

# Microfluidics and cell-free synthetic biology in the development of new diagnostic and therapeutic platforms

Présentée le 5 août 2021

Faculté des sciences et techniques de l'ingénieur  
Laboratoire de caractérisation du réseau biologique  
Programme doctoral en biotechnologie et génie biologique

pour l'obtention du grade de Docteur en médecine et ès sciences (MD-PhD)

par

**Grégoire MICHIELIN**

Acceptée sur proposition du jury

Prof. B. Deplancke, président du jury  
Prof. S. Maerkl, directeur de thèse  
Prof. V. D'Acremont Genton, rapporteuse  
Prof. F. C. Simmel, rapporteur  
Prof. C. Merten, rapporteur

# Acknowledgements

My first thanks go to Sebastian for welcoming me in the laboratory of biological network characterization (LBNC). I was happy to join a lab doing such interesting science combining microfluidics and synthetic biology. I am really grateful for the opportunity I had to work very independently on my encapsulation project, but also to benefit from your input and from exciting collaborations with my colleagues. Thank you to Prof. Bart Deplancke as President for my thesis defense, and to the members of the jury Prof. Valérie D'Acremont, Prof. Friedrich Simmel and Prof. Christoph Merten for the evaluation of my thesis and oral presentation, your interest and useful questions and comments which give me a great motivation for the future. Thank you to my PhD mentor Prof. Olaia Naveiras, as well as to Prof. Bruno Correia, Prof. Li Tang and Prof. Kamiar Aminian for taking part in my first year candidacy examination. I had the chance to get the incredible support from Prof. Esther Amstad and all her fantastic group members. It was a privilege to use devices developed for the production of emulsions by droplet microfluidics, have a perfect hands-on training at the SMaL lab and to have the freedom to work on it back in LBNC. I would like to thank Prof. Kai Johnsson to offer me a position in his lab after my medical studies and for all the preparation and help in obtaining the SNSF MD-PhD grant. Even though I didn't get the chance to work in the lab and perform my intended project on a point-of-care sensor for phenylalanine blood levels, I was deeply interested in the semi-synthetic bioluminescent sensors and I am very happy to see its successful development carried out and I hope that we will see them soon in the clinics.

During the long process of entering the MD-PhD programme and applying for the SNSF grant, I was lucky to have Prof. Lorenz Hirt as a fantastic mentor. Your kindness, interest in my project, and help in preparing the numerous successive presentations were extremely valuable. I would like to thank Prof. Ivan Stamenkovic for the amazing dedication to motivate medical students in joining research. Thank you to Prof. Daniel Hohl as well and the other members of the Lausanne



MD-PhD commission in evaluating my project proposition, and to Thérèse Liechti for her help in all the administrative steps. I also received incredible support on the clinical side in pediatrics, and I would like to thank Prof. Eliane Roulet-Perez and Dr. Sebastien Lebon to spark my great interest in pediatric neurology which convinced me to pursue my training in pediatrics, as well as Prof. Andrea Superti-Furga, Prof. Umberto Simeoni, and Prof. Bernard Laubscher for accepting me in the pediatrics training and for showing great interest in my project and my career.

An immense thank you to Helen and Martine for their help with everything administrative and beyond and thanks to all my colleagues from LBNC: Kristina, Francesca and Francesco who always brought such great atmosphere in the lab, Ekaterina and her high energy maybe coming from her super diet, Nadanai who has been such an amazing colleague sharing good science, good kwak, good food, good music, Professor Ivan ensuring we have high level discussions in all situations and with whom we shared so many great moments in iGEM or in our summer schools, Zoe who is such a talented scientist and the most amazing colleague, always displaying true kindness to everyone around, Simone with his generosity and the best set of jokes, translated or in original version, Barbora who gives so much to make sure everything is in its right place in and out of the lab, Fabien who brings the very needed French touch, version chocolatine, Rohan who is so talented and helped me so much in making microcapsules, Michael who didn't stay long enough but whose passion for science and medicine always brings great discussions, Ming with his dedication to grow millions of yeast cells per week, Shiyu creating millions of yeast cells per week, Evan looking at millions of yeast cells per week, all fantastic colleagues of the yeast team with whom we spend great moments inside and outside the lab, Julia who is an inspiration for working in the lab while being a full-time parent, I hope I can do as well as she does, Josh and all my amazing new colleagues, Amir whose motivation is a great help in our COVID-19 project, Laura who is as daring in the lab as she is on a ski slope, Moustafa and Daniel who I had the chance to work with in iGEM and I am happy to have now as colleagues, and Ragu, Maria, Federico, Rafael, Julian, Fatemeh and Ferdinand who I look forward to spending time with in the lab. A special thank you goes to the SFM2019 summer school participants and organizing team, first and foremost to Tim, my MD-PhD colleague with whom we shared all the steps of the programme, to Flavia and Ale (and of course Ivan again!), and to Roger for his enthusiasm for medical research, the trust he has in the next generation of MD-PhDs, and his hospitality at "Le Bourbaki".

When I started the thesis, I was lucky to still have my chemist friend Aurélien on campus and it

was great to share with you the impressions of starting a PhD, big thanks to you and also to all my chemist friends with whom we shared so many great moments during our studies and maybe spent too much time on a particular terrace on campus. Thank you to all my childhood friends, it gave me incredible strength to go on the challenges I faced knowing that you have been and will always be there by my side trusting I would succeed in everything I do, saying "ça va le faire Greg, on se fait pas de souci pour toi". I have met incredible people along the way in the medical school and in my boarding school job, so thank you to my doctor friends and to all my "frères tuteurs". My chemistry studies at EPFL were incredibly stimulating years, and I was lucky to end on such a high note by doing my project in my brother Olivier's lab, and I would like to thank all the lab members and especially Vincent who is such an amazing person and scientist.

Thank you Olivier for sparking my enthusiasm for research, I vividly remember the first time you showed me and the family some protein structures accessed from PDB and also your fancy coloured silicon graphics machine. Merci aussi pour tous les beaux moments et discussions qui m'ont motivé tout au long de mon parcours. Merci Anne pour m'avoir montré dans toute ton humanité la beauté de la médecine, mon souvenir restera toujours de quand tu avais ramené des échantillons de selles d'un certain voyage et que tu m'avais initié à l'identification de parasites au microscope. Merci Papa pour m'avoir donné la passion de la chimie, une partie de moi aurait sûrement aimé faire autre chose pour ne pas trop marcher dans tes traces, mais comment ne pas tomber sous le charme de belzébules ou de toutes les histoires de tes aventures au labo de chimie avec tes cobayes/élèves du gymnase de la cité. Merci Julie, les mots et les actions manquent toujours pour exprimer l'amour d'un frère pour sa petite soeur, je t'admire tellement pour ton intelligence si étincelante, ta sensibilité unique, et pour tout l'amour que tu sais donner autour de toi. Merci Maman pour m'avoir montré ce qu'est un amour inconditionnel, la générosité absolue, la pureté de ton coeur. Je ne serais rien sans toi et tout ce que tu m'as donné tout au long de ma vie. Merci à vous Mamy et Papy qui m'avez montré tant de choses magnifiques, de générosité dans chaque instant, et combien votre hospitalité remplit de bonheur ceux qui vous entourent. Merci Fanny, tu es la femme de ma vie, mon shared brain, mon amoureuse, mon soutien absolu, ma partenaire de voyages, d'aventures et pour la plus belle aventure qui nous attend. Merci Sam d'être déjà si présent dans ma vie, mais d'avoir pris suffisamment de temps dans le ventre de ta maman, j'ai même réussi à finir ce projet de thèse. Maintenant je peux tranquillement regarder vers l'avenir et vers le plus magnifique projet, devenir papa.

# Abstract

In phenylketonuria, absence or malfunction of the phenylalanine hydroxylase enzyme results in toxic accumulation of phenylalanine in the body. An injectable recombinant enzyme therapy was recently approved and has the potential to improve the quality of life of patients with phenylketonuria. Cell-free protein production uses cytosolic extract of prokaryotic or eukaryotic cells and offers flexibility in biomanufacturing at different scales, accelerates prototyping, and allows decentralized production of therapies by using freeze-dried protein expression systems. In this thesis, we show that we can express the therapeutic enzyme phenylalanine ammonia lyase in home-made cell-free protein expression systems. By using a spectrophotometric enzymatic assay, we show that the enzyme is active and converts phenylalanine to the non-toxic metabolite trans-cinnamic acid. The cell-free expression system can be freeze-dried and still produces active therapeutic enzyme, which would allow the decentralized production of this enzyme replacement therapy. However, the cost associated per dose would be too high with the current cell-free expression system, and improvements in protein yields and costs per reaction will be required to offer decentralized production of enzyme replacement therapy for phenylketonuria.

Another opportunity to improve the quality of life of patients with phenylketonuria would be to propose an oral enzyme replacement therapy. For this purpose, we developed a platform to produce biocompatible semi-permeable microcapsules made of poly-(PEG-DA 250 g/mol) to encapsulate the therapeutic enzyme and protect it from proteolytic digestion. Our results show that the microcapsules are semi-permeable, thermally and mechanically stable, and resistant to incubation in simulated gastric and intestinal fluid. Proteins and active enzymes were successfully encapsulated, but the pore size was slightly too large and would allow the transport of proteolytic enzymes across the capsules shell, thus requiring further improvements for oral enzyme replacement therapy in phenylketonuria.

To demonstrate the potential of the semi-permeable capsules for different applications, we encapsulated proteins, enzymes, magnetic beads, DNA, bacteria or yeast cells inside the liquid core of the microcapsules. This biocompatible microencapsulation platform could be used in the building of innovative encapsulated diagnostic and therapeutic systems containing active biomolecules or living cells.

During the COVID-19 pandemic, we developed a solution to help in the conduction of serological epidemiological studies for the detection of anti-SARS-CoV-2 antibodies. We integrated a decentralized capillary blood collection, dried blood samples shipping, and centralized processing and analysis on a microfluidic chip for high-throughput nano-immunoassays. The microfluidic assay analyzes sample with volumes of a few nanoliters and reduces reagents consumption per datapoint by 2 or 3 orders of magnitude thus offering the potential to greatly reduce costs. The nano-immunoassay was validated with serum samples from 155 PCR-confirmed patients and 134 pre-pandemic negative control sera and showed 100 % specificity and 98 % sensitivity in duplicate measurements. We also show evidence of the good performance of collecting dried blood spots with glucose test strips or two commercial microsampling devices followed by testing with the nano-immunoassay.

Keywords: phenylketonuria, enzyme, replacement, cell-free, microfluidic, encapsulation, immunoassay, dried, blood, microsampling

# Résumé

Dans la phénylcétonurie, une absence ou une mauvaise fonction de l'enzyme phénylalanine hydroxylase résulte en une accumulation toxique de phénylalanine dans le corps. Une enzyme recombinante injectable a récemment été approuvée et a le potentiel d'améliorer la qualité de vie des patients avec phénylcétonurie. La production de protéines *cell-free* utilise un extrait cytosolique de cellules prokaryotes ou eukaryotes et a le potentiel d'offrir de la flexibilité dans la biomanufacture à différentes échelles, d'accélérer le prototypage de procédés, et de permettre la production décentralisée de thérapies grâce à l'utilisation de systèmes de production de protéines *cell-free* lyophilisés. Dans cette thèse, nous montrons que l'enzyme thérapeutique phénylalanine ammonia-lyase peut être exprimée dans un système de production de protéines *cell-free* développé dans le laboratoire. En utilisant un test enzymatique spectrophotométrique, nous montrons que l'enzyme produite est active et convertit la phénylalanine en acide trans-cinnamique, un composé non toxique. Le système de production de protéines *cell-free* peut être lyophilisé et conserve sa capacité de production de l'enzyme thérapeutique active. Cependant, les coûts associés avec la méthode utilisée de production de protéines *cell-free* sont trop élevés. Des améliorations au niveau du rendement ou une réduction des coûts par réaction seront nécessaires pour offrir une production décentralisée de thérapies de remplacement enzymatique pour la phénylcétonurie.

Une opportunité d'améliorer la qualité de vie de patients avec phénylcétonurie serait de proposer une thérapie de remplacement enzymatique par voie orale. Dans ce but, nous avons développé une plateforme pour la production de microcapsules biocompatibles et semi-perméables faites en poly-(PEG-DA 250 g/mol) afin d'encapsuler l'enzyme thérapeutique et la protéger de sa dégradation par des enzymes protéolytiques. Nos résultats montrent que les capsules sont semi-perméables, résistantes aux contraintes mécaniques ou de température, et résistent à une incubation dans du liquide gastrique ou intestinal simulé. Des protéines et enzymes peuvent être encapsulées avec

succès, mais la taille des pores des capsules est un peu trop grande puisqu'elle permettrait le passage d'enzyme protéolytiques, et des modifications seront donc nécessaires pour permettre leur utilisation pour la thérapie de remplacement enzymatique par voie orale. Pour montrer le potentiel des capsules semi-perméables dans différentes applications, nous avons encapsulé différentes protéines, enzymes, billes magnétiques, des molécules d'ADN, des bactéries ou des levures dans le coeur liquide des microcapsules. Cette technique de microencapsulation biocompatible pourrait donc être utilisée dans le développement de nouvelles technologies diagnostique ou thérapeutiques grâce à des biomolécules ou cellules encapsulées.

Durant les premières phases de la pandémie de COVID-19, nous avons développé une solution pour aider à la réalisation d'études épidémiologiques par sérologies pour la détection d'anticorps anti-SARS-CoV-2. Nous avons intégré un procédé qui permet la collection décentralisée de sang capillaire, d'envoi d'échantillons de sang séché, et l'extraction et analyse de manière centralisée grâce à un dispositif microfluidique pour effectuer des nano-immunoessais à haut débit. Le test microfluidique nécessite un échantillon de quelques nanolitres et réduit la consommation de réactif par 2 à 3 ordres de grandeurs pour chaque point de mesure. Le nano-immunoessai a été validé avec des échantillons de sérum provenant de 155 patients ayant présenté un test PCR positif et de 134 patients contrôles prélevés avant la pandémie et le test a démontré une spécificité de 100 % et une spécificité de 98 % pour des analyses effectuées en duplicat. Nous montrons également de bonnes performances lors de la collecte de gouttes de sang séché avec des bandelettes pour glycémie ou avec deux dispositifs commerciaux de collecte de micro-échantillons et leur analyse avec le nano-immunoessai microfluidique.

Mots-clés: phenylcétonurie, enzyme, remplacement, *cell-free*, microfluidique, encapsulation, immunoessai, sang, séché, microéchantillon

# Contents

<b>Acknowledgements</b>	<b>1</b>
<b>Abstract</b>	<b>4</b>
<b>Résumé</b>	<b>6</b>
<b>1 Motivations</b>	<b>14</b>
1.1 Context of the thesis . . . . .	14
1.2 Aims of the thesis . . . . .	16
<b>2 Cell-free expression of a therapeutic enzyme for the treatment of PKU</b>	<b>17</b>
2.1 Introduction . . . . .	17
2.1.1 Phenylketonuria . . . . .	17
2.1.2 PKU management and therapeutic opportunities . . . . .	18
2.1.3 Recombinant enzyme replacement therapy . . . . .	19
2.1.4 Cell-free protein expresion . . . . .	21
2.1.5 Decentralized cell-free manufacturing of biopharmaceuticals . . . . .	22
2.2 Results . . . . .	25
2.2.1 Cell-free expression of PAL . . . . .	25
2.2.2 Lyopreservation of cell-free expression system . . . . .	32
2.2.3 Non-natural amino acid co-translational incorporation . . . . .	34
2.2.4 Cell-free expression of protein nanocompartments . . . . .	38
2.3 Discussion . . . . .	41

<b>3</b>	<b>Direct encapsulation of active biomolecules in semi-permeable microcapsules templated from double-emulsions</b>	<b>43</b>
3.1	Introduction . . . . .	44
3.1.1	Background . . . . .	44
3.1.2	Semipermeable microcapsules for enzyme immobilization . . . . .	45
3.1.3	Compartmentalized cell-free reactions . . . . .	47
3.2	Towards microcapsules templated from double-emulsions . . . . .	60
3.3	Results . . . . .	78
3.3.1	PEG-DA microcapsules templated from double-emulsions . . . . .	78
3.3.2	Production of semi-permeable poly-(PEG-DA 250) capsules . . . . .	80
3.3.3	Direct encapsulation of proteins and enzymes . . . . .	83
3.3.4	Encapsulated DSD reactions . . . . .	87
3.3.5	Immobilization on streptavidin-coated magnetic nanoparticles . . . . .	90
3.3.6	Encapsulation of bacteria and yeast cells . . . . .	93
3.4	Discussion . . . . .	97
<b>4</b>	<b>A high-throughput microfluidic nano-immunoassay for detecting anti-SARS-CoV-2 antibodies in serum or ultra-low volume dried blood samples</b>	<b>100</b>
4.1	Background . . . . .	101
4.2	Preprint . . . . .	104
4.2.1	Abstract . . . . .	104
4.2.2	Introduction . . . . .	105
4.2.3	Results . . . . .	107
4.2.4	Discussion . . . . .	115
4.2.5	Acknowledgments . . . . .	119
4.2.6	Author contributions . . . . .	119
4.2.7	Competing interests . . . . .	120
4.3	Contribution . . . . .	120
4.4	Outlook . . . . .	120
<b>5</b>	<b>Conclusion</b>	<b>122</b>



<b>6 Appendix</b>	<b>126</b>
6.1 Materials and Methods Chapter 2 . . . . .	126
6.2 Materials and Methods Chapter 3 . . . . .	130
6.3 Materials and Methods Chapter 4 . . . . .	134
6.4 Supplementary Figures Chapter 3 . . . . .	139
6.5 Supplementary Figures Chapter 4 . . . . .	143
 <b>Bibliography</b>	 <b>155</b>
 <b>Curriculum vitae</b>	 <b>190</b>

# List of Figures

2.1	Cell-free expression of <i>Av</i> PAL enzyme . . . . .	26
2.2	Cell-free expression of <i>Av</i> PAL enzyme and Ni-NTA spin column purification . . . . .	27
2.3	Enzymatic activity of <i>Av</i> PAL cell-free reaction . . . . .	28
2.4	Cell-free expression of <i>Av</i> PAL enzyme and purification with magnetic particles . . . . .	29
2.5	Enzymatic activity of purified <i>Av</i> PAL or dialyzed <i>Av</i> PAL cell-free reaction . . . . .	30
2.6	Enzymatic activity of freeze-dried cell-free expression systems of <i>Av</i> PAL . . . . .	31
2.7	Trehalose as a lyoprotectant for air-drying of cell-free protein expression systems . . . . .	32
2.8	Freeze-dried cell-free protein expression systems . . . . .	33
2.9	Simplified cell-free protein expression system and freeze-drying . . . . .	35
2.10	Cotranslational incorporation of L-azidohomoalanine using PURE expression system . . . . .	36
2.11	Cotranslational incorporation of L-azidohomoalanine using lysate expression system . . . . .	37
2.12	Cell-free expression of encapsulin protein nanocompartments . . . . .	38
2.13	Cell-free coexpression of encapsulin protein nanocompartments and sfGFP cargo loading . . . . .	39
3.1	Compartmentalized cell-free reactions . . . . .	48
3.2	Communication using cell-free transcription translation . . . . .	57
3.3	Fluorinated oil continuous phase for the production of W/W/O double-emulsions . . . . .	61
3.4	Mineral oil continuous phase for the production of W/W/O double-emulsions . . . . .	62
3.5	Addition of highly hydrophilic polysaccharidic polymer for improved phase separation . . . . .	63
3.6	Addition of DEAP photoinitiator in the continuous phase as a separation agent . . . . .	64
3.7	Addition of HMPP photoinitiator in the continuous phase . . . . .	65
3.8	Water-in-(PEG-DA 250)-in-oil double-emulsions . . . . .	67
3.9	Water-in-(PEG-DA 250)-in-water double-emulsion stability . . . . .	69

3.10	Polymerized capsules from water-in-(PEG-DA 250)-in-water double-emulsion . . . . .	70
3.11	Polymerized capsules are impermeable to small fluorophores . . . . .	71
3.12	No pores formed when illuminated through polpropylene tubes . . . . .	73
3.13	Stability of poly-(PEG-DA 250) microcapsules to physical challenges . . . . .	74
3.14	Stability of poly-(PEG-DA 250) microcapsules to chemical challenges . . . . .	75
3.15	Production of semipermeable microcapsules in a PDMS device with 3D geometry . .	79
3.16	PEG-DA 250 microcapsules are semi-permeable and the pore size can be adjusted by changing the porogen . . . . .	81
3.17	Direct encapsulation of proteins inside semi-permeable PEG-DA 250 capsules . . . .	84
3.18	Direct encapsulation of active enzymes in semi-permeable PEG-DA 250 microcapsules	86
3.19	Immobilization of DNA strand displacement reaction in semi-permeable microcap- sules and implementation of a two-layer signalling cascade . . . . .	88
3.20	Encapsulated streptavidin-coated magnetic nanobeads functionalized with anti-EGFP antibody . . . . .	91
3.21	Immobilization of DNA strand displacement reaction on encapsulated streptavidin- coated magnetic nanobeads . . . . .	92
3.22	Encapsulation and culturing of bacteria expressing a fluorescent protein . . . . .	94
3.23	Encapsulation of yeast cells expressing a fluorescent protein . . . . .	96
4.1	High-throughput microfluidic nano-immunoassay for anti-SARS-CoV-2 antibody de- tection . . . . .	108
4.2	Nano-immunoassay validation . . . . .	111
4.3	Ultra-low volume whole blood sampling and processing . . . . .	112
4.4	Ultra-low volume dried blood method characterization . . . . .	115
4.5	Ultra-low volume patient sample collection and analysis . . . . .	116
4.6	NIA performance table and conceptual home-based sample collection and centralized NIA analysis . . . . .	118
6.1	Microcapsules with decanol porogen are impermeable to 500 kDa FITC-dextran . . .	139
6.2	Semi-permeable microcapsules with ethylhexanol porogen . . . . .	140
6.3	Semi-permeable microcapsules with octanol porogen . . . . .	141
6.4	Interior/exterior fluorescence ratios of 10 kDa RITC-dextran and EGFP . . . . .	142

6.5	Evaluation of SARS-CoV-2 antigens . . . . .	143
6.6	NIA measurements for a range of sample dilutions . . . . .	144
6.7	NIA replicates . . . . .	145
6.8	Device-to-device variation . . . . .	146
6.9	Complete serum dilution data . . . . .	147
6.10	Technical replicates for ultra-low volume whole blood sampling methods . . . . .	153
6.11	FITC spotting tracer . . . . .	154

# 1

## Motivations

### 1.1 Context of the thesis

During my doctoral thesis, I explored multiple directions with the same goal of developing new diagnostic or therapeutic tools. All my different efforts were made in the direction of advancing healthcare, and I hope that my modest contributions done during this thesis will help in any possible way. Before starting this project, I obtained an MD-PhD grant from the Swiss National Science Foundation to work with Professor Kai Johnsson and develop point-of-care sensors for phenylalanine. Such technology would help patients with a disease called phenylketonuria in managing their treatment by closely monitoring their blood phenylalanine levels. During my medical studies and the long process of obtaining this support, I got very interested in this disease and I was looking forward to work on a project that could directly benefit patients. However, a few weeks after receiving the grant, Professor Johnsson informed me that he accepted a position as Max Planck institute director in Heidelberg, meaning I had to find another hosting lab at EPFL.

I was fortunate to join Professor Sebastian Maerkl lab, and we decided to keep working on the subject of phenylketonuria. We explored some new ways of producing the therapeutic enzyme phenylalanine ammonia lyase (PAL) with the use of cell-free expression systems, which could open the possibility to produce the therapeutic enzyme on-demand and in a decentralized way. We also sought to engineer some protection against proteolytic digestion to allow its use as an oral replacement therapy. For that purpose, we considered the use of unnatural amino acid incorporation in the cell-free produced enzyme, which could facilitate the process of enzyme PEGylation used to protect the enzyme. Another protection method we considered was the use of protein nanocompartments

which could form a protease resistant compartment and protect their cargo.

Finally, we started a collaboration with Professor Esther Amstad and the SMaL lab at EPFL to produce semipermeable microcapsules that would allow the encapsulation and protection of the therapeutic PAL enzyme, while allowing the transport of phenylalanine. The production of microcapsules templated from double-emulsions produced with microfluidics ended up forming the most important part of my research project. This has proven to be a difficult task, first setting up a droplet microfluidic method to produce double-emulsions, finding a suitable biocompatible capsule material, and polymerizing semipermeable capsules possessing nanopores of appropriate size cutoff. Encapsulation of enzymes or different active biomolecules in semi-permeable microcompartments not only has interest for enzyme delivery, but also for other applications in therapeutics, diagnostics, or in basic research. We explored different applications that could benefit from the development of our semipermeable microcapsules, such as the encapsulation of DNA strand displacement (DSD) reactions, and we are confident that the microcapsules could be used for other interesting applications in the future.

During the last year of my thesis, our lab was momentarily shut down due to the COVID-19 pandemic. I took some time to help remotely the center of precision oncology in CHUV, Lausanne. In the team, we entered electronic case report forms to allow a clinical monitoring of the oncology patients affected with COVID-19. Later, the lab was partly reopened as part of the EPFL COVID-19 task force, and focused on the development of a microfluidic high-throughput nanoimmunoassay platform for SARS-CoV-2 antibody testing. I was fortunate to join the team formed by my colleagues Zoe Swank, Hon Ming Yip and Chun-Jie Cai and work on this platform. I had a primary involvement on the preanalytical part, exploring the compatibility of dried blood sampling and extraction with the nano-immunoassay platform. This work is ongoing in collaboration with the Geneva University Hospitals and I am particularly happy to participate in this research effort with direct implications for the clinics. I look forward to seeing the collaboration continue and bring new developments in this project supported by the Swiss National Science Foundation (NRP-78).

## 1.2 Aims of the thesis

- The first aim of the thesis is to develop a cell-free expression system for the decentralized or on-demand production of the therapeutic enzyme PAL, and to develop methods that could be used together with cell-free expression and would protect PAL from proteolytic degradation or from eliciting an immune response.
- The second aim of the thesis is the production of biocompatible semi-permeable microcapsules which could be loaded with active enzymes such as PAL or other active biomolecules.
- The third aim of the thesis is the development of a platform for the detection of anti-SARS-CoV-2 antibodies by decentralized collection of blood samples and testing on a microfluidic high-throughput nanoimmunoassay.

## 2

# Cell-free expression of a therapeutic enzyme for the treatment of PKU

## 2.1 Introduction

### 2.1.1 Phenylketonuria

Phenylalanine hydroxylase (PAH) deficiency is an inborn error of metabolism resulting in a deficient or absent hydroxylation of the essential amino acid phenylalanine to tyrosine. It is an autosomal recessive genetic disease that affects the PAH gene on chromosome 12q23.2, with more than 500 different mutations reported [1]. The classical form of the disease is called phenylketonuria (PKU), and it is present in 1 in 8000 newborns in Switzerland (neoscreening.ch). Dr. Asbjörn Fölling, a Norwegian physician and chemical engineer, discovered the disease in 1934 by linking the mental retardation observed in patients to the high concentration of phenylpyruvic acid that he was able to isolate from their urine [2]. The disease could be diagnosed by the reaction of ferric chloride with excess phenylpyruvic acid present in patient's urines, and the role of phenylalanine accumulation in the clinical presentation of PKU and its autosomal recessive transmission were identified [3]. The clinical presentation consists of central nervous system injury, fair skin and hair, and elevated levels of phenylalanine metabolites in urine. Accumulation of phenylalanine saturates the large neutral amino acid transporter (LNAAT), which impairs the transport and metabolism of other amino acids in the brain. Additionally, the missing product of phenylalanine hydroxylation, tyrosine, is an important neurotransmitter precursor; tyrosine is an essential precursor in the biosynthesis



of L-DOPA, dopamine, and catecholamines, but also in the biosynthesis of melanin. Finally, the degradation of the accumulated phenylalanine occurs via alternative metabolic routes, leading to the production and excretion of phenylpyruvate, phenylacetate and other metabolites in the urine, accounting for the characteristic particular odor of the patient’s urine [1]. The mainstay of PKU management was introduced in the 1950s with the adoption of low-phenylalanine diet in the form of low protein regime supplemented with the remaining amino acids [4, 5, 6]. Another important milestone was the development of neonatal screening programs using the bacterial inhibition test proposed by Robert Guthrie [7][8], allowing to place PKU patients on the appropriate diet early enough to mitigate most of the harmful effects of hyperphenylalaninemia during development.

### **2.1.2 PKU management and therapeutic opportunities**

As presented above, the mainstay of the current treatment consists in adopting from the very first weeks of life a restrictive, low-protein diet, further supplemented with medical foods containing the required amino acids except phenylalanine. While this helps in preventing most of the severe consequences of PKU, it can be difficult for some patients to remain in recommended levels of phenylalaninemia and neurophysiological problems can be encountered [1]. Although PKU is a rare disease, its extensive characterization at the clinical, genetical, physiological, and biochemical levels, the awareness gained through neonatal screening programs, together with the availability of preclinical models, has made it an attractive area of research for both academia and the pharmaceutical industry [9]. Despite multiple efforts, the only FDA approved drug until 2018 for the management of phenylketonuria has been Sapropterin, a synthetic analog of tetrahydrobiopterin, which was introduced in 2007. Unfortunately, not more than a third of PKU patients benefit from this therapy as it is not able to lower phenylalanine levels in patients with certain PAH mutations [10]. Enzyme replacement therapy, which provides an exogenous supply of a bacterial phenylalanine ammonia lyase (PAL) to convert excess phenylalanine into the non-toxic transcinnamic acid, would allow most patients to be relieved from their restrictive diets [11]. After years of research and development (discussed in section 2.1.3), a subcutaneous self-injectable pegylated PAL called Pegvaliase or PEG-PAL was approved in the US in 2018 [12] and in 2019 in Europe, marking another more recent milestone in PKU management. Other approaches are being explored, for example by administering the therapy with engineered red blood cells to express an active enzyme, but the company Rubius therapeutics stopped its developments following unconvincing results from the ini-

tial patient treatment in clinical trial NCT04110496. Gene therapy is also advancing towards the clinic with different candidates entering phase 1/2 clinical trials such as HMI-102 from Homology medicine (clinical trial NCT03952156), or BMN 307 from Biomarin (clinical trial: NCT04480567). Gene therapies are attractive as a one-off treatment option, with successes in clinical trials for different indications such as hemophilia A with Biomarin’s valoctocogene roxaparvovec [13]. However, there remain some questions about the duration of efficacy which is of particular significance since the treatment cannot be administered again due to immunization against the adeno-associated virus (AAV) vector used, leading to FDA rejecting the application for Biomarin’s hemophilia A gene therapy, asking for additional data on long term efficacy. Instead of using viral vectors to deliver DNA information for the expression of the therapeutic enzyme, Moderna is investigating at a preclinical stage the use of its mRNA delivery platform for the treatment of PKU mRNA-3283 and has filed patents towards this use (WO2015061491A1). While gene therapies will certainly play an important role in PKU treatment, an oral replacement therapy would offer a comfortable route of administration to patients and its reversible and titrable action would provide an alternative treatment option with facilitated adoption. Early preclinical studies have shown positive results when administering PEGylated PAL to mice by oral gavage [14], but a high dose of enzyme was required to obtain a significant reduction in phenylalaninemia, even with PEGylation and selection of mutations to improve protease resistance. Using its proprietary protein engineering technology, Codexis developed an improved variant of PAL, further strengthening its proteolytic resistance, as well as improving its manufacturability, resulting in the enzyme CDX-6114 which entered a phase I clinical trial (NCT04085666) and will be developed in partnership with Nestlé health science. Alternatively, developments in synthetic biology led to new therapeutic opportunities by engineering non-colonizing probiotics metabolizing phenylalanine in the digestive tract [15] and are currently the focus of Phase II clinical trials.

### 2.1.3 Recombinant enzyme replacement therapy

As the focus of this thesis will be on the use of recombinant enzyme replacement therapy, we will present in more details the developments leading to the approved injectable enzyme replacement therapy for PKU and efforts made in using it for oral enzyme replacement therapy. The first proposition for enzyme replacement therapy in PKU patients was made as early as 1978 when Ambrus *et al.* immobilized phenylalanine ammonia lyase (PAL) in extracorporeal reactors [16].

While successful in reducing phenylalanine levels, it was not practical as a chronic treatment and was not adopted. In 1980, Hoskins *et al.* encapsulated PAL purified from *Rhodotorula glutinis* yeast (*Rg*PAL) in hard gelatin capsules with enteric coating, but no significant reduction in phenylalanine blood levels were observed [17]. In 1985, Thomas Chang proposed to use "artificial cells" obtained from emulsification of a solution of PAL and hemoglobin in collodion, forming capsules with a cellulose acetate thin shell [18]. The administration of the PAL-containing artificial cells to rats was effective in lowering blood phenylalanine levels, but no further developments were made because of the lack of availability in PAL. In 1999, Sarkissian *et al.* cloned the yeast *Rhodospiridium toruloides* PAL gene (*Rt*PAL) in *E. coli* and were able to produce it in large quantities, and showed that it was amenable for reduction of phenylalaninemia leading to a renewed interest in this enzyme [19]. However, the large quantity of enzyme necessary for oral therapy or the reduced efficacy after repeated injections due to immune effects motivated further investigations and developments [20]. One method to prevent recombinant products from eliciting an immune response and reducing their efficacy is to use PEGylation as was developed for adenosine deaminase (PEG-ADA) used in the treatment of severe combined immunodeficiency (SCID) [21]. PEGylation was applied to human phenylalanine hydroxylase (PAH) and other PAH enzymes, but the requirement of a cofactor makes it less ideal compared to PAL [22]. Indeed, the PEGylation procedure was used soon after on *Rt*PAL which successfully reduced immunogenicity of the product while preserving its therapeutic enzymatic activity [23, 24, 25]. The last important step in obtaining an effective enzyme replacement therapy for PKU was the discovery of cyanobacterial PAL enzymes, notably from *Anabaena variabilis*, *Av*PAL. These enzymes have comparably smaller size while presenting comparable catalytic activities [26], and thermal stability and proteolytic resistance was enhanced after engineering two cysteine residues into serines (C503S and C565S) [27]. Finally, the PEGylation of *Av*PAL formed the product used in the injectable enzyme replacement therapy for phenylketonuria after years of collaborative development between academic and industrial partners [20]. While the approval of an injectable enzyme replacement therapy is an immense success, there would still be great benefits for patients to use the recombinant enzyme as an oral therapy. To this goal, the *Av*PAL enzyme was further engineered by substituting a chymotrypsin sensitive residue (F18A) and was either immobilized in silica particles or PEGylated to improve its proteolytic resistance [28]. However, the modifications resulted in decreases in enzyme catalytic activity with only modest improvement in its stability and resistance *in vitro*. Nevertheless, different formulations

were evaluated in a preclinical mouse model of PKU [29] and the triple mutant *Av*PAL PEGylated with 5 kDa PEG was shown as a promising candidate, with a significant and important reduction of blood phenylalanine levels in treated mice [14]. However, the dose administered was important with about 15 units of enzyme per dose in this small animal preclinical model. In comparison, the subcutaneously injectable enzyme is administered at 20 mg or 40 mg per dose in an adult human, which represents around 40 or 80 units of enzyme. Efforts are still ongoing to provide protection to the recombinant enzyme for example by immobilizing the enzyme in mesoporous silica particles [30], or by more extensive protein engineering by Codexis.

#### **2.1.4 Cell-free protein expression**

Cell-free or in vitro transcription-translation makes use of the machinery of living cells for the conversion of DNA based genetic constructs into the corresponding RNA and protein, without the need for maintaining cell integrity and its basic metabolic processes [31]. Extracts from various prokaryotes, eukaryotes, and plants, or even reconstituted systems can be used [32]. The most common commercial cell extracts were developed by using *E. coli* [33, 34], wheat germ [35, 36], or rabbit reticulocytes [37]. More recently, other eukaryotic lysates obtained from insect [38], chinese hamster ovary (CHO) [39] or human [40, 41] cells were made available. A plant-based system using tobacco-BY2 cells presents the highest protein expression in batch format with yields up to 3 mg/mL of reaction [42, 43]. A reconstituted system called “PURE” is also available, where all the necessary machinery components for protein expression are produced recombinantly and purified [44]. Detailed protocols for the in-house preparation of *E. coli* extracts are established [45], and high throughput production of different extracts is possible with little infrastructure by using sonication to lyse bacterial cells [46], making it widely available for research laboratories. In 2011, Zawada *et al.* presented the first large-scale production using an *E. coli* cell-free production system following the current Good Manufacturing Practices (cGMP) for drug production [47]. A detailed examination of the components necessary for the cell-free reaction led to a drastically simplified and cheaper energy supplementation with potassium glutamate as the sole energy source, further converted to higher energy molecules and ATP through active metabolism and oxidative phosphorylation [48], improving on the previously described Cytomim system [49]. This allowed the creation of Sutro biopharma which successfully uses cell-free for the bulk production of biopharmaceuticals such as antibody-drug conjugates [50] or bispecific antibodies [51], leveraging additional

advantages of cell-free biomanufacturing such as non-natural amino acid incorporation or rapid prototyping. More traditional biopharmaceutical companies such as Ipsen also recognized the utility of cell-free, notably in the production of toxins since it can facilitate biocontainment and safety measures and limit the risk of accidental exposition for production operators [52]. Further advances in cell-free transcription translation led to the demonstration of its potential for the portable and on-demand protein synthesis from lyophilized systems in a "just-add-water" format [53, 54]. Indeed, freeze-drying of the cell-free expression system allows for easier storage and distribution, and simple production of the desired product upon rehydration. Moreover, lyophilization was shown to completely remove any bacterial contamination from the cell-free system, making it ideal for portable diagnostics and therapeutics applications [55]. This makes lyophilized systems ideal for teaching purpose as well and we proposed it as an "educational cell-free mini kit" in the EPFL iGEM project 2017 and a similar concept was developed into the BioBits<sup>TM</sup> kits [56, 57, 58].

### **2.1.5 Decentralized cell-free manufacturing of biopharmaceuticals**

While the approval of PEGylated-PAL (Palynziq) enzyme replacement therapy for PKU is a great achievement, the centralized manufacturing of the enzyme, chemical modification with PEG, purification, cold storage and distribution [59], and taking into account the investments associated with its development, translates in a year of treatment costing close to 200'000 \$. Considering the important research and development efforts which were necessary to develop Palynziq, it could be even more difficult to see therapies developed for diseases with smaller patient cohorts, or where the clinical benefits of enzyme replacement therapy would not be large enough to justify high costs. Indeed, biologics and enzyme replacement therapies in particular are very expensive, but manufacturers can argue that their proposition is cost-effective when considering quality adjusted life years (QALYs) gained using the therapy, even though in some cases this calculation is not in favor of enzyme replacement therapy [60]. In addition, there are difficulties in creating a biosimilar market to increase competition and drive costs down [61]. As a result, a great tension is created from the desire to produce ever more individualized therapeutics and addressing rare or neglected diseases, while on the other end using bulk centralized production of biopharmaceuticals which can be distributed to the largest market possible, or with exclusivity and control of pricing for a prolonged period of time [62]. A completely different approach which would circumvent some of the hurdles posed by the current model would be to completely decentralize the production of

biopharmaceuticals for patients via magistral preparation [63, 64]. Schellekens *et al.* propose that biopharmaceuticals could be produced using small scale bioreactors at the point-of-care for a unique patient, which would exempt it from the usual regulations. They estimated the bedside production of recombinant human  $\alpha$ -glucosidase (rhGAA) to 1491 \$/gram compared to the 11'948 \$/gram of the commercial equivalent Myozyme. A great concern in biopharmaceutical production is the occurrence of adverse events due to improper manufacturing. In centralized production, security is improved by the quality management systems in place which reduce such events, but non-identified problems can have consequences for a large number of patients. Moreover, failure to meet quality requirements at the final formulation of the active ingredient is responsible for the majority of shortages of injectable drugs [65]. This can be even more critical when the active ingredient is produced in cells, where the contamination of a cell-line can result in shortages as was the case in 2009 for Fabrazym, requiring a rapid decision on resource allocation to mitigate the effects of the shortage on Fabry disease patients [66, 67]. These considerations point to potential advantages of decentralized manufacturing where only one patient would be affected in case of a production problem, and the production of biopharmaceuticals of clinical quality for human therapeutics has been demonstrated at appropriately small scales using a *Pichia pastoris* expression system [68]. Although the lead time from sequence of interest to produced protein using this cell-based expression system was already considered short at around 16 weeks, the use of cell-free expression systems could drastically reduce it and allow true on-demand production of therapeutics [69]. Using a lyophilized cell-free expression system would further facilitate the decentralized manufacturing of proteins, with the rehydration of the shelf-stable extract with DNA instructions necessary for the production of the desired biopharmaceutical, such as cytotoxic onconase [54], antimicrobial peptide cecropin B or Diphtheria vaccine [53]. The cell-free production is compatible with downstream processes and the purification is even facilitated as no cell separation or cell-lysis step is required after protein expression. This allowed researchers to recombinantly express and purify recombinant human erythropoietin (rhEPO) and recombinant human granulocyte-macrophage colony-stimulating factor (rhGM-CSF) in less than 24 hours [70, 71]. With a lyophilized cell-free expression system and combining the expression and purification steps on a single microfluidic chip, Murphy *et al.* [72] could even obtain purified active cecropin B within 6 hours. As an extreme use case of biopharmaceuticals production in a low-resource setting, the NASA is conducting research programs using cell-free expression for the biomanufacturing in space during long-term flights [73]. In this chap-

ter, we will explore the cell-free production of the therapeutic enzyme *AvPAL*, hoping to further strengthen the potential for decentralized manufacturing of biopharmaceuticals.

## 2.2 Results

In this section, we present the results obtained for the cell-free expression of the therapeutic enzyme *Av*PAL in commercial and home-made lysate (2.2.1) and the use of dried cell-free systems for decentralized protein production (2.2.1). We also present preliminary experiments exploring methods to provide protection to the recombinant enzyme such as non-natural amino acid incorporation which could be used as reactive handles for PEGylation of *Av*PAL (2.2.3), or production of protease resistant protein nanocompartments which can be loaded with a protein cargo (2.2.4).

### 2.2.1 Cell-free expression of PAL

A plasmid was ordered and synthesized through Integrated DNA technologies (IDT) which contains the sequence for *Av*PAL codon optimized for expression in *E. coli* [74] and modified with 3 mutations, C503S and C565S for reduced aggregation [27] and F18A for improved protease resistance [28]. The plasmid also contains a T7 promoter and terminator, and a C-terminal hexahistidine tag. The cell-free protein expression system was produced in-house according to the protocol from Kwon and Jewett [46] and Sun *et al.* [45]. *Av*PAL was expressed from the plasmid template using either a commercial Promega *E. coli* S30 extract for 1h or a home-made system for 3h. The 25  $\mu$ L reaction was supplemented with FluoroTect<sup>TM</sup> GreenLys tRNA to incorporate lysine-BODIPY in the expressed proteins for subsequent on-gel fluorescence detection.

With this system, only newly synthesized proteins will incorporate the lysine-BODIPY and made visible as bands on the gel, together with the charged-tRNAs themselves. This greatly helps in confirming expression of proteins even at low concentrations which could not be visualized on a coomassie-stained gel, or would be superimposed with other proteins present in the reaction mix. We observe a clear single band slightly below the 63 kDa ladder mark in reactions where the DNA template for *Av*PAL is added, close to the expected size of 64 kDa in the monomeric form. The band is present both when a commercial Promega S30 T7 expression system for circular DNA was used and when we used a home-made *E. coli* cell-free extract supplemented with an energy solution provided by the group of Prof. Richard murray at Caltech [45]. The synthesis capacity of the cell-free expression systems was also shown by the production of luciferase when using the positive control circular DNA included in the commercial kit, as evidenced by a clear band slightly above 32 kDa present when using either commercial or home-made extracts. This results show that



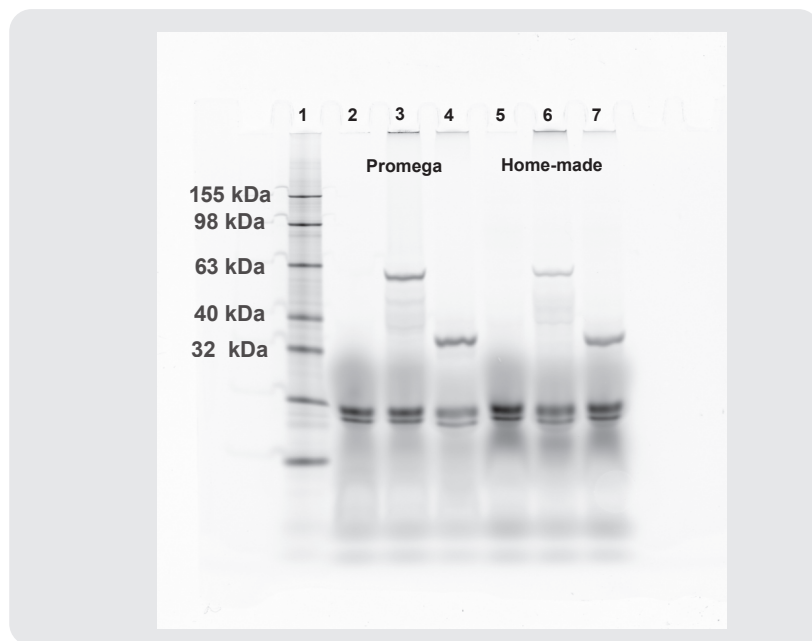


Figure 2.1: **Cell-free expression of *AvPAL* enzyme.**

Fluorescent scan of an SDS page gel. The cell-free reaction was supplemented with tRNA-lysine-BODIPY allowing in-gel fluorescent detection of synthesized proteins. A band of expected size above 60 kDa is observed both in the commercial and in the home-made cell-free expression system. The included positive control also shows luciferase expression. Lanes: (1) ladder (2) blank (3) *AvPAL* (4) luciferase (5) blank (6) *AvPAL* (7) luciferase. (2-4) Promega S30 T7 expression system, (5-7) Home-made expression system.

the engineered therapeutic enzyme *AvPAL* can be expressed both in commercial and home-made cell-free expression systems.

We next tried to scale-up the reactions performed using home-made cell-free extracts to 4 x 50  $\mu$ L of reaction in order to synthesize sufficient protein for purification steps at a small scale. For such low volumes, we used Ni-NTA spin columns (Qiagen) for the purification of the His-tagged *AvPAL* enzyme. Aliquots of the reaction and of the different purification steps were loaded on an SDS-page gel for an estimation of the synthesized and purified *AvPAL* (Fig. 2.2). It is difficult to assess *AvPAL* expression in the reaction mixture loaded in the gel, as an endogenous band is present in the cell-free extract around 64 kDa even without addition of template DNA. The band looks slightly thicker when the *AvPAL* template DNA is added to the reaction, but it is hard to confirm that *AvPAL* is expressed based on this observation. However, we see a strong band in the elution

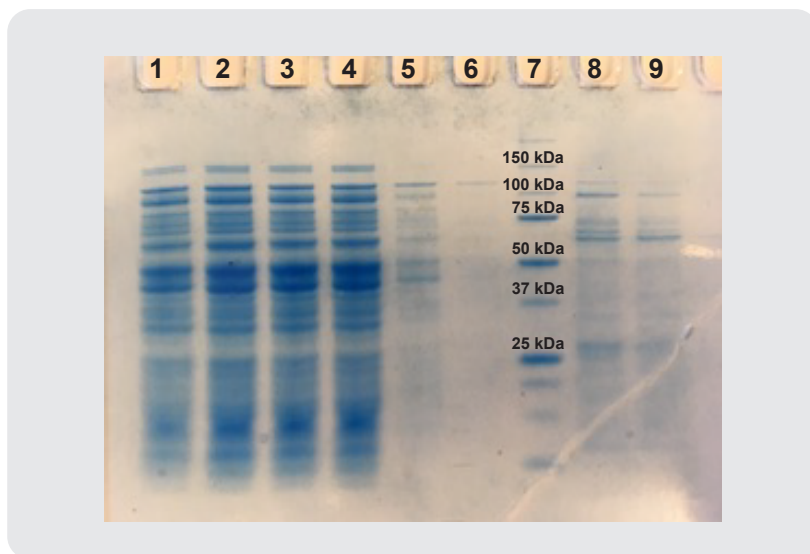


Figure 2.2: **Cell-free expression of *Av*PAL enzyme and Ni-NTA spin column purification.** SDS page gel of endpoint reaction products and the different purification steps. Lanes: (1) blank (2) *Av*PAL expression (3 and 4) flow-through (5 and 6) wash (7) ladder (8 and 9) elution

fractions 1 and 2 at around 64 kDa. Unfortunately, the eluate also contains other proteins and the purity is not satisfactory as it appears to be below 50 % based only on the visual inspection of the SDS-page gel. Even though we could not purify the *Av*PAL enzyme with sufficient purity, this experiment allowed us, after purification, to visualize bands migrating at a distance corresponding to the size of *Av*PAL and confirm its expression in our home-made cell-free expression system.

As the expression and purification of cell-free expressed *Av*PAL enzyme were difficult to assess on a SDS-page gel due to the relatively low protein yields, we chose to directly evaluate the enzymatic activity of cell-free expressed *Av*PAL. In order to evaluate the enzyme activity of the cell-free reactions, we used a spectrophotometric assay to measure the enzymatic conversion of L-phenylalanine into trans-cinnamic acid. Trans-cinnamic strongly absorbs UV light at 270 nm with an extinction coefficient measured at  $21700\text{ M}^{-1}\text{ cm}^{-1}$  in our system, and thus an increase in absorbance can be correlated to *Av*PAL enzymatic activity. As a positive control, we use recombinant *Rg*PAL (Sigma-Aldrich) which is supplied as a 7.4 mg/mL solution with 1 unit/mL specific activity. One unit of enzyme is defined as converting 1  $\mu\text{mole}$  of L-phenylalanine to trans-cinnamic acid at pH 8.5 at 30°C based on the protocol provided by the supplier. The measured absorbance increase was linear and allowed us to calculate an activity for the commercial solution of 7.32 units/mL

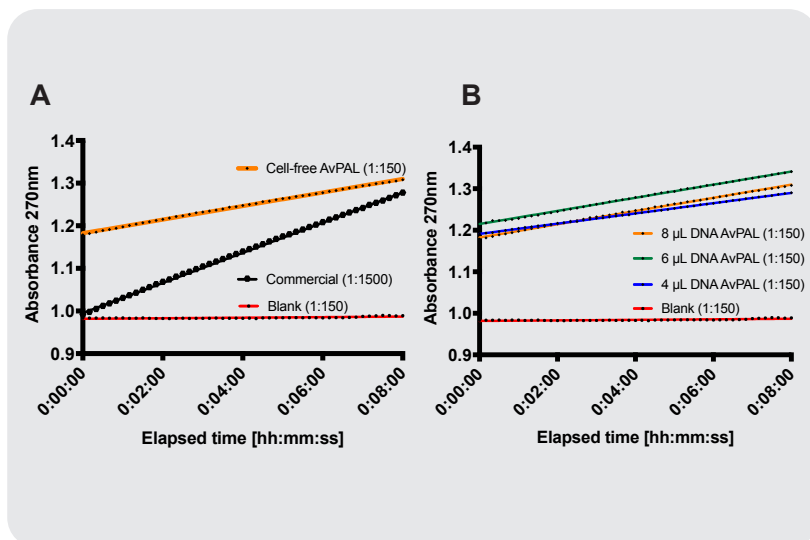


Figure 2.3: **Enzymatic activity of *AvPAL* cell-free reaction.**

Absorbance increase at 270 nm after conversion of phenylalanine to trans-cinnamic acid. **(A)** Commercial recombinant enzyme solution activity was measured for comparison at 7.32 units/mL. **(B)** Activity measured from endpoint cell-free reactions after expression of *AvPAL* with different relative DNA template input. 4  $\mu$ L: 0.26 units/mL, 6  $\mu$ L: 0.33 units/mL, 8  $\mu$ L: 0.33 units/mL. DNA template concentration of 134 ng/ $\mu$ L.

(Fig. 2.3, A), which is in close agreement with the expected 7.4 units/mL. In the same day, we measured the activity of cell-free expression reactions of *AvPAL* directly from the reaction mixture, without any purification step. The activity measured was as high as 0.33 units/mL (Fig. 2.3, B). This activity per volume unit would correspond to an active enzyme concentration of 292  $\mu$ g/mL in the reaction mixture if we assume a specific activity of *AvPAL* of 1.13 units/mg as was reported by Kang *et al.* [28]. A point to note is the initial higher absorbance measured for the cell-free reaction mixtures compared to the blank or the commercial enzyme solution, which can be explained by the presence in the cell-free reaction of molecules which are not related to the trans-cinnamic enzymatic production but absorb at 270 nm, such as the DNA template used for expression. This could also result from the conversion of L-phenylalanine present in the cell-free reaction and converted to trans-cinnamic acid by the newly produced *AvPAL*. In any case, the initial absorbance does not affect the estimation of activity per volume unit as only the slope of the absorbance increase in linear regime is used for the activity calculations. By using a spectrophotometric assay, we could

therefore demonstrate that cell-free reactions expressing *Av*PAL are enzymatically active in converting L-phenylalanine to trans-cinnamic acid, and estimate a cell-free synthesis of close to 300  $\mu\text{g/mL}$  of active *Av*PAL enzyme.

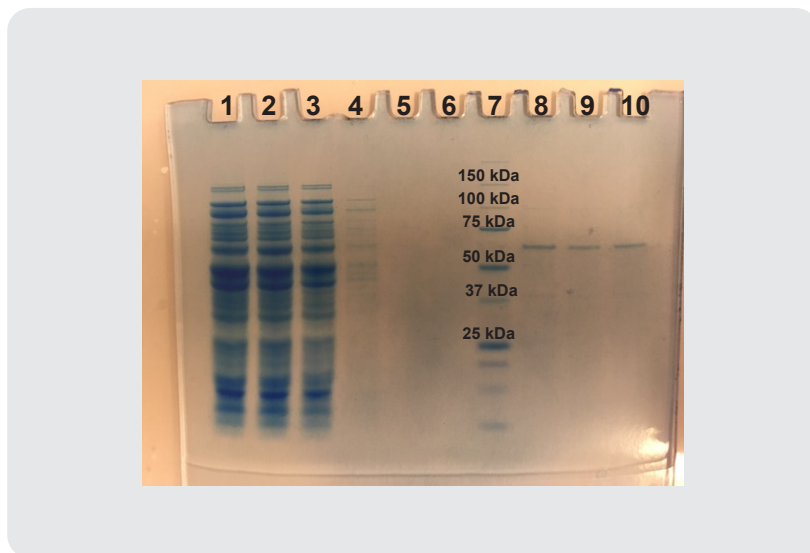


Figure 2.4: **Cell-free expression of *Av*PAL enzyme and purification with magnetic particles.**

SDS page gel of reaction products and the different purification steps. Lanes: (1) blank (2) *Av*PAL expression (3) flow-through (4 to 6) wash (7) ladder (8) elution (9) dialyzed in PBS (10) dialyzed in Tris-HCl.

Having demonstrated that the non-purified cell-free expressed *Av*PAL enzyme is enzymatically active, we tried to improve its purification from the reaction mixture. For this purpose, we selected a different small scale purification method by using Ni-NTA coated magnetic beads (MagneHis<sup>TM</sup>, Promega). 5 x 50  $\mu\text{L}$  reactions were pooled and purified following the standard protocol provided by the supplier. The 250  $\mu\text{L}$  of reaction were eluted in a final volume of 500  $\mu\text{L}$ . It was again difficult to see the band corresponding to *Av*PAL expression in the reaction mixture, although we see a slightly thicker and darker band at the expected size (Fig. 2.4). After elution however, we observed a strong single band between the 50 kDa and 75 kDa protein ladder references. The visual inspection suggested a good purity of the *Av*PAL protein, and we measured a protein concentration of 340  $\mu\text{g/mL}$  in the eluate. Unfortunately, the enzymatic activity of the purified enzyme was only 0.04 units/mL, which was not improved when the purified enzyme was dialysed against

PBS or Tris-HCl to exclude a potential interference of imidazole or other components of the elution buffer (Fig. 2.5, A). This activity per unit of volume would represent a specific activity of around 0.1 units/mg of *Av*PAL enzyme, which is an order of magnitude lower than expected.

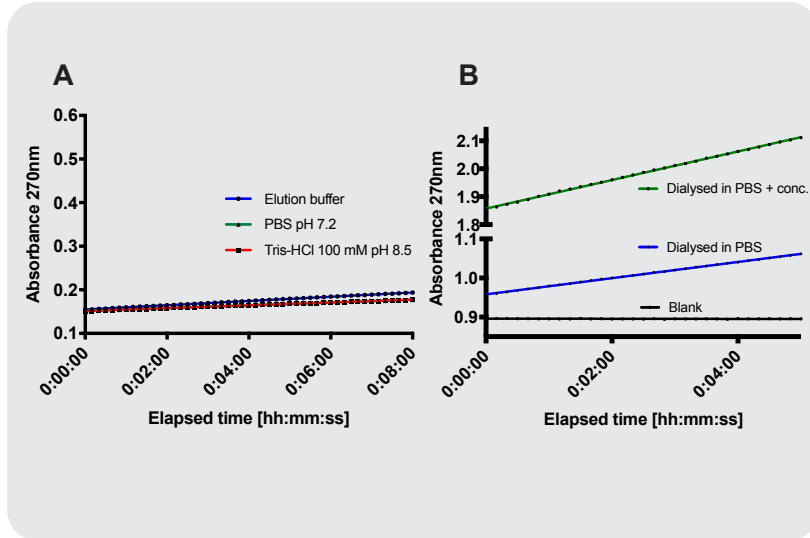


Figure 2.5: **Enzymatic activity of purified *Av*PAL or dialyzed *Av*PAL cell-free reaction.** Absorbance increase at 270 nm after conversion of phenylalanine to trans-cinnamic acid. **(A)** Activity of purified *Av*PAL enzyme in elution buffer: 0.04 units/mL, and subsequent dialysis in PBS: 0.027 units/mL or Tris-HCl: 0.026 units/mL. **(B)** Activity of *Av*PAL cell-free expression reaction endpoint directly dialyzed with a 20 kDa membrane in PBS: 0.43 units/mL and concentrated with a 5 kDa cut-off centrifugal filter unit: 1.06 units/mL.

We again showed that the cell-free reaction expressing *Av*PAL yields a comparably strong activity with 0.43 units/mL of reaction mixture, which was dialyzed in PBS to help remove any potential interference with the enzymatic assay (Fig. 2.5, B). We could further maximize the activity per unit of volume to 1.06 units/mL by simply concentrating the solution with a 5 kDa cut-off centrifugal filter unit. In conclusion, while we show that the his-tagged *Av*PAL enzyme could be purified from the cell-free expression reaction, the specific activity of the purified product is greatly reduced. In the reaction mixture directly, and based on the expected enzyme specific activity, we can estimate that close to 400  $\mu$ g/mL of active *Av*PAL were synthesized. In comparison, the maximum yields reported for cell-free expression systems based on *E. coli* extract are just a little over 2 mg/mL for the synthesis of a model fluorescent protein [75].

One advantage of using cell-free systems for the expression of therapeutic proteins or enzymes would be the possibility to have distributed manufacturing of the cell-free expressed therapeutic. However, the cell-free reaction components are usually stored in  $-80^{\circ}\text{C}$  freezers which would make it very difficult to use outside of a dedicated facility. We therefore tried to express *AvPAL* from a freeze-dried cell-free expression system and assessed the cell-free expression system stability when stored at room temperature. The cell-free reactions were assembled by combining all the components necessary for the reaction, namely the cell-free extract, buffer, energy solution, and *AvPAL* DNA template, and were immediately flash-frozen in liquid nitrogen and freeze-dried overnight. The productivity of the rehydrated freeze-dried cell-free expression system was more than half of the freshly prepared one (Fig. 2.6, A). After 1 week of storage, the productivity was still present, but it was almost completely lost after 2 weeks of storage. We also tried using another freeze-dried system using an extract from *E. coli* cells grown on 2xYTPG medium and a simplified energy solution, but no activity was observed in any of the reactions (Fig. 2.6, B).

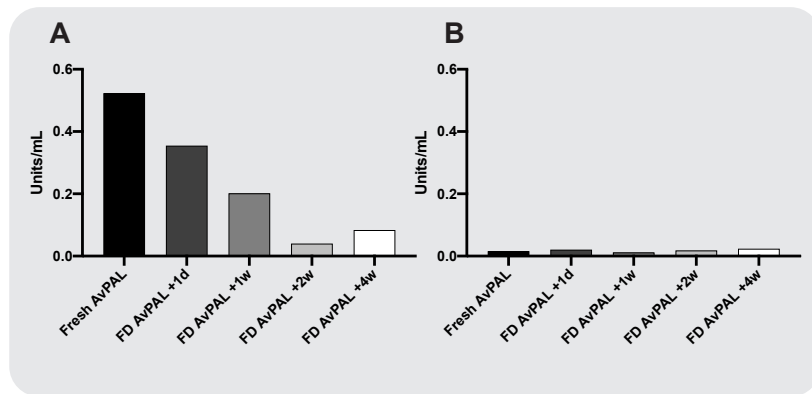


Figure 2.6: **Enzymatic activity of freeze-dried cell-free expression systems of *AvPAL*.**

Bar plots of enzymatic activity observed in fresh or freeze-dried cell-free expression systems. **(A)** Lysate preparation with cells grown on LB and standard energy solution. *AvPAL* enzymatic activity is present after its synthesis in freeze-dried cell-free expression system. Fresh: 0.52 units/mL, freeze-dried: 0.35 units/mL, +1 week: 0.20 units/mL **(B)** Lysate preparation with cells grown on 2xYTPG and simplified energy solution. No significant enzymatic activity.

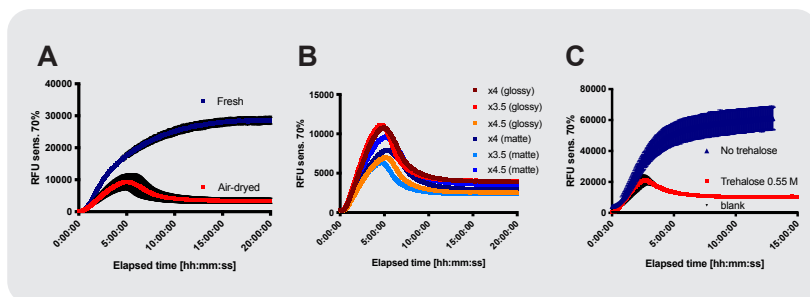


Figure 2.7: **Trehalose as a lyoprotectant for air-drying of cell-free protein expression systems.**

Plate reader fluorescence measurements of EGFP synthesis in cell-free expression systems. **(A)** Addition of trehalose to CFPS allows for air-drying in a 37°C incubator with some residual EGFP expression. **(B)** The lysate supplemented with trehalose was dried as 30  $\mu$ L drops either on a glossy or matte side of a silicon mat. The pellets were rehydrated with water 3.5, 4 or 4.5 times their dried weight. **(C)** Trehalose supplementation has a detrimental effect on EGFP synthesis with a stop in expression and decrease in fluorescence after a few hours of reaction.

### 2.2.2 Lyopreservation of cell-free expression system

In this section, we develop on our attempts to establish a dried cell-free expression system to help in its conservation at room temperature for easier distributed protein production. First, we tried to replicate a protocol proposed by Karig *et al.* [76] which added the lyopreservative trehalose to cell-free extract or to the complete cell-free reaction, and then air-dried the cell-free expression system in a 37°C incubator. The dried reactions formed glassy pellets which could be easily recovered and rehydrated with water to start the reaction. While we could still observe some EGFP expression, the fluorescence measured on a platereader during the timecourse of the cell-free expression reaction was much lower than in a normal reaction with reagents stored at -80°C and freshly thawed before use (Fig. 2.7 A and B). Varying the proportion of water used to rehydrate the pellets did not result in any marked change in EGFP expression (Fig. 2.7 B). The kinetics of the fluorescence signal were highly unusual as there was an initial increase in EGFP signal followed by a decrease in fluorescence. In batch reactions, a plateau in fluorescent signal is generally observed after a few hours of cell-free protein expression as the EGFP synthesis is halted, but we never observed a decrease in fluorescence. We measured again the cell-free protein expression kinetics of a freshly

prepared reaction supplemented with trehalose, and we could observe the same decrease (Fig. 2.7 C). It is therefore probable that trehalose is responsible for an increased degradation of the EGFP fluorescent signal, and also a potential interference with the transcription and translation of EGFP from the template DNA, or with the DNA template itself. Although we could still obtain some protein production with this air-dried system, the very low productivity would make it incompatible with the distributed manufacturing of proteins required in significant quantities.

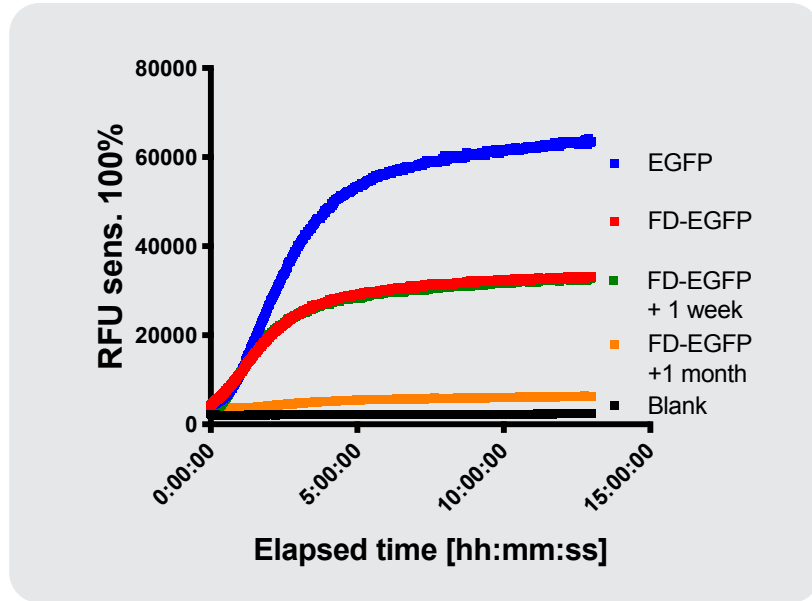


Figure 2.8: **Freeze-dried cell-free protein expression systems.**

Plate reader fluorescence measurements of EGFP synthesis in freeze-dried cell-free expression systems. EGFP protein synthesis is possible with freeze-dried systems with close to 50 % productivity retained. The freeze-dried expression system remains active for a week at room temperature.

Freeze-drying is another lyopreservation method which has been proposed for the preservation of cell-free systems for their use in distributed diagnostics or therapeutics [77, 53]. The procedure for the freeze-drying of cell-free systems required the use of snap freezing in liquid nitrogen, followed by the sublimation of the aqueous phase in a low temperature vacuum. We assembled cell-free protein expression reactions complete with extract, energy solution and DNA template which were immediately snap frozen and freeze-dried overnight in a benchtop apparatus (Labconco) as was also presented earlier for the expression of *AvPAL* (Fig. 2.6). Almost 50 % of the EGFP synthesis yield is achieved compared to the freshly prepared reactions, and the productivity stays at similar



levels after a week of storage at room temperature, while expression is almost completely abolished after 1 month of storage (Fig. 2.8). We also produced *E. coli* BL21 DE3 extracts which were grown on 2x YT or 2xYTPG medium instead of LB and used a simplified energy solution to supplement the cell-free expression reaction. This protocol developed by Cai *et al.* [48] drastically reduces the reagent costs of cell-free protein production by 95 %. The simplified solution contains only T7 polymerase, amino acids, monophosphate nucleotides, glutamate as an energy source, buffering agents, and removed most of the cofactors or high energy molecules usually provided. While the protocol is greatly simplified, it still maintains very good EGFP synthesis yields, and also has a favorable stability upon freeze-drying and storage at room temperature (Fig. 2.9). It should be reminded however that this extract preparation and energy solution protocol was unfortunately not compatible with the expression of *Av*PAL (Fig. 2.6). We note that the *Av*PAL template DNA used in both the standard and simplified protocol were the same, and also that the cell-free expression systems were from the same batch when expressing *Av*PAL or EGFP. Therefore, there must be an incompatibility of the simplified cell-free expression system with the expression of *Av*PAL for which there is no direct explanation based on our experimental results.

### 2.2.3 Non-natural amino acid co-translational incorporation

The open nature of cell-free systems allows for the direct introduction of different additives to the reaction mixture. Here we explored the introduction of non-natural amino acids (nnAA) to the cell-free expression system which can be later used as reactive handles for chemical modifications of the expressed proteins, which would make it attractive for the facilitated PEGylation of therapeutic enzymes. It is possible to use certain small nnAAs such as the methionine non-natural analogue azido-homoalanine (AHA) for residue specific incorporation in bacterial cells [78], and we tried AHA residue-specific incorporation in cell-free as it would not require any addition of modified aaRS/tRNA pairs and was shown to work in cell-free [79]. The incorporation of an azide group would permit the reaction with PEG derivatives using click-chemistry, such as using copper-catalyzed azide-alkyne cyclo-addition [80] or copper-free azide reaction with strained alkynes [81]. We first used the PURE expression system ("protein synthesis using recombinant elements") [44] which presents the advantage of being virtually free of amino acids in the reaction mixture apart from the ones supplied by the user. This allowed us to completely remove methionine and replace it with AHA for residue-specific co-translational incorporation of this nnAA. Indeed, we show that

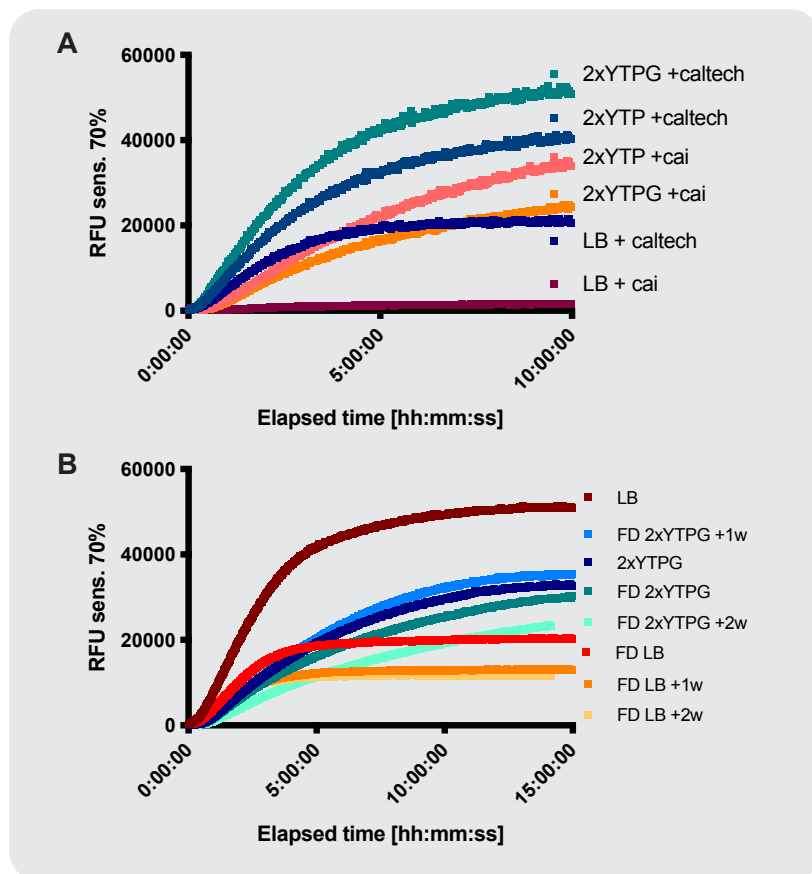


Figure 2.9: **Simplified cell-free protein expression system and freeze-drying.** Plate reader fluorescence measurements of EGFP synthesis in simplified cell-free protein expression systems. **(A)** EGFP expression with CFPS systems using lysate from cells grown on 2xYTP, 2xYTPG or LB, combined with standard energy solution (caltech) or simplified (cai). Only the 2xYTP or 2xYTPG grown lysates can be used in conjunction with the simplified energy solution **(B)** The simplified CFPS systems can be freeze-dried and displays a good retention of EGFP synthesis productivity after storage at room temperature for 1 or 2 weeks.

when the methionine in PURE expression system is replaced with AHA, we can synthesize EGFP with co-translational incorporation, as evidenced by the band of same size and intensity as the band obtained when using all standard amino acids (Fig. 2.10). We also confirm that omitting the methionine impairs EGFP synthesis as no corresponding protein band can be observed on the gel, indicating that no significant amount of methionine is present in the PURE system.

As the yields obtained with PURE are generally low compared to *E. coli* lysate systems and

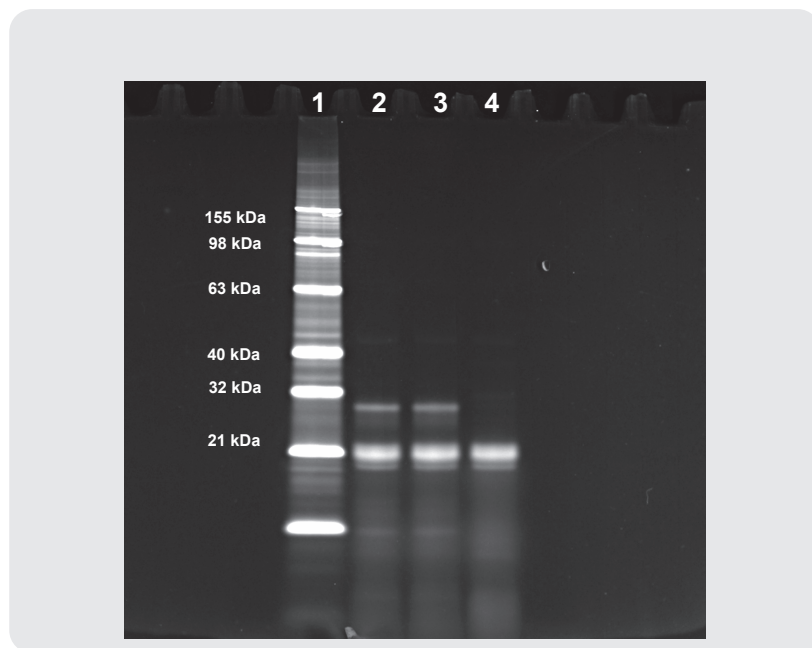


Figure 2.10: **Cotranslational incorporation of L-azidohomoalanine using PURE expression system.**

Fluorescent scan of an SDS-page gel electrophoresis. The cell-free reaction was supplemented with tRNA-lysine-BODIPY allowing in-gel fluorescent detection of synthesized EGFP and 19 amino acids (AA) excluding methionine. Lanes: (1) Ladder (2) 19 AA + methionine (3) 19 AA + L-azidohomoalanine (4) 19 AA. A band of expected size around 30 kDa is observed when either methionine or L-azidohomoalanine is added to the 19 AA mixture.

the costs are significantly higher per unit of produced proteins, we tried to incorporate AHA using a lysate system. Recognizing that the *E. coli* extract should contain significant amounts of methionine, we washed the extract extensively in Buffer A by repeated steps of dilution and centrifugal concentration. The productivity of such "washed" extract is significantly reduced and we also observed that it was not compatible with the use of the simplified energy solution (Fig. 2.11, A). Even after extensive washes of the extract, there is still protein synthesis present when the supplied energy solution does not contain any methionine or AHA, indicating that residual methionine is still present in the washed extract (Fig. 2.11, B). These observations show that we would need to make some significant improvement on the lysate expression system for residue-specific co-translational incorporation of AHA, and it might be preferable to supplement the cell-free expression system with plasmids encoding for an orthogonal aaRS/tRNA pair and use it in site-directed incorporation.

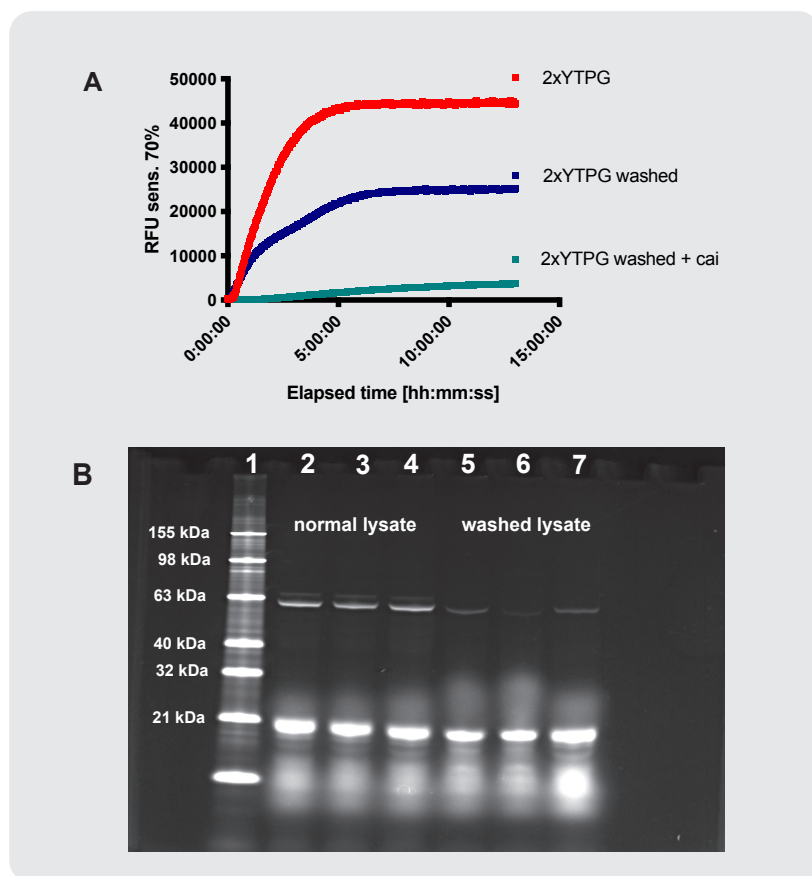


Figure 2.11: **Cotranslational incorporation of L-azidohomoalanine using lysate expression system.**

(A) Plate reader fluorescence measurements of EGFP synthesis in normal and washed cell-free protein expression systems. The CFPS is still active with a reduction in productivity when using a standard energy solution, but is not functional when using the simplified energy solution. (B) Fluorescent scan of an SDS-page gel electrophoresis. The cell-free reaction was supplemented with tRNA-lysine-BODIPY allowing in-gel fluorescent detection of synthesized EGFP and 19 amino acids (AA) excluding methionine. Normal lysate: (1) Ladder (2) 19 AA + methionine (3) 19 AA + L-azidohomoalanine. Washed lysate: (4) 19 AA (5) 19 AA + methionine (6) 19 AA + L-azidohomoalanine (7) 19 AA. A band of expected size around 60 kDa is observed when omitting methionine or L-azidohomoalanine pointing to lysate contribution to the available methionine pool. Washed lysate did not suppress it and the expression appears lower.

#### 2.2.4 Cell-free expression of protein nanocompartments

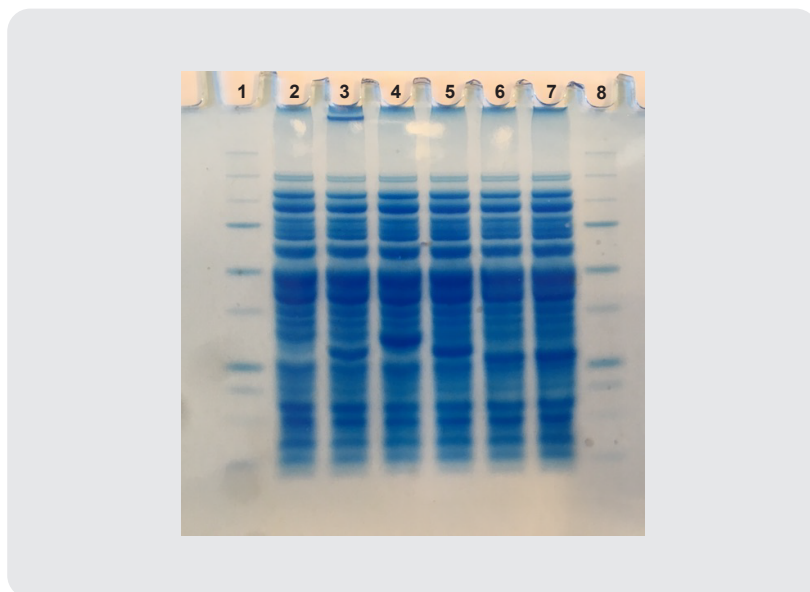


Figure 2.12: **Cell-free expression of encapsulin protein nanocompartments.**

SDS-page gel of endpoint cell-free reactions. Lanes: (1) Ladder (2) blank (3) encapsulin (4) encapsulin-sfGFP 30aa tag (5) encapsulin-sfGFP 15aa tag (6) encapsulin-sfGFP 5aa tag (7) encapsulin-sfGFP 5aa tag. A band corresponding to a megadalton protein assembly is observed in the encapsulin expression reaction. No band is observed when using plasmids coding for encapsulin and sfGFP with cargo-loading tags.

Another possibility we considered to protect cell-free expressed proteins or enzymes from degradation was the use of protein nanocompartments called encapsulin. Encapsulin are compartments composed of a single protein type which self-assembles into a 60-mer to form a spherical compartment [82]. Proteins can be loaded inside these approximately 25 nm large compartments with the help of a specific sequence at the C-terminus described as a cargo-loading tag. We first expressed the proteins from the plasmids gifted by Professor David Savage through AddGene in a standard home-made cell-free reaction, and we observe expression of encapsulin as evidenced by a band at around 30 kDa which corresponds to the size of one monomer. We also note the presence of a band at the very top of the gel which would correspond to the encapsulin megadalton assembly (60 x 30 kDa) (Fig. 2.12). On the same gel, we can see bands corresponding to the expression of sfGFP with cargo-loading tags with a length of 30, 15 or 5 aminoacids. The sfGFP-encapsulin plasmids were

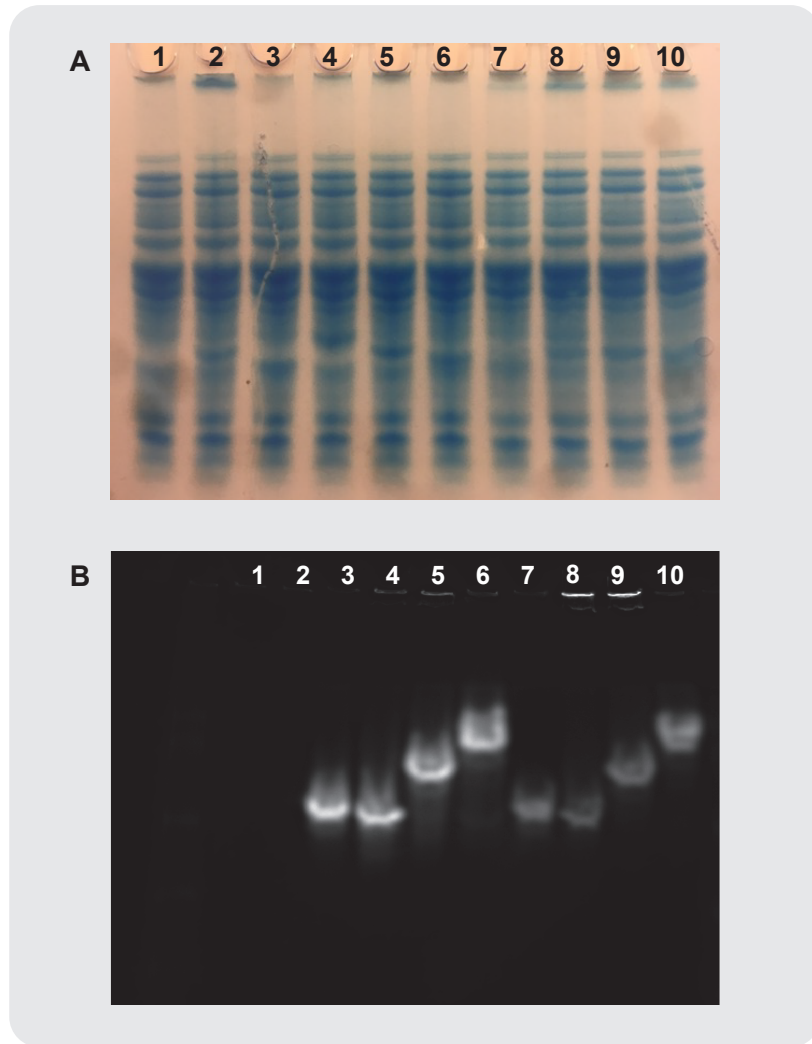


Figure 2.13: **Cell-free coexpression of encapsulin protein nanocompartments and sfGFP cargo loading.**

**(A)** SDS-page gel of endpoint cell-free reactions. Lanes: (1) blank (2) encapsulin (3) EGFP (4) encapsulin-sfGFP 30aa tag (5) encapsulin-sfGFP 15aa tag (6) encapsulin-sfGFP 5aa tag (7-10) same as lanes 3-6 with additional encapsulin template plasmid. **(B)** Fluorescent scan of a native page gel electrophoresis. The fluorescence of EGFP derivatives can be observed directly in the gel. When encapsulin is coexpressed with sfGFP having 30aa or 15aa cargo loading tags (lanes 9 and 10), a fluorescent band is observed on the top of the gel.

designed to allow the coexpression of encapsulin and the tagged sfGFP, but there was probably an error in the received plasmids with the absence of an RBS before the encapsulin gene. To overcome

this issue, we added two DNA templates in the same cell-free reaction when required: the plasmid encoding for the encapsulin only and the plasmid encoding for the sfGFP with cargo-loading tag. We observe again that the sfGFP-encapsulin plasmids do not yield any visible band for encapsulin expression, but when we add the encapsulin plasmid to these reaction, there is a band present on the top of the gel (Fig. 2.13 A). To demonstrate that the sfGFP is loaded inside the protein nanocompartments, we loaded the samples on a native gel and measured the sfGFP fluorescence as it would not be denatured and still visible on a gel. We see a strong fluorescent signal on the top of the wells where both encapsulin and sfGFP with 30 or 15 amino-acid tags plasmids are added in the reaction (Fig. 2.13 B). We can therefore conclude that encapsulin and tagged sfGFP are coexpressed and that sfGFP is loaded into the compartments for the two longer cargo-loading tags. Finally, we tried to produce expression templates for a small monomeric phenylalanine hydroxylase cvPAH fused with a cargo loading tags by assembly PCR, but we were not successful in obtaining the desired PCR constructs. Moreover, additional protein engineering would probably be required to successfully use enzyme-encapsulin nanoreactors, which discouraged us to further explore this option for protecting the therapeutic enzyme.

## 2.3 Discussion

In this work, we show that the therapeutic protein *AvPAL* can be expressed in cell-free expression systems. We demonstrate that *AvPAL* can be purified at a small scale using magnetic beads, with the purified enzyme displaying lower specific activities than expected. The cell-free reactions expressing *AvPAL* have enzymatic activity in converting phenylalanine to trans-cinnamic acid with activity around 0.5 units/mL of reaction. We also show that the cell-free expression system can be freeze-dried and still produce active *AvPAL*, and that the freeze-dried system remains productive for at least a week when stored at room temperature. While these results are encouraging, the limitations we identified are mostly related to the costs associated with the production of *AvPAL* for enzyme replacement therapy. Indeed, to produce the equivalent of a single dose of 20 mg of *AvPAL*, at least 40 mL of cell-free reaction would be needed based on our experiments. With an estimated cost of 30 \$/mL of reaction using the standard method for the production of cell-free extract and energy solution [45], this would amount to 1200 \$ for a single dose, and this only represents the costs associated with protein expression. Using a simplified system, the costs per mL of reaction should be reduced by 95 % [48], which would represent 6\$ for a 20mg dose. Unfortunately, while the simplified system was functional in expressing a fluorescent protein and was compatible with freeze-drying, we could not express any active *AvPAL*. There are other optimized systems for cell-free expression with yields up to 2.3 mg/mL of protein per reaction [75], and some methods which could produce proteins at costs as low as 0.36 \$/mg [83, 84], which could make cell-free expression systems cost-effective. We recognize that cell-free expression of enzymes for replacement therapies are particularly challenging due to the large quantity of product required for every dose which are given repeatedly and on a long-term, making bulk production more cost-effective and thus limiting the interest of decentralized manufacturing. However, whether it is for enzyme replacement therapy or other biopharmaceuticals, we can expect technological advances to further reduce the costs associated with cell-free production by increasing yields of reactions of prolonging the duration of expression with continuous-exchange expression systems [85], and novel microfluidic designs using continuous-exchange could eventually produce proteins at the point-of-care with higher yields [86]. Forward-looking, we could imagine completely cell-free self-sustaining systems for biopharmaceutical production, following recent advances in bottom-up engineering of replication [87], use of in-vitro transcribed tRNAs [88], ribosomal RNA synthesis, assembly and



translation [89], regeneration of protein components of the transcription-translation machinery [90], and which could even be fueled by light [91, 92]. This could be combined with linear DNA templates prepared by PCR assembly and amplification [93, 94], or plasmids obtained by *in vitro* cloning [95] or benchtop DNA synthesizers such as the BioXp<sup>TM</sup> 3200 system [96], completely bypassing the use of cells at any stage of the production of biopharmaceuticals.

## Acknowledgments

I would like to thank my colleagues for their collaboration and their help, in particular Barbora Lavickova for the collaboration on *E. coli* extract preparation and cell-free reaction protocol development, Zoe Swank for the collaboration in the preparation of lysate obtained from cells grown in 2xYTP or 2xYTPG and simplified energy solution, and Simone Giaveri for the collaboration on nnAA incorporation in yeGFP using PURExpress system.

3

Direct encapsulation of active  
biomolecules in semi-permeable  
microcapsules templated from  
double-emulsions

## 3.1 Introduction

### 3.1.1 Background

In the previous chapter, we presented the use of cell-free protein expression for the production of recombinant *Av*PAL for enzyme replacement therapy. Regardless of the high costs associated with cell-free production, we demonstrated that point-of-care production of an active PAL enzyme was possible using a freeze-dried cell-free expression system. However, a challenge in the distributed manufacturing of *Av*PAL for enzyme replacement therapy in phenylketonuria is that the production of the enzyme alone would not be sufficient to provide an effective treatment. Indeed, some modification of the enzyme would be required to protect it from proteolytic digestion or to prevent it from eliciting an immune reaction. As presented in Chapter 2, Professor Thomas Chang, a pioneer in the concept of creating "artificial cells", proposed to use semi-permeable microcapsules containing hemoglobin and PAL as microreactors for oral delivery of PAL enzyme [18]. He identified that a large source of circulating phenylalanine was not only directly from dietary intake, but also from enteric recirculation of aminoacids [97]. Therefore, PAL enzyme encapsulated in semi-permeable capsules would deplete pools of phenylalanine, while being protected from the degradation by proteolytic enzymes in the digestive tract. Unfortunately, no recombinant enzyme was available at that time, which effectively stopped the development of PAL enzyme encapsulation for oral delivery. It is more than 20 years later, after recombinant PAL enzyme was available and could be engineered for increased resistance to proteolytic digestion that the idea of oral enzyme delivery was revisited [28, 14]. Recently, the company Synlogic used its synthetic biology expertise to engineer probiotics expressing PAL as microreactors to lower phenylalanine levels, which entered phase II clinical trials [15]. Interestingly, they could confirm the hypothesis of phenylalanine enterorecirculation by injecting labeled phenylalanine subcutaneously in mice and measuring its increase in the gut, confirming the interest in having encapsulated PAL enzyme active in the digestive tract. Owing to the availability of the recombinant PAL enzyme and its demonstrated clinical efficacy, together with advances in droplet microfluidics, we were interested in reviving the concept pioneered by Professor Thomas Chang of engineering microreactors of PAL protected by a semi-permeable capsule. Combining a suitable encapsulation method with cell-free expression systems, one could even imagine creating artificial protocells from the bottom-up which would express an active PAL enzyme and be used for oral enzyme replacement therapy.

### 3.1.2 Semipermeable microcapsules for enzyme immobilization

Encapsulation of active enzymes for oral enzyme replacement therapy would require the microcapsules to respond to a very extensive specifications list. The capsules production and material should be biocompatible, have a thin semi-permeable shell, a small diameter and narrow size distribution, allow the encapsulation of enzymes and proteins, prevent their adsorption to the shell material, resist to pH encountered in the digestive tract, and present good chemical and mechanical stability. Indeed, the capsules should ideally completely retain their integrity during their passage in the digestive tract, contrary to more commonly developed capsules providing a controlled release of their cargo at specific locations by time-dependent or pH-dependent dissolution. Droplet microfluidic technology enables the production of polymer compartments with precisely defined size and structure templated from multiple emulsions with a polymerizable middle phase. While it is possible to use a water-soluble polymer precursor in the middle phase by using aqueous two-phase systems (ATPS) with dextran [98] or PEG derivatives [99] as polymer precursors, neither could show the successful encapsulation of proteins in semi-permeable capsules. The majority of middle-phase polymer precursors are indeed hydrophobic compounds dissolved in organic solvent, such as PEG-PLA [100, 101], methacrylic anhydride [102], polyurea [103, 104], pH-responsive copolymers (DMAEMA- BMA-MMA) [105], , pNIPAM-PLGA + PEG-PLA [106], pH responsive PAA-b-PMMA or DMAEMA- BMA-MMA [105], or photocurable ETPTA [107]. One drawback of using water-immiscible polymer precursors in the middle-phase, is that most of the obtained polymerized compartments are hermetic to the permeation of solutes. Kim et al. [108] however demonstrated that semi-permeable polymeric shells can be fabricated by introducing an inert diluent, or porogen, in the polymer precursor phase. Upon UV polymerization, the non-reactive porogen is excluded from the forming polymer in a process called polymerization-induced phase separation (PIPS). However, the drawback of the polymers used in this study and of most polymers obtained from water-immiscible precursors is the hydrophobicity of the polymerized capsule shell, leading to protein adsorption and preventing the direct encapsulation of proteins or enzymes.

Recently, it was showed that PEG-diacrylate with a molecular weight of 250 g/mol (PEG-DA 250) can be used as a polymerizable middle phase for the production of double-emulsions with a microfluidic capillary device [109]. The researchers also showed that poly-(PEG-DA 250) has a hydrophilicity similar to hydrogels made from water soluble PEG-DA derivatives of higher molecu-

lar weight. Such favorable characteristics allowed them to directly encapsulate fibrinogen without noticeable adsorption to the polymer shell. However, the produced capsules were hermetic and prevented even small molecule dyes to diffuse out of the capsules. To directly encapsulate biological active substances in biocompatible semi-permeable capsules, we combined the favorable characteristics of the low molecular weight PEG-DA 250 with pore formation through polymerization-induced phase separation. In this work, we use a PDMS microfluidic device with a flow-focusing and co-axial non-planar geometry which does not require any surface treatment to produce double-emulsions of water-in-(PEG-DA 250)-in-water. In order to obtain semi-permeable capsules, we used polymerization-induced phase separation (PIPS) to form pores of nanometric size in the capsule shells. By encapsulating fluorescent cargoes of different sizes or placing empty capsules in fluorophore containing solutions, we show that the capsules are semi-permeable with a size cut-off around 40 kDa, allowing the direct encapsulation of proteins and enzymes while permitting transport of smaller (bio)-molecules. Moreover, the capsules are easily stored and manipulated owing to their chemical and physical stability. While the capsules were originally intended for PAL enzyme encapsulation, we could not achieve satisfactory encapsulation of the therapeutic enzyme with sufficient activity retention. However, to explore the broader potential of the microcapsules we tried to encapsulate bacteria and yeast cells. Moreover, we could easily encapsulate streptavidin or even streptavidin-coated magnetic beads which could serve to immobilize different biomolecules inside the microcapsules compartments and leverage the ability of the capsules to communicate with their environment for the development of different applications. As a demonstration, we immobilized DNA strand displacement reactions on streptavidin encapsulated inside the liquid core of microcapsules populations and implement a two-layer signalling cascade.

We believe that our biocompatible microcapsules could be interesting in the bottom-up engineering of more complex biomolecular systems, eventually building non-dividing protocells for example, and to provide a perspective on how our microcapsules compare to existing encapsulation technologies, we will discuss the different types of compartmentalization used for cell-free reactions in the next section.

The section 3.1.3 has been adapted from a recent review. The text and figures presented below are my original contributions, integrating discussions with co-authors and their feedback.

**Reference:** Laohakunakorn, N., Grasemann, L., Lavickova, B., Michielin, G., Shahein, A., Swank, Z. and Maerkl, S.J. (2019). Bottom-up construction of complex biological systems with cell-free synthetic biology. DOI: 10.5281/zenodo.3591964

This work (Laohakunakorn *et al.* [110]) was later published in Front. Bioeng. Biotechnol., 24 March 2020, DOI: 10.3389/fbioe.2020.00213

### 3.1.3 Compartmentalized cell-free reactions

Compartmentalizing cell-free reactions spatially segregates a bulk reaction into smaller units. In addition to being a fundamental requirement in the construction of artificial cells, compartmentalized TX-TL opens up a number of scientific and practical opportunities, such as increased throughput for screening, *in vitro* directed evolution, distributed computation, and programmable communication. Microwell plates with reaction volumes as low as 0.5  $\mu\text{L}$  [111], and microfluidic devices with volumes down to femtoliters [?], have been used to compartmentalize cell-free reactions.

Below, we will cover different types of compartmentalization including emulsions that allow for the rapid generation of multiple small volume compartments; liquid-liquid phase separation which can recapitulate naturally occurring crowded environments; hydrogels of natural or synthetic origin that immobilize DNA or proteinaceous factors and similarly provide a favorable crowded environment; liposomes which can provide a good starting point in the bottom-up assembly of synthetic cells by encapsulating a gene expression system; and other membrane-enclosed compartments with shells composed of polymers or protein-based materials that will expand the repertoire of physicochemical properties and functionalities.

#### Emulsion-based compartments

Emulsion-based compartmentalization allows for the rapid production of reaction vessels with volumes as low as femtoliters [126]. *In vitro* compartmentalization of TX-TL was first described in the context of *in vitro* evolution when Tawfik *et al.* [127] encapsulated a TX-TL system together with a DNA library of genes coding for an enzyme. Single copies of DNA templates were compartmental-

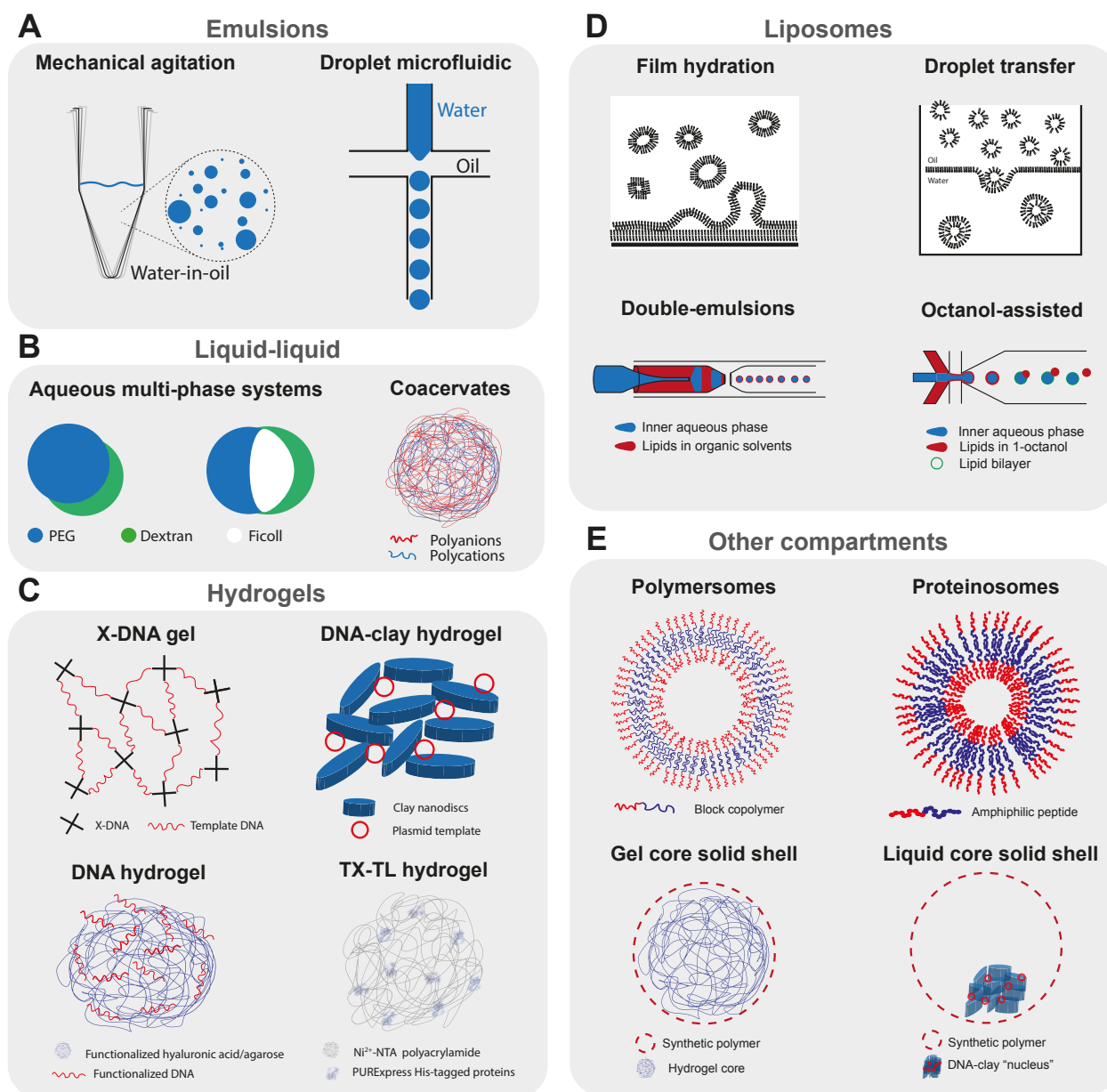


Figure 3.1: Caption next page.

ized in  $\sim 2 \mu\text{m}$  aqueous droplets dispersed in mineral oil, creating the crucial genotype-phenotype linkage [128] which is required for selection and enrichment of improved enzymes. This eventually allowed a complete cycle of directed evolution of phosphotriesterases to be carried out [129].

One major drawback of emulsions produced by bulk methods is the size polydispersity of the obtained compartments (Figure 3.1A). This leads to enzymatic activity being convolved with noise resulting from variation in droplet size, making it difficult to select droplets containing improved

Figure 3.1: **Compartmentalized cell-free reactions.** Schematic representation of the different strategies used to compartmentalize cell-free transcription translation reactions. **(A)** Emulsion-based compartments: polydisperse water-in-oil droplets obtained by mechanical agitation, and microfluidic production of monodisperse droplets. **(B)** Liquid-liquid phase separation: aqueous multiphase systems containing cell-free transcription translation machinery [112], and representation of a complex coacervate. **(C)** Hydrogels: X-DNA linking template DNA and forming a DNA hydrogel [113, 114], a DNA-clay hydrogel [115], hyaluronic acid [116] or agarose [117] functionalized with DNA template, polyacrylamide hydrogel functionalized with  $\text{Ni}^{2+}$ -NTA binding PURExpress His-tagged proteins [118]. **(D)** Liposomes: rehydration of lipid films with an aqueous solution containing TX-TL, droplet transfer method where a lipid-stabilized W/O emulsion is layered on top of a feeding buffer and liposomes transferred to the bottom by centrifugation [119], double-emulsions with ultrathin shells containing lipids in organic solvent [120, 121], and octanol-assisted assembly [122, 123]. **(E)** Other compartments: polymersomes with membrane formed by amphiphilic polymers, proteinosomes with amphiphilic peptides [124], alginate hydrogel coated with various polymers, artificial cells with polymeric shell and liquid core containing a DNA-clay ‘nucleus’ [125].

enzymes. Dittrich *et al.* overcame this limitation using droplet microfluidics to generate monodispersed water-in-oil (W/O) droplets (Figure 3.1A) containing a TX-TL reaction expressing GFP. However, their setup did not allow for the production of droplets containing single DNA copies that gave rise to detectable signals, as would be required for *in vitro* evolution. Using a more efficient TX-TL system and stabilized W/O droplets, Courtois *et al.* were able to obtain efficient transcription and translation from a single DNA copy [130], opening the door for high throughput quantitative evolution experiments in droplets generated by microfluidics. Examples of these include multiple screening rounds to enrich for active hydrogenase [131] and beta-galactosidase enzymes [132].

The use of fluorogenic substrates in enzymatic assays can be problematic in surfactant stabilized emulsions as transport of fluorophores can occur between droplets both in single [133] and double emulsions [134]. Woronoff *et al.* demonstrated an alternative methodology where a proteinogenic amino acid is released after enzymatic turnover and then incorporated in the translation of a reporter protein [135]. Using this approach, they were able to screen for active penicillin acylase enzymes in single gene droplets. The literature contains fewer examples of compartmentalized *in*



*vitro* assays to screen for protein binders. However, two-hybrid and three-hybrid systems have been developed in PURExpress supplemented with *E. coli* core RNAP enzyme [136]. Cui *et al.* used such an *in vitro* two-hybrid system encapsulated in single-emulsion droplets to screen a library of 105 peptide binders in a single day [137].

Recent work using droplets has diversified beyond the high-throughput screening studies discussed in the previous paragraphs to encompass physical effects such as the influence of crowding [138] or droplet size [139, 140, 141] on protein expression. Schwarz-Schilling *et al.* used W/O droplets to compartmentalize streptavidin-coated magnetic beads which act as a scaffold on which complex RNA-protein nanostructures can be built using TX-TL [142]. The high-throughput generation of such compartments is also attractive for the extensive parameter space mapping for genetic network prototyping, as exemplified by the work of Hori *et al.* [143].

### **Liquid-liquid phase separation**

Liquid-liquid phase separation occurs when a water-soluble molecule, generally a polymer, is mixed with another aqueous solution containing either a high salt concentration or another water-soluble polymer. Under certain conditions, the first polymer cannot dissolve in the second solution, and a separation into two distinct phases occurs. The resulting ‘aqueous two-phase system’ (ATPS) can form microscale, membrane-less compartments. The recent discovery that ATPS are ubiquitous in cells has attracted much attention to better understand their role in cell physiology [144]. Recreating cell-free transcription-translation reactions in these systems could help elucidate the properties of such condensates.

Torre *et al.* prepared ATPS of dextran/poly(ethylene glycol) or three-phase systems (A3PS) of dextran/poly(ethylene glycol)/ficoll containing TX-TL by vortexing in mineral oil [112] (Figure 3.1B). In the ATPS, expression of the reporter protein indicated preferential partitioning of the TX-TL machinery to the dextran phase in the ATPS. The A3PS, on the other hand, exhibited lower expression, which was attributed to separation of TX-TL machinery into the different dextran and Ficoll phases, suggesting that different liquid phases could differentially partition TX-TL components.

When a liquid-liquid phase separated compartment consists of a condensate of biological polymers, it is most commonly referred to as a coacervate (Figure 3.1B). These coacervates are characterized by a high degree of macromolecular crowding, exhibiting protein concentrations of up to 272

g/L [145], similar to the *E. coli* cytosol. Such crowding can profoundly influence gene expression. Sokolova *et al.* used a microfluidic device to osmotically concentrate droplets containing lysate, and observed the formation of coacervates in lysate containing 2% PEG-8000 [146]. The resultant reporter gene expression was higher in coacervates than in single phase droplets. The work demonstrated that transcription rates were enhanced in the crowded environment of coacervates, offsetting the lower translation rate. Such observations are in agreement with previous studies in bulk cell-free reactions where macromolecular crowding enhances transcription and impairs translation [147]. To generate monodisperse coacervates in high throughput, Tang *et al.* [148] produced coacervates using a microfluidic device [149] starting from a mixture of carboxymethyl-dextran/polylysine and TX-TL. However, they observed lower gene expression in coacervates compared to the bulk reaction, with results suggesting charge-induced precipitation of the reporter protein after its production. This again indicates that protein expression is sensitive to the partitioning of the TX-TL machinery and that the charge of the coacervate and crowded environment can have opposite effects on yields.

## Hydrogels

Similar environments to coacervates are found in hydrogels, where a highly porous hydrated network provides a crowded environment. Forming gel micropads by cross-linking X-shaped DNA entrapping plasmid DNA, or P-gel, Park *et al.* obtained an up to 94-fold increase in protein production compared to a standard batch reaction [113, 114] (Figure 3.1C). They explained the increase in expression by an enhanced transcription rate due to the higher proximity of gene templates in the crowded DNA gel environment. The P-gel has also been prepared in a microdroplet format [150] and the microgel format was modified with  $\text{Ni}^{2+}$ -NTA to allow the immobilization of the expressed protein on the surface of the microgel [151].

The same group showed that TX-TL was also increased in the presence of a clay hydrogel, which spontaneously forms when mixing hydrated clay in the presence of an ionic solution [115] (Figure 3.1C). DNA and RNA molecules localize to the clay hydrogel and are protected from enzymatic degradation by nucleases. The clay-DNA hydrogels were also formulated into microgels containing magnetic nanoparticles allowing for multiple successive TX-TL reactions after recovery of the magnetic microgel and refreshing of the TX-TL mixture [152]. Finally, clay-DNA microgels have been used as artificial nuclei inside W/O emulsions [152] or inside permeable polymeric capsules [125].

Thiele *et al.* prepared hyaluronic acid functionalized with DNA template and produced porous

hydrogel microparticles, which were further encapsulated in droplets containing TX-TL [116] (Figure 3.1C). They observed efficient GFP protein expression proportional to the number of encapsulated DNA hydrogel beads, with the fluorescent protein diffusing inside the droplet. By using mRNA molecular beacons, they show that the transcribed mRNA remains trapped in the hyaluronic acid/DNA hydrogel, suggesting that transcription and translation both take place inside the hydrogel.

Aufinger *et al.* prepared agarose functionalized with alkynes and coupled to azide-modified DNA, and used it to prepare hydrogel-DNA ‘organelles’ [117] (Figure 3.1C). Transcription organelles contained template DNA coding for mVenus with a toehold switch on the 5’ end of the mRNA, whereas the translation organelles were functionalized with the corresponding toehold trigger. These organelles were re-encapsulated in W/O droplets containing TX-TL, and mVenus expression was observed only in droplets containing both the transcription and translation organelles. As these organelles can offer spatial organization of complex reactions while providing continuous exchange with the environment, they are useful for building more complex modular systems.

Whereas the previous studies focused on immobilizing the DNA template inside hydrogels, Zhou *et al.* immobilized the complete set of PURExpress His-tagged proteins on a polyacrylamide gel functionalized with  $\text{Ni}^{2+}$ -NTA [118] or an anti-His-tag aptamer [153] (Figure 3.1C). The His-tagged proteins, ribosomes, and template plasmids are placed on pre-dried hydrogel particles, which effectively traps the ribosomes and plasmids in the hydrogel network by convection when rehydrated. Sustained gene expression is observed for as long as 11 days when the cell mimics are constantly supplied with fresh feeding buffer.

## Liposomes

Liposomes are compartments encapsulated by a lipid bilayer similar to a cell membrane, making them attractive for the encapsulation of cell-free systems. Liposome technology has been recently reviewed by Stano [154]. Early studies used a film hydration method, where the reaction mix rehydrates a dried lipid film to produce liposomes encapsulating TX-TL (Figure 3.1D). This was deployed to translate peptides [155], proteins [156, 157, 158], and finally a more complex genetic cascade [159]. Noireaux and Libchaber [119] presented a more convenient method of liposome production called droplet transfer, where a lipid stabilized emulsion of the reaction is first formed in oil and then layered on top of the feeding solution (Figure 3.1D). Liposomal vesicles are subsequently

formed by centrifugation. By producing  $\alpha$ -hemolysin *in situ*, which assembled to form pores in the liposome membrane, they were able to constantly supply feeding buffer to the encapsulated reaction and increase the duration of expression up to almost 100 hours.

An interesting improvement in the lipid film rehydration method was presented by Nourian *et al.* where they dried the lipid films on 200  $\mu\text{m}$  glass beads and rehydrated them with PURExpress [160]. This allowed them to use low reaction volumes to produce liposomes in high yield and with high encapsulation efficiency. Moreover, they used phospholipids with shorter acyl chains to produce semi-permeable liposomes and incorporated biotinylated lipids for efficient immobilization of the vesicles on microscope slides.

Droplet microfluidics allows for the generation of double emulsions with ultrathin shells where the middle phase contains dissolved lipids and forms unilamellar vesicles after evaporation of the solvent [161] (Figure 3.1D). Ho *et al.* used this technology to encapsulate a mammalian cell-free system with very high encapsulation efficiency, and observe expression of GFP in the interior of the vesicles as well as expression and assembly of a trans-membrane protein [120]. However, they observed in a consequent study that the surfactant necessary for double emulsion led to aggregation of the mammalian cell-free system [121].

By using triblock copolymer surfactants, Deng *et al.* could control the dewetting of the inner water drop from the middle organic phase thus forming perfectly unilamellar and uniform liposomes, in addition to solvent droplets that could be easily separated [162]. A hierarchical assembly of liposomes inside other liposomes, or vesosomes, through multiple successive encapsulation and dewetting was also demonstrated [163]. *In vitro* transcription of Spinach RNA was carried out in the interior ‘nucleus’ liposome and translation of mRFP in the surrounding ‘cytoplasm’ liposome, showing great potential towards bottom-up assembly of complex biomolecular structures, even though controlled transfer of mRNA from the interior to the surrounding liposome remains to be implemented. Finally, a similar method called octanol-assisted liposome assembly (OLA) was developed where the middle phase alkane solvents are replaced by octanol containing lipids and undergo rapid dewetting, which could further increase the efficiency and biocompatibility of the encapsulation method [122, 123] (Figure 3.1D).

## Other membrane compartments

Other types of membrane compartments have also been used for cell-free protein expression, such as polymersomes, protein-based membranes, and polymeric shells (Figure 3.1E). Although there exist many different strategies and materials to make capsules [164], the conditions necessary for their production often prevent encapsulating cell-free systems. Martino *et al.* [101] used a microfluidic capillary device to generate template double-emulsion for the direct encapsulation of a cell-free expression system inside polymersomes composed of PEG-*b*-PLA copolymer and PLA homopolymer to increase their stability. They successfully expressed an MreB protein which formed patches inside the aqueous core and also adhered to the membrane.

Vogele *et al.* used a film rehydration method similar to the one used for liposome production but with amphiphilic elastin-like peptides as building blocks, which formed vesicles upon rehydration with a TX-TL system [124] (Figure 3.1E). They demonstrate that the expression of the elastin-like peptide led to its successful integration into the membrane and an increase in the size of the vesicles after a few hours of expression. Schreiber *et al.* also used amphiphilic peptides to form vesicles and encapsulate a cell-free expression system, and show the production and incorporation of amphiphilic peptide in the membrane [165]. It will be interesting to see in future studies if pore-forming proteins can be incorporated in these ‘growing’ protein-based membranes, which might allow for prolonged and higher protein expression, as was observed for cell-free protein expression in liposomes. By encapsulating a cell-free extract in millimeter-sized alginate beads coated with polycationic chitosan [166], silica [167], or polyethyleneimine [168], researchers could show continuous expression of eGFP (Figure 3.1E). However, the core of the capsules presented in the previous studies is in a gel format and it is difficult to assess how well the capsules perform as no absolute quantification of the protein levels was provided.

To our knowledge, the only example to date where cell-free protein expression was demonstrated in liquid core-solid shell polymeric capsules was by Niederholtmeyer *et al.* where they produced porous polyacrylate capsules containing a DNA-clay hydrogel nucleus [125] (Figure 3.1E). The capsules’ pores are large enough to allow access by large macromolecules including ribosomes. Transcription-translation from the template DNA immobilized in the clay-DNA hydrogel ‘nucleus’ can be achieved by immersing the capsules in a cell-free expression system. But, as the shell material leads to adsorption of proteins on the capsule surface and the pores are too large to retain the TX-

TL machinery, the direct encapsulation of cell-free systems inside polymeric capsules remains to be demonstrated. Such direct encapsulation in synthetic polymeric capsules would be valuable as they could present attractive properties such as high mechanical and chemical stability, as well as tunable porosity, based on the type of shell material and the fabrication method used.

### Physical effects of compartmentalization

The effect of the compartment size and interface composition can have notable effects on gene expression. Initial work in Yomo's group showed that expression in sub-picoliter PDMS compartments severely hampered GFP synthesis, whereas quartz glass microcompartments passivated with amino acids showed expression as high as 41% of the test tube reaction with no dependence on compartment volume in a range from 40 fL to 7 pL [169]. They later showed that synthesis of  $\beta$ -glucuronidase (GUS) with fourth-order reaction kinetics was favored in smaller compartments while GUS substrate depletion was rapidly occurring, pointing to an ideal compartment volume [139, 170].

No size dependence on GFP synthesis was observed in a range from 1 to 100  $\mu\text{m}$  in liposomes composed of a mixture of different phosphatidylcholine (PC) or phosphatidylglycerol (PG) lipids and cholesterol [171], in contradiction to previous reports where PG had inhibitory effect on protein synthesis [172]. In lipid stabilised droplets, the charge of the lipid used could also influence the synthesis rate, but in this case the relatively more negative PG lipid was favoured over phosphatidylethanolamine (PE) or PC [141]. Sakamoto et al. [140] proposed a model with three regimes where there could be activation, no regulation, or repression at the surface. In droplets stabilized by PC lipids, they observed protein expression that did not scale with the droplet volume  $R^3$ , but with  $R^4$  for droplets with radii below 17  $\mu\text{m}$ , suggesting surface repression in their system. Other effects could explain variations in fluorescence intensity, such as the exchange of solutes between droplets which is influenced by the composition of the carrier oil, lipid or surfactant, as well as the radius of the droplets [134].

The compartmentalization of biochemical reactions in smaller volumes increases the gene expression stochasticity as only a few molecules are present in each compartment. Hansen et al. [138] suggest that such randomness can be explained by extrinsic noise, which results from the Poisson distribution of encapsulated reagents of the cell-free system, and intrinsic noise, which results from molecular crowding and other parameters such as the stochasticity of the gene expression reac-

tions or relative plasmid distributions. They co-encapsulated CFP and YFP plasmids in droplets with varying levels of crowding, and observed an increase in intrinsic noise with increased levels of crowding. Intrinsic noise in gene expression can also arise from the stochastic partitioning as was strikingly observed in liposomes prepared in dilute solutions of transcription-translation system [173]. A small number of compartments ( $< 0.5\%$ ) displayed detectable eGFP gene expression, whereas no expression occurred in free solution raising interesting questions about the mechanism of loading of the solute mixture.

High variability in gene expression was also observed in liposomes prepared in PURE solutions of normal concentration and interestingly gave rise to some compartments displaying particularly high or long lasting gene expression [174]. These large variations due to stochastic partitioning are interesting as a mechanism to generate diversity in the population, as recently discussed in a review by Altamura *et al.* [175]. Understanding and harnessing these physical effects of compartmentalization potentially offers yet another way of controlling cell-free gene expression.

## Communication

Cellular communication is fundamental in biology and responsible for many processes ranging from development to tissue homeostasis. Following the successful developments in compartmentalizing cell-free systems, the next logical challenge consists of engineering inter-compartment communication. On-chip artificial cells consisting of DNA brushes were interconnected in series by microfluidic channels, and communication is achieved by diffusion of molecules, which can be tuned by adjusting channel geometry [176] (Figure 3.2A). Diffusion of a  $\sigma^{28}$  activator from one compartment to the next led to sequential switching of a bistable genetic circuit. In a follow-up study, Tayar *et al.* used a non-linear activator-repressor oscillator in compartments coupled by diffusion and observed that the oscillators could be synchronized and tuned by geometric control of diffusion [183]. A key demonstration was that such reaction-diffusion systems could spontaneously form spatial patterns in good agreement with theory.

Moving away from microfluidic chips could potentially allow for the engineering of more complex, dynamic consortia of communicating compartments or even tissue-like assemblies. Schwarzschild *et al.* used capillaries to align W/O droplets encapsulating cell-free extracts as well as *E. coli* cells [177] (Figure 3.2B, top). The bacteria and cell-free systems contained either an AND gate circuit expressing GFP in response to isopropyl  $\beta$ -D-1-thiogalactopyranoside (IPTG) and acyl

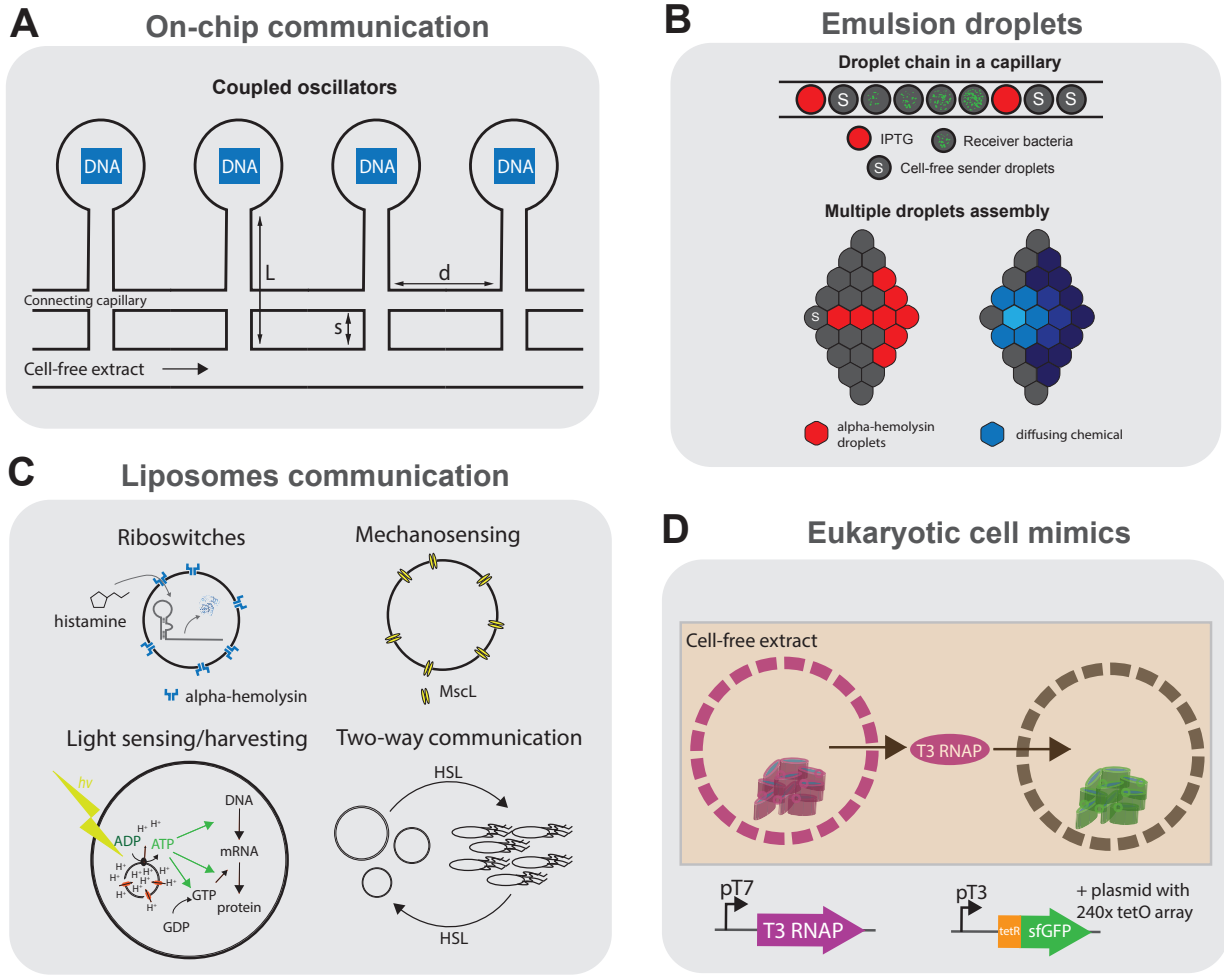


Figure 3.2: Caption next page.

homoserine lactone (AHL), or a sender circuit producing AHL in response to IPTG. Communication could be established between sender droplets and droplets containing the AND gate, in a cell-free-to-bacteria or bacteria-to-cell-free direction.

Dupin *et al.* used a micromanipulator to arrange multiple directly adjacent W/O droplets in a lipid-in-oil bath, forming a lipid bilayer interface between the compartments [178] (Figure 3.2B, bottom). They show direct communication between sender droplets containing arabinose (ARA) or AHL and droplets containing a responder circuit. By using an incoherent feed-forward loop genelet circuit containing an RNA binding to 3,5-difluoro-4-hydroxybenzylidene imidazolinone (DFHBI), they observe the propagation of the DFHBI signal along multiple successive interconnected droplets. Finally, by encapsulating a positive feedback circuit expressing  $\alpha$ -hemolysin in



Figure 3.2: **Communication using cell-free transcription translation.** Schematic representation of the different platforms using cell-free transcription translation reactions for communication. **(A)** Artificial cells on chip: DNA compartments are connected to a cell-free reaction feeding channel and interconnected by another capillary allowing the coupling of the compartments [176]. **(B)** Emulsion droplets: top, water-in-oil droplets containing small molecule activators, bacteria or cell-free genetic circuits arranged in a glass capillary [177]; bottom, multiple lipid-stabilized droplets assembled with a micromanipulator with some droplets containing pore forming  $\alpha$ -hemolysin [178]. **(C)** Sensing and communication with liposomes: liposomes encapsulating histamine-sensitive riboswitches [179], mechanosensing using MscL pores [180, 181], light-driven ATP synthesis using bacteriorhodopsin and ATP synthase [91], and two-way communication between liposomes and bacteria using various AHLs [182]. **(D)** Eukaryotic cell mimics: microporous polymeric capsules containing a DNA-clay hydrogel 'nucleus' are immersed in cell-free transcription translation. The expressed T3 polymerase can diffuse and activate transcription-translation in another compartment.

response to ARA, they observe an increased variability in protein expression levels among droplets, which they describe as 'a primitive form of cellular differentiation'.

Liposomes can more closely recapitulate cellular systems. Lentini *et al.* rehydrated liposomes containing a genetic circuit using a riboswitch responding to theophylline to express  $\alpha$ -hemolysin and release co-encapsulated IPTG (Figure 3.2C). By incubating *E. coli* with these liposomes acting as signal translators, the bacteria could effectively respond to theophylline in the medium [184]. They later demonstrated that two-way communication is possible between the artificial cells and bacteria by responding to and secreting different AHLs [182] (Figure 3.2C). They even devised a 'cellular Turing test' where they compare the expression of quorum sensing genes of *V. fischeri* in the presence of either artificial cells or in a consortium of bacteria. They measure that the artificial cells would be 39% 'life-like', but warn that this estimation does not consider that the artificial cells are not fully genetically encoded. Rampioni *et al.* [185] developed synthetic cells which could send quorum sensing molecule C4-HSL to the pathogenic *P. aeruginosa*. Such synthetic cells could have interesting theranostic applications once equipped with additional sensing capabilities such as those discussed in this section.

Two-way communication has been implemented in various contexts, from buffer conditions ideal for artificial cells, to more simple environments such as water or PBS [186]. Other communication

modalities have also been explored, such as osmoregulation using a mechanosensitive MscL channel incorporated into liposomes, which opens due to membrane stress in hypotonic environments [180, 181]. Impressively, Berhanu *et al.* encapsulated proteoliposomes containing ATP synthase and bacteriorhodopsin inside liposomes [91] (Figure 3.2C). The artificial cells were able to convert photons to a proton gradient inside the proteoliposomes and drive the synthesis of ATP by ATP synthase, fueling the TX-TL system, effectively making these artificial cells capable of light sensing and even photosynthetic activity.

More complex communication between liposomes was presented by Adamala *et al.*, where they use artificial cells containing either bacterial or mammalian TX-TL systems and use small molecules to communicate between the prokaryotic and eukaryotic artificial cells containing different genetic circuits and cascades [187]. However, the sensing of small molecules is limited to known transcriptional regulators or the theophylline riboswitch. Dwidar *et al.* engineered a riboswitch for the biologically relevant small molecule histamine into liposome-based artificial cells, which could respond to the presence of histamine in a variety of programmed ways [179] (Figure 3.2C). Finally, liposome-based artificial cells expressing *Pseudomonas* exotoxin A were injected *in vivo* inside mice tumors and an increase in caspase activity was shown [188], suggesting their potential use in therapeutic or diagnostic applications.

One major limitation of liposomes is the difficulty in implementing signaling mediated by protein factors, as only small signalling molecules can cross the lipid bilayer with the help of the  $\alpha$ -hemolysin pore. The polymeric capsules presented by Niederholtmeyer *et al.* (as discussed in section 3.1.3) are permeabilized by 200–300 nm pores, allowing for the exchange of polymerases and even ribosomes [125]. The authors show a basic form of quorum sensing where the reporter expression increases sharply at a threshold of 400 cell-mimics per 4.5  $\mu$ L droplet of TX-TL.

Models have been recently proposed to help understand and implement communication using cell-free systems. These include studies of quorum sensing [189] and the design of spatially distributed compartments [190]. More complex spatial assemblies of compartments capable of communication [191], combined with computation by cell-free TX-TL genetic circuits or other *in vitro* computation methods (such as DNA strand displacement reactions [192], the Polymerase-Exonuclease-Nickase (PEN) DNA toolbox [193], or transcriptional ‘genelet’ circuits [194]), and integration with orthogonal technologies such as electronics [195] may one day allow for the bottom-up engineering of programmable tissues with distributed functional capabilities.

## 3.2 Towards microcapsules templated from double-emulsions

This section presents the initial steps conducted during my project leading to the final protocol using water-in-(PEG-DA 250)-in-water together with polymerization-induced phase separation (PIPS) to produce semi-permeable and biocompatible poly-(PEG-DA 250) microcapsules. We first present the use of water-in-water-in-oil (W/W/O) production using a fluorinated oil and fluorinated surfactants, with PEG-DA 575 as an aqueous middle phase with the idea of using aqueous two-phase systems to generate capsules. Next, we adapted the protocol to use a mineral oil outer phase using commonly available surfactants such as Span-80. As these methods would lead to the production of microspheres and not microcapsules due to insufficient phase-separation, we tried to modify the aqueous innerphase by supplementing it with a highly hydrophilic polysaccharidic polymer. Trying to obtain phase separation, we used a high concentration of photoinitiator in the oil phase to act as a separating agent which would draw the PEG-DA rich phase towards the water/oil interface. As methods relying on phase separation were not robust in the production of microcapsules, we explored using a middle phase which could be directly UV polymerized. We started using PEG-DA 250 due to its immiscibility with both water and mineral oil, and potentially better characteristics than other UV polymerized acrylate polymers. Using mineral oil as an outer phase, it was difficult to prevent the double-emulsion from dewetting, even with the addition of surfactants. We next explored using a production system completely avoiding the use of oil by directly using water-in-(PEG-DA 250)-in-water, and supplementing the water phases with PVA to act as a surfactant. The double-emulsion stability was limited and required some optimization of the different phases compositions, notably aiming to have similar phase densities. The addition of a surfactant to the middle phase was next evaluated which finally allowed the robust production of microcapsules. However, the obtained capsules were mostly impermeable to small solutes, so we explored the addition of an inert diluent or porogen to the PEG-DA 250 middle phase. By using butyl-acetate as a porogen, we could finally obtain semi-permeable microcapsules when UV intensity was sufficient and not blocked by the use of UV-absorbing tubes.

### Fluorinated oil outer phase

The initial strategy for the production of semi-permeable microcapsules was to use W/W/O double emulsions, which is an aqueous two-phase system in oil emulsion. The system was chosen with

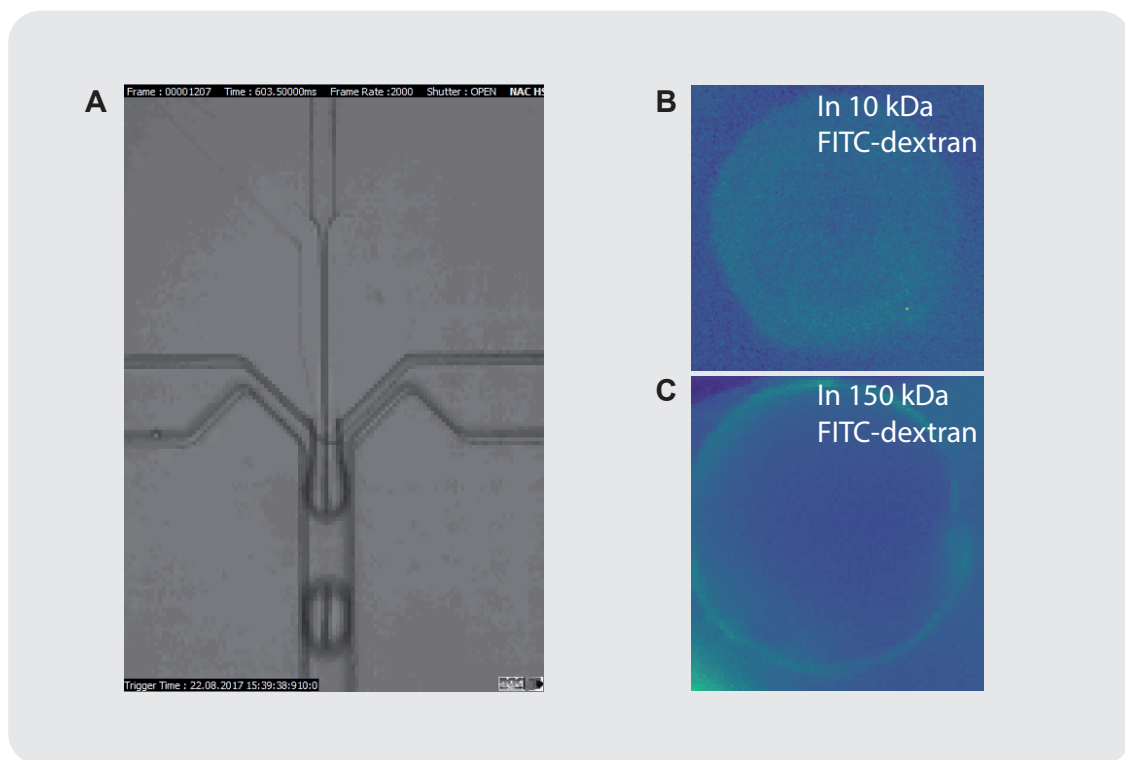


Figure 3.3: **Fluorinated oil continuous phase for the production of W/W/O double-emulsions.** Preliminary experiments using fluorinated oil HFE with fluorinated surfactants as continuous phase. The high salt inner phase is not phase separating from the PEG-DA and leads to the production of microspheres.

the perspective of using PEG-diacrylate as polymerizable middle phase for the production of a biocompatible hydrogel shell. For these initial steps, we largely benefited from the expertise of Professor Esther Amstad's group (SMaL) at EPFL, and their advice in the fabrication and operation of non-planar PDMS device for the production of double-emulsions. We used a fluorinated oil together with fluorinated surfactants developed in their lab based on triblock copolymers of PEG and perfluorinated polyether [196]. The operation of the device required a surface treatment of the collection channel with a silane compound to prevent the wetting of the channel walls and failure of the double-emulsion production. We could obtain some droplets using such device and fluid components, but we were not successful in obtaining a proper aqueous two-phase system inside the droplets. We used a high salt inner phase with 15% NaCl and a middle phase with 50% PEG-DA 575 g/mol which did not phase separate in the emulsion. This resulted in the formation of poly-(PEG-DA 575) microspheres and we could not obtain any microcapsules (Fig. 3.3).

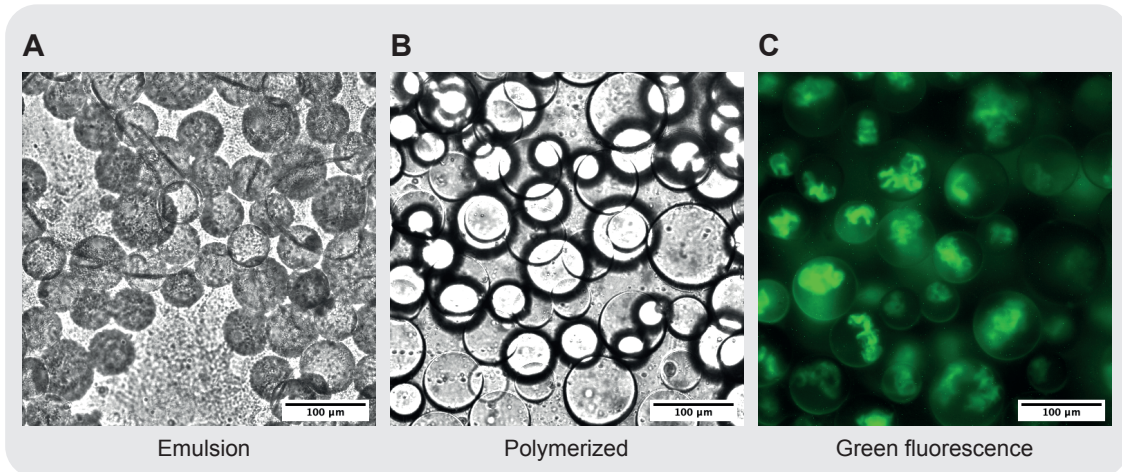


Figure 3.4: **Mineral oil continuous phase for the production of W/W/O double-emulsions.** Preliminary experiments using mineral oil with Span80 non-ionic surfactant as continuous phase. The aqueous inner phase is not phase separating from the PEG-DA and leads to the production of microspheres. EGFP contained in the inner phase is trapped in the poly-(PEG-DA 575) hydrogel formed after UV polymerization.

### Mineral oil outer phase

After setting up a dropmaking station in our lab with three computer-controlled syringe pumps (New Era), we did a few unsuccessful initial trials of using fluorinated oil and surfactants with

persisting problems of channel wetting or droplets coalescence, preventing the production of microcapsules. We then turned to mineral oil and commercial non-ionic surfactants instead as they were readily available in the lab. It was still possible to generate droplets, and we tried to encapsulate EGFP as a model protein in the interior of the capsules. However, we observed again that there was no phase separation of the two aqueous phases, resulting in the formation of poly-(PEG-DA 575) microspheres. The EGFP protein fluorescent signal was observed in the polymerized microspheres as inhomogeneous bundles of fluorescent material (Fig. 3.4).

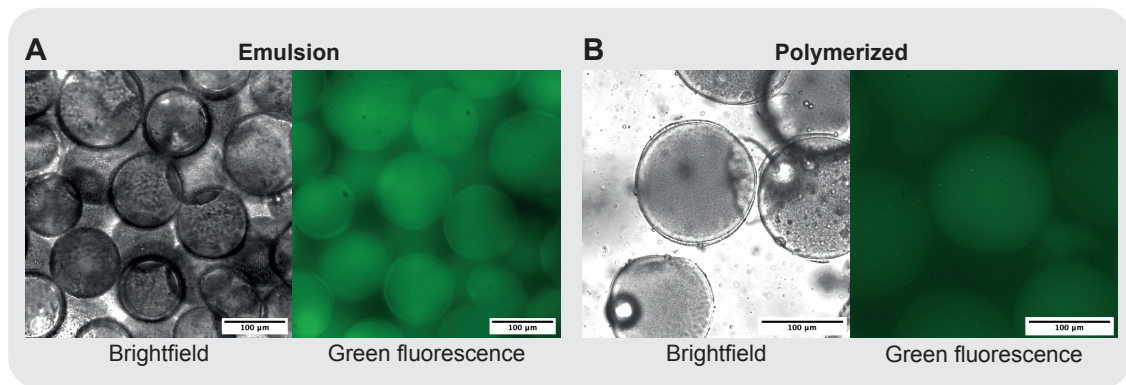


Figure 3.5: **Addition of highly hydrophilic polysaccharidic polymer for improved phase separation.** Ficoll-400 was added to the inner phase to help in the formation of the aqueous two-phase system. Some outer ring in the produced droplets is visible in the emulsions. The appearance after polymerization suggests the formation of hydrogel microspheres.

### Aqueous two-phase system

In order to improve the phase separation between the two aqueous phases, we added Ficoll-400, a highly hydrophilic polysaccharidic polymer, to the inner phase and kept using PEG-DA 575 as a middle phase. After production, it appeared that a thin rim was created on the droplets which could indicate phase separation. However, after UV polymerization we obtained only microspheres (Fig. 3.5). It is possible that the outer rim was actually composed of the Ficoll-rich phase while the center of the droplets was the PEG-DA 575 rich phase, leading to the formation of microspheres after polymerization. It is also possible that the double-emulsion dewets before or upon polymerization. We tried adding a surfactant in the middle phase, but could not obtain microcapsules.

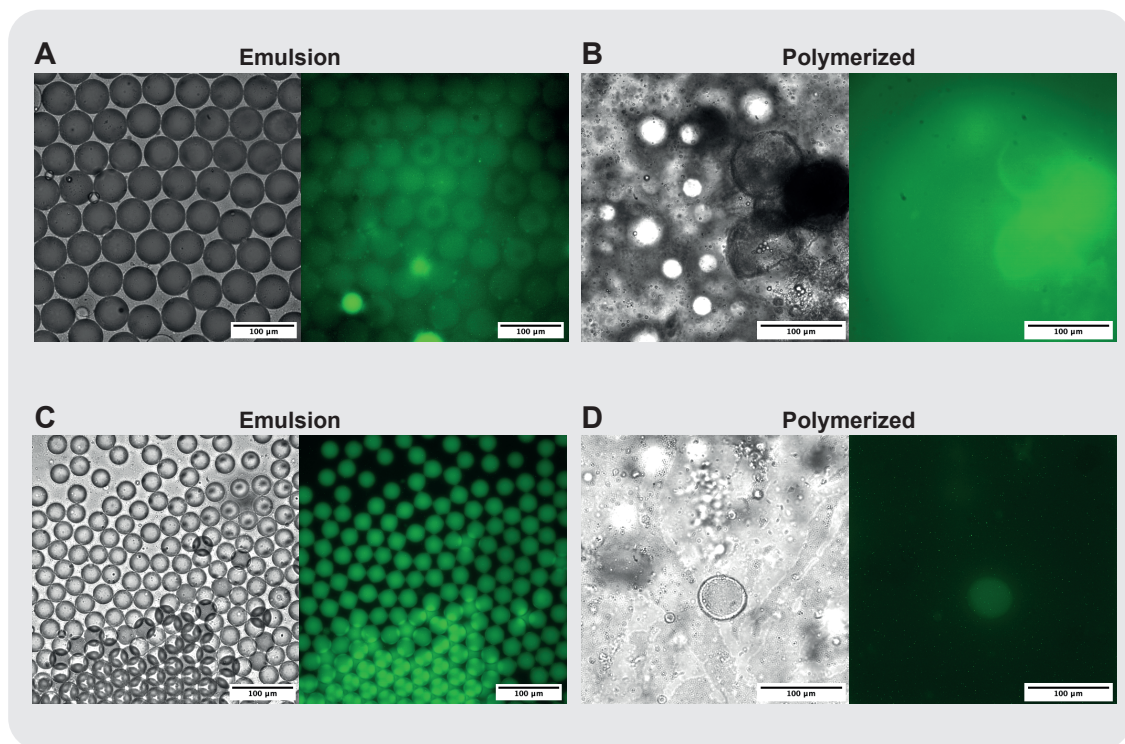


Figure 3.6: **Addition of DEAP photoinitiator in the continuous phase as a separation agent.** A photoinitiator (DEAP 30 %) is added to the continuous phase to help in phase separation. The middle phase is composed of 20 % PEG-DA 575 with (A-B) 50 % lysate or (C-D) 10 % PEG 8000. No improvement was observed in phase separation in the emulsions. Some capsules could be obtained after UV polymerization with a fragile thin shell after polymerization at the droplet water/oil interface.



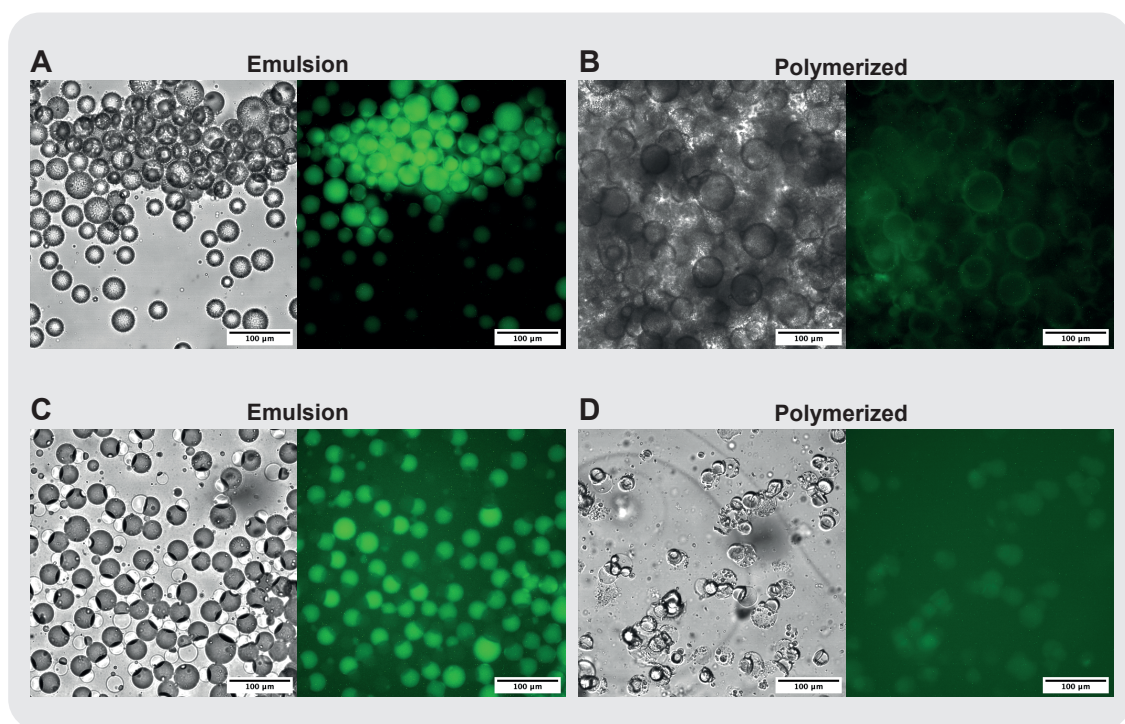


Figure 3.7: **Addition of HMPP photoinitiator in the continuous phase.** A photoinitiator (HMPP 5 %) is added to the continuous phase only. The emulsions evolved to different morphologies depending on their PEG-DA 575 content. 10 % PEG-DA emulsions (A-B) evolved into what resembles a pickering emulsion stabilized by PEG-DA microdroplets. 25 % PEG-DA emulsions (C-D) formed joined aqueous-rich and PEG-DA rich dewetted droplets which were both polymerized after UV exposition.



## Separation agent

Although we did not exhaust ways to improve the phase separation by modifying the inner and middle phase compositions, we decided to try another strategy to help the phase separation as was proposed by Choi *et al.* [197]. They proposed the use of a photoinitiator (2,2-diethoxyacetophenone, DEAP) dissolved in a high 30 % (w/v) concentration in the outer oil phase to act as a separation agent. We could not see any phase separation in the obtained emulsions, but we obtained some microcapsules after UV polymerization (Fig. 3.6). It is not clear however if the photoinitiator helped in phase separation, or simply that its high concentration in the outer phase and absence of photoinitiator in the inner and middle phase resulted in a small outer layer of the droplets being polymerized. We also tried adding the photoinitiator usually added to the PEG-DA middle phase (2-hydroxy-2-methyl-propiophenone, HMPP) directly in the outer oil phase at a 5 % (v/v) concentration. Again, we could obtain some particles of different morphologies depending on the concentration of PEG-DA 575 used in the middle phase. Some further exploration of the different phases compositions might result in the finding of appropriate conditions for the production of W/W/O double-emulsions. However, the difficulties in operation, poor stability of the emulsions and unclear contributions of various factors to the final morphologies of the obtained particles led us to explore different ways to produce microcapsules templated from double-emulsions.

## Water-in-(PEG-DA 250)-in-oil

During our initial tests, one observation we made during was that PEG-DA with the lowest molecular weight of 250 g/mol was not miscible with water. This seemed as a problem since we could not dilute it with water as was done for PEG-DA 575, and it was not possible to form emulsions when we used it in an experiment with a fluorinated oil outer phase. However, we realised that its immiscibility with water would make it possible to produce double-emulsions with a PEG-DA 250 middle phase. The polymerized poly-(PEG-DA 250) would then provide a good shell material as an alternative to other photocurable acrylate oils such as ethoxylated trimethylolpropane triacrylate (ETPTA) or trimethylolpropane triacrylate (TMPTA). Our first experiments aimed at producing water-in-(PEG-DA 250)-in-oil double-emulsions as templates for the production of microcapsules. Even though the production of such double-emulsions was possible in the non-planar microfluidic chip, the double-emulsion stability was very limited when we observed them on a cell-counting slide

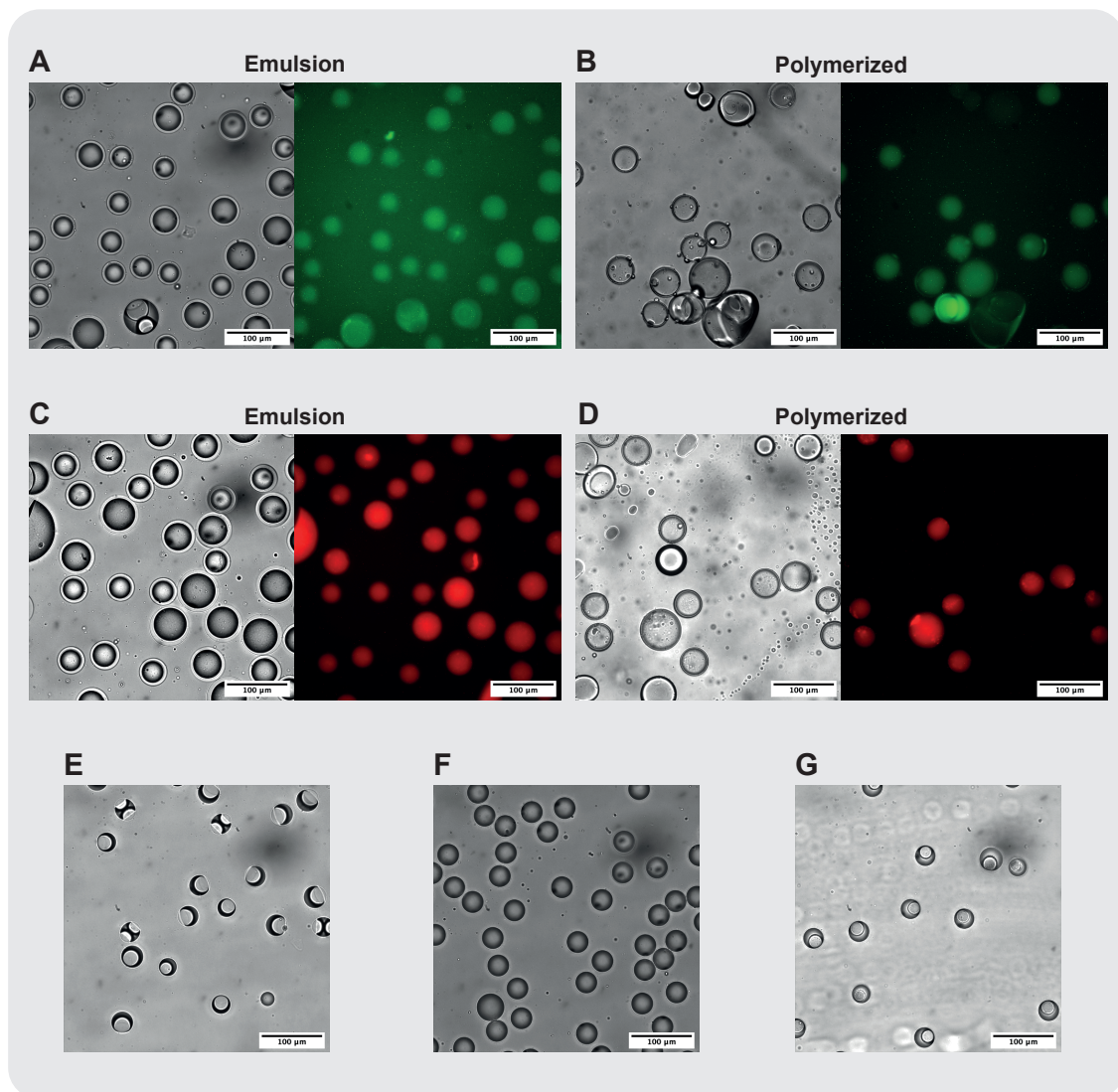


Figure 3.8: **Water-in-(PEG-DA 250)-in-oil double-emulsions.** Using PEG-DA 250 as a middle phase, it is possible to generate double-emulsions and obtain microcapsules after UV polymerization. Both 4 kDa FITC-dextran (A-B) and rhodamine (C-D) were encapsulated. The stability of the double-emulsion was short when observed on a cell-counting slide, resulting in polydisperse capsules. Increasing the surfactant concentration to 15 % in the oil (E), and adding 20 % 1-decanol (F) or 20 % butyl-acetate (G) to the middle phase did not improve the stability significantly.

(Fig. 3.8, A and C). This resulted in polymerized capsules with a large variation in their morphologies (Fig. 3.8, B and D) and relatively low yield of recovered material. We tried different ways to improve the stability of the double-emulsion such as adding 10 % PVA to the inner phase (Fig. 3.8, A and C), increasing the surfactant concentration in the oil phase (Fig. 3.8, E), or adding a mild solvent to the PEG-DA 250 middle phase such as 20 % 1-decanol or 20 % butyl-acetate (Fig. 3.8, F and G). Despite the problems in stability of the double-emulsions, the combination of water-in-(PEG-DA 250)-in-oil was the first time we could produce microcapsules with a robust polymeric shell and motivated us to keep using PEG-DA 250 as a polymer precursor.

### **Water-in-(PEG-DA 250)-in-Water double-emulsion stability**

After a few attempts with a mineral oil outer phase, we rapidly explored the possibility to use a water-in-(PEG-DA 250)-in-water system. We used PVA in both inner and outer phases which acts both as a surfactant and to increase the aqueous phase viscosity and density. Varying the PVA concentration and the flowrates of the different phases, we were able to produce double-emulsions in dripping or short-jetting regime (Fig. 3.15). Moreover, we could use the non-planar PDMS devices without any surface treatment without noting any wetting of the channel by the PEG-DA 250 middle phase. The different phases composition not only had an impact on the drop-making, but were also critical in providing good double-emulsion stability. Using 5 % PVA in the inner and outer phases led to good chip operation, but was not providing a good double-emulsion stability, as we observed dewetting after a few seconds when placed on a cell-counting slide (Fig. 3.9, A-C). Increasing the concentration to 10 % PVA improved the stability slightly, but the double-emulsions were still very short-lived, preventing the collection of a batch of decent size to be polymerized (Fig. 3.9, D-F).

To stabilize double-emulsions, not only the surface energies need to be adequate [198], but the phase densities need to be closely matched, or require the formation of ultrathin shells where the dewetting will be slowed down by a lubrication effect [199]. While the shells formed are relatively thin at about 5-10  $\mu\text{m}$  thickness, this did not provide added stability to the double-emulsions as this effect is important for capsules with much thinner shells, which could be achieved in the future by using devices to remove excess middle phase [200, 201]. To improve the matching of densities, it is necessary to either increase the density of the inner phase, with the density of the aqueous PVA solution which should be between 1.00 and 1.02 g/mL at 25°C [202], or decrease the density of the

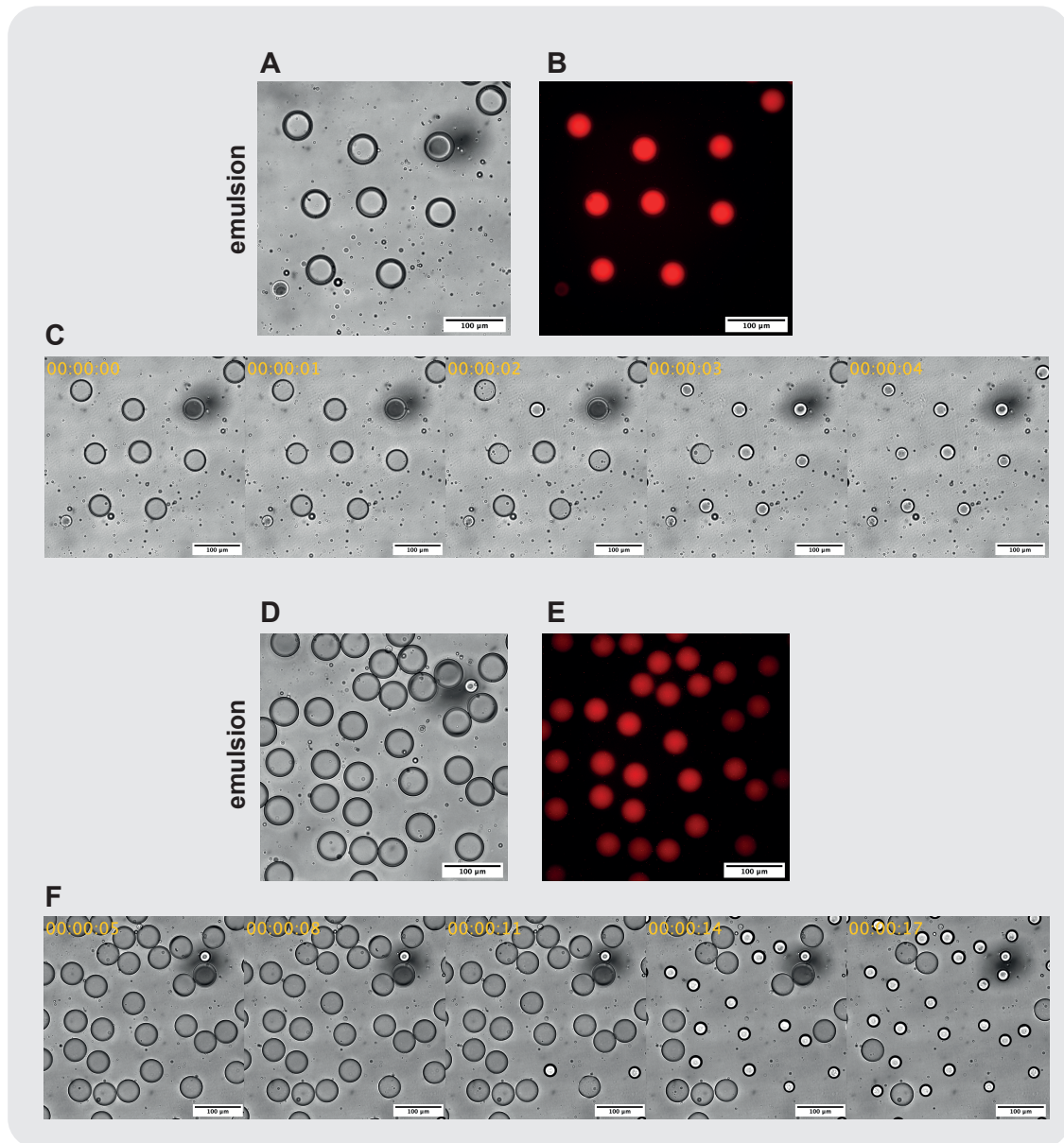


Figure 3.9: **Water-in-(PEG-DA 250)-in-water double-emulsion stability.** Using PEG-DA 250 as a middle phase, it is possible to generate double-emulsions with aqueous inner and outer phase. (A-B) Using 5 % PVA surfactant in the aqueous phases to produce monodisperse double-emulsions. (C) The emulsion stability is short on a cell-counting slide. (D-E) Using 10 % PVA in the aqueous phases. (F) The stability of the double-emulsion on a cell-counting slide is improved but too short-lived for UV polymerization in batch.

middle phase, with a density of PEG-DA 250 of 1.11 g/mL at 25°C.

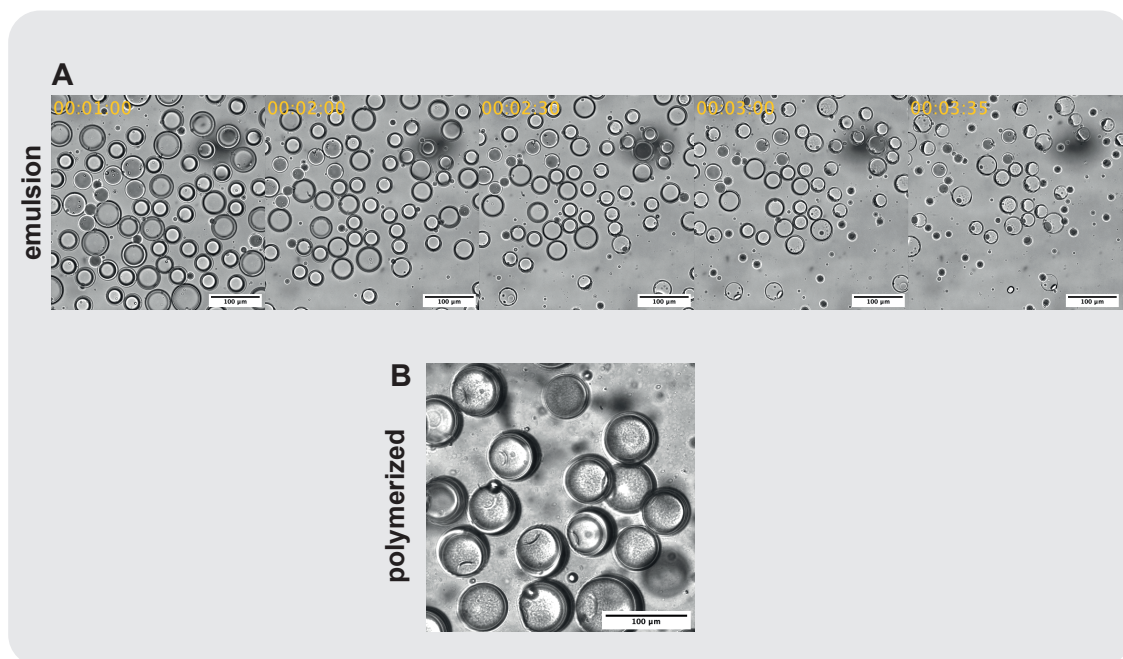


Figure 3.10: **Polymerized capsules from water-in-(PEG-DA 250)-in-water double-emulsion.** (A-B) Addition of 10 % glycerol to a 5 % PVA aqueous inner phase provided better emulsion stability, with a portion of droplets remaining after a few minutes on a cell-counting slide. (B) Microcapsules were obtained after UV polymerization in batch.

By adding 10 % of glycerol to a 5 % PVA inner aqueous phase, we could indeed stabilize the double-emulsions sufficiently to allow the collection of double-emulsions and their UV polymerization. The double-emulsions were stable for a few minutes when placed on a cell-counting slide (Fig. 3.10), which represents an additional stress compared to their situation in the collection tube. The improved stability is demonstrated by the possibility to polymerize the capsules in batch and obtain capsules of homogeneous morphology and recovered in good yields. While further improvements on capsules stability will be presented below, this formed an important step as these were the first capsules obtained from poly-(PEG-DA 250) templated from water-in-(PEG-DA 250)-in-water double-emulsions.



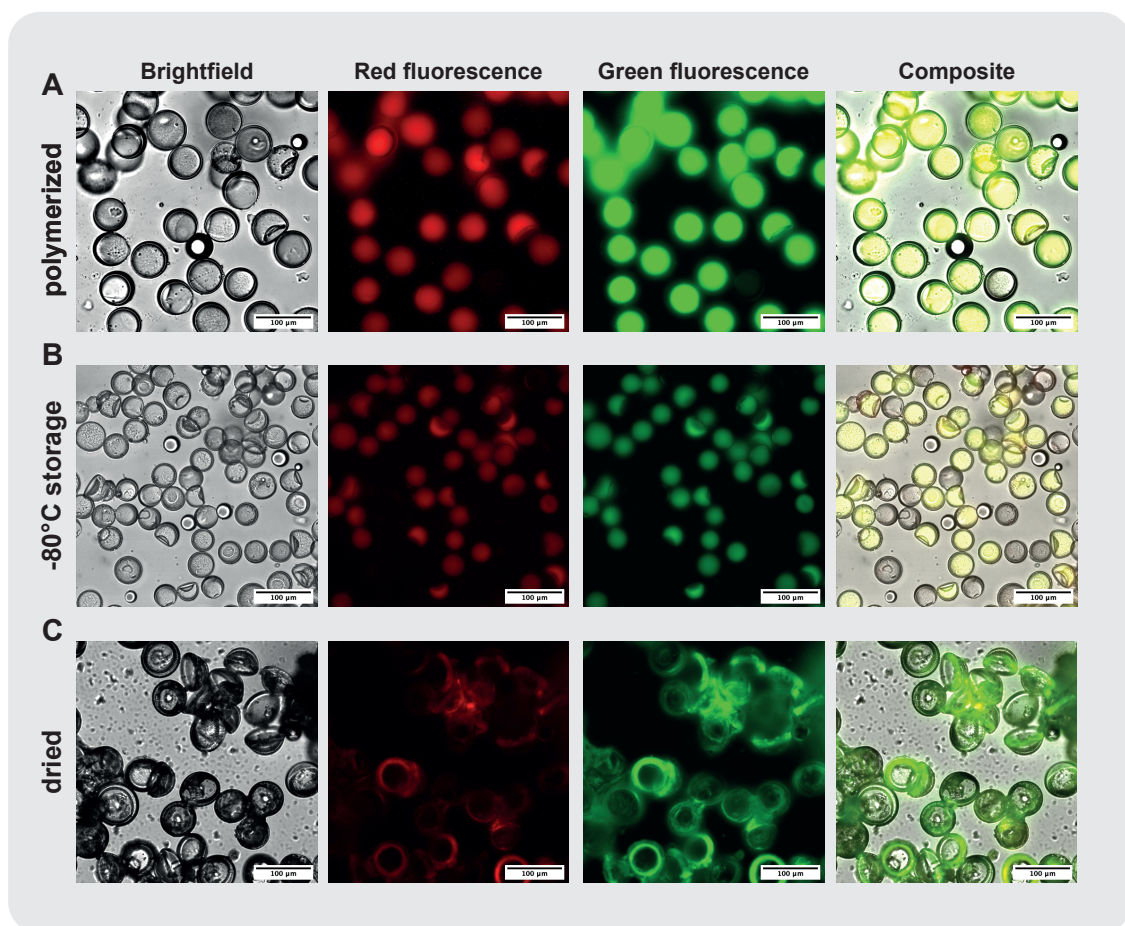


Figure 3.11: **Polymerized capsules are impermeable to small fluorophores.** The short molecular weight PEG-DA forms a polymer network with pore sizes preventing the exchange of small solutes. Coencapsulated rhodamine or 10 kDa FITC-dextran were retained in the interior of the capsules. (A) After multiple aqueous washes. (B) After storage at -80°C for 19 days. (C) After drying on a glass slide.

## Capsules permeability

After the successful production of poly-(PEG-DA 250) capsules, we assessed their permeability to fluorescent molecules of different molecular weights. We first encapsulated small molecule fluorophore sulforhodamine and a small molecular weight 10 kDa FITC-dextran. We observed that the fluorophores were retained in the interior of the capsules, even after rounds of extensive aqueous washes, storage at  $-80^{\circ}\text{C}$  for 19 days or after being dried on a glass slide (Fig 3.11). This is not unexpected as poly-(PEG-DA 250) has been shown to form a highly biocompatible resin which is impermeable and has been used notably in the fabrication of 3D-printed microstructures [203, 204]. This was also confirmed by the production of hermetic poly-(PEG-DA 250) microcapsules as presented by Nam *et al.* [109]. However, this would greatly limit the applications of such microcapsules, as the only way to release a cargo or to put in contact the interior of the capsules and their environment would be by an irreversible mechanical or chemical degradation of their shells.

In order to make the polymeric shell semi-permeable, we decided to use a process called polymerization-induced phase separation which was used by Kim *et al.* to form pores in ETPTA microcapsules [108]. We added an inert solvent to the PEG-DA 250 middle phase, which does not participate in the formation of the polymer network and will form small islands of unpolymerized material connected to form a nanoporous network. The addition of a mild solvent, such as butyl-acetate, decanol, 2-ethylhexanol, octanol or 2-heptanone to the middle phase does not impair the device operation and we did not observe any obvious swelling of the PDMS. The solvents also help in reducing the density of the middle phase to better match the density of the aqueous phases, which results in more stable double-emulsions (Fig. 3.12, emulsion). We also note that to improve the stability of the double-emulsions, it was highly beneficial to add 1 or 1.5 % of Span80 surfactant to the middle phase [199]. Regarding the capsule permeability however, the capsules produced with 15 % butyl-acetate porogen retained the small molecular weight fluorophores in their lumen even after polymerization and repeated washes (Fig. 3.12, polymerized). The UV polymerization was conducted by illuminating from the side of a 1.5 mL polypropylene tube with a 100W mercury arc lamp for 30 seconds. The polypropylene tubes absorb a significant amount of UV light, particularly in the lower wavelengths, and this could have led to a slower polymerization process. However, it could be overcome by using custom-made PDMS chambers or simply using UV transparent cuvettes

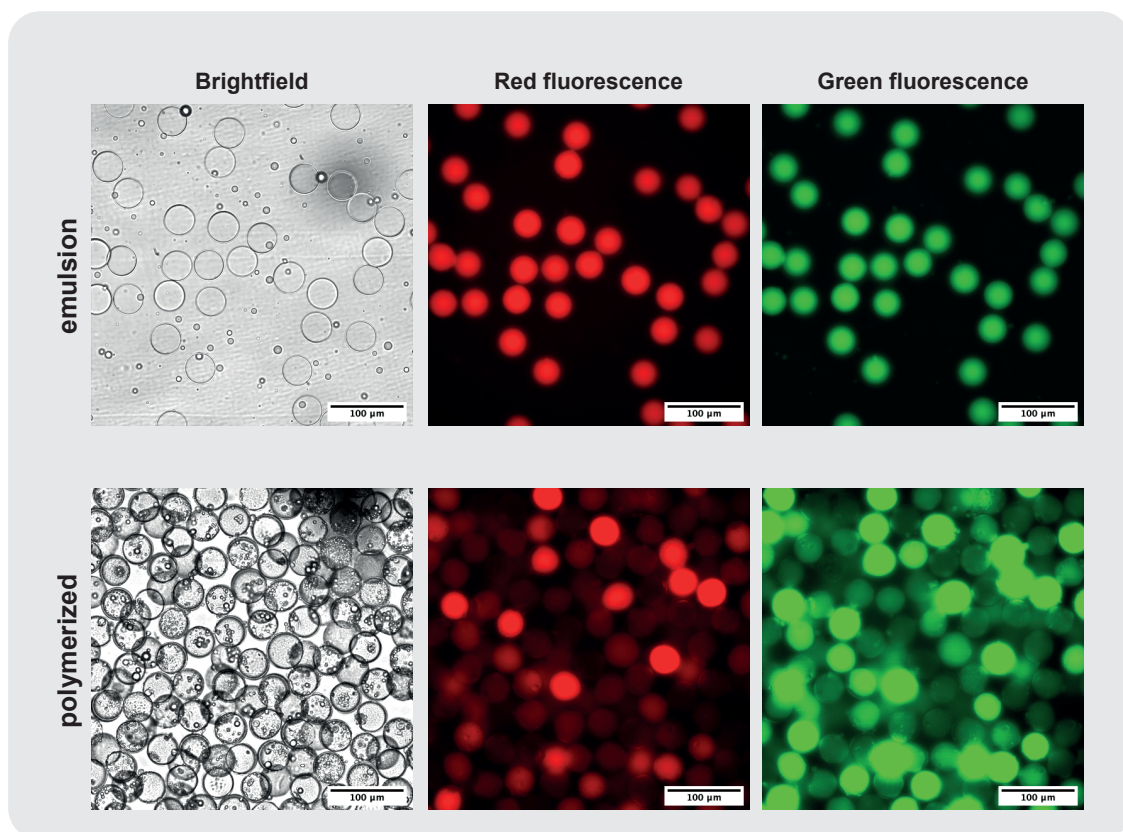


Figure 3.12: **No pores formed when illuminated through polypropylene tubes.** Butyl-acetate porogen was added to the PEG-DA 250 middle phase. The double-emulsion stability is improved by the addition of butyl-acetate and Span80 to the middle phase. Monodisperse capsules are obtained after UV polymerization with the total light from a mercury arc lamp focused on the side of a 1.5 mL polypropylene tube. Both sulforhodamine and 10 kDa FITC-dextran are retained inside the microcapsules.



(UVettes, Eppendorf), which were used throughout the rest of the project for the production of semi-permeable microcapsules.

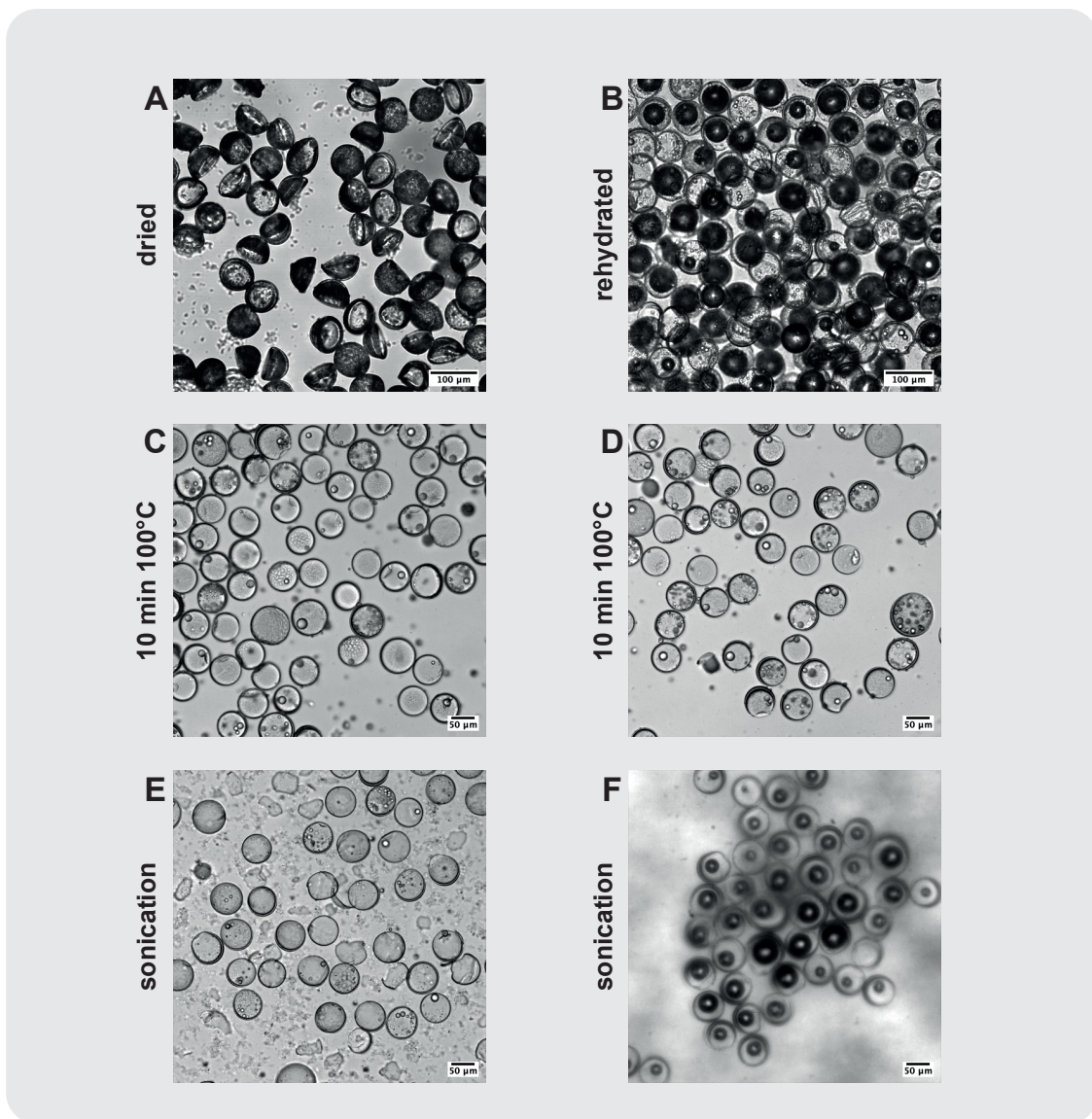


Figure 3.13: **Stability of poly-(PEG-DA 250) microcapsules to physical challenges.** Microcapsules were (A) air dried on a glass slide and (B) rehydrated by addition of buffer. The capsules recover their spherical shape after rehydration and some contain a gas drop that gradually dissolves. The capsules are resistant to (C-D) boiling, and (E-F) sonication to a lesser extent. Broken capsules debris are observed (E) as well as nucleation of gas bubbles inside the capsules (F).

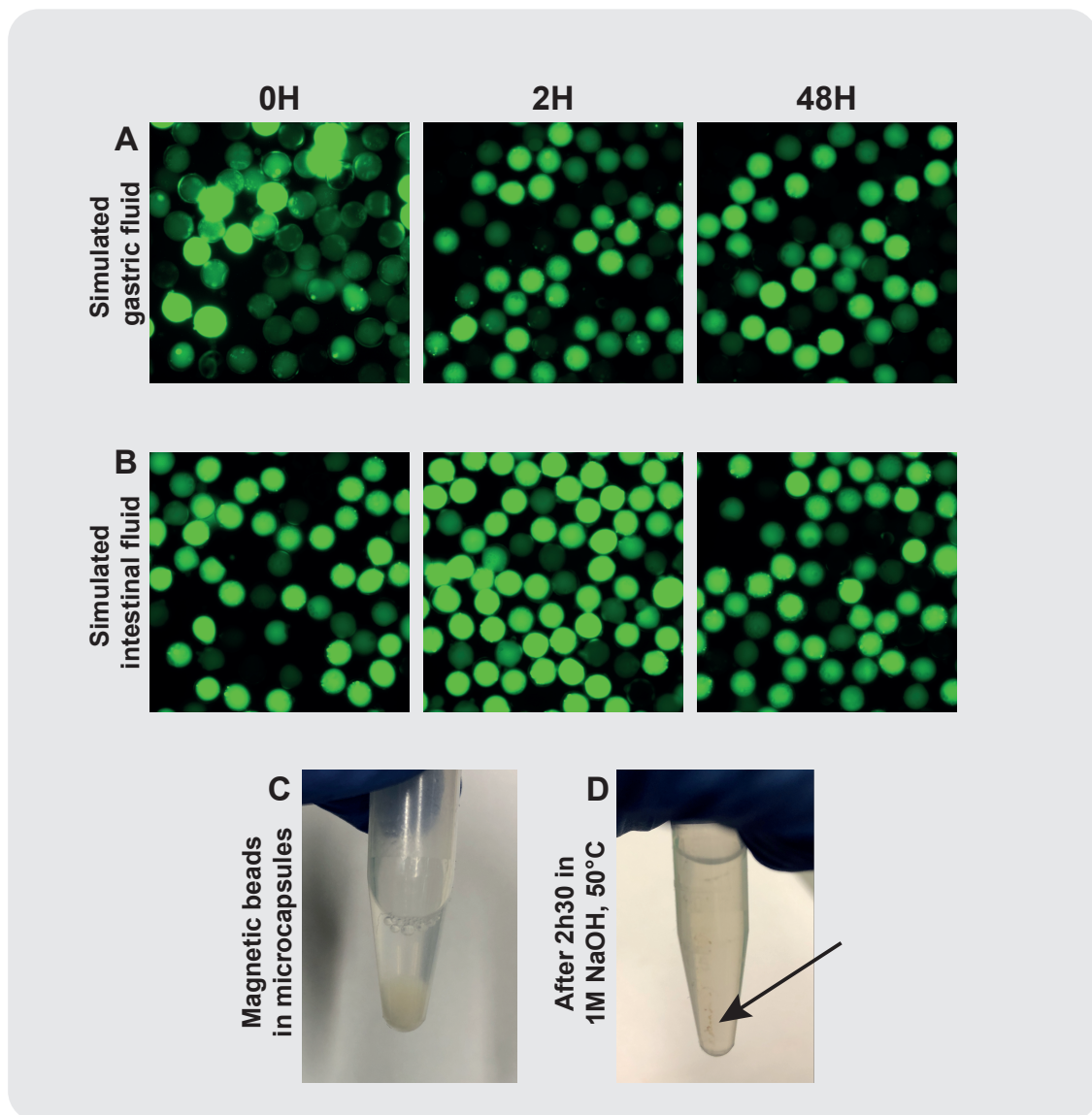


Figure 3.14: **Stability of poly-(PEG-DA 250) microcapsules to chemical challenges.** Microcapsules containing 500 kDa FITC-dextran were challenged with (A) Simulated gastric fluid, (pH 1.2) and (B) Simulated intestinal fluid (pH 6.8). The capsules are intact and retain the fluorescent cargo after 48H of incubation. Microcapsules hydrolysis in 1 M NaOH leads to complete dissolution of the capsules after 2h30 at 50°C. Magnetic nanoparticle containing capsules pellet (C) and magnetic particles released from the dissolved capsules (D). The tube was placed 2 minutes on a magnetic stand and a brown particles are attracted to the side of the tube (black arrow).

## Physical and chemical stability

Finally, we present here the favourable physical and chemical stability of the poly-(PEG-DA 250) semi-permeable microcapsules. As a first observation, the polymerized microcapsules are very easily recovered after their production, as they can withstand repeated centrifugal washes and pipetting steps or vortexing. They settle rapidly in PBS supplemented with 0.1 % Tween20 to form a white pellet which can be easily disturbed by pipetting up and down to resuspend the capsules. To observe the capsules, we found it very convenient to simply load them on cell-counting slides (Countess<sup>TM</sup>, ThermoFisher). The capsules can be air-dried on a glass slide and they buckle into a lenticular shape, before recovering their original shape after rehydration (Fig. 3.13, A-B). The capsules are also resistant to boiling for 10 minutes, and virtually no broken capsules or debris were observed (Fig. 3.13, C-D). The only method we used that could significantly damage the microcapsules was by using a sonication tip immersed in a 1 mL solution of microcapsules to deliver 400 J in a 10s ON 10s OFF cycle at 50% amplitude (Fig. 3.13, E-F). We could even observe capsules floating at the surface, due to the presence of gas bubbles in their interior, which were probably formed by cavitation inside the capsules and had not burst. In conclusion, the microcapsules have remarkable physical stability which make them adapted to a large range of operating conditions. We also assessed the resistance of the poly-(PEG-DA 250) microcapsules to chemical challenges. As the initial intended application for the semi-permeable microcapsules was to develop an oral enzyme delivery platform, we first investigated their resistance after incubation in simulated gastric fluid (SGF) or in simulated intestinal fluid (SIF)(Fig. 3.14, A and B). Even in the very acidic pH 1.2 of the SGF, no damage or release of the cargo was observed. We note that we had to wash the capsules and place them back in a PBS solution to obtain the images after 2 hours and 48 hours, as the low pH would completely abolish the 500 kDa FITC-dextran fluorescent signal. However, it can be observed that the signal was completely recovered without loss of cargo after exchange to PBS with neutral pH. Unsurprisingly, the more gentle pH 6.8 of SIF did not lead to any degradation of the microcapsules or release of their cargo. The poly-(PEG-DA 250) contain ester bonds which can be hydrolyzed, making it ultimately biodegradable [205]. The hydrolysis can be accelerated by adding a base and heating the solution to 50°C. To aid in visualizing the degradation of the capsules, we used microcapsules containing magnetic nanobeads, and placed them in 1 M NaOH for 2h30 at 50°C (Fig. 3.14, C and D). It can be observed that the white pellet of microcapsules is completely

dissolved after incubation, and we could see free magnetic nanoparticles in solution, which were attracted to the side of the tube after placing it against a magnetic stand. In conclusion, the poly-(PEG-DA 250) microcapsules are resistant to chemical challenges, and particularly important is their stability in pH encountered in the digestive tract. On the other hand, the capsules can be readily dissolved in basic conditions, allowing the recovery of certain cargo or to perform reactions on the encapsulated material, such as DNA extraction and amplification [99].

### 3.3 Results

#### 3.3.1 PEG-DA microcapsules templated from double-emulsions

Poly(ethylene glycol) diacrylate of 250 g/mol molecular weight (PEG-DA 250) can be used to form water-in-(PEG-DA 250)-in-water double-emulsions. As PEG derivatives are generally considered biocompatible, bioinert and ultimately biodegradable [205], we experimented using various PEG-DAs of low molecular weight, such as PEG-DA 700 g/mol, PEG-DA 575 g/mol and PEG-DA 250 g/mol as precursors for the production of microcapsules after photopolymerization by UV illumination. For PEG-DA with molecular weights of 575 g/mol or higher, their water miscibility prevented us to readily form double-emulsions. We attempted to use a continuous oil phase and to produce an aqueous two-phase system by adding high molecular weight Ficoll in the aqueous inner phase, but could not obtain well defined core-shell structures. Leonavicene et al. recently showed that a high molecular weight PEG-DA (8000 g/mol) is indeed necessary to obtain a two-phase system and form core-shell capsules using PEG-DA as a capsule material [99]. However, we identified PEG-DA 250 as a potential polymer precursor due to its water immiscibility, as was also reported by Nam *et al.* [109]. This property of PEG-DA 250 allowed us to use it as the middle phase in double-emulsions and was compatible with droplet generation in a PDMS device (Fig. 3.15, A). To form the double-emulsions, we used an aqueous continuous phase supplemented with 10% PVA. The PEG-DA 250 middle phase was supplemented with a photoinitiator (HMPP) and surfactant (Span80), with the optional addition of a mild organic solvent. We produced monodisperse double-emulsions in a jetting regime with flowrates of 2500  $\mu\text{L/hr}$  for the aqueous continuous phase, 200  $\mu\text{L/hr}$  for the PEG-DA 250 middle phase, and 250  $\mu\text{L/hr}$  for the aqueous inner phase (Fig. 3.15, top panel). Interestingly, the double-emulsions could be generated without requiring any surface treatment of the device owing to the non-planar geometry of the PDMS device which prevented wetting of the collection channel by the more hydrophobic middle-phase. We collected double-emulsions in batches of 15 minutes before UV polymerization without noticing any problem in double-emulsion stability.

In the jetting regime, we observed the formation of small satellite droplets and a few droplets of larger size, but the double-emulsions themselves were consistent in size. After double-emulsion generation, we polymerized the core-shell capsules by UV-illumination in batch and obtained monodisperse capsules with a mean diameter of 62  $\mu\text{m}$  (Fig. 3.15C,D). The coefficient of variation was close

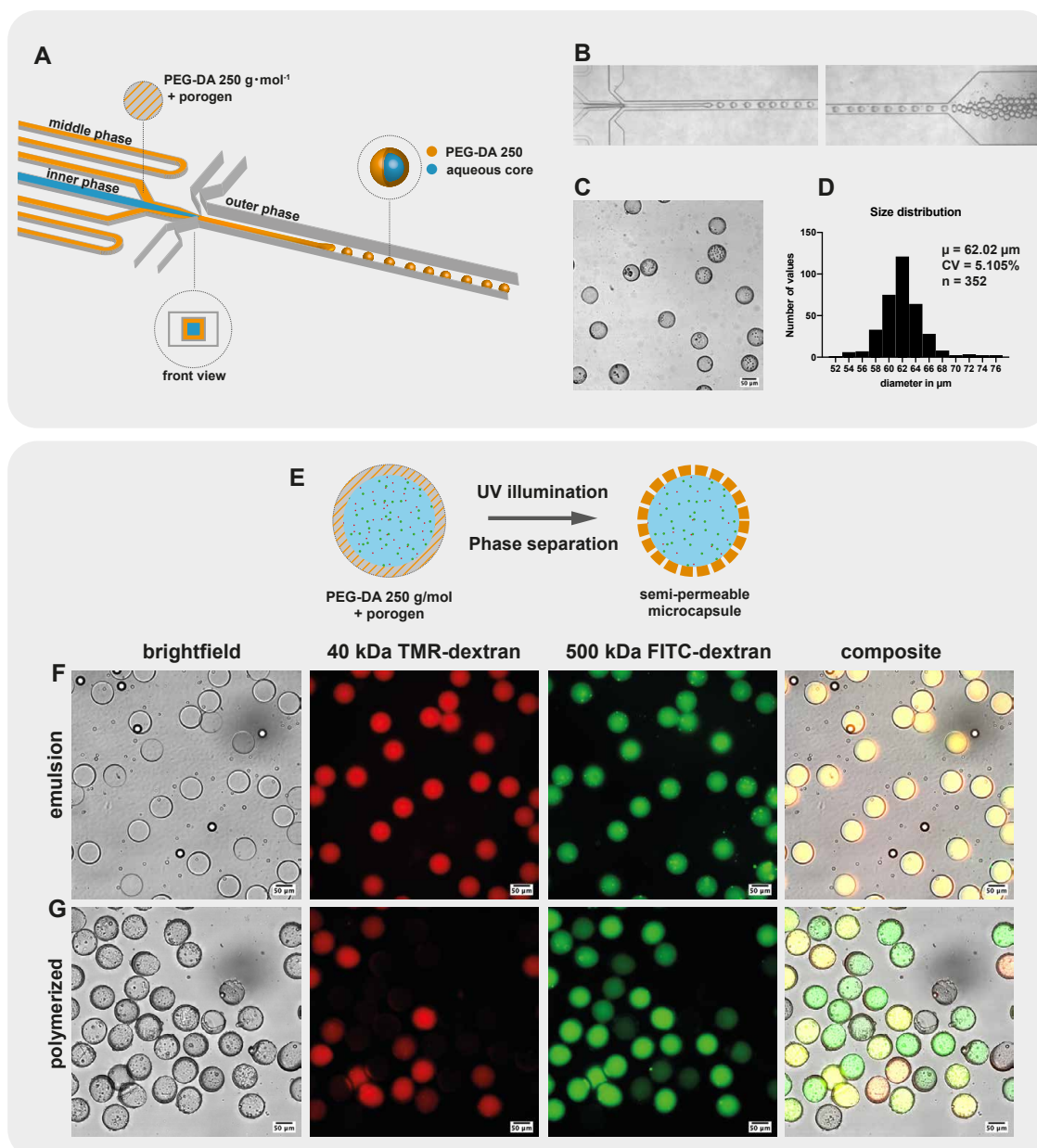


Figure 3.15: **Production of semipermeable microcapsules in a PDMS device with 3D geometry.** (A) Schematic representation of the PDMS device with 3D geometry. W/O/W double-emulsions are generated with a PEG-DA 250 middle phase encapsulating an inner aqueous core. (B) Micrographs of the PDMS device operation. Double-emulsions are produced in jetting regime without the need for surface treatment. (C) Brightfield image of microcapsules obtained after UV polymerization of the collected double-emulsion. (D) Size and size distribution of a representative batch of polymerized microcapsules. (E) Schematic representation of polymerization-induced phase separation (PIPS) upon UV illumination. 15 % Butyl-acetate (porogen) is mixed with PEG-DA 250 to form semi-permeable microcapsules. (F) In the collected double-emulsion, both high molecular weight 500 kDa FITC-dextran and lower molecular weight 40 kDa RITC-dextran are retained in the inner aqueous phase. (G) After UV polymerization and PIPS, pores are formed in the capsules shell and capsules become semi-permeable.

to 5 %, in accordance with previous results using similar PDMS devices [206] (see figure1). The thickness of the capsule shell was estimated from inspecting microscope images to be between 5 and 10  $\mu\text{m}$  thick. Our results not only confirmed the observation from Nam *et al.* [109] that water-immiscible PEG-DA 250 is a suitable polymerizable middle phase, but demonstrated its compatibility with double-emulsion generation in a PDMS device which did not require any surface treatment, and resulted in the production of monodispersed poly-(PEG-DA 250) microcapsules with thin shells.

By using droplet microfluidic to generate double-emulsions, we can directly encapsulate cargoes by adding them to the aqueous inner phase. The inner aqueous phase containing 10 % PVA can be supplemented with a water soluble cargo for its direct encapsulation into the polymerized capsules. By adding 500 kDa FITC-dextran to the inner aqueous phase, we observed a fluorescent signal from the dextran derivative in the double-emulsion, and almost all capsules retained the 500 kDa FITC-dextran after polymerization. Interestingly, we note that the speckled fluorescent signal in some double-emulsions evolves into a completely homogeneous aspect filling the interior of the polymerized capsules. Importantly, the homogenous profile in the polymerized capsules also suggests that the encapsulated FITC-dextran does not adsorb to the poly-(PEG-DA 250) shell. We noted that the fraction of inner phase available for direct encapsulation is important as the 10 % PVA solution can be mixed with another aqueous solution down to a final concentration of 2 % PVA and still produce double emulsions polymerized into microcapsules. Therefore these results demonstrated the possibility to directly encapsulate water-soluble cargo into the poly-(PEG-DA 250) capsules without noticeable adsorption of the cargo to the capsule material.

Moreover, the polymerized capsules were stable, and their cargo was retained in their lumen for prolonged times. The capsules are mechanically stable and can be pipetted and vortexed extensively without noticeable change in their morphology. An investigation of their physical and chemical stability demonstrated the great resistance of the microcapsules and is presented in Section 3.2.

### 3.3.2 Production of semi-permeable poly-(PEG-DA 250) capsules

To produce semi-permeable capsules, we used the mild inert solvent butyl-acetate mixed in the middle phase which serves as a porogen in polymerization induced phase separation (PIPS). Obtaining small pores in microcapsules can be a significant challenge, and we chose to use PIPS which was



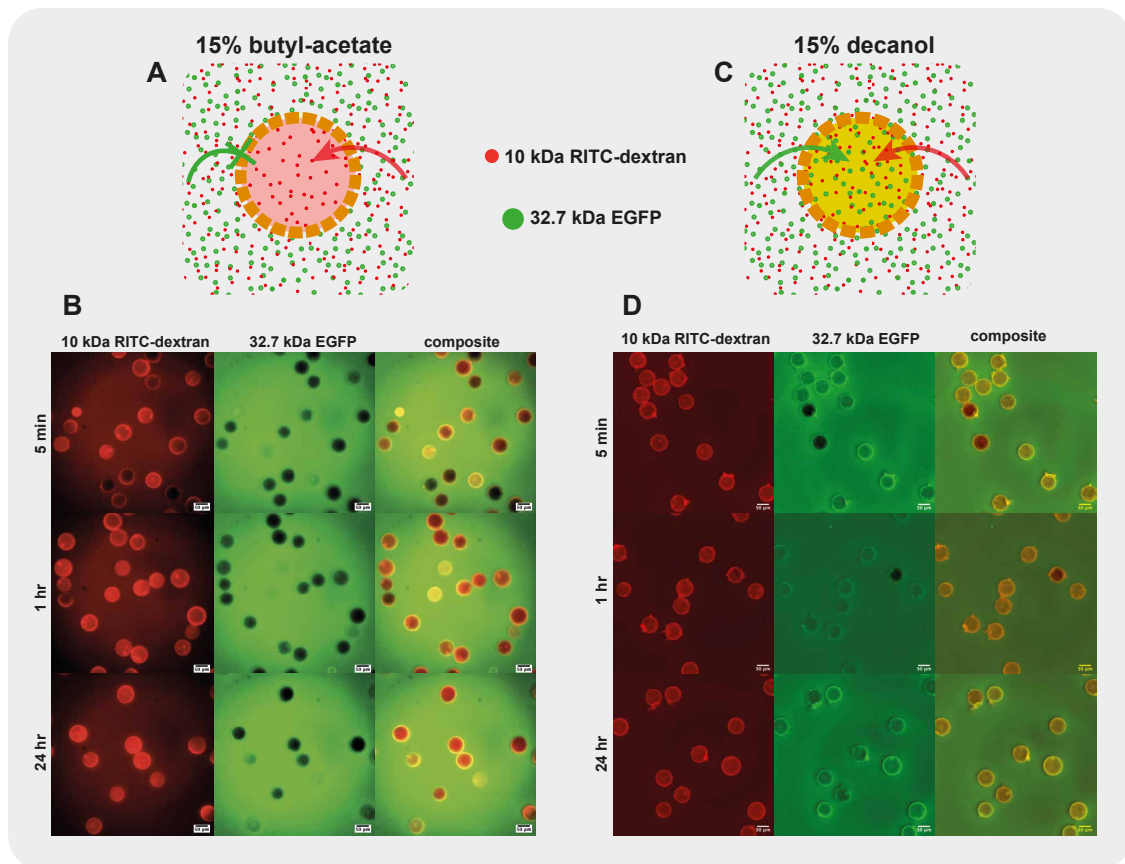


Figure 3.16: **PEG-DA 250 microcapsules are semi-permeable and the pore size can be adjusted by changing the porogen.** Schematic representation of PEG-DA 250 microcapsules produced using (A) 15 % butyl-acetate or (C) 15 % 1-decanol as porogen. 15 % butyl-acetate microcapsules selectively allow the permeation of 10 kDa RITC-dextran while excluding 32.7 kDa EGFP. The larger pore size of microcapsules produced with 15 % 1-decanol as porogen allows the diffusion of both fluorescent molecules. Microcapsules produced using (B) 15 % butyl-acetate or (D) 15% 1-decanol porogen are immersed in a solution containing 10 kDa RITC-dextran and 32.7 kDa EGFP. The evolution of the fluorescent signal in the Cy3 and FITC channels is observed after 5 minutes, 1 hour and 24 hours. While microcapsules produced using 15 % 1-decanol are permeable to both fluorescent molecules, we clearly observe the selective permeability of microcapsules produced using 15 % butyl-acetate as a porogen.



previously employed in the production of semi-permeable microcapsules [207, 108]. To encapsulate cargos relevant for different biological applications, we used butyl-acetate as it was described by Kim *et al.* [108] to form nanopores with diameter below 30 nm in a thin shell composed of a cross-linked network of ethoxylated trimethylolpropane triacrylate (ETPTA) and glycidyl methacrylate (GMA). Pores of nanometric size should allow the loading of large biomolecules such as proteins or enzymes, while allowing the transfer of solvents, small molecules, peptides, or even small proteins across the capsule shell. To evaluate the permeability of the capsules, we added 500 kDa FITC-dextran and 40 kDa TMR-dextran to the inner aqueous phase, and observed that almost 90% of the polymerized capsules retained the 500 kDa FITC-dextran after the capsules were extensively washed by successive centrifugation in excess of buffer and followed by a 24h incubation (Fig. 3.15, G). On the other hand, only about 40% of the capsules retained the lower molecular weight 40 kDa TMR-dextran. These results show that some capsules are semi-permeable, as evidenced by the capsules in which only the higher molecular weight fluorophore is retained. Even though the size cut-off could not be precisely determined from this experiment, we can estimate it to be well below 500 kDa and potentially close to the size of the smaller fluorophore, 40 kDa.

To better characterize the semi-permeability, we prepared empty capsules and placed them in a solution of fluorescent molecules of different molecular weights (Fig. 3.16). We placed empty capsules produced using 15 % butyl-acetate porogen in a solution containing both 10 kDa RITC-dextran and 32.7 kDa EGFP (Fig. 3.16, A and B). We observed that most capsule showed a relatively rapid increase in signal in the red fluorescent channel, corresponding to the lower molecular weight 10 kDa RITC-dextran. After 1 hour incubation, most capsules showed red fluorescent signal in their core, and all capsules displayed a high red fluorescent signal after 24h incubation. At the same time, the majority of these capsules showed no increase in signal in the green fluorescent channel corresponding to the 32.7 kDa EGFP. By superimposing the signal from the two fluorescent channels, we could clearly see that a majority of the capsules were semi-permeable and exclude EGFP for at least 24h while allowing diffusion of the 10 kDa RITC-dextran into their interior. We note however some variability in the permeability of the capsules, with some capsules appearing permeable to EGFP already after a few minutes of incubation, while a few capsules still excluded 10 kDa RITC-dextran after 1 hour.

We observed that by using 1-decanol as a porogen, we obtained semi-permeable capsules with a different size cutoff. The use of 1-decanol was reported by Kim *et al.* [108] to create larger

pores in the ETPTA/GMA polymer shell due to a different interaction parameter of 1-decanol with the forming polymer. Here, we show that capsules produced with 15 % 1-decanol porogen in PEG-DA 250 also resulted in higher permeability than capsules produced with the butyl-acetate porogen (Fig. 3.16, C and D). We saw an increase in green fluorescent signal corresponding to 32.7 kDa EGFP in the interior of the capsules after only a few minutes incubation and all capsules' interior were fluorescent after 24 h. In addition, all capsules were completely permeable to 10 kDa RITC-dextran. However, in contrast to ETPTA/GMA capsules using 1-decanol porogen, our capsules weren't permeable to the larger 500 kDa FITC-dextran even after 48h incubation. To complement our study on polymerization induced phase separation, we also selected water-immiscible porogens which should have different interaction parameters with the polymerizing poly-(PEG-DA 250), such as 2-ethyl-hexanol, octanol, or heptanone. In our experiments, we could not observe a strong influence in the obtained size cut-off when using butyl-acetate or one of the other porogens. However, the possibility to select different porogens might be useful depending on the required application, considering for example that heptan-2-one is a food additive authorized by the FDA. These results demonstrated that it is possible to tune microcapsule permeability by varying porogen composition, and that a selection of porogens are compatible with our microfluidic production of semi-permeable microcapsules.

### 3.3.3 Direct encapsulation of proteins and enzymes

Next, we showed that we can directly encapsulate proteins in semi-permeable poly-(PEG-DA 250) microcapsules without loss of function or adsorption to the polymeric shell. We directly encapsulated recombinant 32.7 kDa EGFP inside our microcapsules by adding it to a final concentration of 2  $\mu\text{g/mL}$  in the inner aqueous phase. The fluorescence signal can be observed in the double-emulsion without any sign of precipitation, and once polymerized the capsules display a homogeneous fluorescent profile, without any sign of adsorption of the protein to the capsule material (Fig. 3.17, E and G). After prolonged incubation in PBS, we saw that a proportion of the capsules did not contain any fluorescent signal, consistent with previous observations when encapsulating 40 kDa TMR-dextran (Fig. 3.17, E and F). This observation could be explained by broken capsules releasing their content, or could also suggest a permeability cutoff close to the size of these fluorescent molecules. We also expect some variability in the pore size of the capsules due to the batch UV polymerization process, as the received UV intensity could slightly differ depending on the po-

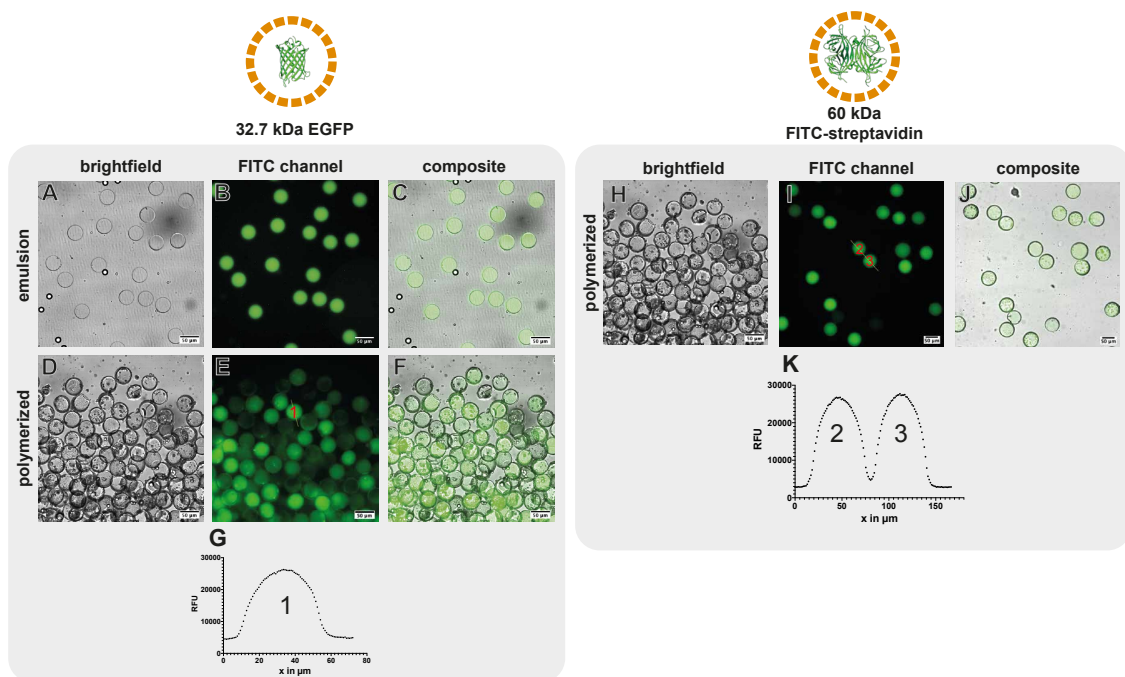


Figure 3.17: **Direct encapsulation of proteins inside semi-permeable PEG-DA 250 capsules.** EGFP is added to the aqueous inner phase for direct encapsulation. (A, B, C) Microscope images of the produced double-emulsion showing a fluorescent signal in the FITC channel corresponding to the double-emulsion's aqueous inner phase. (D, E, F) After polymerization, the fluorescent signal is still present in the interior of most capsules. Some variability in the pore size or a size cutoff close to the 32.7 kDa EGFP results in some protein leakage. (G) Fluorescent profile from the capsule shown in panel E. The fluorescent profile suggests a homogeneous distribution of EGFP in the interior of the capsule without protein adsorption to the shell material. (H, I, J) Microscope images of polymerized capsules containing FITC-streptavidin after direct encapsulation. A fluorescent signal is present in all capsules, suggesting that the pore size is too small for the FITC-streptavidin diffusion. (K) Fluorescent profile across two capsules from panel I. The profile suggests a homogeneous distribution of FITC-streptavidin in the interior of the capsule without protein adsorption to the shell material.

sition of the capsule in the cuvette. We encapsulated another model protein by adding 60 kDa FITC-labelled streptavidin (Biolegend) in the aqueous inner phase to a final concentration of 50  $\mu\text{g/mL}$ . Again, we observed a strong fluorescent signal in the capsules after polymerization. The fluorescent signal profile in the polymerized capsules indicates no sign of protein adsorption on the capsule shell, confirming our previous observation with EGFP encapsulation (Fig. 3.17, I and K). With the larger molecular weight of the 60 kDa FITC-streptavidin, we saw that most polymerized capsules contained fluorescent signal after aqueous washes, pointing to a size cutoff below the size of FITC-streptavidin. Altogether, we confirmed that the poly-(PEG-DA 250) shell obtained after UV polymerization is compatible with direct protein encapsulation. The materials used did not lead to adsorption of proteins to the capsule shell and the polymerization-induced phase separation process formed pores sufficiently small to retain proteins with sizes of 32.7 kDa and above.

After the successful encapsulation of proteins, we loaded enzymes and assessed their activity after encapsulation. As a first model enzyme, we chose bioluminescent luciferase for direct encapsulation into the semi-permeable microcapsules. We used a commercially available recombinant GFP-luciferase fusion protein (econoLuciferase<sup>TM</sup>, Biosynth), which allows for the detection and quantification of enzyme encapsulation by fluorescence. The molecular weight of the fusion protein being over 90 kDa should also warrant the proper retention of the enzyme in the interior of the microcapsules. Indeed, we saw that both the double-emulsion and polymerized capsules contained a fluorescent signal from the econoLuciferase fluorescent fusion protein. In both cases, we observed a speckled distribution of the fluorescent signal which might be due to some level of precipitation in the 10 % PVA inner solution (Fig. 3.18, A and B). However, after washes and incubation in PBS, the fluorescent signal became homogeneous and remained present in more than 20% capsules after a year of storage at 4°C. Most importantly, the capsules containing econoLuciferase generated a strong bioluminescent signal in a bioluminescent assay. The econoLuciferase-containing capsules were placed in a solution containing D-luciferin, and we measured a bioluminescent signal two orders of magnitude higher than the signal observed for negative control empty capsules (Fig. 3.18, C). However, we measured an almost 10 times higher bioluminescent signal for non-encapsulated econoLuciferase compared to the signal obtained from econoLuciferase-containing capsules, while also observing that the fluorescent signal from GFP was 10 times higher for the solution of non-encapsulated luciferase. Considering the respective dilutions in the free and encapsulated enzyme solutions, we estimate that around 5 % of the GFP-luciferase is encapsulated and retains fluorescent

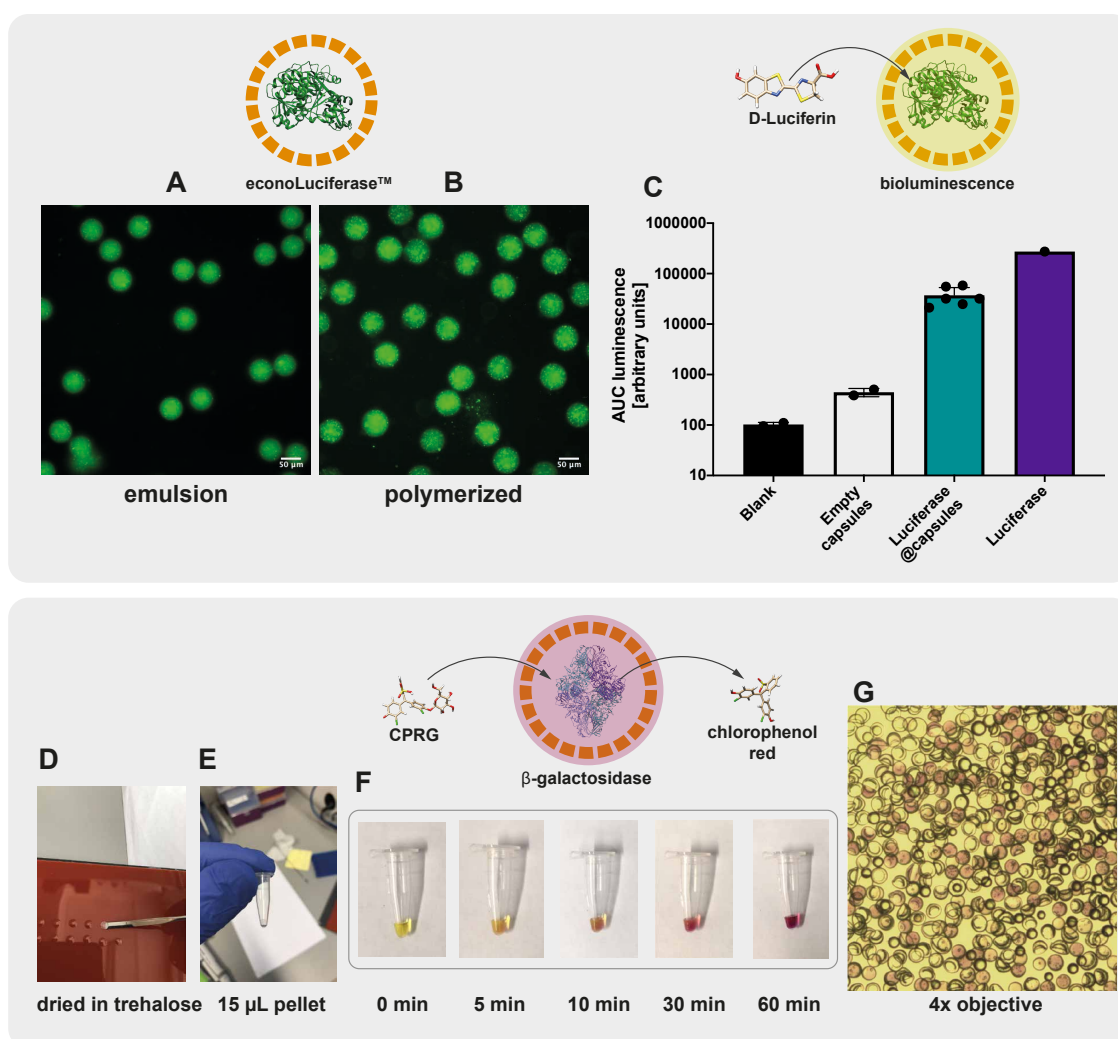


Figure 3.18: **Direct encapsulation of active enzymes in semi-permeable PEG-DA 250 microcapsules.** A commercial luciferase-GFP fusion protein is directly encapsulated in semi-permeable capsules. The fluorescent fusion protein allows for the visualization of the enzyme (**A**) in the double-emulsion, and (**B**), in the polymerized capsules. (**C**) The encapsulated econoLuciferase™ shows a strong signal in a bioluminescent assay. Direct encapsulation of  $\beta$ -galactosidase. (**D**, **E**) Enzyme-containing capsules are dispersed in trehalose and air-dried at 37°C. (**F**) After rehydration with a solution containing CPRG, the substrate is hydrolyzed to chlorophenol red. (**G**) The solution is imaged with a color camera mounted on an inverted microscope with 4x magnification. Capsules display a purple color in their interior, indicative of  $\beta$ -galactosidase enzymatic activity.

signal or enzymatic activity. This loss in fluorescent signal and enzymatic activity was relatively high, which might be caused by the different capsule production steps, from inner phase formulation, loading in syringes, microfluidic double-emulsion production, double-emulsion collection, batch UV polymerization, multiple aqueous washes, and overnight storage at 4°C. Therefore, the retention of activity appears reasonable using this direct encapsulation process, and an optimization of the different production parameters could potentially improve the activity of the enzyme-loaded capsules. These results demonstrate that a bioluminescent enzyme can be encapsulated in poly-(PEG-DA 250) microcapsules with an appreciable retention of its catalytic activity, while the semi-permeable shell allows shuttling of the enzyme substrate D-Luciferin into the core of the microcapsules to generate a strong bioluminescent signal.

In a second example, we demonstrated that capsules can be dried and rehydrated while preserving enzyme functionality. We encapsulated  $\beta$ -galactosidase, a tetrameric enzyme with a total molecular weight of 465 kDa which should be retained in the interior of the semi-permeable capsules, and initial enzymatic assays using chlorophenol red- $\beta$ -D-galactoside substrate (CPRG) showed that enzymatic activity was indeed present in  $\beta$ -galactosidase-loaded capsules. To show that enzyme-containing capsules can be dried and still retain some activity, we dispersed  $\beta$ -galactosidase-containing capsules in a 0,5 M trehalose solution and dried small drops overnight in an incubator at 37°C resulting in trehalose pellets (Fig. 3.18, D and E). After rehydrating the dried pellets with a CPRG solution, we saw a change in color upon enzymatic conversion of the yellow CPRG to chlorophenol red. We observed by the naked eye that the color change happens at the location of the capsules, and visualization with a 4x objective showed that the interior of some capsules turn to an intense purple red color (Fig. 3.18, F and G). Although the obtained images did not serve as a quantification of the chlorophenol red concentration, they clearly showed that the conversion of CPRG to chlorophenol red occurred inside the  $\beta$ -galactosidase containing capsules. These results demonstrated the possibility for the direct encapsulation of an active enzyme into semi-permeable microcapsules, and we additionally showed that capsules can be air-dried in a lyoprotective solution of trehalose and still retain their encapsulated enzyme activity after rehydration.

### 3.3.4 Encapsulated DSD reactions

We were interested in building complex biomolecular systems as they are representative of how the capsules could be used for sensing and responding to a stimulus, which would be of importance for

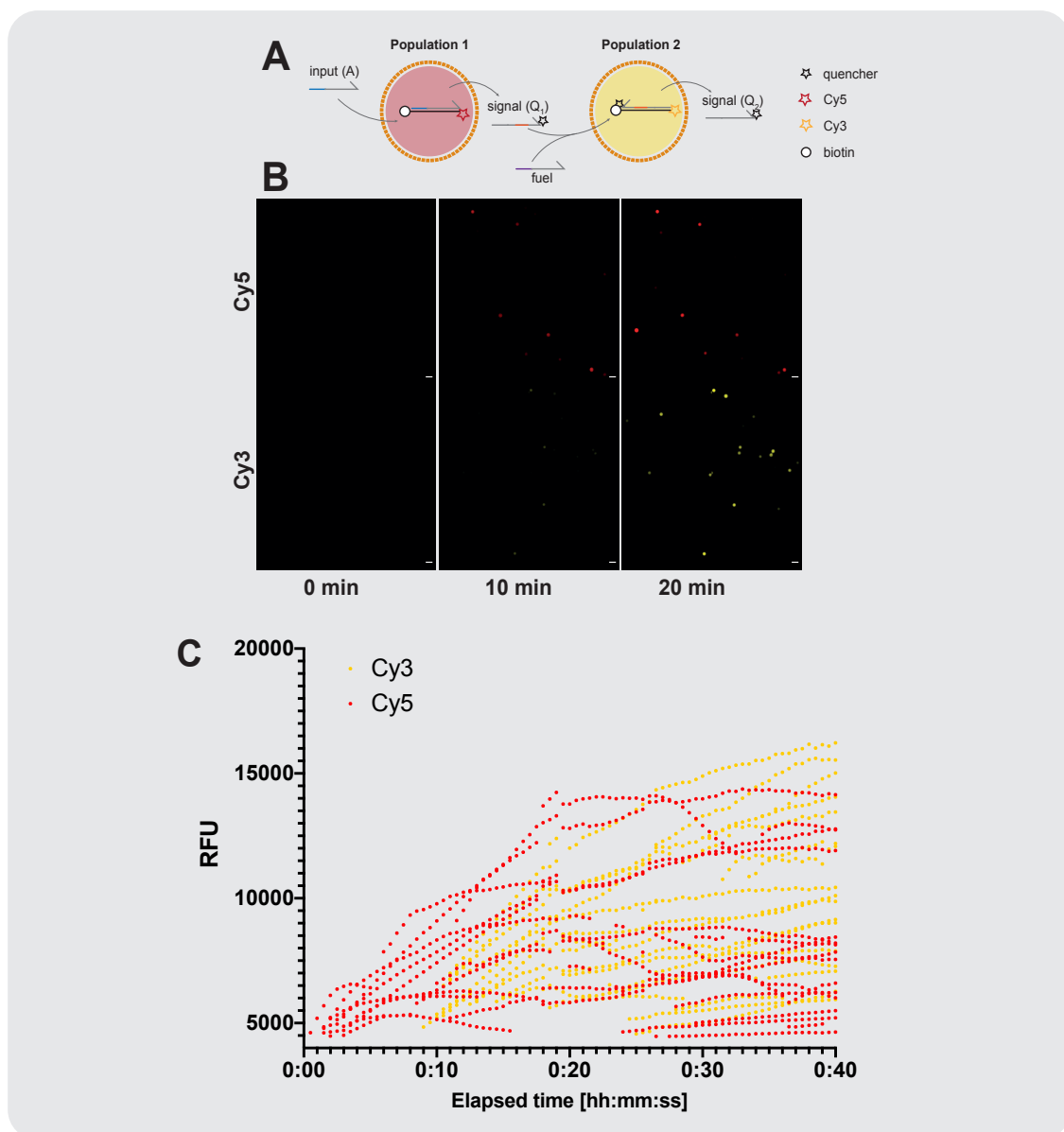


Figure 3.19: **Immobilization of DNA strand displacement reaction in semi-permeable microcapsules and implementation of a two-layer signalling cascade.** (A) Schematic representation of the two-layer signalling cascade as depicted in Joesaar *et al.* [192] (B) Implementation of the two-layer signalling cascade in poly-(PEG-DA 250) capsules. The two capsules populations are mixed and imaged on a cell-counting slide immediately after addition of 50 nM input strand (A). An increase in Cy5 and Cy3 fluorescent signals is observed corresponding to the activation of the first and second populations, respectively. (C) Mean intensity of automatically detected particles. An increase in the Cy5 signal is observed corresponding to the activated first population of capsules. After the release and diffusion of the signal strand (Q<sub>1</sub>) to the second capsule population, an increase in Cy3 signal is observed corresponding to their subsequent activation.

diagnostic and therapeutic, or theranostic applications. As a demonstration for the potential of the semi-permeable poly-(PEG-DA 250) microcapsules, we used capsules containing FITC-streptavidin to immobilize DNA strands to build a two-layer signaling cascade of DNA strand displacement (DSD) reactions. It has been recently demonstrated that DSD reactions can be performed in proteinosome microcapsules [208] and serve as a model of protocellular communication and distributed biomolecular computation [192]. Here, we used capsules containing FITC-streptavidin presented in the previous sections to immobilize biotinylated DNA strands and complementary strands, following the design from Joesaar et al. [192]: We implemented a two-layer signalling cascade by functionalizing a first population of capsules with a transducer DSD gate responding after toehold displacement from a ssDNA input strand (A), which leads to the release of a signal strand (Q1) and unquenching of a Cy5 fluorophore. The (Q1) signal strand can in turn activate a second population of capsules functionalized with a transducer-amplifier DSD gate releasing a second signal strand (Q2), this time unquenching a Cy3 fluorophore. We also added a fuel strand which acts as an amplifier by allowing the toehold displacement and reuse of signal strand (Q1) which can again activate other capsules of the second population. The two capsule populations were mixed together and the two-layer signalling cascade was activated upon addition of the input strand (A). In our experiment, we mixed the two capsules populations, added 50 nM input strand (A), and loaded the freely moving capsules in a cell counting chamber. We first measured a Cy5 signal increase corresponding to the first population of capsules containing the first DSD transducer gate. After a time lag of a few minutes, we saw a subsequent increase in Cy3 signal corresponding to the second population of capsules containing the transducer-amplifier DSD gate (Figure 3.19). We observed a Cy5 increase in about 10 capsules of the first population and Cy3 increase in about 15 capsules of the second population. The activation of the two-layer cascade could be modified by changing the concentration of input strand (A). By increasing it to 100 nM, the activation of the first population was greatly accelerated and amplified, to the point where early activation was difficult to capture considering the time required to set up the microscope measurements. On the other hand, reducing (A) concentration to 10 nM led to a much slower and lower levels of activation of the first population. In all cases, we observed a lag of 5 to 10 minutes between the activation of the first population, signal transduction, and finally the activation of the second population. While this is a succinct implementation of the recently developed compartmentalized DSD reactions, these results demonstrated that DSD reactions can be efficiently encapsulated in our semi-permeable



microcapsules and employed to build communicating biomolecular systems.

### 3.3.5 Immobilization on streptavidin-coated magnetic nanoparticles

The possibility to immobilize biomolecules by diffusion through the capsules shell and interaction with an encapsulated binding partner is attractive as it could offer many different applications, starting from the same material. Here we explored the possibility to encapsulate streptavidin-coated magnetic nanobeads which can be further used as a binding partner for biotinylated molecules. We prepared batches of microcapsules containing 10 % (v/v) or 20 % (v/v) of streptavidin-coated magnetic nanobeads solution. The capsules were produced using either butyl-acetate as porogen or 1-decanol to provide larger pores. Using the microcapsules with larger pores, we could immobilize biomolecules as large as biotinylated antibodies, which could be useful for the immobilization of a large variety of secondary binding partners without requiring them to be biotinylated. As a proof of concept, we immobilized a biotinylated anti-GFP antibody (Abcam, ab6658) by diffusion inside the microcapsules with large pores and containing the streptavidin-coated microcapsules.

After functionalization with the anti-EGFP antibody, the microcapsules are incubated with an EGFP solution and we show that EGFP is immobilized inside the functionalized capsules (Fig. 3.20, B). The immobilization is specific to the capsules with anti-EGFP antibodies as the same microcapsules containing magnetic nanoparticles did not display significant EGFP signal when they were not functionalized with the biotinylated antibody (Fig. 3.20, A). One possible explanation for the increase in signal in the antibody functionalized capsules would be a passive trapping of the anti-GFP antibody in the lumen of the capsules. However, it can be observed on higher magnification that the EGFP fluorescence is colocalized with the 130 nm magnetic particles which can be identified as small aggregates following centrifugation during the washing steps (Fig. 3.20, C). This points to a successful immobilization of biotinylated anti-GFP antibody on the magnetic nanobeads and subsequent binding of EGFP. Following such proof-of-concept, this method could be used to purify biomolecules from complex matrices, effectively combining a size-exclusion and affinity purification in a single-step. Alternatively, immunoassays could be implemented in capsules where a detection antibody could be added in a final step, and the signal quantified by measuring the signal intensity or counting the number of capsules with a positive or negative signal, similar to other digital assay formats.

As another proof-of-concept for the use of semi-permeable microcapsules preloaded with streptavidin-

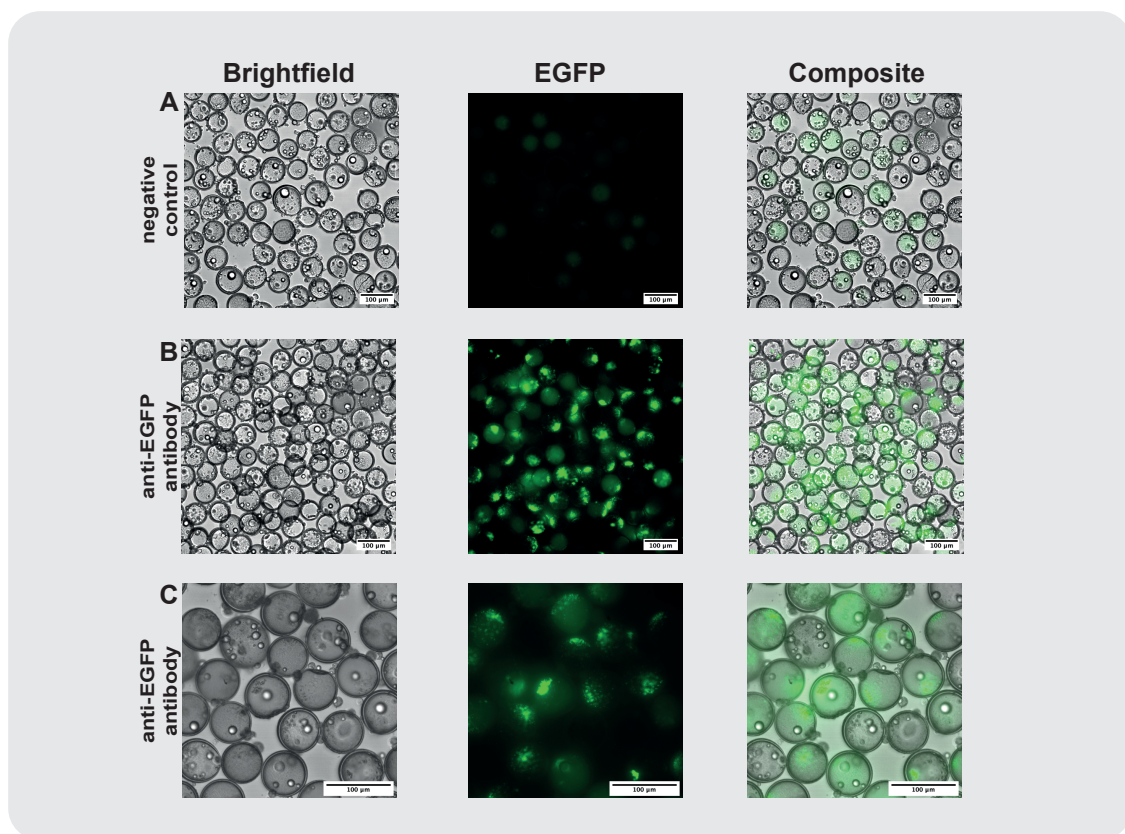


Figure 3.20: **Encapsulated streptavidin-coated magnetic nanobeads functionalized with anti-EGFP antibody.** The large pores microcapsules containing the magnetic nanoparticles were incubated in biotinylated anti-GFP antibody (25 µg/mL) overnight at 4°C. The capsules were washed 3 times and incubated in 10 µg/mL EGFP overnight at 4°C. After washing, the capsules were imaged with (B) 20x and (C) 40x magnification. The negative control (A) consists of the same magnetic nanobeads containing microcapsules without incubation in anti-EGFP antibody.

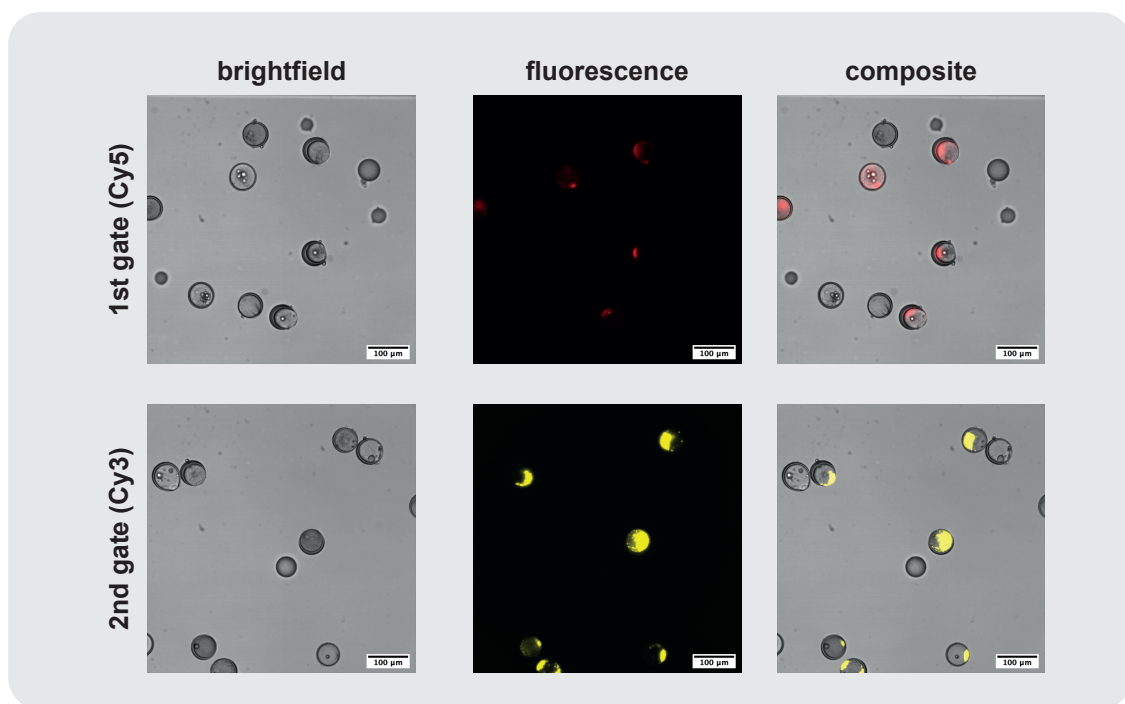


Figure 3.21: **Immobilization of DNA strand displacement reaction on encapsulated streptavidin-coated magnetic nanobeads.** Microcapsules were loaded with a magnetic nanobeads solution 20 % (v/v) and two capsules populations were functionalized with the 1st and 2nd DSD gate of a two-layer signalling cascade. The DSD reaction cascade is activated by addition of an input DNA strand and the fluorescence is measured after 20 minutes of incubation.

coated magnetic nanobeads, we used the small pores microcapsules to implement the same DSD reactions as presented in the previous section. The microcapsules containing the nanobeads were incubated with the biotinylated strands and complementary strands composing the DSD reactions. It was possible to implement single DSD reactions, as well as the complete two-layer signalling cascade. The procedure to prepare the microcapsules remains identical to the protocol used for the microcapsules containing FITC-streptavidin. Two populations were individually functionalized with the first and second gate respectively, and mixed before activation with a DNA input strand. The two-layer cascade proceeded similarly to the DSD reactions immobilized on FITC-streptavidin and a fluorescent signal from the activated gates could be observed. After 20 minutes of incubation, we see that about half of the capsules have a Cy5 signal and half of the capsules have a Cy3 signal, corresponding to the activation of the first and second gate (Fig. 3.21). As was noted before, the signal is not uniformly dispersed in the interior of the capsules, but appears as small clumps where the magnetic nanobeads are located, which should not affect the DSD reactions negatively. These results show that the semipermeable microcapsules with streptavidin-coated magnetic nanobeads can be utilized to implement complex DSD reactions. This principle could be used to prepare more complex biomolecular systems, and by using nanobeads with Ni-NTA or other custom functionalization it could be possible to immobilize large sets of different biomolecules with orthogonal tags.

### 3.3.6 Encapsulation of bacteria and yeast cells

To conclude our survey of the possibilities offered by the semi-permeable poly-(PEG-DA 250) microcapsules, we explored the encapsulation of bacteria or yeast cells. Encapsulation of living organisms in microcapsules could open up a large number of applications, from directed evolution of enzymes to therapeutic use of encapsulated cells.

First, we used *E. coli* bacterial cells grown overnight and loaded them to 20 % (v/v) in the inner aqueous phase. The cells produce a yeGFP protein which allows to easily visualize them with fluorescence. While we noted some small clumps of bacteria being formed and released in the filter region after the chip inlet, this did not prevent the operation and we could successfully produce successive batches of capsules for a total operation time of about an hour. The emulsion was assessed on a cell-counting slide and we could see the presence of bacteria in the inner aqueous phase of the double-emulsions (Fig. 3.22, emulsion). The capsules were polymerized by UV exposition for 30s

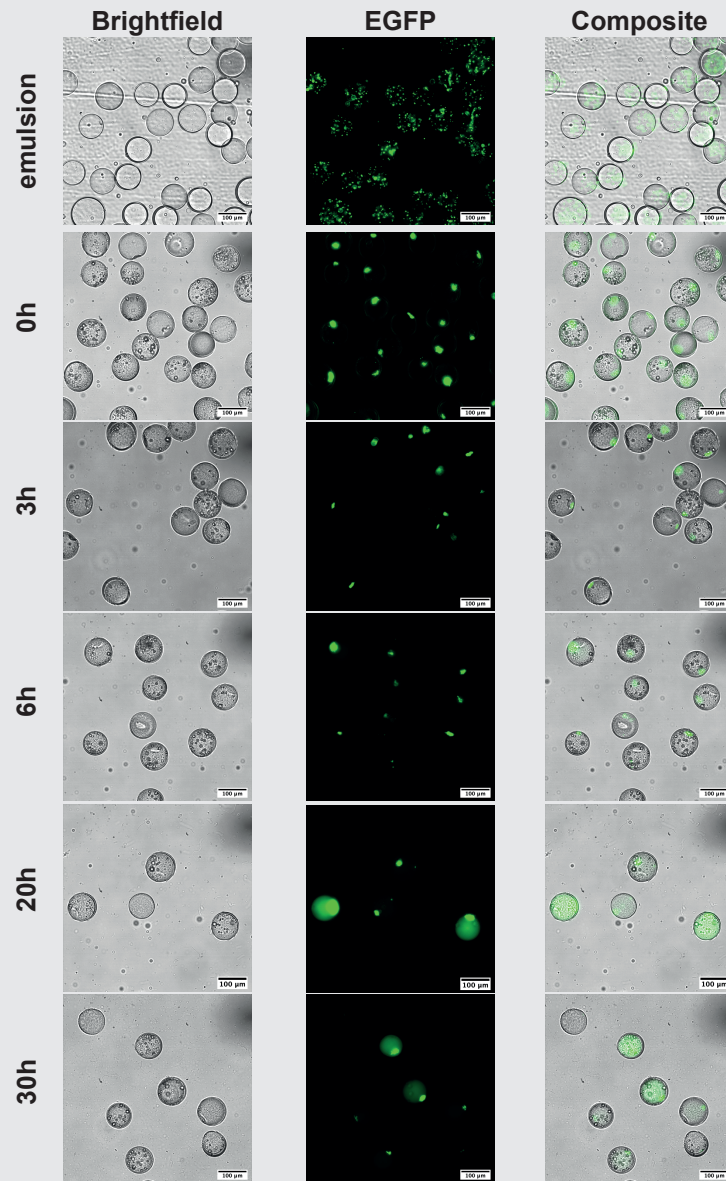


Figure 3.22: **Encapsulation and culturing of bacteria expressing a fluorescent protein.** Bacteria expressing a fluorescent protein are visible in the aqueous interior of double-emulsions. After UV polymerization and aqueous washes fluorescent bacteria are still present. After incubation at 37°C in LB medium, some capsules display an increase in fluorescent signal.

and washed extensively in buffer PBS-(Tween20 0.1 %) to remove the porogen, and then placed in LB medium for incubation at 37°C with shaking. The fluorescent bacterial cells were visible inside the microcapsules and formed small aggregates, probably resulting from the centrifugation steps of the buffer washes (Fig. 3.22, 0h). After prolonged incubation in LB at 37°C, some capsules display a diffuse fluorescent signal which could correspond to the outgrowth of bacterial cells in the interior of the capsules (Fig. 3.22, 20h and 30h). An alternative explanation would be the mechanical dissociation of the bacterial aggregates observed initially, but this would result in a picture where all capsules present a similar diffuse signal. In this case, we see a clear difference between capsules which contain the initial fluorescent aggregate and no or little diffuse fluorescence, and capsules with a high diffuse fluorescence and the aggregate still present in the capsules. After 30h of culturing, a majority of the microcapsules present a high fluorescent signal. Additional experiments should be performed to conclude that encapsulated bacteria can be cultured inside the microcapsules, for example comparing with bacteria placed in PBS-(Tween20 0.1 %) buffer and incubated at 37°C with shaking as a negative control. These results are encouraging indications that bacteria can be encapsulated and their culturing will be the focus of further investigations.

In addition to bacteria, we also encapsulated yeast cells in the semi-permeable microcapsules. An overnight culture of constitutively fluorescent yeast cells was mixed with the inner aqueous phase at 20% (v/v) and used in microcapsules production. During the double-emulsion generation, we noted again the presence of yeast aggregates passing down the inner phase channel. Nevertheless, the operation was stable and we were able to collect multiple batches of polymerized microcapsules. The presence of encapsulated yeast cells was confirmed by observation on the microscope, and with 60x magnification individual cells could be observed inside the capsules (Fig. 3.23). The yeast cells were fluorescent and appeared to have a normal morphology. However, we did not observe any change in number of yeast cells or change in signal inside the microcapsules after 2 days of culturing. Providing a longer culturing time might be beneficial, but the culture medium became contaminated with bacteria which prevented further culturing. Appropriate care and working under the flame should have minimized the risk of contamination, but the production of capsules and their washing was not performed in a sterile environment, making it difficult to prevent any contamination. In conclusion, the encapsulation of yeast cells inside the microcapsules is also demonstrated, and further studies will explore culture conditions.

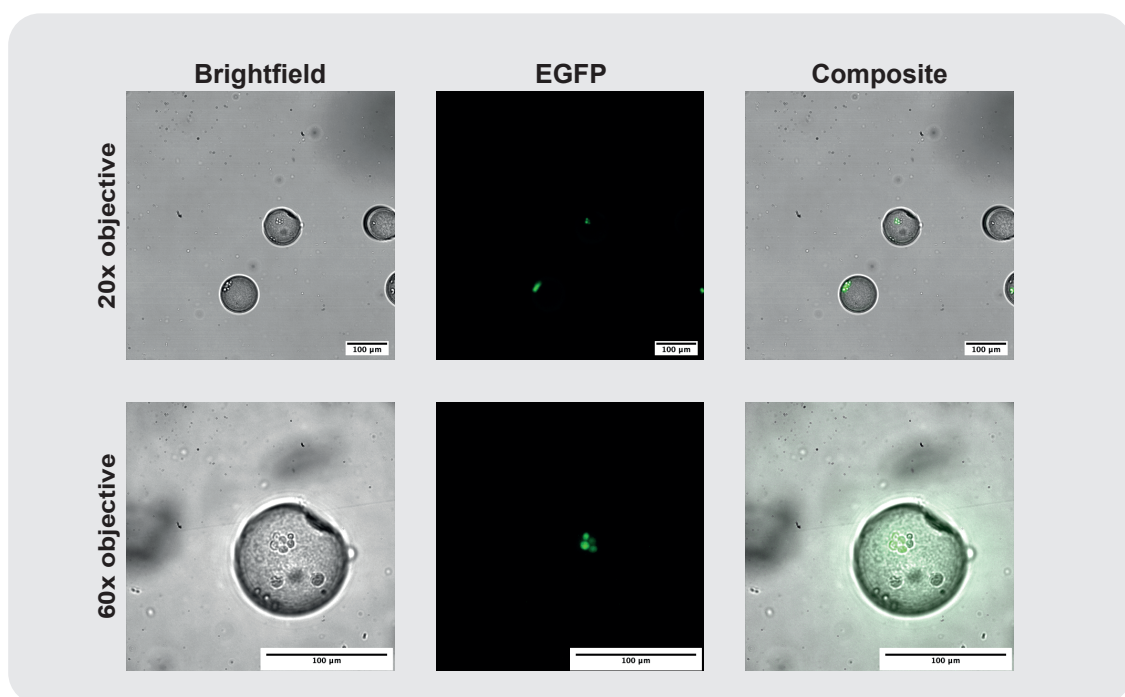


Figure 3.23: **Encapsulation of yeast cells expressing a fluorescent protein.** Yeast cells expressing a fluorescent protein are visible in the aqueous interior of UV polymerized capsules. With a 60x magnification, individual fluorescent yeast cells can be observed inside capsules.

### 3.4 Discussion

In this work, we present the production of biocompatible and semipermeable poly-(PEG-DA 250) microcapsules and their use for encapsulation of proteins, enzymes, DNA, or even bacteria and yeast cells with retained functionality. First, we show that PEG-DA 250 can be used as a polymerizable middle phase for the production of microcapsules templated from water-in-(PEG-DA 250)-in-water double-emulsion. The generation of such double-emulsion does not require the use of a co-axial capillary device [109], but can be produced in a PDMS device with non-planar geometry which does not require any surface treatment [209]. The relatively simple method and reproducibility in the fabrication and use of untreated PDMS device for the production of poly-(PEG-DA 250) microcapsules should make this method available for interested labs with access to soft lithography fabrication. By adding an inert diluent to the PEG-DA 250 middle phase, we show that semipermeable microcapsules can be formed by polymerization-induced phase separation (PIPS). This technique was previously used in the formation of semi-permeable microcapsules made from other acrylate based polymers such as blends of ETPTA/GMA [108] or EDGMA/GMA [207]. While the semi-permeability of the capsules was demonstrated, no direct encapsulation of biological components was achieved, apart from the encapsulation of plasmid DNA in the ETPTA/GMA microcapsules in Niederholtmeyer *et al.* [125]. It is interesting to note that the plasmid DNA contained in these capsules could serve as a protein expression template after immersion in a cell-free transcription translation system. However, the ETPTA/GMA capsule had to be reacted first with amino-PEG12-alcohol to prevent the adsorption of proteins on the capsules shell. Moreover, this also indicates that the direct encapsulation of proteins or enzymes would have been precluded by the use of such polymers. Here, we confirm previous observation from Nam *et al.* [109] that poly-(PEG-DA 250) microcapsules do not lead to the adsorption of biomolecules and in particular of proteins or enzymes, allowing their direct encapsulation in the interior of the semi-permeable microcapsules. The encapsulated proteins show no sign of adsorption even after prolonged times of more than a year in some cases. Moreover, the very small pores obtained by PIPS when using butyl-acetate as a porogen can be estimated to be close to or even smaller than the hydrodynamic radius of the 32.7 kDa recombinant EGFP protein. This will allow for the encapsulation of a variety protein, enzymes, RNA, DNA or (bio)-molecule of interest as long as their size is not smaller than this cut-off. We show that the encapsulation of active enzymes is possible and that the semi-



permeability of the capsules overcomes the opposing challenges of the stable encapsulation without release of the enzyme, while at the same time allowing the diffusion of reactants and products in and out of the capsules. Alternatively, we propose that the encapsulation of streptavidin, functionalized magnetic beads or other functionalized molecules of appropriate size can serve as an immobilization partner for smaller molecules. In future developments, this could serve to immobilize peptides and small proteins with appropriate tags, or even small molecules, which could be activated or released upon sensing of an external stimulus. This is demonstrated by the immobilization on encapsulated streptavidin of short strands of DNA modified with a biotin handle, which served in the implementation of a two-layer signalling cascade from DNA strand displacement (DSD) reactions. While the original implementation of DSD reactions in microcompartments proposed by Joesaar *et al.* [192] was performed in proteinosomes, we show that our semi-permeable microcapsules are adapted for the design of such complex synthetic biology application. The semi-permeability of proteinosomes produced by Joesaar *et al.* probably present more narrow size cut-offs as it is primarily defined by the length of the cross-linking agent and size of the protein used. However, their production in a shaken emulsion results in a range of capsules sizes, which required the use of a microfluidic device containing traps and valves for the loading and perfusion of the proteinosomes population. As the authors note, it should be possible to obtain proteinosomes with narrow size distribution by using microfluidic production methods [210]. Our microcapsules show a very narrow size distribution, and their convenient manipulation allows us to rapidly image them on a simple cell counting slide. Indeed, one attribute of our microcapsules is their chemical and physical stability, which should allow to prepare such distributed computing systems, store them and manipulate them repeatedly without concerns in the compartments stability. Consortia of functional compartments are indeed of key interest in the bottom-up construction of complex biomolecular systems [110, 211] and we hope that our work will contribute to these exciting and challenging developments. To add some flexibility and other features to our microcapsules, we show that the immobilization of biomolecules can be achieved after encapsulation not only using encapsulated FITC-streptavidin, but also with functionalized magnetic nanoparticles, which can be used to immobilize an anti-GFP antibody and subsequent binding of EGFP from the surrounding solution, or to implement DSD reactions with the same success as when using encapsulated FITC-streptavidin. We also show preliminary evidence that even live bacteria or yeast cells can be encapsulated and suggest that bacteria are able to multiply after cultivation. While these are very preliminary results, such possibility would open up

a wide array of synthetic biology application by encapsulating cells with diagnostic or therapeutic functionalities. Regarding the encapsulation of the therapeutic enzyme PAL, further improvements need to be made to obtain microcapsules capable of containing active PAL enzyme and protect it from proteolytic digestion. Indeed, preliminary experiments showed that the enzymatic activity of PAL in capsules was reduced, similar to what we observed with econoLuciferase encapsulation. Moreover, the semipermeable capsules size cutoff is probably just large enough to allow the entry of proteases such as trypsin and chymotrypsin with sizes around 25 kDa. However, we believe that it will be possible to form smaller pores by changing the porogen or adjusting its concentration, or alternatively to use protease inhibitors co-encapsulated with PAL to protect it from proteolytic digestion. In conclusion, we envision our biocompatible microencapsulation platform to have broad applications in the building of innovative encapsulated diagnostic and therapeutic systems containing active biomolecules or living cells.

## Acknowledgments

We thank Rohan Thakur for his contribution in setting up the syringe pumps in our lab and for his contributions in initial platform development. We thank Jui-Chia Chang, Gianluca Etienne and the SMaL lab at EPFL, for supplying us with the photomask and for their help with preliminary experiments.

4

**A high-throughput microfluidic  
nano-immunoassay for detecting  
anti-SARS-CoV-2 antibodies in serum  
or ultra-low volume dried blood  
samples**

## 4.1 Background

Serological surveys studying the presence of anti-SARS-CoV-2 antibodies are an important tool in better understanding the evolution of COVID-19 pandemic and multiple studies have been conducted in different places and setting worldwide, such as patients hospitalized in New York [212] or Glasgow [213], healthcare workers caring for COVID-19 patients in Korea [214], households in Brazil [215] or the population in Geneva [216]. In Switzerland, a nationwide program has been implemented, in which multiple seroprevalence studies studying different aspects of COVID-19 spread will be conducted and coordinated [217]. With close to 30'000 tested subjects, this study requires the involvement of multiple entities, and will rely on the collection of 7.5 mL to 20 mL of blood by venipuncture and analyse serum or plasma samples using an immunoassay developed in-house using a trimerized full Spike antigen on a Luminex platform [218]. Such program should provide high quality data on the levels of anti-SARS-CoV-2 antibodies in the population and subpopulations selected by profession, such as health care workers, food retailers, post office employees, or selected by specific risk, such as nursing home residents or asylum seekers, to name a few examples of this great initiative. In the spring of 2020, our lab got involved as part of the EPFL task force on COVID-19 with the goal of providing tools to facilitate the conduction of large epidemiological surveys measuring the levels of anti-SARS-CoV-2 antibodies. Indeed, conducting large epidemiological surveys can present significant challenges with human resources, logistics and cost associated with sample collection and analysis. A high-throughput nano-immunoassay technology developed previously in the lab [219, 220] was proposed to detect anti-SARS-CoV-2 antibodies. With its open platform, the microfluidic chip can be repurposed to perform different immunoassays, and promising results were rapidly obtained in detecting anti-SARS-CoV-2 antibodies in serum by using the same trimerized full Spike protein antigen used by Fenwick *et al.* [218] and produced by the EPFL protein production and structure core facility. While the microfluidic nano-immunoassay offers high-throughput and reduced consumption of sample and reagents per assay, such advantages might be offset by the requirement of obtaining serum samples in a centralized entity such as a hospital, where the infrastructure is generally well suited to analyze large numbers of blood samples obtained by venipuncture in a fully automated way. In order to offer the possibility to conduct serological surveys in lower resources settings, whether it is in countries lacking a dense health-care network, or in accessing subjects living in more remote areas, we explored the possibility to

use decentralized sample collection using blood microsampling. We believe that combining such sample collection with high-throughput, low sample volume and reduced costs nano-immunoassays would offer a great addition to existing options. This could indeed satisfy many of the criteria as proposed by the WHO for the selection of diagnostic tests, ASSURED: Affordable, Sensitive, Specific, User-friendly, Rapid and robust, Equipment-free, Deliverable to end-users [221, 222]. In the current landscape of assays available for anti-SARS-CoV-2 serological surveys, two main options are offered, which are on one hand the use of standard ELISAs or clinical immunoanalyzers, and on the other hand the use of lateral flow immunoassays (LFIA). LFIAs have advantages related to the criteria of being affordable, user-friendly, rapid and robust, equipment-free, deliverable to end-users, and generally have sufficient specificity [223], which would make them an attractive tool for serological studies. However, most of the LFIAs suffer from low sensitivity [224, 225, 226]. The sensitivity could be even lower than reported when considering samples from subjects in the general population who have not been PCR confirmed [227]. An additional limitation of LFIAs results from the qualitative visual readout, which can be ambiguous to interpret, does not provide any information on antibody levels and does not give a digital readout which can be easily recorded. Moreover, the test is destructive in the sense that no sample is left for further reanalysis.

On the other hand, immunoassays performed on serum or plasma using ELISA or clinical immunoanalyzers [228, 218, 224, 229] offer very good performance characteristics with generally 100 % specificity and sensitivity above 98 %. However, these tests require a large infrastructure and the use of large volumes of samples generally obtained by venipuncture. To facilitate sample collection and the logistics associated with serosurveys, some studies have proposed to combine the use of microsampling with standard immunoassays. The most commonly used microsampling method consists in placing capillary blood specimen on filter paper and then elute subpunches in buffer before analysis as has been used for neonatal screening programs, allowing for the measurement of anti-SARS-CoV-2 antibodies with good agreement with serum samples [230, 231, 232]. However, the results can be altered by the hematocrit concentration which would result in an under or overestimation of the antibody levels [233]. By using a microfluidics-assisted collection of capillary blood on a device called Hemaxis<sup>TM</sup>, it would be possible however to obtain dried blood spots of defined volumes which can be entirely eluted for a precise control of analyte concentration without influence of the hematocrit levels [234]. To obtain the same precise control of the sample volume, some groups have used another technology called volumetric absorptive microsampling (VAMS)

[235] which allows to collect a capillary blood sample of defined volume on the polymeric tip of devices called Mitra<sup>®</sup>. The samples are eluted by placing the polymeric tips in microplates containing buffer and the supernatant is analyzed with a standard immuno-assay [236, 237]. While this use of microsampling is very promising, the sample volume requirements for the analysis were important, with at least 100  $\mu\text{L}$  of eluted sample for standard ELISA [237] or 200  $\mu\text{L}$  with a Roche Elecsys assay [236]. This would imply that not more than 1 datapoint can be obtained from a 20  $\mu\text{L}$  capillary blood sample eluted in 200  $\mu\text{L}$  buffer using Roche Elecsys. Using our nanoimmunoassays, only a few nanoliters are consumed per datapoint, and only 20  $\mu\text{L}$  of eluted sample are necessary to be placed in the 384-well source plate used for the spotting step required to load the samples in our assay. This allowed us to chose HemaXis<sup>TM</sup> and Mitra<sup>®</sup> devices collecting only 10  $\mu\text{L}$  of sample making it even more convenient for end-users. With such low-volume requirements, we even explored the possibility to use glucose test strips collecting 0.6  $\mu\text{L}$  of capillary blood and eluted in only 30  $\mu\text{L}$  of buffer. The different dried blood collection methods would allow the collection at the point-of-care, with simplified logistics, reduced biosecurity risks by virus safely contained in the dried state, and eluted in detergent-containing buffer thereby inactivating envelopped viruses such as SARS-CoV-2 [238]. We also considered alternatives to the microsampling technologies we used, such as devices that can directly separate serum from blood obtained by fingerprick at the point-of-care [239, 240, 241, 242]. While there are a number of devices available, they had the drawback of presenting higher costs and generally required higher volumes to be obtained from the fingerprick. Although it might be important to obtain serum to test for certain analytes where whole blood samples are not compatible with analysis, it was not the case for the detection of anti-SARS-CoV-2 antibodies. Finally, the use of saliva samples could be interesting due to its relatively simple collection, and it has been successfully used in the detection of anti-SARS-COV-2 [243]. However, the sensitivity observed in samples collected more than 21 days post-symptom onset was only 84.2 % when used in conjunction with EuroImmun IgG ELISA kit. In addition, the sample collection is not significantly more convenient than a fingerprick, and the sample processing steps are not as well established as for dried blood samples. We believe that blood obtained via fingerprick and placed on microsampling devices for controlled volume collection is a convenient sampling method and has great complementarity with the microfluidic high-throughput nano-immunoassay, and we present the work performed in collaboration with University Hospitals of Geneva in section 4.2.

## 4.2 Preprint

The work presented in this section has been made available as a preprint in *medRxiv*, 2020.

**Authors:** Zoe Swank, Grégoire Michielin, Hon Ming Yip, Patrick Cohen, Diego O. Andrey, Nicolas Vuilleumier, Laurent Kaiser, Benjamin Meyer, Sebastian Maerkl

**Reference:** Swank Z, Michielin G, Yip HM, Cohen P, Andrey DO, Vuilleumier N, et al. A high-throughput microfluidic nano-immunoassay for detecting anti-SARS-CoV-2 antibodies in serum or ultra-low volume dried blood samples. *medRxiv*. Cold Spring Harbor Laboratory Press; 2020 Oct 29;26:1033–5. DOI: 10.1101/2020.10.07.20208280

This work is licensed under the Creative Commons Attribution 4.0 International License  
<http://creativecommons.org/licenses/by/4.0/>

### 4.2.1 Abstract

Novel technologies are needed to facilitate large-scale detection and quantification of SARS-CoV-2 specific antibodies in human blood samples. Such technologies are essential to support seroprevalence studies, vaccine clinical trials, and to monitor quality and duration of immunity. We developed a microfluidic nano-immunoassay for the detection of anti-SARS-CoV-2 IgG antibodies in 1024 samples per device. The method achieved a specificity of 100% and a sensitivity of 98% based on the analysis of 289 human serum samples. To eliminate the need for venipuncture, we developed low-cost, ultra-low volume whole blood sampling methods based on two commercial devices and repurposed a blood glucose test strip. The glucose test strip permits the collection, shipment, and analysis of 0.6  $\mu$ L whole blood easily obtainable from a simple fingerprick. The nano-immunoassay platform achieves high-throughput, high sensitivity and specificity, negligible reagent consumption, and a decentralized and simple approach to blood sample collection. We expect this technology to be immediately applicable to current and future SARS-CoV-2 related serological studies and to protein biomarker diagnostics in general.

### 4.2.2 Introduction

The emergence of a new coronavirus at the end of 2019, termed severe acute respiratory syndrome coronavirus 2 (SARS-CoV-2), led to an unprecedented global public health crisis [244]. Within  $\sim 10$  months, it is estimated that SARS-CoV-2 infected 35 million people worldwide and 1 million people died of coronavirus disease 2019 (COVID-19) caused by SARS-CoV-2 [245]. As SARS-CoV-2 causes mainly mild disease or infection presents without symptoms, many cases are not captured by direct testing in the acute phase of disease [246]. However, to estimate infection fatality rate and guide public health decisions, it is of utmost importance to establish the true spread or prevalence of the virus by identifying how many people have been exposed [247, 248].

Detection of anti-SARS-CoV-2 antibodies using highly sensitive and specific assays can help answer these questions. Several seroprevalence studies have already been conducted, demonstrating rather low seroprevalence rates even in areas that were severely affected [249, 250, 251, 252]. Such data show that herd immunity through natural infection is far from being reached. However, these studies are merely snapshots of an evolving situation, both in time and space. Therefore, there is a sustained need for seroprevalence studies to be continuously conducted in order to monitor virus spread and to keep policy makers informed. In addition, tens to hundreds of thousands of blood samples will need to be tested to determine antibody titers for each SARS-CoV-2 vaccine phase 3 clinical trial and a large number of samples will need to be tested to monitor immune responses after a vaccine has been approved and rolled-out. Such studies are cumbersome and expensive to perform as they require large-numbers of serum samples to be obtained by venipuncture and analysed by highly sensitive and specific immunological assays to classify samples or to provide quantitative information on antibody titers.

Several assays, such as enzyme-linked immunosorbent assays (ELISA) or chemiluminescent immuno-assays (CLIA), are commercially available, but mainly rely on serum drawn by venipuncture. These tests are also rather expensive, with reagent costs on the order of 3-10 USD per test. Alternatively, in-house ELISAs are difficult to standardize and require high amounts of recombinant antigen, usually around 100ng per sample [248]. Other recently developed methods such as miniaturized high-throughput ELISAs that use low microliter volumes suffer from lower sensitivity [253], and ultra-sensitive assays based on digital ELISA have a low sample throughput of 68 tests per hour [254]. The comparatively high cost of these assays and the reliance on serum samples



taken by venipuncture are considerable hurdles to performing large-scale studies under normal circumstances, but especially so during a pandemic, when sample collection can put clinical staff and study participants at risk. Lateral flow assays (LFAs) can be performed at the point of care or at home requiring only a "drop" of whole blood, but the sensitivity and specificity of these assays is often insufficient [255, 256, 257] and LFAs are relatively expensive at ~22 USD per test. Furthermore, LFAs provide test results but no blood samples are being collected which could be used for follow-up analyses.

There is therefore a clear need for new technologies to supersede existing methods such as ELISA, CLIA, and LFAs. Novel technologies should be capable of high-throughput, low-reagent consumption, low-cost per test, high sensitivity and specificity, and be compatible with ultra-low volume whole-blood samples in the low or even sub-microliter range that can be obtained via a simple fingerprick. Biomarker detection using dried whole blood on filter paper or other devices would have tremendous advantages as it can be collected by untrained individuals at home. The samples could then be conveniently shipped by regular mail at ambient temperature to a central laboratory for analysis and test results returned electronically via a mobile app or email.

In this study we developed and validated a nano-immunoassay (NIA) that analyses 1024 samples in parallel on a single microfluidic device the size of a USB stick. NIA reagent consumption and corresponding costs are roughly 1000 times less than a standard ELISA. Based on the analysis of 134 negative and 155 positive control sera, NIA achieved a specificity of 100% and a sensitivity of 98% when RT-PCR was used as a reference. NIA performed as well as a standard ELISA for samples obtained more than 20 days post onset of symptoms, and performed better than ELISA for samples obtained less than 20 days past onset of symptoms, indicating that NIA is more sensitive than ELISA for the analysis of early timepoint samples with lower antibody titers. We go on to demonstrate that NIA can be used to measure anti-SARS-CoV-2 antibodies in ultra-low volume dried whole blood samples, eliminating the need for venipuncture blood collection. We tested two commercial blood collection devices: Neoteryx's Mitra<sup>®</sup> and DBS System SA's HemaXis<sup>™</sup> DB10, and show that it is possible to repurpose low-cost and widely available blood glucose test strips for sample collection and shipment. Samples could be stored up to 6 days at room temperature with minimal sample degradation and all three methods yielded better results than an ELISA performed on standard serum samples collected from the same individuals.

## 4.2.3 Results

### 4.2.3.1 Nano-immunoassay development

We adapted a MITOMI based [258, 259] 1024 NIA device previously applied to vaccine adjuvant screening [260] and the detection of inflammatory and cancer related protein biomarkers in serum [261] to the detection of anti-SARS-CoV-2 IgG antibodies. The NIA device described here is a simplified version of the original 1024 serum analyzer chip and more similar to the original MITOMI device with slightly enlarged chambers to accommodate spotted patient samples. The microfluidic device is a standard two-layer polydimethylsiloxane (PDMS) device [262], consisting of a flow and a control layer. Fluids in the flow layer can be manipulated with pneumatic valves formed by the control layer. The device contains 1024 unit cells, each consisting of an assay and a spotting chamber (Figure 4.1A). Patient samples are spotted onto an epoxy-coated glass slide using a contact-printing microarray robot, on top of which the PDMS device is aligned and bonded. Patient samples are initially isolated by actuating the neck valve and the surface of the assay chamber is patterned with biotinylated bovine serum albumin (BSA-biotin) and neutrAvidin, leaving a circular surface region coated with neutrAvidin beneath the MITOMI button. Afterwards, biotinylated anti-His antibody is flowed through the device, enabling the subsequent immobilization of a His-tagged SARS-CoV-2 antigen. Patient samples are then solubilized and the sandwich valves are closed, allowing any SARS-CoV-2 specific antibodies to diffuse into the assay chamber and bind the surface immobilized antigen. The MITOMI button is closed following an incubation period and any unbound material is washed away. A secondary antibody labeled with phycoerythrin (PE) is flowed to detect the presence of antibodies bound to the SARS-CoV-2 antigen (Fig. 4.1B, C).

We optimized the NIA for detection of anti-spike IgG antibodies in human serum by first testing several different spike antigen variants and identified the in-house produced trimerized full-length spike protein as the most suitable antigen (Fig. 6.5). The use of trimerized full length spike and spike-receptor binding domain (RBD) both resulted in high signal intensities and low-background. We decided on using the trimerized full-length spike protein as it most closely resembles the natural conformation of the SARS-CoV-2 spike protein. As a proof-of-concept we added chimeric anti-spike antibody at different concentrations into human serum, spotted each dilution, and showed that NIA could quantify anti-spike antibody concentrations (Fig. 4.1D, E). Based on this sandwich immunoassay we estimate that our limit of detection (LOD) is around 1 nM IgG. To permit the

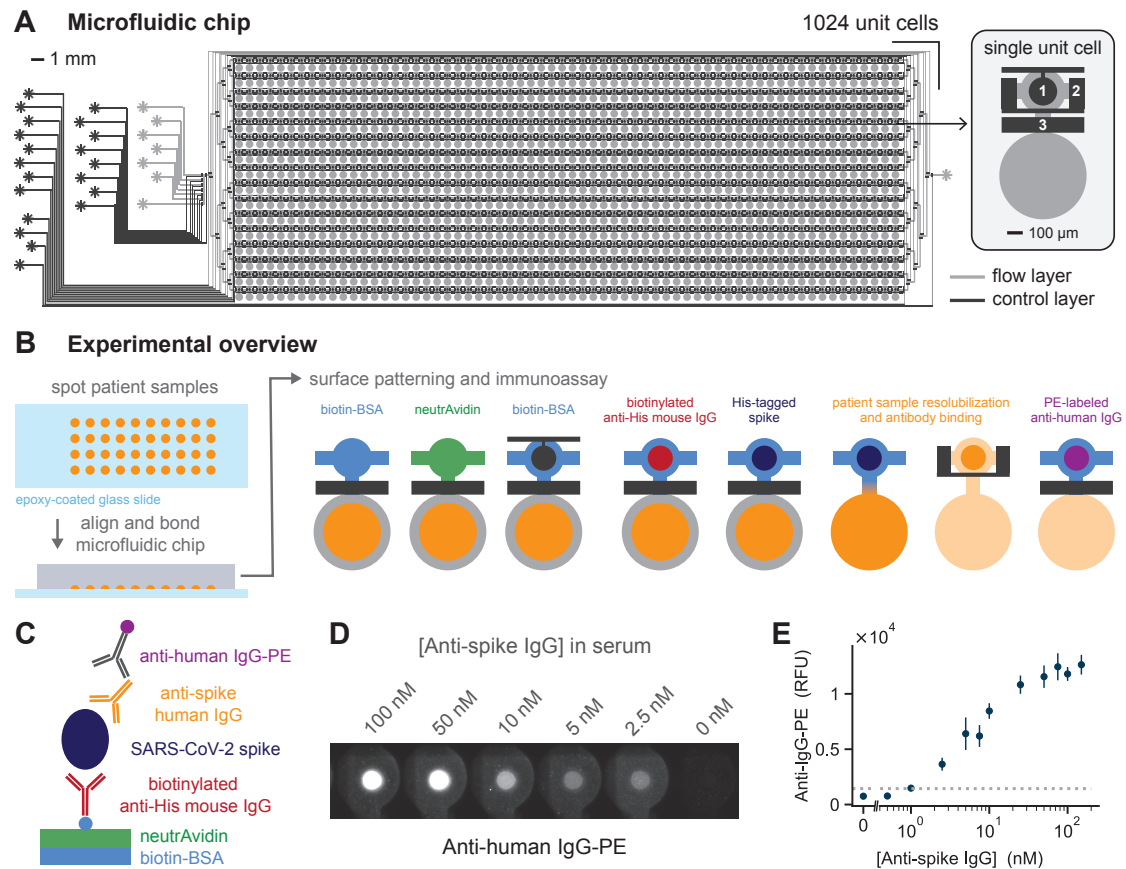


Figure 4.1: **High-throughput microfluidic nano-immunoassay for anti-SARS-CoV-2 antibody detection.** (A) The two-layer microfluidic chip design consists of 1024 unit cells. Each unit cell in turn contains two sections: an immunoassay chamber (top) and a spotting chamber (bottom). Control valves include the button (1), sandwich (2) and neck (3) valves. (B) A schematic of the experimental process, starting with the spotting of patient samples, followed by chip alignment and bonding, biotin-BSA and neutrAvidin surface patterning, and lastly the immunoassay for detection of anti-SARS-CoV2 antibodies. Surface patterning and immunoassay are shown for a single unit. During the experiment all unit cells are processed in parallel. (C) Schematic of the on-chip sandwich immunoassay. (D) Fluorescence images of anti-human IgG-PE signal for a given concentration of anti-spike antibodies present in human serum. (E) Quantification of the anti-human IgG-PE signal for a range of anti-spike concentrations spotted. The dashed horizontal line indicates the LOD.

analysis of patient sera in a standard, biosafety level 1 (BSL-1) laboratory we developed a simple treatment protocol that renders the sera BSL-1 compatible. This was achieved by conducting a short heat-inactivation step, followed by the addition of Triton X-100 to a final concentration of 1% [263]. Dried whole blood samples could be safely handled in a BSL-1 environment without requiring any pre-treatment steps.

#### **4.2.3.2 Nano-immunoassay validation**

We validated the high-throughput NIA for the detection of SARS-CoV-2 anti-spike IgG antibodies with 289 serum samples, collected from 155 PCR-confirmed SARS-CoV-2 infected individuals and 134 pre-pandemic negative samples collected in 2013/14 and 2018. Different serum sample dilutions, ranging from no dilution to a 1:256 dilution, were spotted to determine the optimal value (Fig. 6.6). NIA achieved a maximum specificity and sensitivity of 100% and 98%, respectively, at a serum dilution of 1:8 (Fig. 4.2A, 6.6) and a receiver operator characteristic (ROC) curve with an area under the curve (AUC) equal to 0.99 (Fig. 4.2B). In parallel, ELISA was used to validate the presence of anti-spike(S1) IgG in the same patient samples (Fig. 4.2C) resulting in a good correlation ( $R^2=0.87$ ) between NIA and ELISA measurements (Fig. 4.2D). As the serum samples were obtained from patients at different time points post onset of symptoms we plotted the NIA results according to when samples were obtained (Fig. 4.2E). We also analyzed NIA and ELISA results split into samples obtained on or before 20 days post onset of symptoms (DPOS) and samples obtained after 20 days post onset when antibody responses are usually fully developed (Fig. 4.2A, C). If DPOS was not known for a given patient, then days post diagnosis (DPD) was used instead. Performance in terms of specificity and sensitivity between NIA and ELISA are similar for samples obtained after 20 days past onset of symptoms, but NIA outperforms ELISA for samples collected on or before 20 days post onset in terms of sensitivity by 13 percentage points (Fig. 4.2F).

Each sample dilution was tested in triplicate, enabling us to test up to 336 different samples or sample dilutions on a single device. In order to determine if it would be possible to further increase throughput by reducing the number of replicates we randomly selected one or two of the three 1:8 dilution replicates and calculated ROC curves, specificity, and sensitivity (Fig. 6.7). We found that using duplicates only slightly reduced sensitivity from 98% to 97%, whereas using a single measurement lowered sensitivity to 95%, all the while retaining a 100% specificity. Given that using duplicate measurements led to only a minimal change in sensitivity, it will be possible to increase

throughput to 512 samples analyzed in duplicate per device. Additional gains in throughput are theoretically possible by scaling the device itself, with MITOMI devices containing up to 4160 unit cells having been demonstrated in the past [264].

To assess device to device reproducibility we tested all serum samples (1:8 dilution) on two separate devices which resulted in a correlation of  $R^2 = 0.98$  (Fig. 6.8A). We then correlated the measurements from one of those devices to the measurements made on six other devices and again observed a good correlation of  $R^2 = 0.95$  (Fig. 6.8B). In the first case the same sample solution was used for spotting two devices, whereas in the second case the two measurements being compared came from separately prepared patient sample dilutions. Additionally we compared the anti-IgG-PE signal measured for a reference serum dilution series on three separate devices and computed an average coefficient of variation equal to 11.7% for the dilutions measured (Fig. 6.8C, D).

To determine quantitative antibody titers in each serum sample, we fit data from the full dilution series to a saturation binding curve model, enabling us to extract the dilution equivalent to the half-maximum signal for each serum sample ( $EC_{50}$ ) (Fig. 4.2G, 6.9). Using the calculated  $1/EC_{50}$  value, we again analyzed the NIA results, resulting in a specificity and sensitivity of 100% and 98%, respectively (4.2H). Lastly, we compared the  $1/EC_{50}$  values to values obtained from a single 1:8 dilution and found an excellent correspondence between those two measurements (Fig. 4.2I), indicating that a single measurement returns accurate quantitative information on antibody concentrations. Only at very high antibody titers does the signal saturate for the 1:8 dilution. Using two measurements of a 1:8 and one slightly higher dilution could therefore maximize throughput, specificity, and sensitivity of NIA, and return accurate antibody titer values.

#### **4.2.3.3 Ultra-low volume whole blood collection and analysis**

The NIA platform proved to be highly specific and sensitive when applied to standard serum samples. We recognized that use of serum samples limits the applicability of our and other methods to samples collected by venipuncture, which has to be performed by trained personnel in hospitals or point of care settings. Venipuncture requires large volumes of blood in the 5 mL range, considerable downstream sample processing, and a cold chain from point of sample collection to point of analysis. Large-scale seroprevalence studies are thus challenging to conduct, especially when including remote or large geographic areas. Establishing a large-scale, low-cost, and widely accessible serology platform necessitates the development of venipuncture alternatives. For this reason,

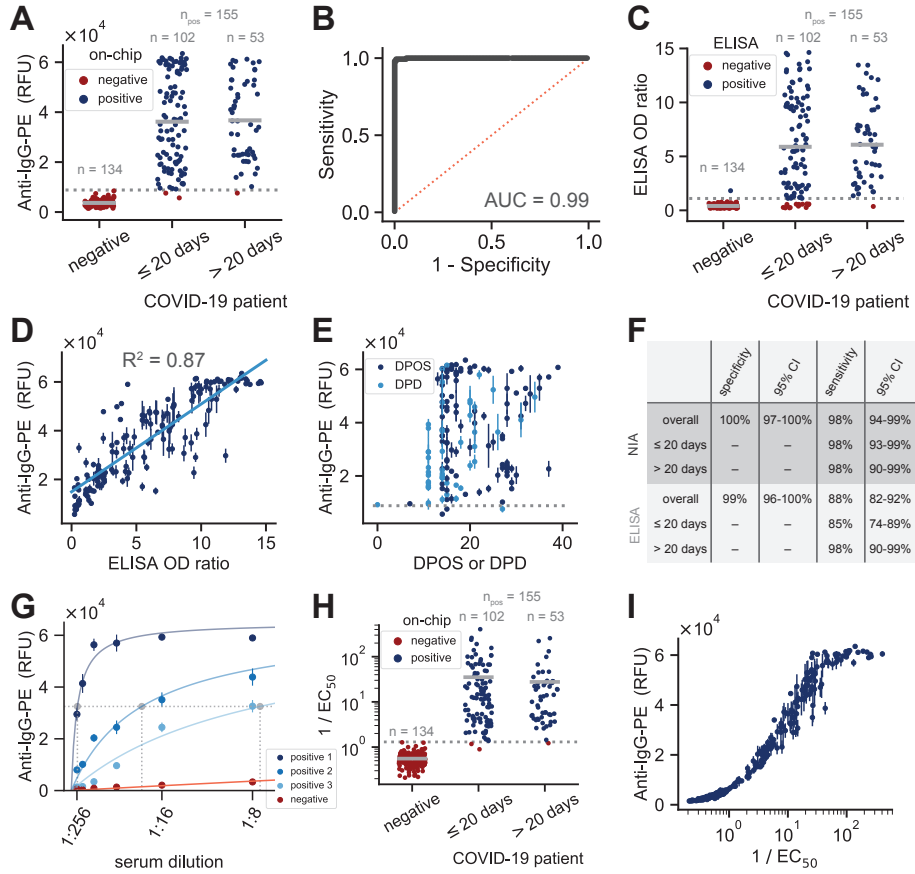


Figure 4.2: **Nano-immunoassay validation.** (A) NIA anti-IgG-PE signal for serum samples obtained from SARS-CoV-2 negative individuals (obtained in 2013/14 and 2018) or SARS-CoV-2 RT-PCR confirmed positive patients. Measurements shown are for a 1:8 dilution of each serum sample. Data points represent mean values of 3 replicates from a single chip. A total of 6 devices were run to collect this data. (B) ROC curve corresponding to the measurements shown in panel A. (C) ELISA OD ratios for the same serum samples as in A. (D) Correlation between NIA and ELISA measurements. Data points represent means  $\pm$  SD ( $n = 3$ ). (E) NIA measurements plotted versus days past onset of symptoms or days post diagnosis. Data points represent means  $\pm$  SD ( $n = 3$ ). (F) Specificity and sensitivity for NIA and ELISA. The dashed grey lines in A, C, and E indicate the cutoff used for the specificity and sensitivity calculations. (G) Examples of curve fits for three positive and one negative patient sample. The horizontal dashed line indicates half maximal binding and the three dashed vertical lines correspond to the  $EC_{50}$  values determined for each of the positive samples. (H)  $1/EC_{50}$  categorized according to whether the sample was negative or from an RT-PCR confirmed positive patient. (I) Anti-IgG-PE signal for a 1:8 dilution of each serum sample versus  $1/EC_{50}$ .

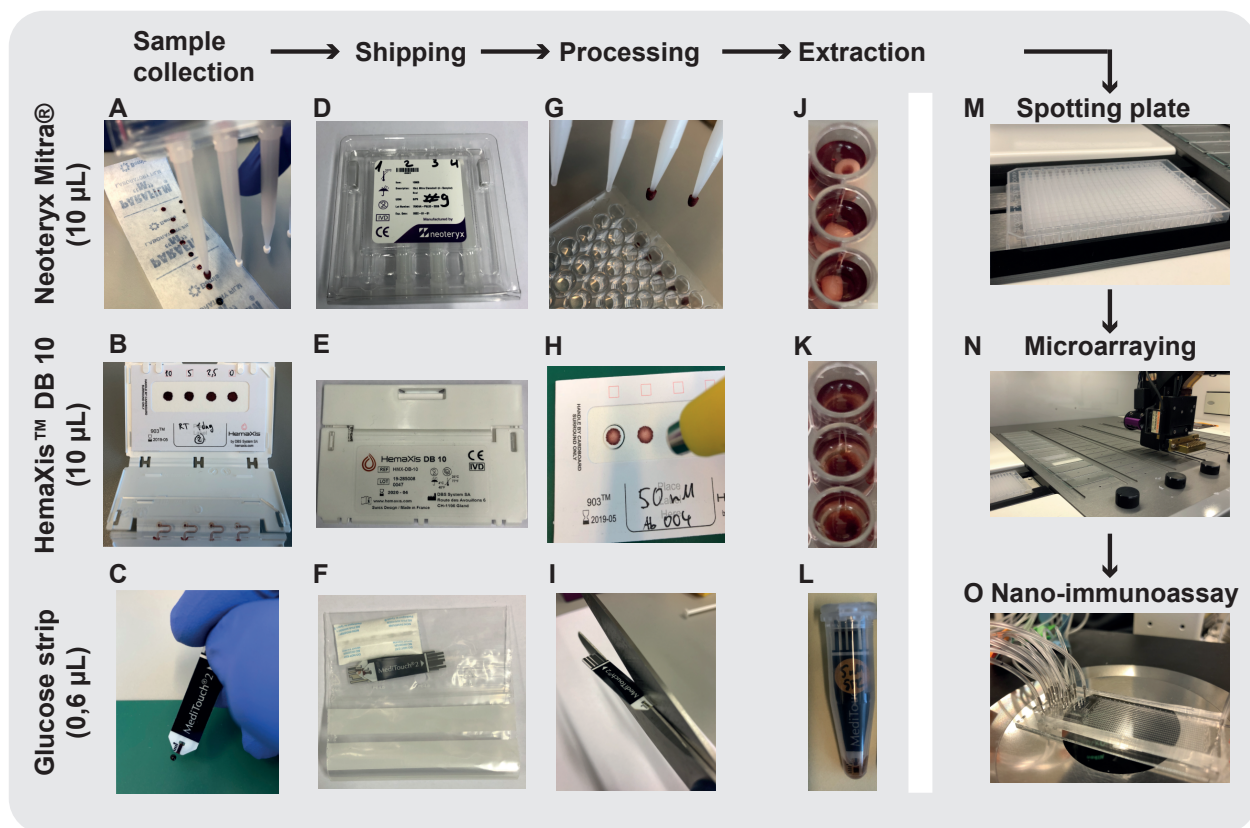


Figure 4.3: **Ultra-low volume whole blood sampling and processing.** Three devices were tested for ultra-low volume whole blood sampling and extraction: Neoteryx Mitra®, DBS System SA HemaXis™ DB10, and glucose test strips. 10 µL whole blood is collected by the (A) Mitra® and (B) HemaXis™ DB10 devices. (C) 0.6 µL whole blood is collected by the blood glucose test strip. (D-F) Blood samples are dried, allowing the devices to be shipped under ambient conditions by regular mail. (G-I) The devices are processed upon arrival at the laboratory. (G) Mitra® tips are removed and placed in a 96 well plate, (H) HemaXis™ DB10 cards are punched and the filter discs placed in a 96 well plate, (I) and the glucose test strip is cut to size and placed in an Eppendorf tube. (J-L) Blood samples are extracted in a buffer solution by overnight incubation at 4°C, followed by transfer to a spotting plate (M). Samples are then microarrayed (N), and analyzed with the NIA device (O).

we developed a sample collection and processing pipeline that enables us to carry out NIA with ultra-low volume, dried whole blood samples obtainable by a simple fingerprick. We tested three different methods to collect, ship, process, extract, and analyze dried whole blood samples (Fig. 4.3). We tested two commercially available devices that collect 10  $\mu\text{L}$  of whole blood: Neoteryx Mitra<sup>®</sup> and DBS System SA HemaXis<sup>™</sup> DB10. We also explored the possibility of repurposing existing blood glucose test strips (Medisana, MediTouch 2) for whole blood collection and shipping. The glucose test strips collect 0.6  $\mu\text{L}$  of whole blood which is approximately twenty times less than what is required by the commercial devices and 10,000 times less blood than obtained by venipuncture. Furthermore, blood glucose test strips are cheap at less than 0.5 USD per strip and widely available, potentially avoiding any supply bottlenecks during a pandemic. The two commercial devices by comparison cost 5-10 USD or 1.25 - 2.5 USD per sample.

We evaluated the three collection methods by spiking human whole blood with different concentrations of anti-spike IgG and collected the blood with each collection device. We then extracted the dried blood from each device and spotted the samples for NIA analysis. We first tested an aqueous EDTA solution and sonication for extraction [265], but the use of this buffer resulted in large and inconsistent spots during microarraying. We then tested PBS (1% BSA) or PBS (1% BSA, 0.5% Tween-20) [266] extraction buffers with overnight incubation at 4°C and found that the addition of 0.5% Tween-20 greatly improved the assay (data not shown). With this optimized sample extraction workflow we were able to quantitate anti-spike IgG from the dried blood samples (Fig. 4.4A-C).

To assess the variability of each sampling method we collected whole blood spiked with anti-spike IgG three separate times and compared the on-chip antibody signal (Fig. 6.10A-C). We calculated the coefficient of variation for the technical repeats for each anti-spike concentration tested and found that it did not exceed 15% for any of the three collection methods with an average CV of 5.7%, 7.7%, 9.2% for Mitra<sup>®</sup>, HemaXis<sup>™</sup> DB10, and the glucose test strips (Fig. 6.10D). Although, there may be further variability introduced depending on how each individual collects his or her own blood sample, each device uses a hard-coded method to collect a specific volume of blood that leads to low variability for NIA antibody detection.

As we expect these blood sampling devices to be used decentralized, followed by shipping with regular mail to a central laboratory for analysis, an important factor to assess was sample stability. To determine stability of anti-spike IgG antibodies we allowed the blood to dry on each



device followed by storage for two and six days at room temperature (23°C) before extraction and testing (Fig. 4.4D-F). Furthermore, depending on the climatic conditions, samples sent by post may be subject to higher temperatures, therefore we also stored the devices for 1 day at 55°C. For the Mitra<sup>®</sup> device we observed very little sample degradation after 6 days of storage at room temperature and slight sample degradation when stored at 55°C for one day. Very similar results were obtained for the glucose test strips. The HemaXis<sup>TM</sup>DB10 devices were the most sensitive to prolonged and high temperature storage, but still resulted in sufficient signal for accurate quantitation.

Having established that ultra-low volume dried blood samples can be analyzed on the NIA platform, we tested the method with ultra-low volume whole blood patient samples collected with each of the three collection methods. As a surrogate for capillary blood we used 36 EDTA-whole blood samples from 21 RT-PCR confirmed COVID-19 patients and 15 presumed negative patients hospitalized for other reasons that served as negative controls. We collected whole blood samples in Geneva followed by shipping via regular mail to Lausanne for analysis. All positive samples are early seroconverts obtained within 14 days post diagnosis, and thus even standard, large-volume serum samples are challenging to analyze (Fig. 4.2C). For reference measurements we prepared plasma from EDTA-whole blood samples and performed S1 ELISA assays on the same patient samples.

We directly compared results obtained by ELISA performed on standard large-volume serum samples to NIA measurements performed on ultra-low volume dried whole blood samples collected with the three collection methods and processed as described above (Fig. 4.5). ELISA detected SARS-CoV-2 specific antibodies in 62% of all COVID-19 patient samples and found no detectable antibodies in any of the 15 presumed negative samples. For the three sampling methods we set the threshold between positive and negative calls to the intensity of the second highest negative sample. All three methods identified the same 62% anti-SARS-CoV-2 IgG positive samples as the reference ELISA, but the Mitra<sup>®</sup> method was able to detect antibodies in 33% additional RT-PCR positive samples and the HemaXis<sup>TM</sup> DB10 and glucose strip methods were able to detect an additional 29%. This proof of concept study demonstrates that ultra-volume whole blood samples can be collected and analyzed on the NIA platform. Surprisingly, even difficult to quantitate samples obtained within the first 14 days post onset of symptoms could be analyzed with this approach.

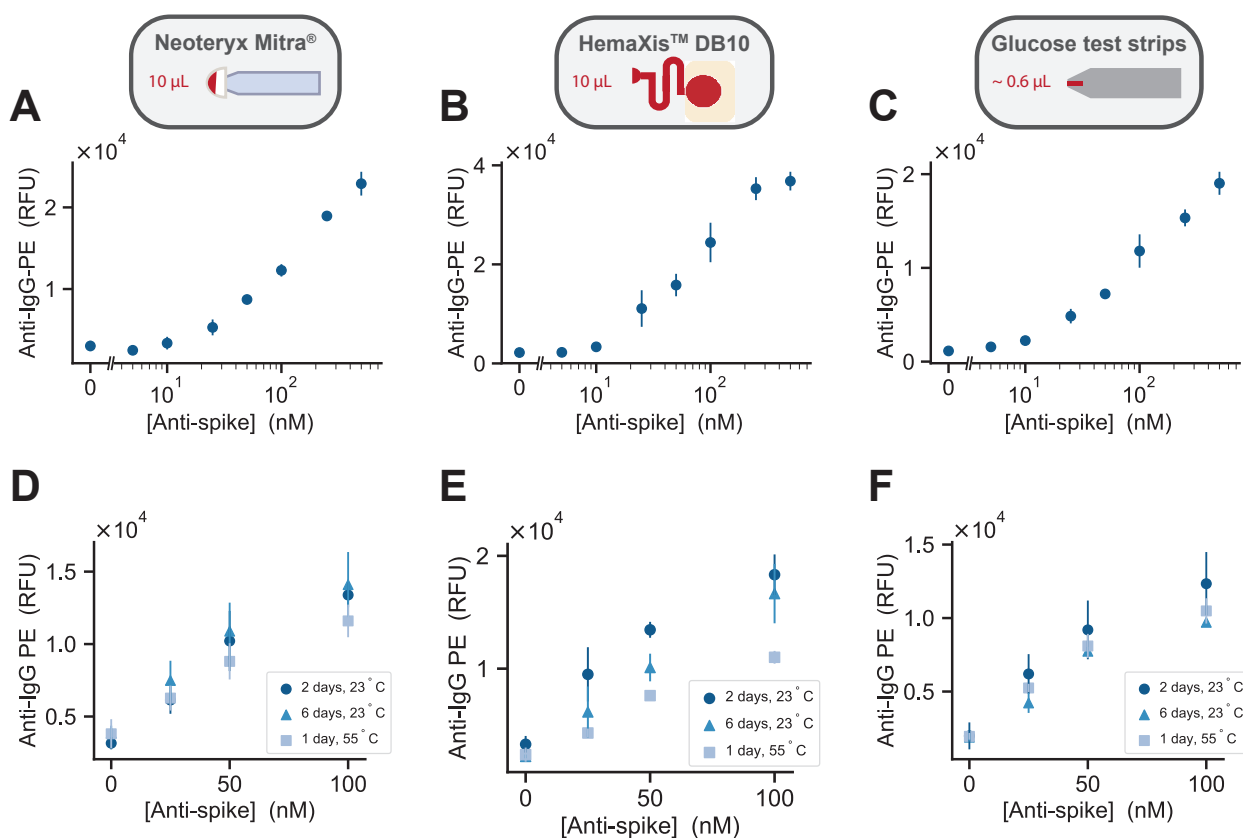


Figure 4.4: **Ultra-low volume dried blood method characterization.** The figure is organized into three columns each corresponding to the respective sampling method: Neoteryx Mitra®, HemaXis™ DB10, and glucose test strips. **(A-C)** NIA anti-IgG-PE signal versus concentration of anti-spike IgG present in dried whole blood samples collected with each of the three sampling methods. Data points represent means  $\pm$ SD (n=4). **(D-F)** Sample stability testing. NIA anti-IgG-PE measurements versus anti-spike IgG concentration. Blood samples were dried and then stored on each collection device for 1 day or 6 days at 23°C, and 1 day at 55°C.

#### 4.2.4 Discussion

We developed and validated a high-throughput nano-immunoassay device capable of analyzing 1024 samples in parallel. Detecting the presence of SARS-CoV-2 anti-spike IgG antibodies the method achieved a specificity of 100% and a sensitivity of 98% based on the analysis of serum samples from 155 positive SARS-CoV-2 infected and 134 negative individuals, performing as well or better than standard ELISA (Fig. 4.6A). In addition to generating accurate binary classification of samples,

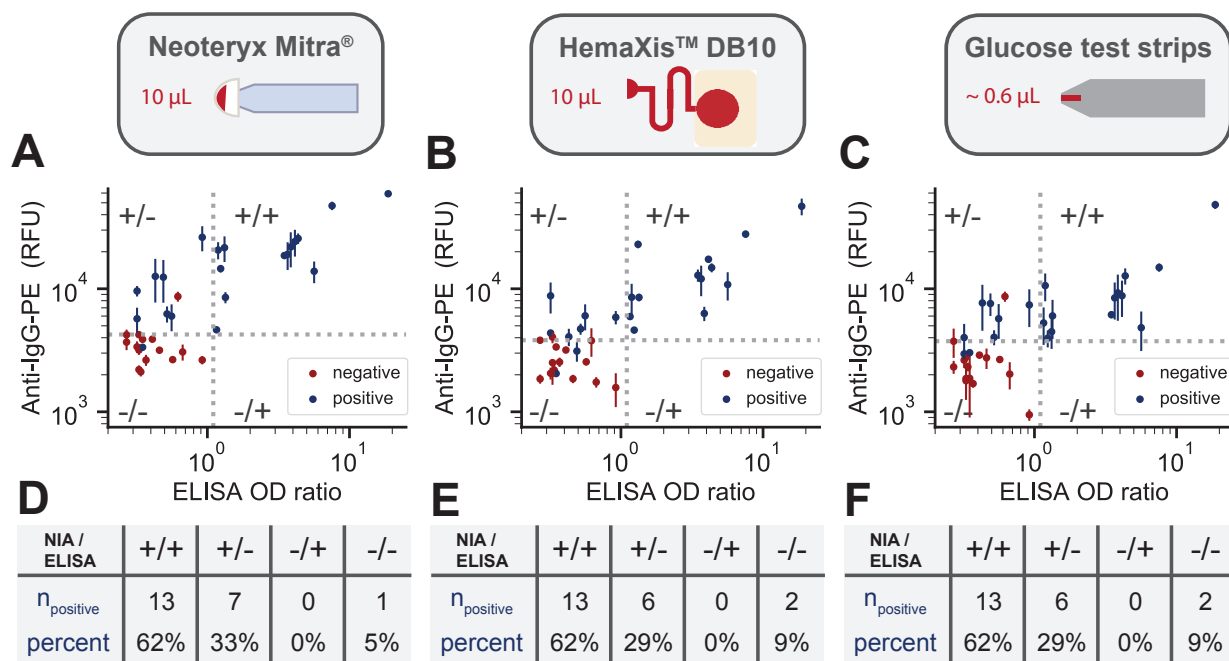


Figure 4.5: **Ultra-low volume patient sample collection and analysis.** (A-C) NIA anti-IgG-PE signal versus ELISA OD ratio for whole blood patient samples collected using each of the three sampling methods: Neoteryx Mitra®, DBS Systems SA HemaXis™ DB10, and glucose test strips. Data points are colored either blue or red corresponding to whether the samples were presumed positive or negative. The vertical dashed line represents the positive-negative cutoff for ELISA and the horizontal dashed line represents the chosen cutoff for the NIA measurements set equal to the 2nd highest negative measurement. Data points represent means  $\pm$ SD ( $n=4$ ). (D-F) Number of blue data points for each quadrant in plots A-C, respectively, along with the percentage of positive data points per quadrant.

NIA is also capable of returning accurate antibody titers.

The method developed here is applicable to the large-scale characterization of serum samples collected as part of epidemiological studies, identify donors for plasma therapy, and vaccine trial support. A single researcher can achieve a throughput of 1-2 devices, or 512 - 1024 samples per day (analyzed in duplicate) in a small research laboratory not dedicated or equipped for high-throughput molecular diagnostics. Due to increases in efficiency, a small team of 3 can likely achieve a throughput of 6 devices or 3'072 samples per day (analyzed in duplicate). By comparison, the number of RT-PCR tests performed in all of Switzerland ranged from 6'000 to 18'000 tests per

day between April and September 2020. Consumables, reagent consumption, and associated costs are negligible with NIA, which is an important consideration when compared to the high reagent cost of ELISAs and when considering potential reagent shortages that may be encountered during critical phases in a global pandemic.

Platform capabilities could be further expanded in the near term. We previously demonstrated that the platform can be used to perform multiplexed analysis, allowing 4 or more biomarkers to be tested for each sample [260, 267, 261]. This would allow the analysis of multiple antigens, cytokines, or inflammatory markers to provide insights into prior virus exposures and the response to infection. We also previously demonstrated that kinetic rate measurements can be performed in high-throughput with this method [268] and that digital ELISAs can be performed using the same technology in instances where lower limits of detection may be required [269, 254].

To enable large-scale studies we placed specific emphasis on the development of simple, low-cost, and ultra-low volume sample collection strategies and integration of these workflows with the nano-immunoassay platform. We characterized three blood sampling devices and tested all of them with patient samples. Two of these methods are commercially available devices: Mitra<sup>®</sup> from Neoteryx and HemaXis<sup>™</sup> DB10 from DBS System SA. We also explored the possibility of repurposing low-cost, and readily available blood glucose test strips for blood sample collection and shipment. The two commercial devices allow the collection of a minimal volume of 10  $\mu\text{L}$  whereas the blood glucose test strip collects as little as 0.6  $\mu\text{L}$  whole blood. Such small volumes allow untrained personnel to fingerprick and collect whole blood, eliminating the need for phlebotomists and the inconvenience of visiting a hospital or point of care location. The collected blood is allowed to dry on the devices, and we could show that these dried blood samples can be analyzed after 6 days of storage at ambient temperatures eliminating the need for a cold chain.

The combination of a high-throughput, highly specific and sensitive nano-immunoassay, and the ability to analyze minute volumes of dried blood samples has enormous potential for SARS-CoV-2 serology, epidemiological studies, vaccine trial and therapeutic development support. Further areas of use could be large-scale seroprevalence studies in low- and middle-income countries [271] without sufficient in-country laboratory capacity by sending specimens by international mail. Especially in the current SARS-CoV-2 pandemic, population-based seroprevalence studies could elucidate some urgent questions such as the impact of COVID-19 in Africa [272].

New technology and method developments such as those reported here will make it possible

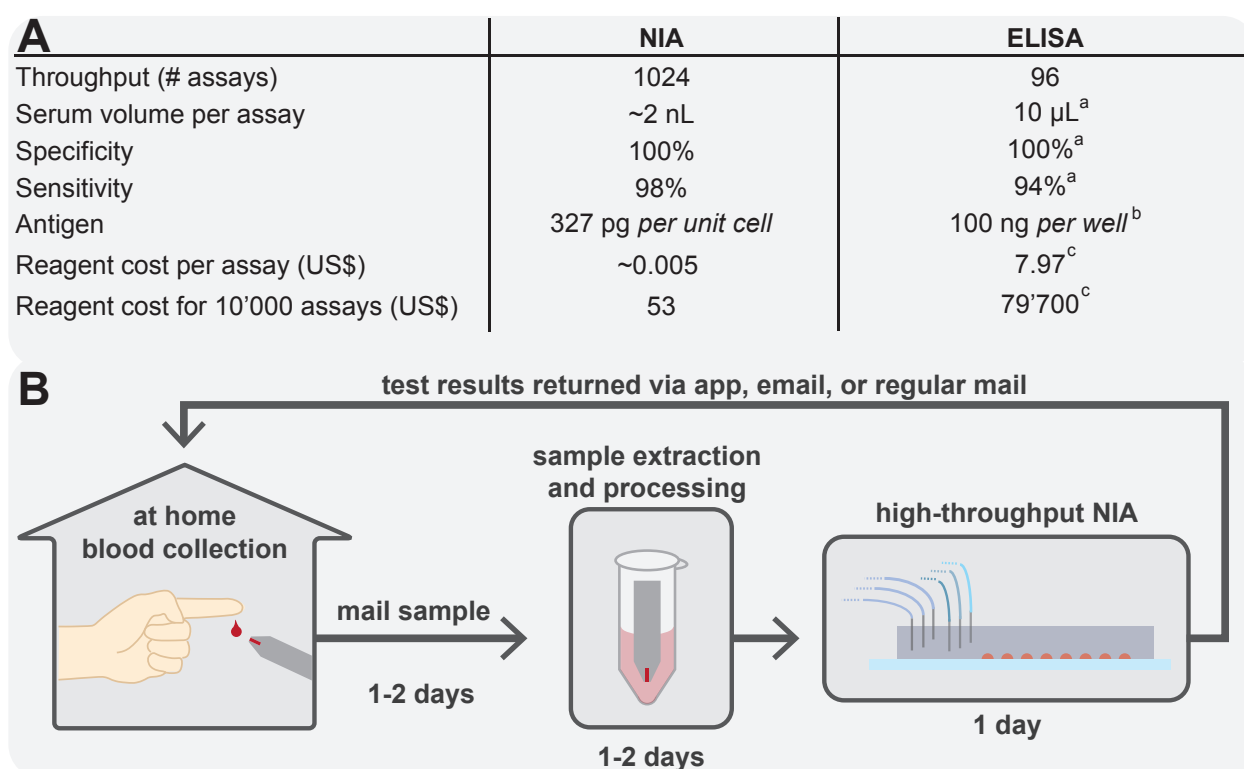


Figure 4.6: **NIA performance table and conceptual home-based sample collection and centralized NIA analysis.** **(A)** Comparison between the high-throughput NIA platform and standard ELISA. Sensitivity and specificity values are based on serum sample analysis for both NIA and ELISA. <sup>a</sup> based on EuroImmun ELISA kit (EI 2606-9601)[270], <sup>b</sup>[266], <sup>c</sup> price based on abcam ELISA kit (ab274342). **(B)** A NIA based diagnostic workflow that uses decentralized ultra-low volume whole blood sample collection, shipping via regular mail, and centralized sample processing and analysis on a high-throughput NIA platform. Test results are analyzed and interpreted and then reported back via mobile app, email, or regular mail.

to overcome the current centralized molecular diagnostics paradigm, which is focused on hospitals and point of care settings rather than on patients and individuals seeking simple, affordable, and convenient molecular diagnostics. The need to visit a clinic is an inconvenience for everyone and can be an insurmountable obstacle for many. The requirement for venipuncture blood collection, sample pre-treatment, and expensive ELISAs prohibits broad testing and contributes to high health care costs. NIA makes it possible for individuals to purchase a simple blood sampling kit containing a lancet, a blood sampling device, and a return mail envelope, at a local pharmacy or supermar-

ket (Fig. 4.6B). The kit can be used easily and conveniently in the privacy of one’s own home, where a simple fingerprick is made and the blood collected by the device. The device with the collected blood can then be sent without special biosafety requirements by regular mail to a central laboratory which analyzes the blood sample for one or more biomarkers, interprets the data, and returns the test results to the individual via smart phone, email, or regular mail. Furthermore, each blood sample is sufficient to conduct many molecular diagnostic assays with NIA. The whole process from kit purchase to results could take less than a week, which is fast enough for a vast majority of tests that are not particularly time critical. Decentralized and simple sample collection coupled with centralized, next-generation high-performance molecular tests will broaden access to molecular diagnostics, and increase the use of testing. During a global pandemic, such technologies could enable the collection of critical epidemiological data, provide instrumental data for vaccine development, and provide information to individuals on their health status.

#### **4.2.5 Acknowledgments**

We would like to thank the Protein Production and Structure Core Facility team at EPFL, specifically Dr. David Hacker, Dr. Florence Pojer, Dr. Kelvin Lau, Laurence Durrer and Soraya Quinche for production and purification of Spike 2P in mammalian cells. We thank Neeraj Dhar and the McKinney lab at EPFL for their help in sample inactivation in BSL-3. We thank Isabelle Armvernez for technical assistance as well as Barbara Lemaitre and Catia Machado Delgado for sample preparation. We kindly thank DBS System SA for generously providing us with HemaXis<sup>TM</sup> DB10 devices. This work was supported by the European Research Council under the European Union’s Horizon 2020 research and innovation program Grant 723106 (SJM), SNF Project grant 182019 (SJM), SNF NRP 78 Covid-19 grant 198412 (SJM, IE, and BM), EPFL (SJM) and a grant from the Private Foundation of the Geneva University Hospital (IE).

#### **4.2.6 Author contributions**

SJM, BM, and IE developed the project. PC, DOA, NV, LK provided resources and advice on experiments. ZS, GM, HMY, performed experiments. ZS, GM, HMY, IE, BM, SJM, designed experiments, analyzed data, and wrote the manuscript.

### 4.2.7 Competing interests

The authors declare no conflict of interest.

## 4.3 Contribution

My contributions to the project on "A high-throughput microfluidic nano-immunoassay for detecting anti-SARS-CoV-2 antibodies in serum or ultra-low volume dried blood samples" were the following: I primarily worked on the preanalytical part in close collaboration with Dr. Zoe Swank and the rest of the team. I helped in receiving the patient serum samples and setting up the protocol for heat inactivation and 1 % Triton X-100 treatment to allow us to use the samples in our lab. I performed initial developments and optimization in repurposing the glucose test strips for the collection of blood samples. I helped in selecting two commercially-available microsampling device, DBS systems HemaXis<sup>TM</sup> and Neoteryx Mitra<sup>®</sup>, and explored the different extraction parameters useful for interfacing our high-throughput microfluidic platform with this decentralized sample collection method. I prepared and extracted all the samples used in Figure 4.4 and Figure 6.10. I extracted all the samples used in Figure 4.5. In the article, I prepared Figure 4.3 and the comparison table for Figure 4.6. For the methods section, I wrote the part for "whole and dried blood" and helped in other parts as well. Finally, I participated in discussions regarding the project development and article writing, and gave feedback on all the different sections, figures and tables presented in the article.

## 4.4 Outlook

Using our nano-immunoassay platform, we plan on providing the analytical support to conduct serological epidemiological studies with our collaborators in University Hospitals of Geneva, but hopefully also help other studies in Switzerland or elsewhere. In order to better characterize exposure and immunological response to different coronaviruses, we will use trimerized Spike antigens of the four common cold coronaviruses, namely HCoV-OC43, HCoV-HKU1, HCoV-229E and HCoV-NL63 which will be produced at EPFL by following the same strategy to stabilize the Spike protein in the prefusion conformation [273]. With the very low sample and reagent consumption, we should be able to test samples against multiple antigens with a high-throughput and controlled costs. While

an initial proportion of the samples will be obtained from venipunctures at the hospital and serum will be analyzed, we plan to further validate the use of microsampling and support studies conducted in decentralized settings such as schools, with the added advantage of offering a less invasive sample collection method for such vulnerable populations. The platform could also be used to conduct a serological survey throughout Switzerland with patient self-collecting dried blood samples at home, or at a local pharmacy. This could allow to study and compare the immunity developed by populations living in areas with different population density. Without offering the possibility for subjects to draw a sample at their home or at least within reasonable distance, it might be difficult to obtain access to subjects living in more remote areas. At the same time, it will be particularly important to gather information on immunity acquired naturally or with vaccination campaigns in remote areas which could present very different kinetics compared to areas more densely populated and with greater access to healthcare. On a technological level, we expect to further improve the throughput on our platform by some changes from the preanalytical and analytical parts to data analysis steps. For the preanalytical part, we are exploring the use of a pipetting robot to automate steps such as serum sample dilution or preparation of plates for dried blood samples extraction. For the dried blood spots on filter paper, we will also explore the use of a fully automated system which can elute the samples by a flow-through desorption process [274]. For the arraying of samples to be analyzed in the microfluidic chip, we will explore the use of different microarray spotters. One option would be to have multiple affordable benchtop pin-based spotters which we could use in parallel to increase the throughput. Another option would be to try spotters using contact-less dispensing of samples by using technologies such as inkjet dispensing [275]. For the analytical part, different improvements could be explored, like the use of multiple MITOMI buttons in a single assay chamber for multiplexed detection of antibodies to different antigens [219, 220]. We also want to increase automation of the protocol by using solenoid valves with computer control so we can initially prepare the fluidic sample and control lines and then run the assay in an automated or semi-automated fashion with checkpoints allowing for visual inspection at critical steps of the protocol. This would allow a single operator to more conveniently run multiple microfluidic assays in parallel. Finally, we would like to improve on the automated image analysis pipeline, which could be potentially integrated with a laboratory information management system to directly link a registered subject sample with its corresponding data and logs of all the different steps of our nano-immunoassay platform.



## Conclusion

In this thesis, we explored the use of cell-free protein expression systems and its potential for the decentralized production of biopharmaceuticals. We show the successful production of *Av*PAL in a home-made cell-free expression system and that the therapeutic enzyme is enzymatically active. The cell-free expression system can be lyophilized, stored for a week at room temperature, and rehydrated to produce the active *Av*PAL enzyme, which would facilitate the decentralized production of this biopharmaceutical product with this "just-add-water" system. In our hands, the costs and yields associated with cell-free production remain prohibitive for therapies where large amounts of the biopharmaceutical are required for each dose, or require a chronic treatment. However we are confident that technological advances will greatly improve cell-free systems for biomanufacturing, and we imagine that classical biotechnological production could be complemented by a completely *in vitro* approach from DNA synthesis to the final biopharmaceutical product. Such decentralized production of biopharmaceuticals can be already beneficial in the production of therapeutic products where a single dose is required. For example, conjugate vaccines can be produced by a cell-free system expressing carrier proteins and desired glycosylation to offer protection against various pathogens infection[276]. In the case of phenylketonuria, a daily administration of a high dose of enzyme is required for therapeutic efficacy and might therefore limit the advantage of the decentralized smaller scale production. Moreover, recent advances in protein engineering might provide better manufacturability and stability to the therapeutic enzyme, such as enzyme CDX-6114 from Codexis (clinical trial: NCT04085666) developed in partnership with Nestlé health science. The ability to produce large quantities of shelf-stable enzyme in a dried format could hopefully lead to more cost-effective enzyme replacement therapies for phenylketonuria. While protein en-

gineering and classical biotechnological approaches might be adapted to provide solutions in the treatment of phenylketonuria, cell-free synthetic biology and bottom-up bioengineering approaches offer the unique potential to generate biopharmaceuticals in a "digital-to-biological" approach[277]. Shortened timelines in biopharmaceutical production with flexible scales could translate to faster development of therapies for rare diseases where it can be difficult to set up a dedicated biopharmaceutical production line for a very limited number of patients. This work provides evidence that even relatively complex enzymes can be produced in a cell-free expression system, and we believe that other enzymes missing in rare diseases resulting from inborn error of metabolism could be addressed in future research.

In a second part, we developed a protocol for the production of biocompatible and semi-permeable microcapsules with a poly-(PEG-DA 250) shell. We show that the capsules are semi-permeable with a size cutoff around 40 kDa, allowing the direct encapsulation of proteins and enzymes, while permitting transport of smaller proteins, DNA strands, or small molecules across the capsules shell. Moreover, the capsules are easily stored and manipulated owing to their chemical and physical stability. While our initial motivation was to encapsulate the therapeutic enzyme PAL for oral delivery, this will require some further optimization as the pore size of the capsules is still slightly too large to protect it from proteolytic enzymes, which will be further investigated by varying the porogen type and concentration to form smaller pores. With their current composition, we show that the microcapsules have a broad range of potential applications, offering the possibility not only to encapsulate proteins or enzymes, but also cells, or can serve to immobilize other biomolecules in the semi-permeable microcompartments such as DNA strands, which we used to build complex biomolecular systems such as a two-layer signalling cascade using encapsulated DNA strand-displacement reactions. While other microfluidic encapsulation methods have been developed, they generally suffer from inconvenients that prevent the encapsulation of active enzymes for oral delivery. Biocompatible large molecular weight PEG-DA hydrogel capsules have been developed, but the pore size is often larger than a majority of proteins which would lead to their uncontrolled release from the capsule[99]. On the other hand, capsules obtained with photocurable oils can be made semi-permeable by adding porogens to the phase containing the polymer precursor[108], but such materials lead to a strong adsorption of proteins to the capsule material due to their high hydrophobicity[109]. This prevents the direct encapsulation of proteins in such capsules, and also requires an additional step of passivation before placing the capsules in contact

with proteins to prevent their non-specific adsorption[125]. This work provides a method for the microfluidic production of semi-permeable capsules with a polymer composition of low molecular weight PEG-DA compatible with protein and other biomolecules encapsulation. Such properties should allow them to be used in the bottom-up engineering of complex biomolecular systems and in the development of drug-delivery applications.

Finally, we successfully developed a platform for the detection of anti-SARS-CoV-2 antibodies by decentralized collection of blood samples and testing on a microfluidic high-throughput nano-immunoassay. Using a sampling method that can be easily performed at the point-of-care or even at-home, combined with a technology which can offer high performance nano-immunoassay with minimal sample and reagent consumption, has the potential to facilitate the conduction of serological epidemiological studies. The microfluidic nanoimmunoassay analyzes sample with volumes of a few nanoliters and reduces reagents consumption per datapoint by 2 or 3 orders of magnitude thus offering the potential to greatly reduce costs. The nano-immunoassay was validated with serum samples from 155 PCR-confirmed patients and 134 pre-pandemic negative control sera and showed 100 % specificity and 98 % sensitivity in duplicate measurements. We also show evidence of the good performance of collecting dried blood spots with repurposed glucose test strips or with two different commercial microsampling devices, and followed by testing with the microfluidic nano-immunoassay. As the microfluidic device is not restricted to detecting anti-SARS-CoV-2 antibodies and allows to conduct different immunoassays, this platform could also offer a convenient solution for patients and doctors by testing biomarkers commonly used for diagnostic purpose. While other diagnostic platforms currently used in hospitals or large diagnostic laboratories are suitable for the analysis of anti-SARS-CoV-2 IgG levels, they are most suited for the high-throughput analysis of blood samples obtained by venipuncture. The use of dried blood samples can be used in conjunction with automated analyzers, but requires large sample volumes that would consume the whole extracted sample in a single assay[236]. It is also possible to use standard ELISA formats for the analysis of samples obtained from microsampling, but not more than one or two measurements could be performed based on the volume used in a 96-well format, with a trade-off in the sample throughput[237]. Other formats such as 384-well or even 1536-well plates[278] would reduce the sample consumption per assay, but the compatibility with microsampling remains to be demonstrated. We believe that our microfluidic platform provides a unique opportunity to perform high quality immunoassays displaying specificity and sensitivity matching state-of-the-art centralized diagnostic

platforms, while at the same time offering the full compatibility with a convenient decentralized microsampling collection. Moreover, the ultra-low sample requirement allows for multiplexed or repeated testing from samples collected with commercial devices with volumes as low as 10  $\mu\text{L}$ , or even under 1  $\mu\text{L}$  by using repurposed glucose test strips. We envision our platform to offer a direct benefit in performing serological surveys in the current COVID-19 pandemic, but also in personal diagnostics testing other biomarkers in the future.

## 6

# Appendix

## 6.1 Materials and Methods Chapter 2

### Home-made *E. coli* lysate preparation

*E. coli* The protocol used for cell-free extract preparation and cell-free TX-TL reactions is adapted from Sun *et al.* [45] and Kwon and Jewett [46]. BL21 DE3 cells were grown from glycerol stocks overnight in 5 mL LB in a 37°C incubator with 200 rpm agitation. 2 x 1 mL of the preculture were added the next morning to 200 mL of LB medium in 1 L erlenmeyer flasks and culture for 4 hours representing an OD at 600 nm between 1.5 and 2. In order to prepare extracts containing T7 polymerase, 400 µL of 100 nM IPTG was added after 2 hours of culture in each 200 mL culture. The cells were harvested by separating the 200 mL of culture into 4 x 50 mL Falcon tubes and centrifuged for 20 min at 4000 rpm at 4°C. The pellets were washed 3 times in Buffer A (10 mM Tris-acetate, 14 mM magnesium glutamate, 60 mM potassium glutamate, 2 mM DTT). The cells were pelleted again and weighed after removal of the supernatant. The pellets were flash frozen in liquid nitrogen and stored at -80°C before being further processed. For extract preparation, the cells were resuspended in 1 mL of Buffer A per mg of cells in the pellet. It is important at this stage to use Buffer A with freshly added DTT. The cells are lysed by sonication using 50% amplitude with 10 s pulses followed by 10s off to prevent overheating. The cells are placed in an ice-water bath in round bottom 2 mL tubes, and care should be taken to place the sonication tip as deep as possible in the tube without touching its walls. We usually split the resuspended cells in 1 mL aliquot and deliver a total energy of 400 J, but if necessary the total energy can be adapted depending on the volume

[46]. When successful, the sonication should yield a darker and more transparent solution than the starting off-white thick suspension of cells. After lysis, the extract is clarified by centrifugation for 10 min at 12000 rpm at 4°C. The supernatant is carefully removed and incubated at 37°C with shaking for 90 min as an optional "run-off" reaction. The extract is centrifuged again for 10 min at 12000 rpm at 4°C and the supernatant is harvested. It is preferable to be conservative and lose a little portion of extract to remove only the supernatant to prevent contamination of the lysate with cells or cell debris which could reduce its activity. The supernatant was aliquoted, flash frozen in liquid nitrogen and stored at -80°C before use.

### **Cell-free TX-TL reactions**

Cell-free expression reactions are set up by mixing 25 % lysate, 25 % Buffer A (with DTT freshly added), 25 % energy solution, and the 25 % left are composed of the DNA template completed with nuclease free water. The energy solution used is 4x concentrate and its composition is described in Sun *et al.* [45] and corresponds to the "Caltech" standard energy solution which uses 3-PGA as energy source, or in Cai *et al.* [48] and corresponds to the "simplified" energy solution which uses only glutamate. As an important note, the "simplified" energy solution can be used only in conjunction with lysate prepared from cells grown on 2xYTP or 2xYTPG medium. The cell-free reactions were conducted in volumes of 10 µL in 384-well microplates at 29°C on a platereader, or 25 µL or 50 µL reactions in 1.5 mL tubes in a thermomixer at 29°C or 37°C with agitation.

### **AvPAL expression and purification**

AvPAL expression was performed as described above in 50 µL reactions with 500 to 1000 ng of plasmid template DNA. The 1.5 mL tubes were placed in a thermomixer at 37°C or 29°C with agitation at 600 rpm. Expression of AvPAL using S30 T7 High-Yield protein expression system was performed following the manufacturer's protocol (Promega). For labeling of proteins with lysine BODIPY, 1 µL of FluoroTect<sup>TM</sup> GreenLys (Promega) was added in 25 µL of cell-free reaction. For purification, we used either Ni-NTA spin columns (Qiagen) or MagneHis<sup>TM</sup> Ni-particles (Promega) following manufacturers instructions. For SDS-page gel inspection, 5 µL of the reaction were mixed with 5 µL Laemmli Buffer (Sigma-Aldrich) and heated at 100°C for 2 min before loading on the gel. The gel was run for 10 min at 100 V, followed by 35 min at 150 V. The gel was stained 1 h in Coomassie and washed overnight with destaining solution replaced multiple times.

## Enzymatic activity measurements

The enzymatic assay for PAL activity measurement was performed according to the recombinant enzyme supplier instruction (Sigma-Aldrich). A calibration curve for absorbance of trans-cinnamic acid was measured and an extinction coefficient at 270 nm was calculated. For the assay 100 mM Tris-HCl pH 8.5 buffer was prepared and 3 mM L-phenylalanine was diluted in the same buffer. The enzymatic reaction was performed by mixing 200  $\mu$ L of L-phenylalanine solution, 90  $\mu$ L of DI water, and 10  $\mu$ L of sample and pipetting this solution in a quartz cuvette. The absorbance increase was measured at room temperature every 10 s for 5 to 10 min. The absorbance increase was linear and the slope was used for activity calculations with the definition of 1 Unit of enzyme converting 1  $\mu$ mole of L-phenylalanine to trans-cinnamic acid per min at pH 8.5 at 30°C.

## Lyopreservation of cell-free extracts

For the air-drying of lysate, we diluted it 2x in a 1.1 M solution of trehalose in Buffer A. We pipetted 30  $\mu$ L drops on a silicon mat and placed it in a 37°C incubator for 24 h. The dried lysate-trehalose mixture formed pellets which were rehydrated in nuclease-free water and combined with energy solution and DNA template for cell-free expression. For the preparation of freeze-dried cell-free expression reactions, complete reactions with lysate, energy solution and DNA template were assembled, placed in 1.5 mL tubes and flash-frozen in liquid nitrogen. The tubes caps were replaced with ones having holes pierced by a needle and the samples were freeze dried overnight in a benchtop freeze-dryer (FreeZone<sup>TM</sup> Labconco<sup>TM</sup>). To start the cell-free reactions, the freeze-dried reaction pellets were rehydrated with nuclease-free water corresponding to the weight loss upon drying (generally 85-90 %).

## Expression of protein nanocompartments

pET14-Encap, pET14-GFP30\_Encap, pET14-GFP15\_Encap, and pET14-GFP5\_Encap were gifts from David Savage (Addgene plasmid 86405 ; <http://n2t.net/addgene:86405> ; RRID:Addgene\_86405). The bacterial slabs were streaked, single colonies were grown overnight, and plasmids were obtained by miniprep. The expression of encapsulin variants was performed using the standard protocol for cell-free expression. The products were analyzed either on SDS-page gel or on a Native page gel to observe EGFP fluorescence.

## Co-translational incorporation of non-natural amino acids

For the cotranslational incorporation of azido-homoalanine, we used a PURExpress system which does not contain amino acids and tRNAs in the energy solution (NEB E6840S). The 19 amino acids except methionine were added separately at a concentration of 2 mM, and the reaction was performed with either 2 mM methionine, 2 mM azido-homoalanine or no methionine equivalent. tRNAs were also added to the reaction and supplemented with lysine-BODIPY tRNA. The reaction products were visualized on an SDS-page gels using a fluorescent gel scanner for detection of lysine-BODIPY signal. For the cotranslational incorporation of azido-homoalanine in proteins using lysate-based expression systems, the same protocol was used for the separate addition of amino acids. The lysate was either a standard *E. coli* extract, or alternatively the extract was buffer exchanged multiple times with Buffer A using Amicon<sup>®</sup> Ultra 0.5 mL centrifugal filters with 3 kDa cut-off to remove amino acids present in the extract. tRNAs were also added to the reaction and supplemented with lysine-BODIPY tRNA. The reaction products were again visualized on an SDS-page gels using a fluorescent gel scanner for detection of lysine-BODIPY signal.



## 6.2 Materials and Methods Chapter 3

### Microfluidic chip fabrication

The PDMS microfluidic device were produced using standard soft lithography methods and used designs previously established [209, 279]. Transparency films obtained from the SMaL lab from Prof. Esther Amstad at EPFL were used as photo masks for the production of a SU-8 master on a silicon wafer. A master was prepared by using photolithography with the negative photoresist SU-8. A first 40  $\mu\text{m}$  layer of 3025 SU-8 (Microchem) containing the inner and middle phase channel was spin-coated and UV exposed on the first half of the master while the second half was fully exposed. A second 60  $\mu\text{m}$  layer of 3050 SU-8 (Microchem) was spin-coated and UV exposed aligned on top of the features to generate the main channels on both halves of the master. After using the master for PDMS replica moulding, both halves of the design were treated with O<sub>2</sub> plasma for 45 s and bonded to one another.

### Microfluidic microcapsules production

The microfluidic system was operated using syringe pumps (New Era) controlled via a python script written in Professor Adam Abate's lab at UCSF. Syringes were connected to Tygon tubing and the tubing was connected to the chip via metal pins. The flowrates for the inner, middle and outer phase were set to 250, 200, and 2500  $\mu\text{L}/\text{h}$ . The inner phase and outer phase are composed of a 10 wt/wt% aqueous solution of PVA (poly(vinyl alcohol), 13000-23000 g/mol, Sigma-Aldrich). The drop production was observed at the junction and at the collecting channel through a 4x objective with a high-speed digital camera (Fastec HiSpec). The resulting double-emulsion were placed on a cell-counting slide and inspected with a 20x objective in brightfield and fluorescence. The double-emulsions were collected in UV-transparent cuvettes (UVettes, Eppendorf) and illuminated for 30 seconds from the side with the complete spectrum of a 100W Mercury lamp focused on the cuvette. Alternatively, an Omnicure S1500 200W UV curing lamp with standard filter (320nm-500nm) was used and the double-emulsions were illuminated with a probe placed on the top of the cuvette. The polymerized capsules were transferred to a 1.5mL eppendorf tube and washed 10 times in 1 mL cold wash buffer (1xPBS, 0.1 % Tween20) by centrifugation at 2000 rpm for 1.5 minutes at 4°C. Obtained capsules were stored at 4°C in wash buffer.

## Semi-permeable capsules

For the production of semi-permeable capsules, the middle phase was supplemented with 15 % butyl acetate (Sigma-Aldrich) porogen, 1 % Span80 (Fluka) surfactant and 4 % 2-Hydroxy-2-methylpropiophenone (97%, Sigma-Aldrich) photoinitiator. In the direct encapsulation of fluorophores, we supplemented the 10 % PVA inner aqueous phase with 100  $\mu\text{g}/\text{mL}$  of 500 kDa FITC-dextran and 50  $\mu\text{g}/\text{mL}$  TMR-dextran. Fluorophore-containing capsules were washed like previously described and kept in wash buffer at 4°C overnight to ensure pores opening. The capsules were pipetted in a cell-counting slide (Countess??) and fluorescence images were acquired in the Cy3 and FITC channels. For permeability characterization, empty capsules were immersed in a solution containing 10 kDa RITC-dextran and 32.7 kDa EGFP. After different incubation time, fluorescence images were acquired in the Cy3 and FITC channels. Capsules were produced using different porogens by simply replacing the 15 % butyl-acetate with 1-decanol, octanol, 2-ethylhexanol, or 2-heptanone (all from Sigma-Aldrich).

## Direct encapsulation of proteins and enzymes

For the direct encapsulation of proteins, the 10 % PVA inner phase was supplemented with 32.7 kDa recombinant EGFP (Biovision) mixed to a final concentration of 2  $\mu\text{g}/\text{mL}$  or 60 kDa FITC-labeled streptavidin (Biolegend) to a final concentration of 50  $\mu\text{g}/\text{mL}$ . Double-emulsions or polymerized capsules were loaded in a cell-counting chamber and imaged on a microscope with 20x magnification. For the direct encapsulation of enzymes, econoLuciferase<sup>TM</sup> 10 mg/mL solution (Biosynth) was mixed to 4 v/v % in the 10 % PVA inner phase. The double-emulsions and polymerized capsules were loaded in a cell-counting chamber and inspected on a microscope and fluorescence signal was measured. In the bioluminescent assay, 25  $\mu\text{L}$  of blank, empty capsules, econoLuciferase-containing capsules, or free econoLuciferase were mixed with 100  $\mu\text{L}$  of luciferase assay reagent (Promega) in a black 96-well plate and imaged for 50 minutes on a plate reader. The bioluminescent signal was integrated over the duration of the experiment.  $\beta$ -galactosidase aqueous glycerol suspension (Sigma-Aldrich) was mixed to 10 v/v % in the 10 % PVA inner phase. The produced capsules were resuspended in a 0.5 M trehalose solution and 15  $\mu\text{L}$  drops were pipetted on a silicon mat and dried overnight in a 37°C incubator. The resulting dried pellets were recovered in a tube and rehydrated with a chlorophenol red  $\beta$ -D-galactopyranoside (CPRG) solution. The color change was imaged

with a phone camera, or with a color camera (Pike) mounted on a microscope and imaged with a 4x objective.

## DNA-strand displacement reactions

We used capsules containing the 60 kDa FITC-labeled streptavidin for the immobilization of biotinylated DNA strands. The DNA strands were synthesized at IDT with HPLC purification. The DNA sequence and DNA modifications were strictly identical to the one presented in Joesaar et al.[192] and we followed the same protocol for the assembly of two populations of capsules containing the first ( $F_1$ ) or second ( $F_2$ ) gate DSD reactions. Briefly, 40  $\mu$ l of a dispersion of FITC-streptavidin containing capsules, 20  $\mu$ l of 4x buffer and 8  $\mu$ l of biotinylated DNA gate strand ( $F_1$  or  $F_2$ , from a 10  $\mu$ M stock solution) were mixed with a pipette in a 1.5 ml Eppendorf tube and incubated at room temperature for 1 h, followed by addition of 12  $\mu$ l output strand ( $Q_1$  or  $Q_2$ , from a 10  $\mu$ M stock solution), gentle mixing and overnight incubation at 4°C. The excess unbound output strand was removed by removing around 50  $\mu$ l of the supernatant and the capsules were washed 3 times with 400  $\mu$ l of buffer by centrifugation at 1500 rpm, 4°C, and the capsules with the immobilized DSD reaction were stored at 4°C. To perform the double-layer signaling cascade, the two capsules populations were mixed and supplemented with a fuel strand. After the addition of an input strand ( $A$ ) at a concentration of 50 nM, 10 nM or 100 nM, the resulting solution was pipetted in a cell counting chamber (Countess, Thermofisher). To prevent evaporation, the device was placed in a petri dish and surrounded by kimwipes saturated with 1xPBS, allowing for long term imaging of the two-layer signalling cascade. The fluorescent signal for the first gate (Cy5) and second gate (Cy3) was measured with a 200 ms exposure every 30s for a duration of 1 hour. The resulting images were captured in a 3x3 stitch with a 20x objective. For an estimation of the signal increase over the timecourse of the experiment, we used ImageJ and applied a simple minimum thresholding to detect the capsules in each image. We used the "erode" function 5 times to ensure only the capsules were captured, and used the "analyze particles" function to extract the different parameters for particles with circularity over 0.6 and area above 1000  $\mu$ m<sup>2</sup>. For each timepoint of the experiment, the mean intensity of every detected particle was plotted using PRISM.

## Encapsulation of bacteria and yeast cells

*E. coli* cells were grown overnight in LB in a 37°C incubator with shaking. The cells were diluted in the 10 % PVA inner phase by mixing 100 µL of the overnight with 900 µL of the inner phase. The operation of the microfluidic device was done with the same flowrates as described, and the capsules were polymerized for 30s, 10 s or 5s with an Omnicure S1500 200W UV curing lamp with standard filter (320nm-500nm). The capsules were washed in PBS-(Tween-20 0.1 %) and pelleted by centrifugation at 2000 rpm at 4°C, repeated 10 times. For culturing of *E. coli* cells inside the capsules, the buffer was replaced by LB medium and placed in a 37°C incubator with shaking. Yeast cells were grown overnight in YPD in a 30°C incubator with shaking. The cells were diluted in the 10 % PVA inner phase by mixing 100 µL of the overnight with 900 µL of the inner phase. The operation of the microfluidic device was done with the same flowrates as described, and the capsules were polymerized for 30s or 10s with an Omnicure S1500 200W UV curing lamp with standard filter (320nm-500nm). The capsules were washed in PBS-(Tween-20 0.1%) pelleted by centrifugation at 2000 rpm at 4°C and repeated 10 times. For culturing yeast cells inside the capsules, the buffer was replaced by YPD medium and then placed in a 30°C incubator with shaking.

## 6.3 Materials and Methods Chapter 4

### Microfluidic chip fabrication

The designs for the flow and control layer of the device were drawn with AutoCAD software, we then used standard photolithography to fabricate the molds for each layer. Three replicates of the design are fitted onto a 4 inch silicon wafer so that three devices can be made in a single fabrication process. SU-8 negative photoresist was used to create the control channel features (GM 1070, Gersteltec Sarl) with a height of 30  $\mu\text{m}$ , while AZ 10XT-60 positive photoresist (Microchemicals GmbH) was used to generate flow channel features with a height of 15  $\mu\text{m}$ . After development, the flow layer mold was annealed at 180°C in a convection oven for two hours to obtain rounded features. Afterwards each of the wafers was treated with TMCS (trimethylchlorosilane) and coated with PDMS (Sylgard 184, Dow Corning). For the control layer  $\sim 50$  g of PDMS with an elastomer to crosslinker ratio of 5:1 was prepared, whereas for the flow layer a 20:1 ratio of elastomer to crosslinker was spin coated at 1800 rpm to yield a height of  $\sim 50$   $\mu\text{m}$ . Both PDMS coated wafers were then partially cured for 20 minutes at 80°C, after which devices from the control layer were cut out and the inlets for each control line were punched (OD = 889 mm) using a precision manual-punching machine (Syneo, USA). Each control layer is then aligned onto the flow layer by hand using a Nikon stereo microscope. The aligned devices were then placed at 80°C for 90 minutes, allowing the two layers to bond together so that the entire device can then be cut and removed from the flow wafer. After that, the flow layer inlets were punched.

### Immunoassay reagents

For our on-chip immunoassay we used biotinylated mouse anti-His antibodies (Qiagen, 34440) to immobilize His-tagged SARS-CoV-2 antigens on the surface of our assay chambers. The prefusion ectodomain of the SARS-CoV-2 Spike glycoprotein (the construct was a generous gift from Prof. Jason McLellan, University of Texas, Austin [280]) was transiently transfected into suspension-adapted HEK293 cells (Thermo Fisher) with PEI MAX (Polysciences) in Excell293 medium. Incubation with agitation was performed at 37°C and 4.5% CO<sub>2</sub> for 5 days. The clarified supernatant was loaded onto Fastback Ni<sup>2+</sup> Advance resin column (Protein Ark) eluted with 500 mM imidazole, pH 7.5 in PBS. For proof-of-concept experiments, chimeric anti-spike antibodies were purchased

from Sino Biological (40150-D002, 40150-D003, 40150-D004, 40150-D005). We spiked the chimeric anti-spike antibodies into human serum (Sigma-Aldrich, H4522) and whole blood (ZenBio, SER-WB). For detecting human IgG, we used PE labeled goat anti-Human-IgG (Abcam, ab131612).

## **Sample preparation**

### **Serum**

Serum samples were collected from 155 RT-PCR confirmed COVID-19 patients and 134 negative control sera obtained in 2013/14 and 2018 before the start of the pandemic (including 50 children). All samples were collected according to the local ethical guidelines and ethical approval was waived by the ethics committee of the University Hospital of Geneva (HUG). We used days post onset of symptoms (dpos) according to patient history or days post diagnosis (dpd) in case dpos was unknown. All samples were stored at -20°C until analysis. In order to handle patient serum samples in a Biosafety Level 1 laboratory, patient serum samples were heat treated at 56°C for 30 minutes and Triton X-100 (Fisher Scientific) was added to the samples to a final concentration of 1%. In order to optimize spotting parameters and the on-chip immunoassay, proof-of-concept experiments involving human serum spiked with chimeric anti-spike antibodies were also carried out with the addition of Triton X-100. For dilution series experiments, patient serum samples were diluted in a PBS solution containing 2% BSA. Additionally, 10  $\mu$ M FITC-dextran (10 kDa) was added as a tracer to each sample in order to assess whether similar volumes of serum samples were spotted (Fig. 6.11).

### **Whole and dried blood**

Human Whole Blood - Frozen, 10ml was obtained from AMS Biotechnology (Europe). Anti-spike antibodies were added to whole blood to the desired concentration from a stock solution of 2  $\mu$ M. To simulate a fingerprick collection, 15-20  $\mu$ L of whole blood samples were pipetted on parafilm and then collected on the sampling device where 10  $\mu$ L were collected with HemaXis<sup>TM</sup> DB10 (DBS System SA) or Mitra<sup>®</sup> Clamshell (Neoteryx). The samples were dried and then stored in their original container without further protection. Samples were kept at room temperature for 1, 2 or 6 days, or in a 55°C oven for 1 day. The dried blood stored on HemaXis<sup>TM</sup> filter paper were cut using an 8 mm biopsy puncher and scalpel and the tip of the Mitra<sup>®</sup> devices were removed with

tweezers. The samples were placed in a 96-well plate and filled with 200  $\mu\text{L}$  of cold extraction buffer (1xPBS, 1% BSA, 0,5% Tween20) [266] and incubated overnight at 4°C with 300 rpm agitation. Around 150  $\mu\text{L}$  per well of the supernatant was recovered and stored at -20°C until analysis. Alternatively, a small volume of blood (around 0.6  $\mu\text{L}$ ) was collected with a Meditouch 2 glucose test strip (Medisana), dried and stored in a box kept at room temperature for 1,2 or 6 days, or in a 55°C oven for 1 day. Extraction was performed by placing the strip at the bottom of a 1,5 mL tube filled with 30  $\mu\text{L}$  of extraction buffer overnight at 4°C.

As a substitute for capillary blood taken from a fingerprick, we used leftover EDTA whole blood samples drawn from hospitalised COVID-19 patients at different time points post diagnosis for routine clinical laboratory analysis. EDTA whole blood samples were stored at 4°C for a maximum of seven days before they were applied to the dried blood collection devices. 20  $\mu\text{L}$  of EDTA whole blood was pipetted on a parafilm sheet, and collected with a Mitra<sup>®</sup> device or glucose strip. For the HemaXis<sup>™</sup> device, 10  $\mu\text{L}$  of whole blood was directly pipetted on the filter card. The samples were dried for 30 minutes and placed in a plastic bag with silica gel before shipping. The samples were extracted as described above 5 days after collection and shipping, microarray spotted on a glass slide on day 6 and the nano-immunoassay chip was run on day 7. To determine antibodies against SARS-CoV-2 S1 protein by Euroimmun S1 ELISA, EDTA whole blood samples were centrifuged for 5min at 1200x g at 4°C and 200  $\mu\text{L}$  of plasma were stored at 4°C until analysis.

## Enzyme-linked immunosorbent assay

Euroimmun S1 IgG ELISA (Euroimmun AG, Lübeck, Germany, # EI 2606-9601 G) was performed according to the manufacturers instructions and was run on a Dynex Agility (RUWAG Handels AG, Bettlach, Switzerland). OD ratios were calculated by dividing the OD450 of each sample by the OD450 of a calibrator that was run on each plate. Results equal or above OD ratio of 1.1 were considered positive.

## Microarray spotting

25  $\mu\text{L}$  of each sample were loaded into a 384 microwell plate (ArrayIt, MMP384). An MP3 microarray printing pin (Arrayit) was used to spot the samples onto an epoxy-coated glass slide using a QArray2 microarrayer (Genetix). The presence of Triton X-100 in the serum samples had a signif-

icant effect on the spot diameter. To account for this we increased the dimensions of the spotting chamber and set the inking and stamping time to 50 ms and 1 ms, respectively. In addition, it was critical that the ambient humidity was below  $\sim 42\%$ , otherwise the spots would become too large and merge together. After spotting, the PDMS chip was aligned on top of the sample spots using a stereo microscope and bonded over night at  $40\text{ }^{\circ}\text{C}$ .

## Running on-chip immunoassays

Control lines were filled with PBS, attached to the chip and pressurized at 145 kPa. While isolating the spotted sample with the neck valve closed, the lower half of the unit cells were patterned with BSA-biotin (Thermo Fisher, 29130) and neutrAvidin (Thermo Fisher, 3100). First BSA-biotin was flowed at a concentration of 2 mg/mL for 20 minutes, then neutrAvidin was flowed at a concentration of 1 mg/mL for 20 minutes. A flow pressure of 27-34 kPa was maintained for each of the flow steps. Afterwards the button valve was actuated and BSA-biotin was flowed for an additional 20 minutes. In between each of these steps a solution of 0.005% Tween 20 (Sigma, P1379) in PBS was flowed for 5 minutes to wash away any unbound material. After surface functionalization, a  $1\text{ }\mu\text{g/mL}$  solution of biotinylated anti-His antibody in 2% BSA in PBS was flowed for 20 minutes. Next a  $6.7\text{ }\mu\text{g/mL}$  solution of His-tagged SARS-CoV-2 spike protein in 2% BSA in PBS was flowed for 20 minutes. The spike protein solution contained 25% chicken serum (Sigma, C5405), which served to block the surface and reduce non-specific binding. Before each of these steps the solution was first flowed for 2 minutes with the button valves down, allowing the solution to flow evenly into the entire device. After flowing each solution for 20 minutes, a wash step was performed by flowing 0.005% Tween PBS for 5 minutes with the button valves down. Once the spike protein was attached to the surface, the serum spots were re-solubilized by opening the neck valve and allowing 0.005% Tween PBS to flow into the spotting chamber while the outlet valve was closed. The neck valve was then closed and 0.005% Tween PBS was flowed for 5 minutes to prevent cross-contamination of samples in neighboring unit cells. The sandwich valves were then closed and the neck valve was released to allow any antibodies present in the serum spot to diffuse into the assay chamber. After an incubation of 70 minutes the button valve was opened and a second incubation of 60 minutes was carried out, permitting any anti-spike antibodies to bind to the spike protein. Any unbound material could then be washed away by flowing 0.005% Tween PBS for 5 minutes with the button and neck valves closed. A  $5.6\text{ }\mu\text{g/mL}$  solution of anti-IgG-PE



was then flowed for 2 minutes with the buttons down, then for 10 minutes with the buttons up. The buttons were then closed and any unbound detection antibody was washed away by flowing 0.005% Tween PBS for 5 minutes. Each unit cell was then imaged with an exposure time of 300 ms using a Nikon ECLIPSE Ti microscope equipped with a LED Fluorescent Excitation System, a Cy3 filter set, and a Hamamatsu ORCA-Flash4.0 camera (C11440).

## Data analysis

The detection antibody signal was quantified using a custom Python script. ROC analysis was performed using GraphPad Prism. Cutoff values for the NIA measurements were chosen by maximizing both the specificity and sensitivity values.  $EC_{50}$  values were determined by fitting the dilution series data (1:256 - 1:8) for each sample to a saturation binding curve,  $y = \frac{B_{max}x}{x+EC_{50}}$ . For all samples  $B_{max}$  was set to 65000.

## 6.4 Supplementary Figures Chapter 3

In this section we present supplementary figures that were obtained for the further characterization of the microcapsules semi-permeability.

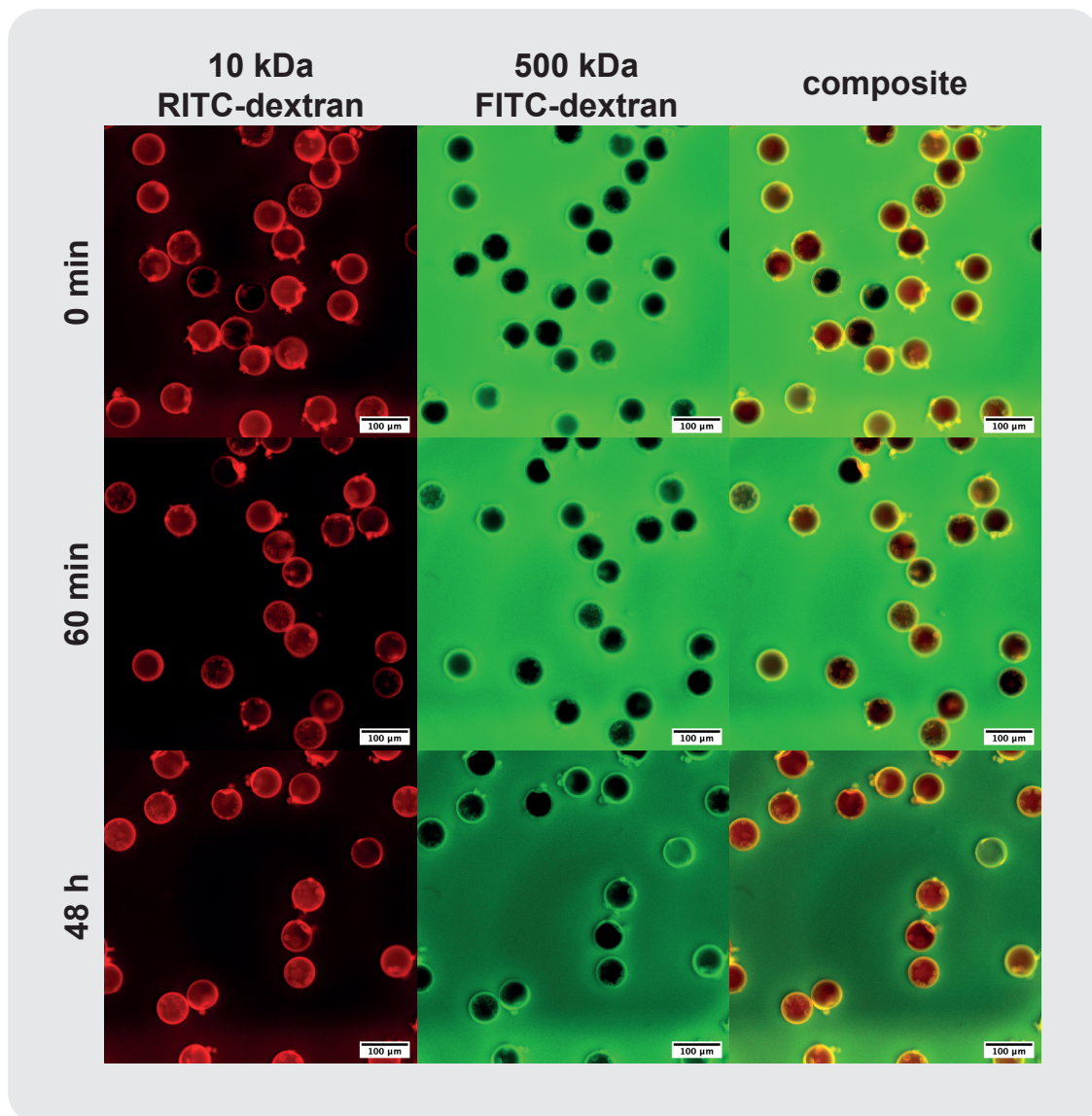


Figure 6.1: **Microcapsules with decanol porogen are impermeable to 500 kDa FITC-dextran.** PEG-DA 250 microcapsules produced with 1-decanol porogen were immersed in a 10 kDa RITC-dextran + 500 kDa FITC-dextran solution. After 48h of incubation, the large molecular weight dextran is still excluded from the capsules.

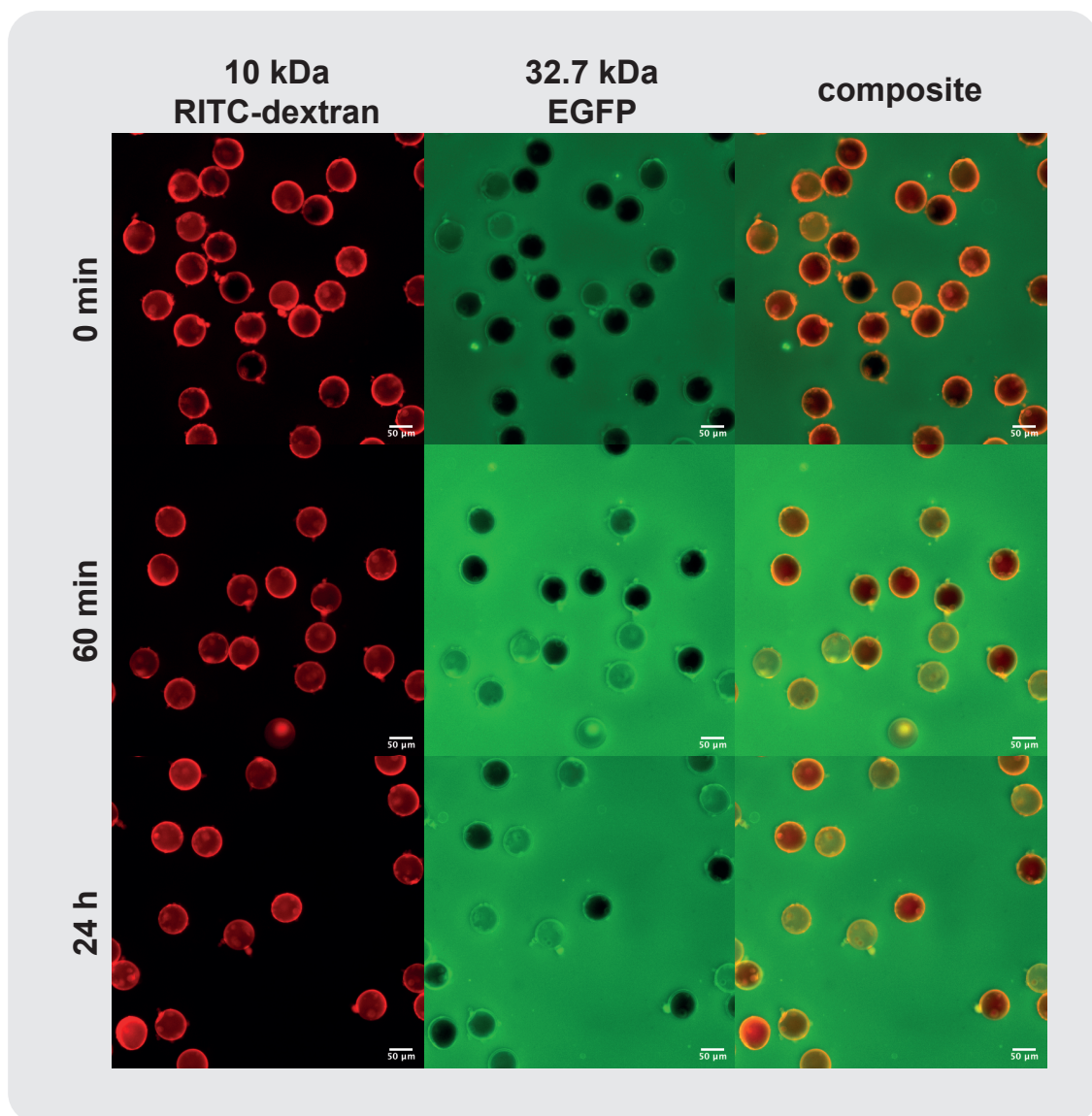


Figure 6.2: **Semi-permeable microcapsules with ethylhexanol porogen.** PEG-DA 250 microcapsules produced with ethylhexanol porogen were immersed in a 10 kDa RITC-dextran + 32.7 kDa EGFP solution. The 10 kDa fluorophore rapidly diffuses inside the capsules, while 32.7 kDa EGFP slowly diffuses over the course of 24 hours.

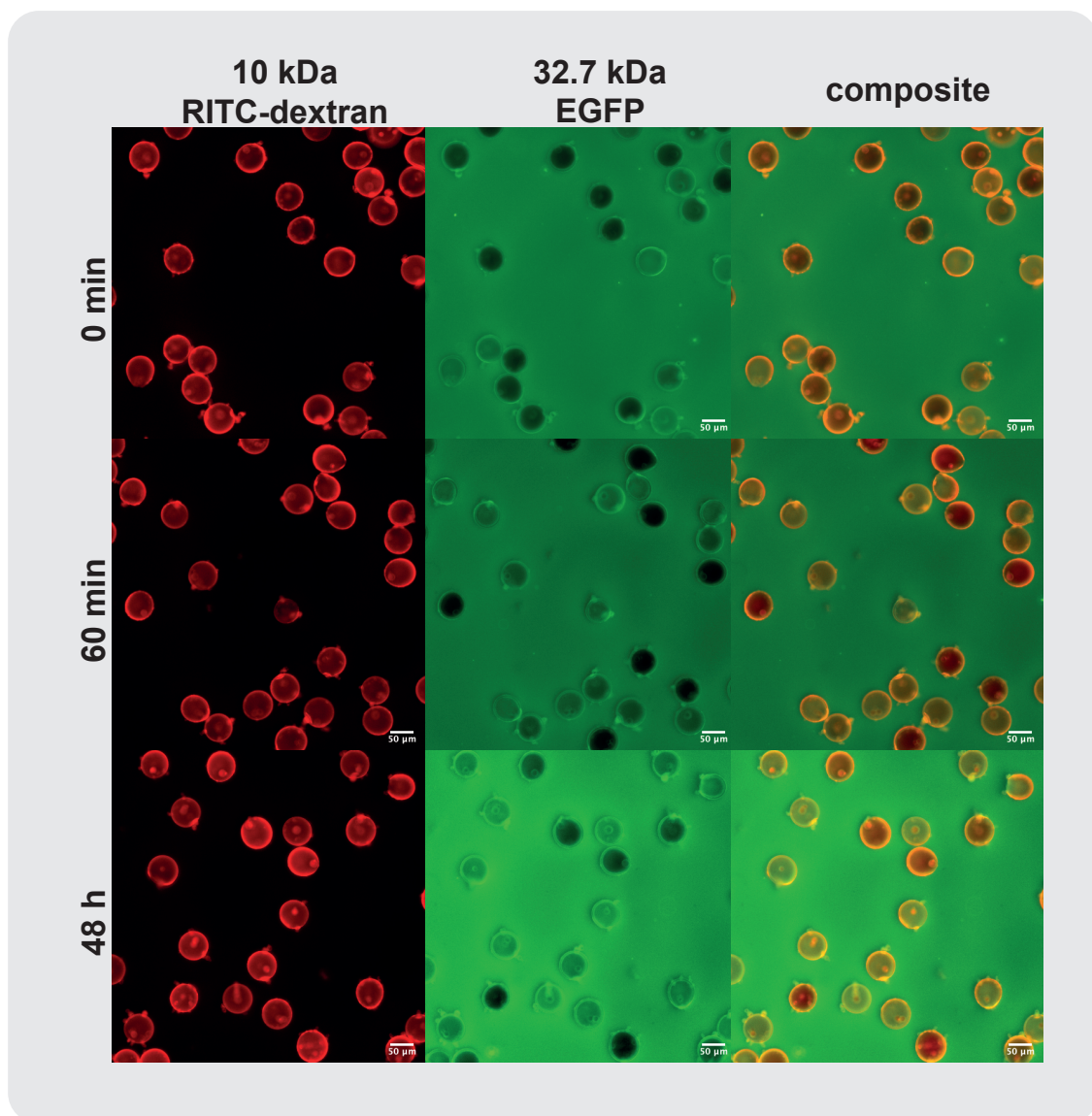


Figure 6.3: **Semi-permeable microcapsules with octanol porogen.** PEG-DA 250 microcapsules produced with octanol porogen were immersed in a 10 kDa RITC-dextran + 32.7 kDa EGFP solution. The 10 kDa fluorophore rapidly diffuses inside the capsules, while 32.7 kDa EGFP slowly diffuses over the course of 24 hours.

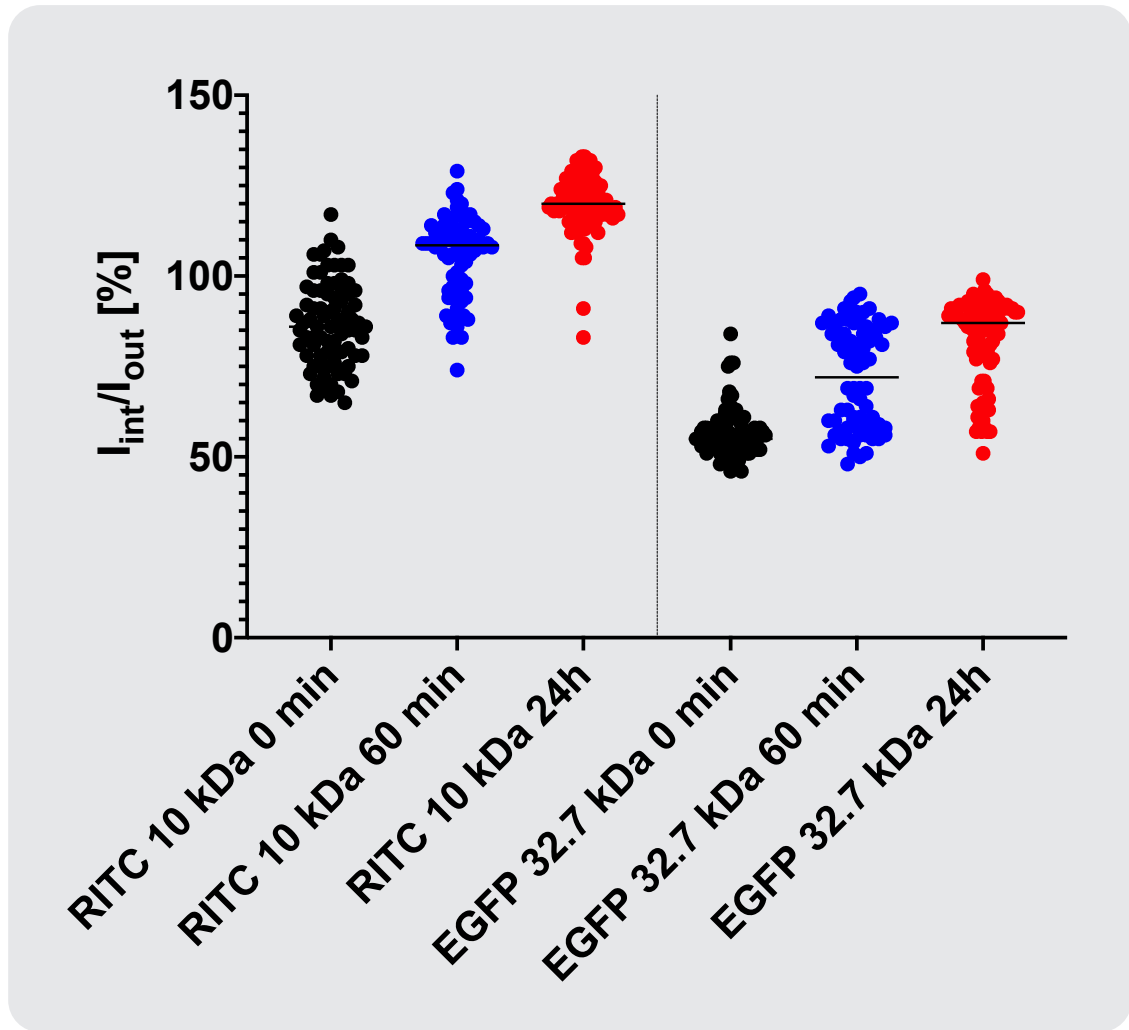


Figure 6.4: **Interior/exterior fluorescence ratios of 10 kDa RITC-dextran and EGFP.** The fluorescence ratio rapidly increases for 10 kDa RITC-dextran and is above 100 % for all but two capsules after 24 hours of incubation. The increase is slower for EGFP and more than 20 % of capsules have a ratio below 75 % after 24 hours.

## 6.5 Supplementary Figures Chapter 4

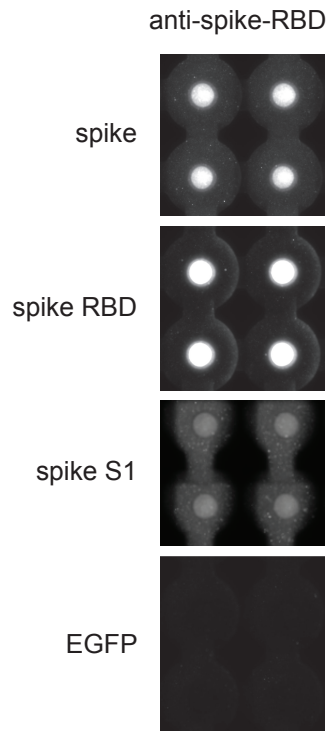


Figure 6.5: **Evaluation of SARS-CoV-2 antigens.** NIA images showing anti-IgG-PE signals obtained when spike, RBD and S1 antigens in combination with an anti-S1 primary antibody were tested. EGFP served as a negative control.



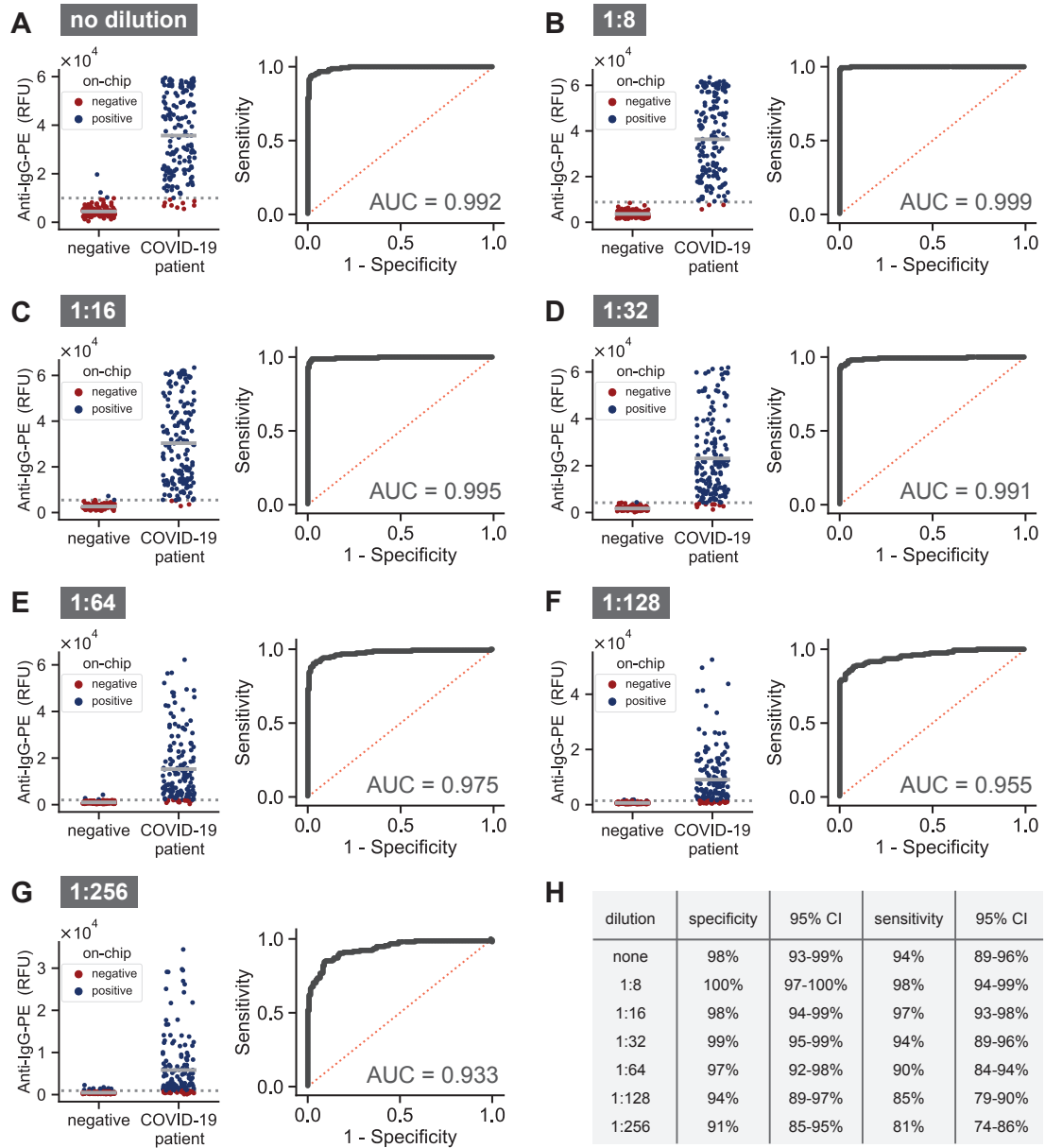


Figure 6.6: **NIA measurements for a range of sample dilutions.** (A-G) NIA measurements for different dilutions of patient serum samples categorized according to whether the sample was pre-pandemic negative or from COVID-19 patients. Data points represent mean values ( $n = 3$ ). Corresponding ROC curves are shown to the right of the plotted data. (H) Specificity and sensitivity values calculated for each dilution according to the dashed cutoff line shown in plots A-G.

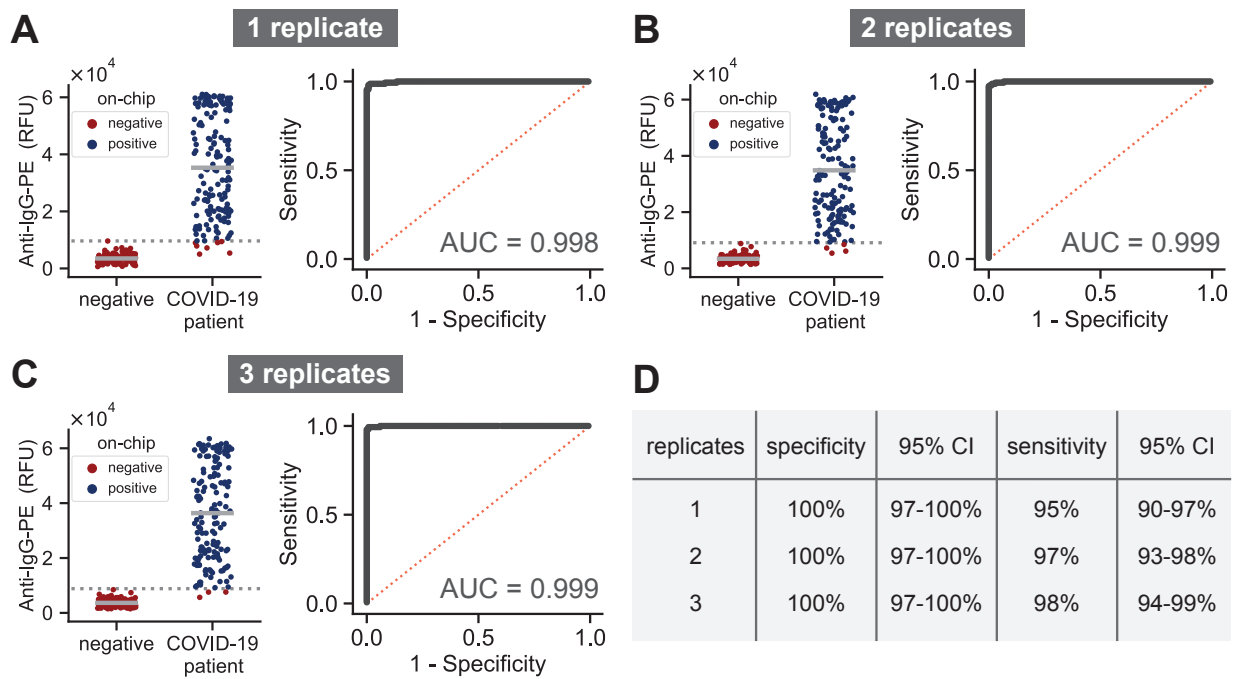


Figure 6.7: **NIA replicates.** (A-C) Mean anti-IgG-PE signal for one, two or three on-chip replicates shown for a 1:8 serum dilution, along with the corresponding ROC curves. (D) Specificity and sensitivity values calculated according number of on-chip replicates and based on the dashed cutoff line shown in plots A-C.



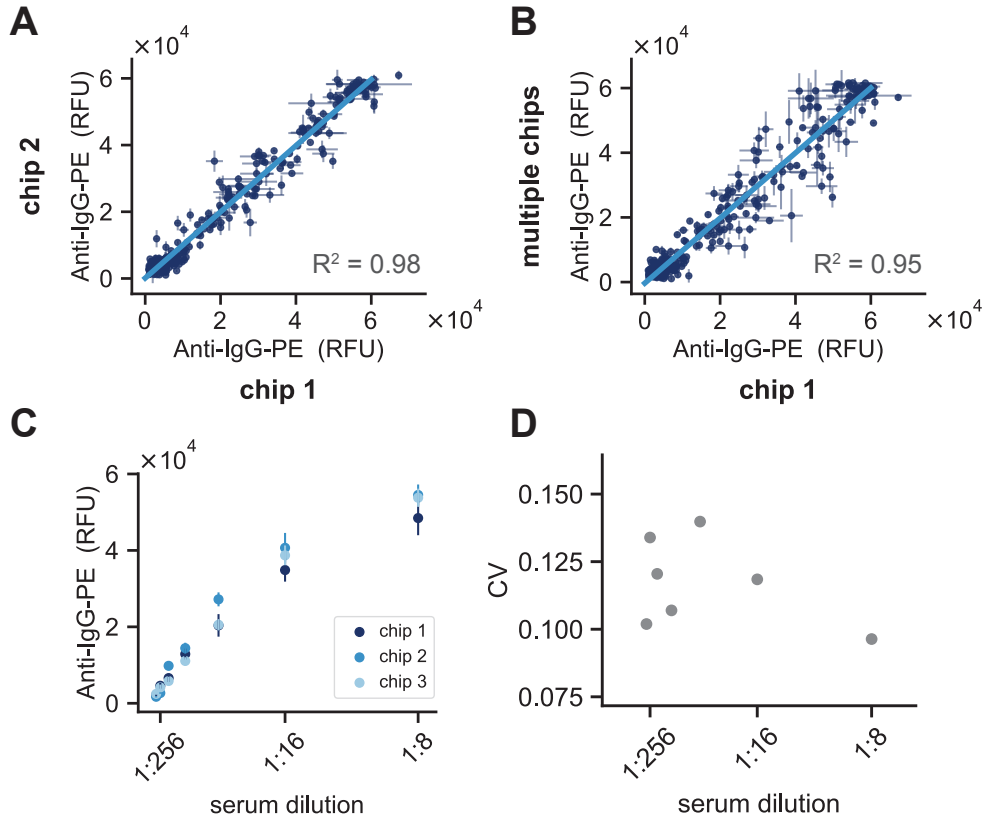


Figure 6.8: **Device-to-device variation.** (A) Correlation of anti-IgG-PE signals obtained from two separate chips that were prepared using the same 1:8 serum sample dilutions. (B) Anti-IgG-PE measurements collected from a total of 6 chips versus measurements for the same samples collected on a single chip. Sample dilutions were prepared separately for each of the chips. (C) NIA measurements for a reference serum dilution series measured on three separate chips. (D) Coefficient of variation calculated for the three measurements of each reference serum dilution.

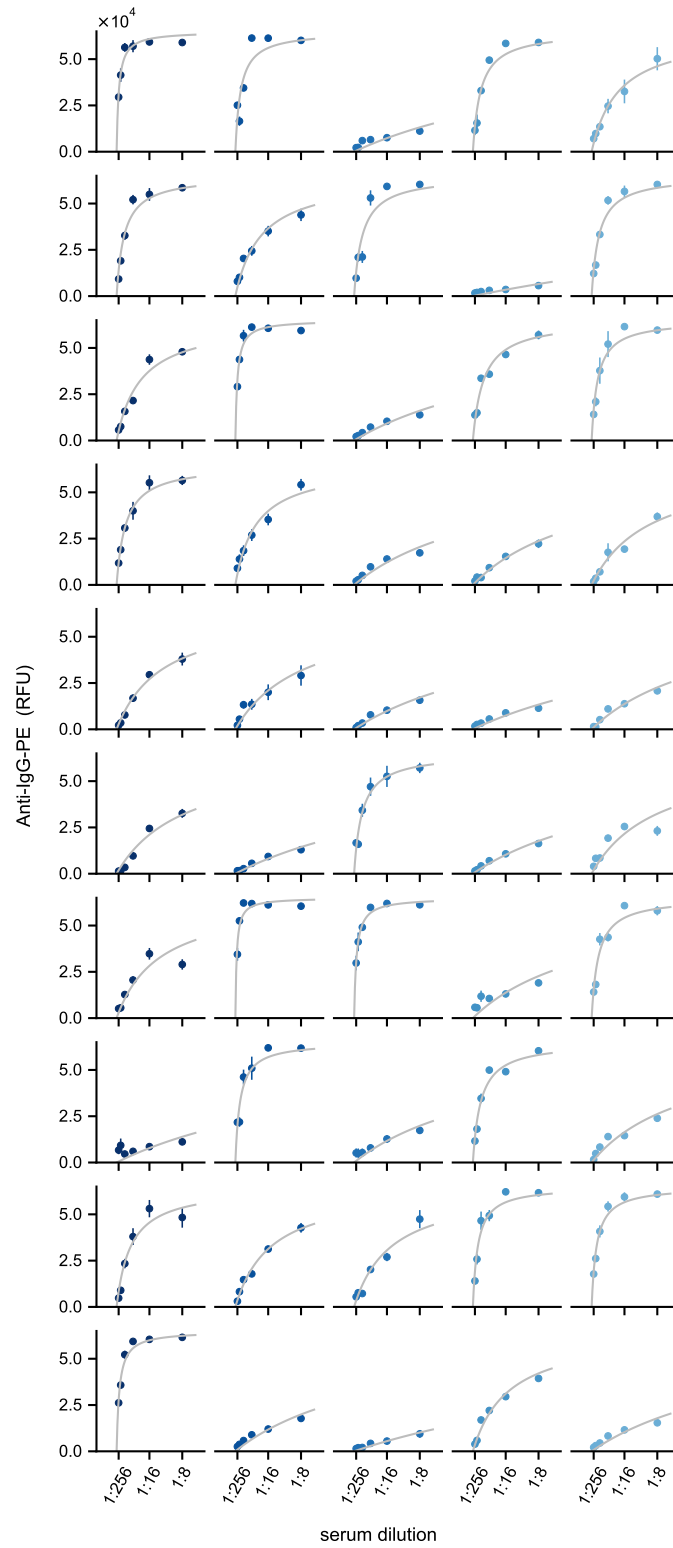


Figure 6.9: **Complete serum dilution data.** Data points are colored blue or red corresponding to dilutions from negative or positive patient serum samples, respectively.

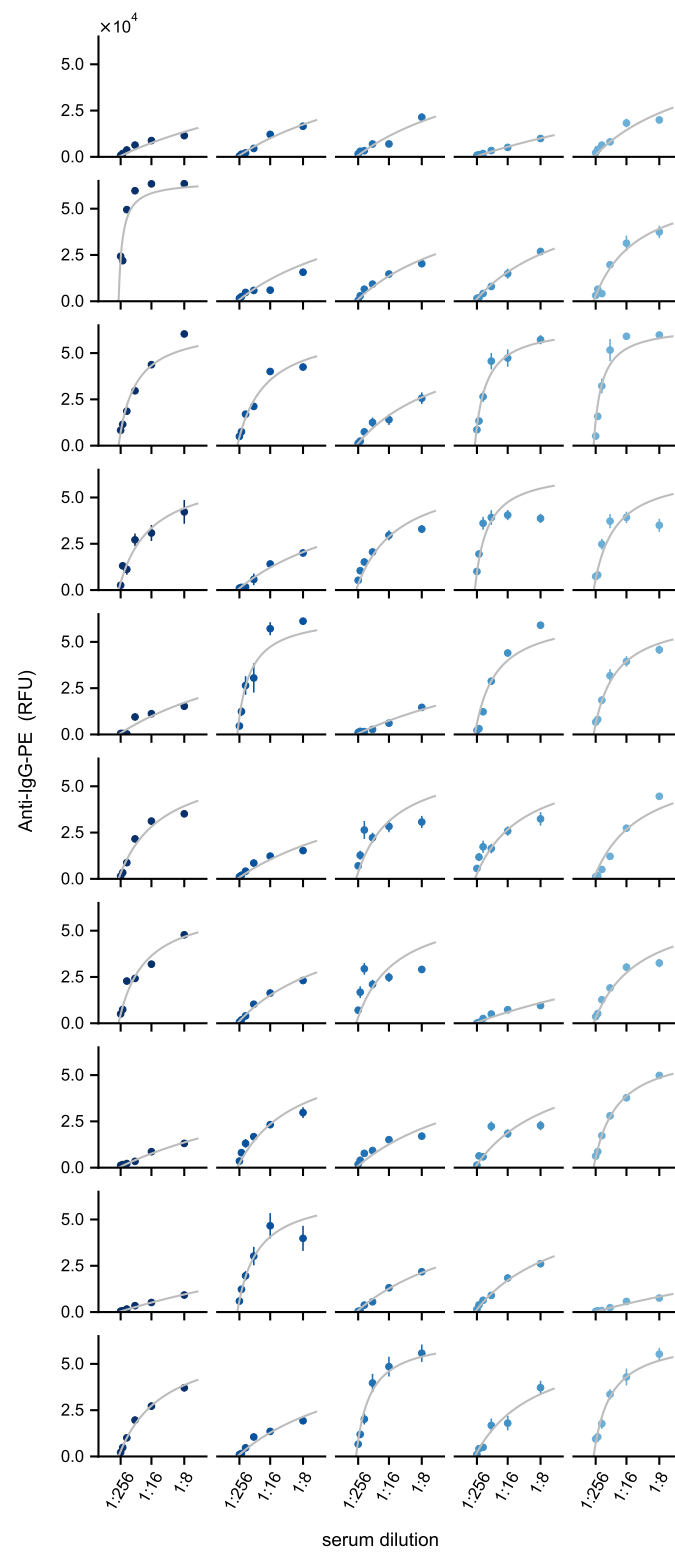


Figure 6.9: **Complete serum dilution data.**

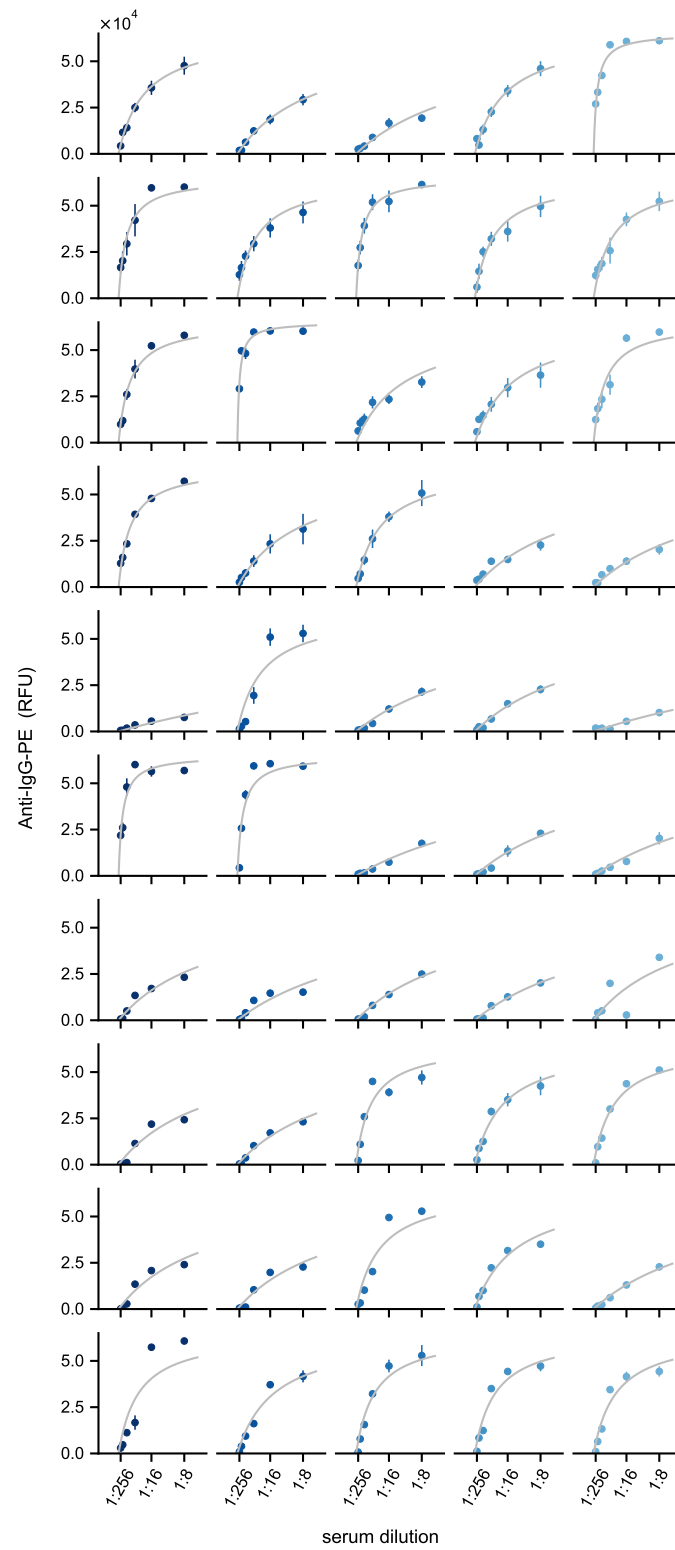


Figure 6.9: **Complete serum dilution data.**

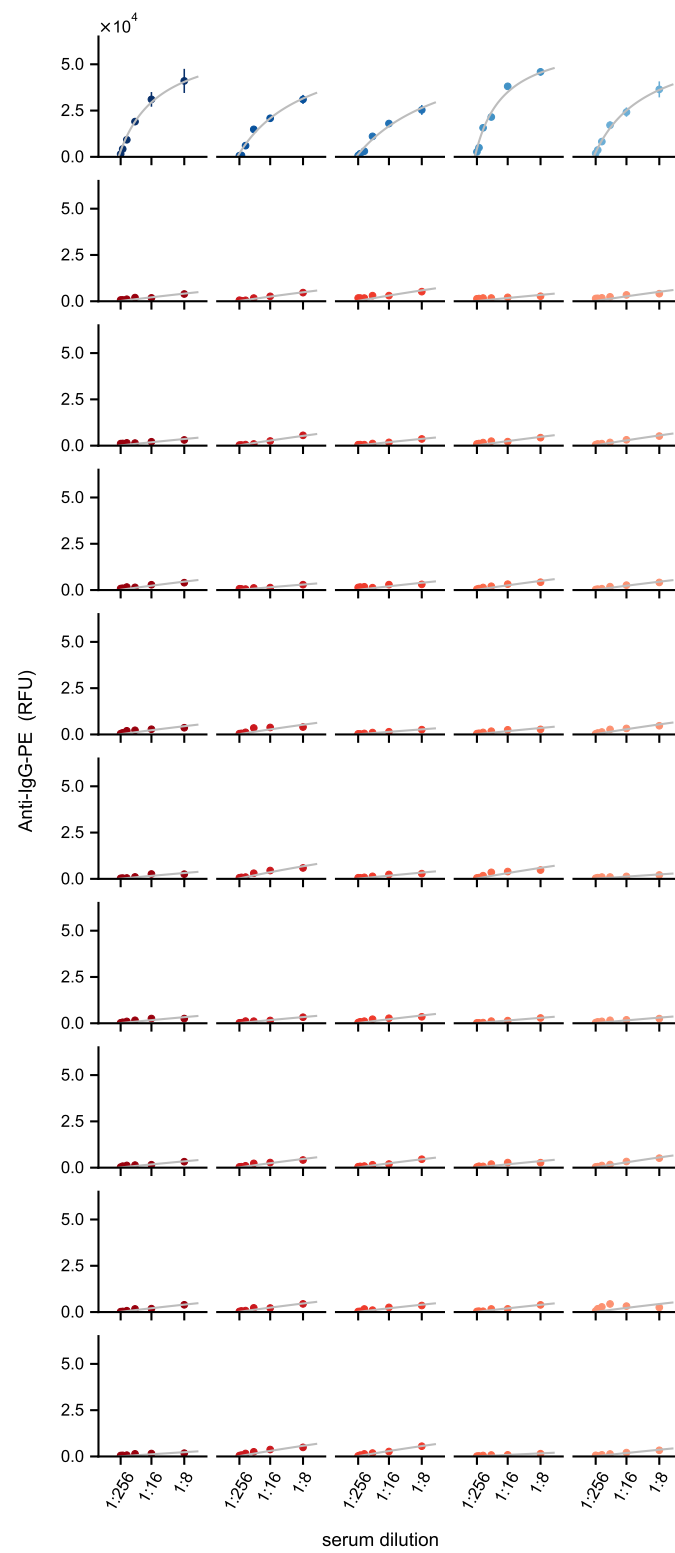


Figure 6.9: **Complete serum dilution data.**

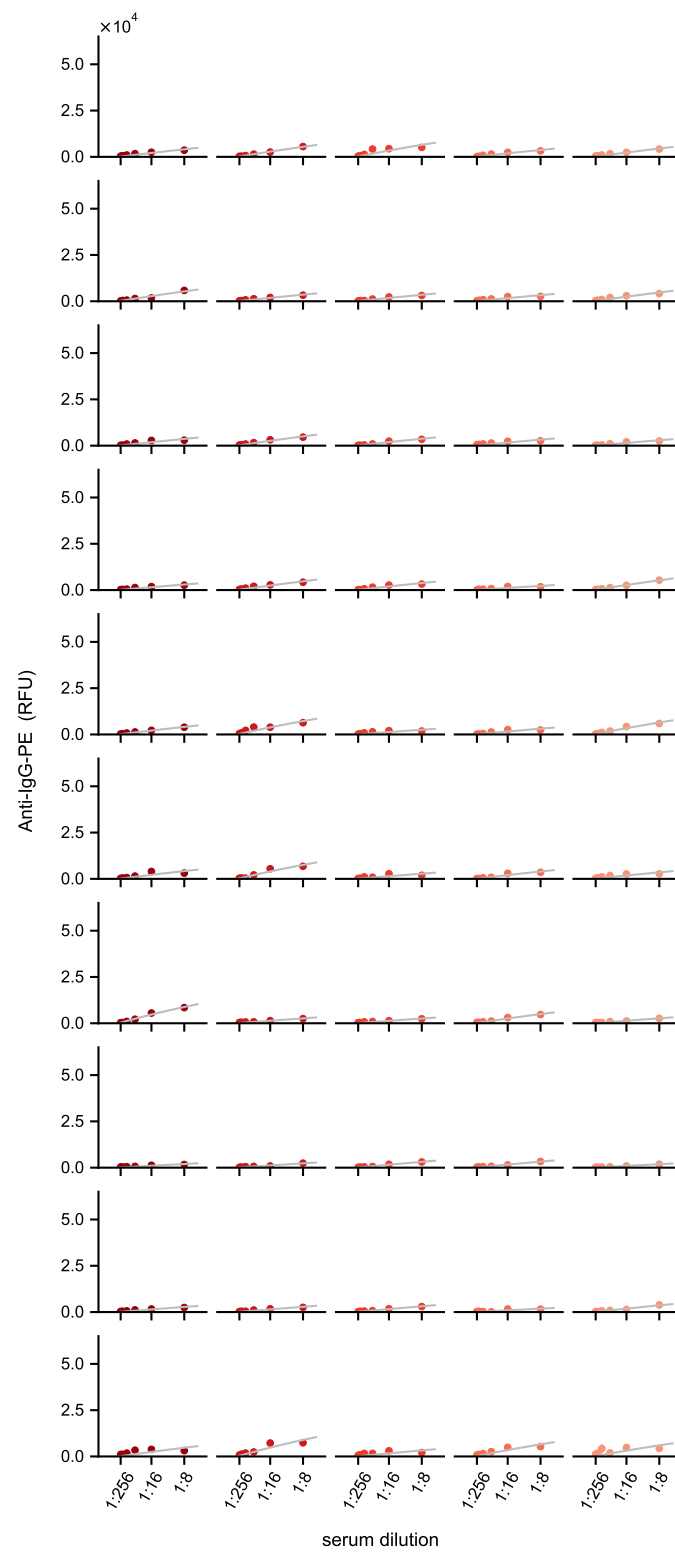


Figure 6.9: Complete serum dilution data.

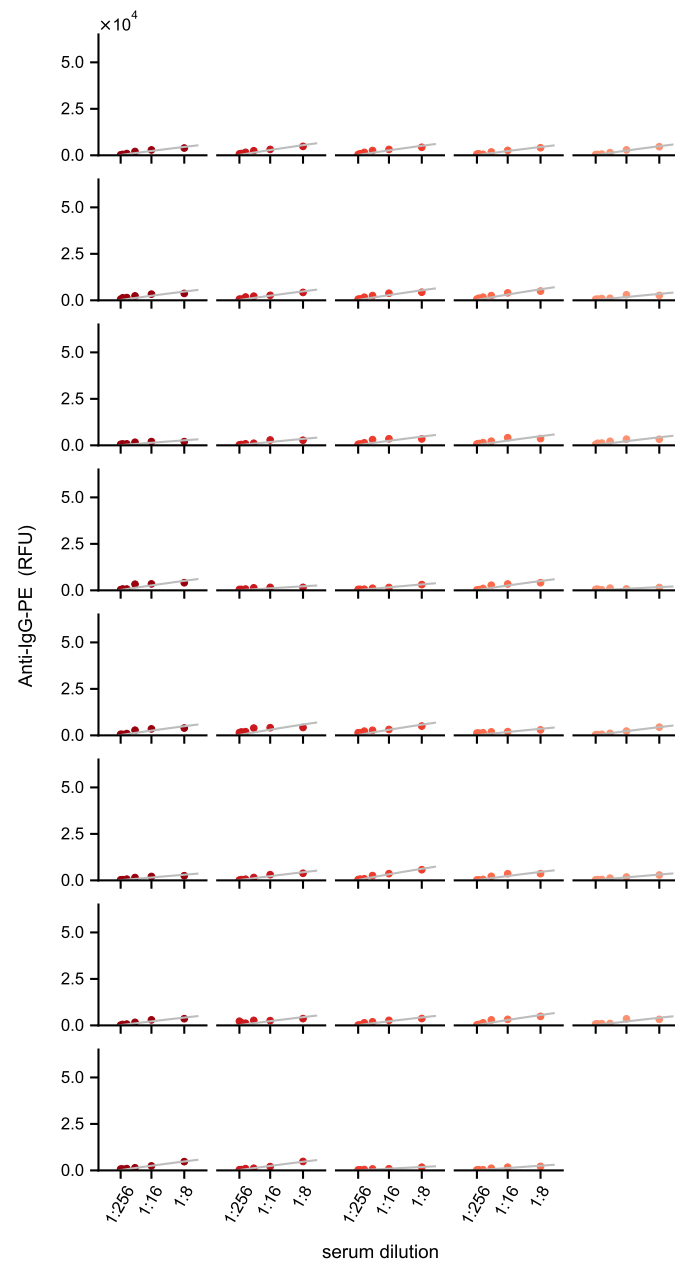


Figure 6.9: **Complete serum dilution data.**

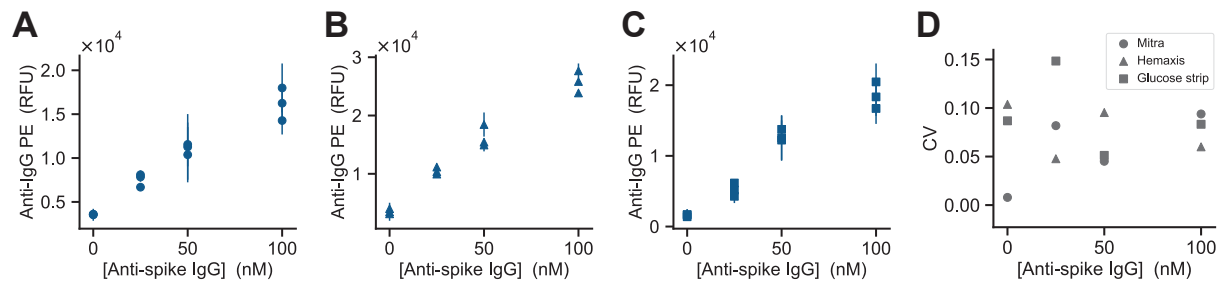


Figure 6.10: **Technical replicates for ultra-low volume whole blood sampling methods.** (A-C) On-chip anti-IgG-PE signal versus the concentration of anti-spike-IgG in whole blood for three technical replicates sampled using each of the three methods: Mitra<sup>®</sup>, HemaXis<sup>™</sup> DB10, and glucose test strips (shown in this order from left to right). (D) Coefficient of variation versus the concentration of anti-spike-IgG for each blood sampling method.



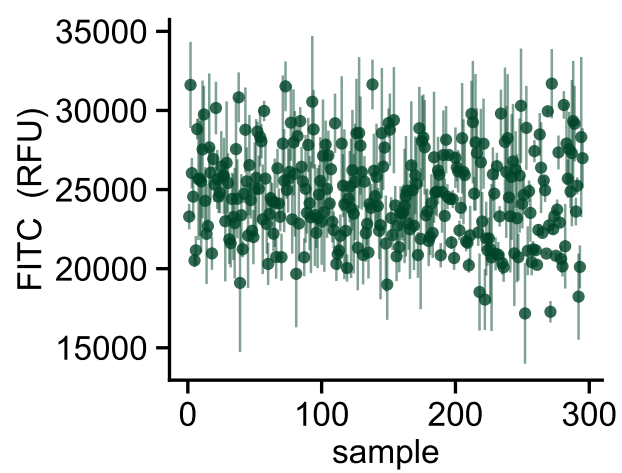


Figure 6.11: **FITC spotting tracer.** FITC-dextran (10 kDa) signal for each serum sample (1:8 dilution). Images were acquired in the spotting chamber after the sample had been resolubilized.

# Bibliography

- [1] J. J. Mitchell, Y. J. Trakadis, and C. R. Scriver, “Phenylalanine hydroxylase deficiency,” *Genetics in Medicine*, vol. 13, pp. 697–707, Aug. 2011.
- [2] Centerwall, SA and Centerwall, WR, “The discovery of phenylketonuria: The story of a young couple, two retarded children, and a scientist,” *Pediatrics*, vol. 105, pp. 89–103, Jan. 2000.
- [3] L. S. PENROSE, “Phenylketonuria; a problem in eugenics.,” *The Lancet*, vol. 1, pp. 949–953, June 1946.
- [4] H. BICKEL, J. GERRARD, and E. M. HICKMANS, “The influence of phenylalanine intake on the chemistry and behaviour of a phenyl-ketonuric child.,” *Acta paediatrica*, vol. 43, pp. 64–77, Jan. 1954.
- [5] L. I. WOOLF, R. GRIFFITHS, and A. MONCRIEFF, “Treatment of phenylketonuria with a diet low in phenylalanine.,” *British medical journal*, vol. 1, pp. 57–64, Jan. 1955.
- [6] M. D. ARMSTRONG and F. H. TYLER, “Studies on phenylketonuria. I. Restricted phenylalanine intake in phenylketonuria.,” *The Journal of clinical investigation*, vol. 34, pp. 565–580, Apr. 1955.
- [7] R. Guthrie, *The introduction of newborn screening for phenylketonuria. A personal history.*, vol. 155 Suppl 1 of *A personal history*. Universitäts-Kinderklinik, Heidelberg, Germany.: Springer-Verlag, July 1996.
- [8] R. Guthrie and A. SUSI, “A SIMPLE PHENYLALANINE METHOD FOR DETECTING PHENYLKETONURIA IN LARGE POPULATIONS OF NEWBORN INFANTS.,” *Pediatrics*, vol. 32, pp. 338–343, Sept. 1963.

- [9] H. L. Levy, “Phenylketonuria: old disease, new approach to treatment.,” *Proceedings of the National Academy of Sciences of the United States of America*, vol. 96, pp. 1811–1813, Mar. 1999.
- [10] N. Al Hafid and J. Christodoulou, “Phenylketonuria: a review of current and future treatments.,” *Translational pediatrics*, vol. 4, pp. 304–317, Oct. 2015.
- [11] N. Blau and N. Longo, “Alternative therapies to address the unmet medical needs of patients with phenylketonuria,” *Expert Opinion on Pharmacotherapy*, vol. 16, no. 6, pp. 000–000, 2015.
- [12] A. Markham, “Pegvaliase: First Global Approval,” *BioDrugs*, vol. 32, pp. 391–395, July 2018.
- [13] K. J. Pasi, S. Rangarajan, N. Mitchell, W. Lester, E. Symington, B. Madan, M. Laffan, C. B. Russell, M. Li, G. F. Pierce, and W. Y. Wong, “Multiyear Follow-up of AAV5-hFVIII-SQ Gene Therapy for Hemophilia A,” *N Engl J Med*, vol. 382, pp. 29–40, Jan. 2020.
- [14] C. N. Sarkissian, T. S. Kang, A. Gámez, C. R. Scriver, and R. C. Stevens, “Evaluation of orally administered PEGylated phenylalanine ammonia lyase in mice for the treatment of Phenylketonuria,” *Molecular Genetics and Metabolism*, vol. 104, pp. 249–254, Nov. 2011.
- [15] V. M. Isabella, B. N. Ha, M. J. Castillo, D. J. Lubkowitz, S. E. Rowe, Y. A. Millet, C. L. Anderson, N. Li, A. B. Fisher, K. A. West, P. J. Reeder, M. M. Momin, C. G. Bergeron, S. E. Guilmain, P. F. Miller, C. B. Kurtz, and D. Falb, “Development of a synthetic live bacterial therapeutic for the human metabolic disease phenylketonuria,” *Nature Biotechnology*, vol. 36, pp. 857–864, Aug. 2018.
- [16] C. M. Ambrus, J. L. Ambrus, C. Horvath, H. Pedersen, S. Sharma, C. Kant, E. Mirand, R. Guthrie, and T. Paul, “Phenylalanine depletion for the management of phenylketonuria: use of enzyme reactors with immobilized enzymes,” *Science (New York, N.Y.)*, vol. 201, no. 4358, pp. 837–839, 1978.
- [17] J. A. Hoskins, G. Jack, H. E. Wade, R. J. Peiris, E. C. Wright, D. J. Starr, and J. Stern, “Enzymatic control of phenylalanine intake in phenylketonuria.,” *The Lancet*, vol. 1, pp. 392–394, Feb. 1980.

- [18] L. Bourget and T. M. Chang, "Phenylalanine ammonia-lyase immobilized in semipermeable microcapsules for enzyme replacement in phenylketonuria.," *FEBS Letters*, vol. 180, pp. 5–8, Jan. 1985.
- [19] C. N. Sarkissian, Z. Shao, F. Blain, R. Peevers, H. Su, R. Heft, T. M. Chang, and C. R. Scriver, "A different approach to treatment of phenylketonuria: phenylalanine degradation with recombinant phenylalanine ammonia lyase.," *Proceedings of the National Academy of Sciences of the United States of America*, vol. 96, pp. 2339–2344, Mar. 1999.
- [20] H. L. Levy, C. N. Sarkissian, and C. R. Scriver, "Phenylalanine ammonia lyase (PAL)<sub>From discovery to enzyme substitution therapy for phenylketonuria,</sub>" *Molecular Genetics and Metabolism*, pp. 218–229, Aug. 2018.
- [21] Y. Levy, M. S. Hershfield, C. Fernandez-Mejia, S. H. Polmar, D. Scudiery, M. Berger, and R. U. Sorensen, "Adenosine deaminase deficiency with late onset of recurrent infections: response to treatment with polyethylene glycol-modified adenosine deaminase.," *The Journal of Pediatrics*, vol. 113, pp. 312–317, Aug. 1988.
- [22] A. Gámez, L. Wang, M. Straub, M. G. Patch, and R. C. Stevens, "Toward PKU Enzyme Replacement Therapy: PEGylation with Activity Retention for Three Forms of Recombinant Phenylalanine Hydroxylase," *Molecular Therapy*, vol. 9, pp. 124–129, Jan. 2004.
- [23] L. Wang, A. Gámez, C. N. Sarkissian, M. Straub, M. G. Patch, G. W. Han, S. Striepeke, P. Fitzpatrick, C. R. Scriver, and R. C. Stevens, "Structure-based chemical modification strategy for enzyme replacement treatment of phenylketonuria," *Molecular Genetics and Metabolism*, vol. 86, pp. 134–140, Sept. 2005.
- [24] A. GAMEZ, C. SARKISSIAN, L. WANG, W. KIM, M. STRAUB, M. PATCH, L. CHEN, S. STRIEPEKE, P. FITZPATRICK, and J. LEMONTT, "Development of Pegylated Forms of Recombinant Phenylalanine Ammonia-Lyase for the Treatment of Classical Phenylketonuria," *Molecular Therapy*, vol. 11, pp. 986–989, June 2005.
- [25] A. Gámez, L. Wang, C. N. Sarkissian, D. Wendt, P. Fitzpatrick, J. F. Lemontt, C. R. Scriver, and R. C. Stevens, "Structure-based epitope and PEGylation sites mapping of phenylalanine ammonia-lyase for enzyme substitution treatment of phenylketonuria," *Molecular Genetics and Metabolism*, vol. 91, pp. 325–334, Aug. 2007.

- [26] M. C. Moffitt, G. V. Louie, M. E. Bowman, J. Pence, J. P. Noel, and B. S. Moore, “Discovery of Two Cyanobacterial Phenylalanine Ammonia Lyases: Kinetic and Structural Characterization  $\dagger, \ddagger$ ,” *Biochemistry*, vol. 46, pp. 1004–1012, Jan. 2007.
- [27] L. Wang, A. Gámez, H. Archer, E. E. Abola, C. N. Sarkissian, P. Fitzpatrick, D. Wendt, Y. Zhang, M. Vellard, J. Bliesath, S. M. Bell, J. F. Lemontt, C. R. Scriver, and R. C. Stevens, “Structural and Biochemical Characterization of the Therapeutic *Anabaena variabilis* Phenylalanine Ammonia Lyase,” *Journal of Molecular Biology*, vol. 380, pp. 623–635, July 2008.
- [28] T. S. Kang, L. Wang, C. N. Sarkissian, A. Gámez, C. R. Scriver, and R. C. Stevens, “Converting an injectable protein therapeutic into an oral form: Phenylalanine ammonia lyase for phenylketonuria,” *Molecular Genetics and Metabolism*, vol. 99, pp. 4–9, Jan. 2010.
- [29] A. Shedlovsky, J. D. McDonald, D. Symula, and W. F. Dove, “Mouse models of human phenylketonuria,” *Genetics*, vol. 134, pp. 1205–1210, Aug. 1993.
- [30] I. P. de Sousa, C. Gourmel, O. Berkovska, M. Burger, and J.-C. Leroux, “A microparticulate based formulation to protect therapeutic enzymes from proteolytic digestion: phenylalanine ammonia lyase as case study,” *Scientific Reports*, vol. 10, pp. 1–11, Feb. 2020.
- [31] G. Rosenblum and B. S. Cooperman, “Engine out of the chassis: Cell-free protein synthesis and its uses,” *FEBS Letters*, vol. 588, pp. 261–268, Jan. 2014.
- [32] S. Chong, “Overview of cell-free protein synthesis: historic landmarks, commercial systems, and expanding applications,” *Current protocols in molecular biology*, vol. 108, pp. 16.30.1–11, Oct. 2014.
- [33] G. Zubay, “In vitro synthesis of protein in microbial systems,” *Annual review of genetics*, vol. 7, no. 1, pp. 267–287, 1973.
- [34] A. C. Chiao, R. M. Murray, and Z. Z. Sun, “Development of prokaryotic cell-free systems for synthetic biology,” *bioRxiv*, pp. 1–38, Apr. 2016.
- [35] B. E. Roberts and B. M. Paterson, “Efficient translation of tobacco mosaic virus RNA and rabbit globin 9S RNA in a cell-free system from commercial wheat germ,” *Proceedings of the*

- National Academy of Sciences of the United States of America*, vol. 70, pp. 2330–2334, Aug. 1973.
- [36] K. Madin, T. Sawasaki, T. Ogasawara, and Y. Endo, “A highly efficient and robust cell-free protein synthesis system prepared from wheat embryos: plants apparently contain a suicide system directed at ribosomes.,” *Proceedings of the National Academy of Sciences of the United States of America*, vol. 97, pp. 559–564, Jan. 2000.
  - [37] H. R. Pelham and R. J. Jackson, “An efficient mRNA-dependent translation system from reticulocyte lysates.,” *European journal of biochemistry*, vol. 67, pp. 247–256, Aug. 1976.
  - [38] M. R. Swerdel and A. M. Fallon, “Cell-free translation in lysates from *Spodoptera frugiperda* (Lepidoptera: Noctuidae) cells.,” *Comparative biochemistry and physiology. B, Comparative biochemistry*, vol. 93, no. 4, pp. 803–806, 1989.
  - [39] A. K. Brödel, A. Sonnabend, and S. Kubick, “Cell-free protein expression based on extracts from CHO cells.,” *Biotechnology and Bioengineering*, vol. 111, pp. 25–36, Jan. 2014.
  - [40] S. Mikami, M. Masutani, N. Sonenberg, S. Yokoyama, and H. Imataka, “An efficient mammalian cell-free translation system supplemented with translation factors,” *Protein Expression and Purification*, vol. 46, pp. 348–357, Apr. 2006.
  - [41] S. Mikami, T. Kobayashi, S. Yokoyama, and H. Imataka, “A hybridoma-based in vitro translation system that efficiently synthesizes glycoproteins,” *Journal of Biotechnology*, vol. 127, pp. 65–78, Dec. 2006.
  - [42] M. Buntru, S. Vogel, H. Spiegel, and S. Schillberg, “Tobacco BY-2 cell-free lysate: an alternative and highly-productive plant-based in vitro translation system,” *BMC Biotechnology*, vol. 14, pp. 5–11, May 2014.
  - [43] S. Schillberg, “Critical Analysis of the Commercial Potential of Plants for the Production of Recombinant Proteins,” pp. 1–10, June 2019.
  - [44] Y. Shimizu, A. Inoue, Y. Tomari, T. Suzuki, T. Yokogawa, K. Nishikawa, and T. Ueda, “Cell-free translation reconstituted with purified components.,” *Nature Biotechnology*, vol. 19, pp. 751–755, Aug. 2001.

- [45] Z. Z. Sun, C. A. Hayes, J. Shin, F. Caschera, R. M. Murray, and V. Noireaux, "Protocols for Implementing an *jemE*/Escherichia coli/*emE* Based TX-TL Cell-Free Expression System for Synthetic Biology," *Journal of Visualized Experiments*, no. 79, pp. 1–14, 2013.
- [46] Y.-C. Kwon and M. C. Jewett, "High-throughput preparation methods of crude extract for robust cell-free protein synthesis," *Scientific Reports*, vol. 5, pp. 8663–8, Mar. 2015.
- [47] J. F. Zawada, G. Yin, A. R. Steiner, J. Yang, A. Naresh, S. M. Roy, D. S. Gold, H. G. Heinsohn, and C. J. Murray, "Microscale to manufacturing scale-up of cell-free cytokine production-a new approach for shortening protein production development timelines," *Biotechnology and Bioengineering*, vol. 108, pp. 1570–1578, Mar. 2011.
- [48] Q. Cai, J. A. Hanson, A. R. Steiner, C. Tran, M. R. Masikat, R. Chen, J. F. Zawada, A. K. Sato, T. J. Hallam, and G. Yin, "A simplified and robust protocol for immunoglobulin expression in Escherichia coli cell-free protein synthesis systems," *Biotechnology Progress*, vol. 31, pp. 823–831, Apr. 2015.
- [49] M. C. Jewett, K. A. Calhoun, A. Voloshin, J. J. Wu, and J. R. Swartz, "An integrated cell-free metabolic platform for protein production and synthetic biology," *Molecular Systems Biology*, vol. 4, pp. 1–10, Oct. 2008.
- [50] E. S. Zimmerman, T. H. Heibeck, A. Gill, X. Li, C. J. Murray, M. R. Madlansacay, C. Tran, N. T. Uter, G. Yin, P. J. Rivers, A. Y. Yam, W. D. Wang, A. R. Steiner, S. U. Bajad, K. Penta, W. Yang, T. J. Hallam, C. D. Thanos, and A. K. Sato, "Production of Site-Specific Antibody–Drug Conjugates Using Optimized Non-Natural Amino Acids in a Cell-Free Expression System," *Bioconjugate Chemistry*, vol. 25, pp. 351–361, Feb. 2014.
- [51] Y. Xu, J. Lee, C. Tran, T. H. Heibeck, W. D. Wang, J. Yang, R. L. Stafford, A. R. Steiner, A. K. Sato, T. J. Hallam, and G. Yin, "Production of bispecific antibodies in "knobs-into-holes" using a cell-free expression system," *mAbs*, vol. 7, pp. 231–242, Jan. 2015.
- [52] J. Jones, J. Tuck, S. Went, and P. Probert, "Development of an In-House Cell Free Extract Process and Robotic Platform for Expression Optimization," *American Pharmaceutical Review*, June 2019.

- [53] K. Pardee, S. Slomovic, P. Q. Nguyen, J. W. Lee, N. Donghia, D. Burrill, T. Ferrante, F. R. McSorley, Y. Furuta, A. Vernet, M. Lewandowski, C. N. Boddy, N. S. Joshi, and J. J. Collins, “Portable, On-Demand Biomolecular Manufacturing,” *Cell*, vol. 167, pp. 248–254.e12, Sept. 2016.
- [54] A. S. M. Salehi, M. T. Smith, A. M. Bennett, J. B. Williams, W. G. Pitt, and B. C. Bundy, “Cell-free protein synthesis of a cytotoxic cancer therapeutic: Onconase production and a just-add-water cell-free system,” *Biotechnology Journal*, vol. 11, pp. 274–281, Nov. 2015.
- [55] M. T. Smith, A. M. Bennett, J. M. Hunt, and B. C. Bundy, “Creating a completely “cell-free” system for protein synthesis,” *Biotechnology Progress*, vol. 31, pp. 1716–1719, Aug. 2015.
- [56] J. C. Stark, A. Huang, P. Q. Nguyen, R. S. Dubner, K. J. Hsu, T. C. Ferrante, M. Anderson, A. Kanapskyte, Q. Mucha, J. S. Packett, P. Patel, R. Patel, D. Qaq, T. Zondor, J. Burke, T. Martinez, A. Miller-Berry, A. Puppala, K. Reichert, M. Schmid, L. Brand, L. R. Hill, J. F. Chellaswamy, N. Faheem, S. Fetherling, E. Gong, E. M. Gonzalzes, T. Granito, J. Koritsaris, B. Nguyen, S. Ottman, C. Palffy, A. Patel, S. Skweres, A. Slaton, T. Woods, N. Donghia, K. Pardee, J. J. Collins, and M. C. Jewett, “BioBits™ Bright: A fluorescent synthetic biology education kit,” *Science Advances*, vol. 4, pp. eaat5107–532, Aug. 2018.
- [57] A. Huang, P. Q. Nguyen, J. C. Stark, M. K. Takahashi, N. Donghia, T. Ferrante, A. J. Dy, K. J. Hsu, R. S. Dubner, K. Pardee, M. C. Jewett, and J. J. Collins, “BioBits™ Explorer: A modular synthetic biology education kit,” *Science Advances*, vol. 4, p. eaat5105, Aug. 2018.
- [58] J. C. Stark, A. Huang, K. J. Hsu, R. S. Dubner, J. Forbrook, S. Marshalla, F. Rodriguez, M. Washington, G. A. Rybnicky, P. Q. Nguyen, B. Hasselbacher, R. Jabri, R. Kamran, V. Koralewski, W. Wightkin, T. Martinez, and M. C. Jewett, “BioBits Health: Classroom Activities Exploring Engineering, Biology, and Human Health with Fluorescent Readouts,” *ACS Synthetic Biology*, vol. 8, pp. 1001–1009, Mar. 2019.
- [59] S. M. Bell, D. J. Wendt, Y. Zhang, T. W. Taylor, S. Long, L. Tsuruda, B. Zhao, P. Laipis, and P. A. Fitzpatrick, “Formulation and PEGylation optimization of the therapeutic PEGylated phenylalanine ammonia lyase for the treatment of phenylketonuria,” *PLoS ONE*, vol. 12, pp. e0173269–17, Mar. 2017.



- [60] S. M. Rombach, C. E. M. Hollak, G. E. Linthorst, and M. G. W. Dijkgraaf, “Cost-effectiveness of enzyme replacement therapy for Fabry disease.,” *Orphanet journal of rare diseases*, vol. 8, p. 29, Feb. 2013.
- [61] A. B. Engelberg, A. S. Kesselheim, and J. Avorn, “Balancing innovation, access, and profits—market exclusivity for biologics.,” *N Engl J Med*, vol. 361, pp. 1917–1919, Nov. 2009.
- [62] Institute of Medicine (US) Committee on Accelerating Rare Diseases Research and Orphan Product Development, M. J. Field, and T. F. Boat, “Rare Diseases and Orphan Products: Accelerating Research and Development,” 2010.
- [63] H. Schellekens, M. Aldosari, H. Talsma, and E. Mastrobattista, “Making individualized drugs a reality.,” *Nature Publishing Group*, vol. 35, pp. 507–513, June 2017.
- [64] “Patient-centered drug manufacture.,” *Nature Publishing Group*, vol. 35, pp. 485–485, June 2017.
- [65] J. Woodcock and M. Wosinska, “Economic and Technological Drivers of Generic Sterile Injectable Drug Shortages,” *Clinical Pharmacology & Therapeutics*, pp. 1–7, Nov. 2012.
- [66] G. E. Linthorst, D. P. Germain, C. E. M. Hollak, D. Hughes, A. Rolfs, C. Wanner, and A. Mehta, “Expert opinion on temporary treatment recommendations for Fabry disease during the shortage of enzyme replacement therapy (ERT),” *Molecular Genetics and Metabolism*, vol. 102, pp. 99–102, Jan. 2011.
- [67] S. Sirrs, “The Fabrazyme shortage—A call to action for metabolic physicians,” *Molecular Genetics and Metabolism*, vol. 102, pp. 4–5, Jan. 2011.
- [68] L. E. Crowell, A. E. Lu, K. R. Love, A. Stockdale, S. M. Timmick, D. Wu, Y. A. Wang, W. Doherty, A. Bonnyman, N. Vecchiarello, C. Goodwine, L. Bradbury, J. R. Brady, J. J. Clark, N. A. Colant, A. Cvetkovic, N. C. Dalvie, D. Liu, Y. Liu, C. A. Mascarenhas, C. B. Matthews, N. J. Mozdierz, K. A. Shah, S.-L. Wu, W. S. Hancock, R. D. Braatz, S. M. Cramer, and J. C. Love, “On-demand manufacturing of clinical-quality biopharmaceuticals,” *Nature Biotechnology*, vol. 36, pp. 988–995, Oct. 2018.

- [69] B. P. Mohr, S. T. Retterer, and M. J. Doktycz, “While-you-wait proteins? Producing biomolecules at the point of need,” *Expert Review of Proteomics*, vol. 13, pp. 707–709, July 2016.
- [70] C. J. Sullivan, E. D. Pendleton, H. H. Sasmor, W. L. Hicks, J. B. Farnum, M. Muto, E. M. Amendt, J. A. Schoborg, R. W. Martin, L. G. Clark, M. J. Anderson, A. Choudhury, R. Fior, Y.-H. Lo, R. H. Griffey, S. A. Chappell, M. C. Jewett, V. P. Mauro, and J. Dresios, “A cell-free expression and purification process for rapid production of protein biologics,” *Biotechnology Journal*, vol. 11, pp. 238–248, Dec. 2015.
- [71] C. J. Sullivan, E. D. Pendleton, and J. Dresios, “Cell-Free Production of Protein Biologics Within 24 H,” in *Recombinant Glycoprotein Production: Methods and Protocols* (V. i. n. Picanço-Castro and K. Swiech, eds.), pp. 95–107, New York, NY: Springer New York, 2018.
- [72] T. W. Murphy, J. Sheng, L. B. Naler, X. Feng, and C. Lu, “On-chip manufacturing of synthetic proteins for point-of-care therapeutics,” *Microsystems & Nanoengineering*, vol. 5, pp. 1–12, Mar. 2019.
- [73] E. Zhao and B. C. Bundy, “Advancing Space Flight Medical Care through On-demand Protein Therapeutic Production Capabilities,” 2019.
- [74] S. L. Lovelock, R. C. Lloyd, and N. J. Turner, “Phenylalanine Ammonia Lyase Catalyzed Synthesis of Amino Acids by an MIO-Cofactor Independent Pathway,” *Angewandte Chemie International Edition*, vol. 53, pp. 4652–4656, Apr. 2014.
- [75] F. Caschera and V. Noireaux, “Synthesis of 2.3 mg/ml of protein with an all Escherichia coli cell-free transcription-translation system,” *Biochimie*, vol. 99, pp. 162–168, Apr. 2014.
- [76] D. K. Karig, S. Bessling, P. Thielen, S. Zhang, and J. Wolfe, “Preservation of protein expression systems at elevated temperatures for portable therapeutic production,” *Journal of The Royal Society Interface*, vol. 14, pp. 20161039–8, Apr. 2017.
- [77] K. Pardee, A. A. Green, T. Ferrante, D. E. Cameron, A. DaleyKeyser, P. Yin, and J. J. Collins, “Paper-Based Synthetic Gene Networks,” *Cell*, vol. 159, pp. 940–954, Nov. 2014.
- [78] K. L. Kiick, E. Saxon, D. A. Tirrell, and C. R. Bertozzi, “Incorporation of azides into recombinant proteins for chemoselective modification by the Staudinger ligation,” *Proceedings of*

- the National Academy of Sciences of the United States of America*, vol. 99, pp. 19–24, Jan. 2002.
- [79] K. G. Patel and J. R. Swartz, “Surface Functionalization of Virus-Like Particles by Direct Conjugation Using Azide-Alkyne Click Chemistry,” *Bioconjugate Chemistry*, vol. 22, pp. 376–387, Mar. 2011.
  - [80] F. Himo, T. Lovell, R. Hilgraf, V. V. Rostovtsev, L. Noodleman, K. B. Sharpless, and V. V. Fokin, “Copper(I)-Catalyzed Synthesis of Azoles. DFT Study Predicts Unprecedented Reactivity and Intermediates,” *Journal of the American Chemical Society*, vol. 127, pp. 210–216, Jan. 2005.
  - [81] J. Dommerholt, F. P. J. T. Rutjes, and F. L. Delft, “Strain-Promoted 1,3-Dipolar Cycloaddition of Cycloalkynes and Organic Azides,” *Topics in Current Chemistry*, vol. 374, pp. 1–20, Mar. 2016.
  - [82] C. Cassidy-Amstutz, L. Oltrogge, C. C. Going, A. Lee, P. Teng, D. Quintanilla, A. East-Seletsky, E. R. Williams, and D. F. Savage, “Identification of a Minimal Peptide Tag for in Vivo and in Vitro Loading of Encapsulin,” *Biochemistry*, vol. 55, pp. 3461–3468, June 2016.
  - [83] F. Caschera and V. Noireaux, “A cost-effective polyphosphate-based metabolism fuels an all E. coli cell-free expression system,” *Metabolic Engineering*, vol. 27, pp. 29–37, Jan. 2015.
  - [84] H.-C. Kim, T.-W. Kim, and D.-M. Kim, “Prolonged production of proteins in a cell-free protein synthesis system using polymeric carbohydrates as an energy source,” *Process Biochemistry*, vol. 46, pp. 1366–1369, June 2011.
  - [85] A. S. Spirin, “High-throughput cell-free systems for synthesis of functionally active proteins,” *Trends in Biotechnology*, vol. 22, pp. 538–545, Oct. 2004.
  - [86] A. C. Timm, P. G. Shankles, C. M. Foster, M. J. Doktycz, and S. T. Retterer, “Toward Microfluidic Reactors for Cell-Free Protein Synthesis at the Point-of-Care,” *Small*, vol. 12, pp. 810–817, Dec. 2015.
  - [87] K. Libicher, R. Hornberger, M. Heymann, and H. Mutschler, “In vitro self-replication and multicistronic expression of large synthetic genomes,” *Nature Communications*, vol. 11, pp. 1–8, Feb. 2020.

- [88] K. Hibi, K. Amikura, N. Sugiura, K. Masuda, S. Ohno, T. Yokogawa, T. Ueda, and Y. Shimizu, “Reconstituted cell-free protein synthesis using in vitro transcribed tRNAs,” *Communications Biology*, vol. 3, pp. 1–11, June 2020.
- [89] M. C. Jewett, B. R. Fritz, L. E. Timmerman, and G. M. Church, “In vitro integration of ribosomal RNA synthesis, ribosome assembly, and translation,” *Molecular Systems Biology*, vol. 9, pp. 1–8, June 2013.
- [90] B. Lavickova, N. Laohakunakorn, and S. J. Maerkl, “A partially self-regenerating synthetic cell,” *Nature Communications*, vol. 11, pp. 1–11, Dec. 2020.
- [91] S. Berhanu, T. Ueda, and Y. Kuruma, “Artificial photosynthetic cell producing energy for protein synthesis,” *Nature Communications*, vol. 10, pp. 1325–10, Mar. 2019.
- [92] T. E. Miller, T. Beneyton, T. Schwander, C. Diehl, M. Girault, R. McLean, T. Chotel, P. Claus, N. S. Cortina, J.-C. Baret, and T. J. Erb, “Light-powered CO<sub>2</sub> fixation in a chloroplast mimic with natural and synthetic parts,” *Science (New York, N.Y.)*, vol. 368, pp. 649–654, May 2020.
- [93] S.-M. Schinn, A. Broadbent, W. T. Bradley, and B. C. Bundy, “Protein synthesis directly from PCR: progress and applications of cell-free protein synthesis with linear DNA,” *New BIOTECHNOLOGY*, vol. 33, pp. 480–487, June 2016.
- [94] Z. Z. Sun, E. Yeung, C. A. Hayes, V. Noireaux, and R. M. Murray, “Linear DNA for Rapid Prototyping of Synthetic Biological Circuits in an Escherichia coliBased TX-TL Cell-Free System,” *ACS Synthetic Biology*, vol. 3, pp. 387–397, June 2014.
- [95] M. Su’etsugu, H. Takada, T. Katayama, and H. Tsujimoto, “Exponential propagation of large circular DNA by reconstitution of a chromosome-replication cycle,” *Nucleic Acids Research*, vol. 45, pp. 11525–11534, Sept. 2017.
- [96] H. Zheng, S. C. Lefebvre, S. R. Smith, T. J. Hanly, Y. Suzuki, and A. E. Allen, “Successful Diatom Transcription Factor Synthesis and Downstream Cloning Using the BioXp™ 3200 System,” *BioTechniques*, vol. 59, pp. 1–2, July 2015.
- [97] T. M. S. Chang, “Therapeutic applications of polymeric artificial cells,” *Nature reviews. Drug discovery*, vol. 4, pp. 221–235, Mar. 2005.

- [98] S. Mytnyk, I. Ziemecka, A. G. L. Olive, J. W. M. van der Meer, K. A. Totlani, S. Oldenhof, M. T. Kreutzer, V. Van Steijn, and J. H. van Esch, “Microcapsules with a permeable hydrogel shell and an aqueous core continuously produced in a 3D microdevice by all-aqueous microfluidics,” *RSC Advances*, vol. 7, pp. 11331–11337, Feb. 2017.
- [99] G. Leonaviciene, K. Leonavicius, R. Meskys, and L. Mazutis, “Multi-step processing of single cells using semi-permeable capsules,” *Lab Chip*, vol. 55, pp. 159–11, 2020.
- [100] H. C. Shum, J.-W. Kim, and D. A. Weitz, “Microfluidic Fabrication of Monodisperse Biocompatible and Biodegradable Polymersomes with Controlled Permeability,” *Journal of the American Chemical Society*, vol. 130, pp. 9543–9549, July 2008.
- [101] C. Martino, S.-H. Kim, L. Horsfall, A. Abbaspourrad, S. J. Rosser, J. Cooper, and D. A. Weitz, “Protein Expression, Aggregation, and Triggered Release from Polymersomes as Artificial Cell-like Structures,” *Angewandte Chemie International Edition*, vol. 51, pp. 6416–6420, May 2012.
- [102] J. G. Werner, B. T. Deveney, S. Nawar, and D. A. Weitz, “Dynamic Microcapsules with Rapid and Reversible Permeability Switching,” *Advanced Functional Materials*, vol. 28, pp. 1803385–10, Aug. 2018.
- [103] I. Polenz, S. S. Datta, and D. A. Weitz, “Controlling the Morphology of Polyurea Microcapsules Using Microfluidics,” *Langmuir*, vol. 30, pp. 13405–13410, Oct. 2014.
- [104] I. Polenz, D. A. Weitz, and J.-C. Baret, “Polyurea Microcapsules in Microfluidics: Surfactant Control of Soft Membranes,” *Langmuir*, vol. 31, pp. 1127–1134, Jan. 2015.
- [105] A. Abbaspourrad, S. S. Datta, and D. A. Weitz, “Controlling Release From pH-Responsive Microcapsules,” *Langmuir*, vol. 29, pp. 12697–12702, Oct. 2013.
- [106] S. S. Datta, A. Abbaspourrad, E. Amstad, J. Fan, S.-H. Kim, M. Romanowsky, H. C. Shum, B. Sun, A. S. Utada, M. Windbergs, S. Zhou, and D. A. Weitz, “25th Anniversary Article: Double Emulsion Templated Solid Microcapsules: Mechanics And Controlled Release,” *Advanced Materials*, vol. 26, pp. 2205–2218, Feb. 2014.
- [107] C.-H. Choi, H. Lee, A. Abbaspourrad, J. H. Kim, J. Fan, M. Caggioni, C. Wesner, T. Zhu, and D. A. Weitz, “Triple Emulsion Drops with An Ultrathin Water Layer: High Encapsulation

- Efficiency and Enhanced Cargo Retention in Microcapsules,” *Advanced Materials*, vol. 28, pp. 3340–3344, Mar. 2016.
- [108] B. Kim, T. Y. Jeon, Y.-K. Oh, and S.-H. Kim, “Microfluidic Production of Semipermeable Microcapsules by Polymerization-Induced Phase Separation,” *Langmuir*, vol. 31, pp. 6027–6034, May 2015.
- [109] C. Nam, J. Yoon, S. A. Ryu, C.-H. Choi, and H. Lee, “Water and Oil Insoluble PEGDA-Based Microcapsule: Biocompatible and Multicomponent Encapsulation,” *ACS Applied Materials & Interfaces*, vol. 10, pp. 40366–40371, Nov. 2018.
- [110] N. Laohakunakorn, L. Grasemann, B. Lavickova, G. Michielin, A. Shahein, Z. Swank, and S. J. Maerkl, “Bottom-Up Construction of Complex Biomolecular Systems With Cell-Free Synthetic Biology,” *Frontiers in Bioengineering and Biotechnology*, vol. 8, pp. 431–26, Mar. 2020.
- [111] R. Marshall, J. Garamella, V. Noireaux, and A. Pierson, “High-throughput Microliter-Sized Cell-Free Transcription-Translation Reactions for Synthetic Biology Applications Using the Echo® 550 Liquid Handler.”
- [112] P. Torre, C. D. Keating, and S. S. Mansy, “Multiphase Water-in-Oil Emulsion Droplets for Cell-Free Transcription–Translation,” *Langmuir*, vol. 30, pp. 5695–5699, May 2014.
- [113] N. Park, S. H. Um, H. Funabashi, J. Xu, and D. Luo, “A cell-free protein-producing gel,” *Nature Materials*, vol. 8, pp. 432–437, Mar. 2009.
- [114] N. Park, J. S. Kahn, E. J. Rice, M. R. Hartman, H. Funabashi, J. Xu, S. H. Um, and D. Luo, “High-yield cell-free protein production from P-gel,” *Nature Protocols*, vol. 4, pp. 1759–1770, Nov. 2009.
- [115] D. Yang, S. Peng, M. R. Hartman, T. Gupton-Campolongo, E. J. Rice, A. K. Chang, Z. Gu, G. Q. M. Lu, and D. Luo, “Enhanced transcription and translation in clay hydrogel and implications for early life evolution,” *Scientific Reports*, vol. 3, pp. 27–6, Nov. 2013.
- [116] J. Thiele, Y. Ma, D. Foscith, M. M. K. Hansen, C. Steffen, H. A. Heus, and W. T. S. Huck, “DNA-functionalized hydrogels for confined membrane-free in vitro transcription/translation,” *Lab Chip*, vol. 14, no. 15, pp. 2651–6, 2014.

- [117] L. Aufinger and F. C. Simmel, “Artificial Gel-Based Organelles for Spatial Organization of Cell-Free Gene Expression Reactions,” *Angewandte Chemie International Edition*, vol. 57, pp. 17245–17248, Nov. 2018.
- [118] X. Zhou, H. Wu, M. Cui, S. N. Lai, and B. Zheng, “Long-lived protein expression in hydrogel particles: towards artificial cells,” *Chemical Science*, vol. 9, no. 18, pp. 4275–4279, 2018.
- [119] V. Noireaux and A. Libchaber, “A vesicle bioreactor as a step toward an artificial cell assembly,” *Proceedings of the National Academy of Sciences of the United States of America*, vol. 101, pp. 17669–17674, Dec. 2004.
- [120] K. K. Y. Ho, V. L. Murray, and A. P. Liu, “Engineering artificial cells by combining HeLa-based cell-free expression and ultrathin double emulsion template,” in *Engineering artificial cells by combining HeLa-based cell-free expression and ultrathin double emulsion template*, pp. 303–318, Elsevier, 2015.
- [121] K. K. Y. Ho, J. W. Lee, G. Durand, S. Majumder, and A. P. Liu, “Protein aggregation with poly(vinyl) alcohol surfactant reduces double emulsion-encapsulated mammalian cell-free expression,” *PLoS ONE*, vol. 12, pp. e0174689–15, Mar. 2017.
- [122] S. Deshpande, Y. Caspi, A. E. C. Meijering, and C. Dekker, “Octanol-assisted liposome assembly on chip,” *Nature Communications*, vol. 7, no. 1, pp. 1–9, 1.
- [123] S. Deshpande and C. Dekker, “On-chip microfluidic production of cell-sized liposomes,” *Nature Protocols*, vol. 13, pp. 856–874, Mar. 2018.
- [124] K. Vogele, T. Frank, L. Gasser, M. A. Goetzfried, M. W. Hackl, S. A. Sieber, F. C. Simmel, and T. Pirzer, “Towards synthetic cells using peptide-based reaction compartments,” *Nature Communications*, vol. 9, pp. 1–7, Sept. 2018.
- [125] H. Niederholtmeyer, C. Chagga, and N. K. Devaraj, “Communication and quorum sensing in non-living mimics of eukaryotic cells,” *Nature Communications*, vol. 9, pp. 1–8, Nov. 2018.
- [126] M. Shojaeian, F.-X. Lehr, H. U. Göringer, and S. Hardt, “On-Demand Production of Femto-liter Drops in Microchannels and Their Use as Biological Reaction Compartments,” *Analytical Chemistry*, vol. 91, pp. 3484–3491, Feb. 2019.

- [127] D. S. Tawfik and A. D. Griffiths, “Man-made cell-like compartments for molecular evolution,” *Nature Biotechnology*, vol. 16, pp. 652–656, July 1998.
- [128] L. E. Contreras-Llano and C. Tan, “High-throughput screening of biomolecules using cell-free gene expression systems,” *Synthetic Biology*, vol. 3, pp. 47–13, July 2018.
- [129] A. D. Griffiths and D. S. Tawfik, “Directed evolution of an extremely fast phosphotriesterase by in vitro compartmentalization,” *Embo Journal*, vol. 22, no. 1, pp. 24–35, 2003.
- [130] F. Courtois, L. F. Olguin, G. Whyte, D. Bratton, W. T. S. Huck, C. Abell, and F. Hollfelder, “An Integrated Device for Monitoring Time-Dependent in vitro Expression From Single Genes in Picolitre Droplets,” *ChemBioChem*, vol. 9, pp. 439–446, Feb. 2008.
- [131] J. A. Stapleton and J. R. Swartz, “Development of an In Vitro Compartmentalization Screen for High-Throughput Directed Evolution of [FeFe] Hydrogenases,” *PLoS ONE*, vol. 5, pp. e15275–8, Dec. 2010.
- [132] A. Fallah-Araghi, J.-C. Baret, M. Ryckelynck, and A. D. Griffiths, “A completely in vitro ultrahigh-throughput droplet-based microfluidic screening system for protein engineering and directed evolution,” *Lab Chip*, vol. 12, no. 5, pp. 882–11, 2012.
- [133] P. Gruner, B. Riechers, B. i. t. Semin, J. Lim, A. Johnston, K. Short, and J.-C. Baret, “Controlling molecular transport in minimal emulsions,” *Nature Communications*, vol. 7, pp. 1–9, Apr. 2019.
- [134] G. Etienne, A. Vian, M. Biočanin, B. Deplancke, and E. Amstad, “Cross-talk between emulsion drops: how are hydrophilic reagents transported across oil phases?,” *Lab Chip*, vol. 18, no. 24, pp. 3903–3912, 2018.
- [135] G. Woronoff, M. Ryckelynck, J. Wessel, O. Schicke, A. D. Griffiths, and P. Soumillon, “Activity-Fed Translation (AFT) Assay: A New High-Throughput Screening Strategy for Enzymes in Droplets,” *ChemBioChem*, vol. 16, pp. 1343–1349, May 2015.
- [136] Y. Zhou, H. Asahara, N. Schneider, P. Dranchak, J. Inglese, and S. Chong, “Engineering Bacterial Transcription Regulation To Create a Synthetic in VitroTwo-Hybrid System for Protein Interaction Assays,” *Journal of the American Chemical Society*, vol. 136, pp. 14031–14038, Aug. 2014.



- [137] N. Cui, H. Zhang, N. Schneider, Y. Tao, H. Asahara, Z. Sun, Y. Cai, S. A. Koehler, T. F. A. de Greef, A. Abbaspourrad, D. A. Weitz, and S. Chong, “A mix-and-read drop-based in vitro two-hybrid method for screening high-affinity peptide binders,” *Scientific Reports*, vol. 6, pp. 1–10, Feb. 2016.
- [138] M. M. K. Hansen, L. H. H. Meijer, E. Spruijt, R. J. M. Maas, M. V. Rosquelles, J. Groen, H. A. Heus, and W. T. S. Huck, “Macromolecular crowding creates heterogeneous environments of gene expression in picolitre droplets,” *Nature Nanotechnology*, vol. 11, pp. 191–197, Oct. 2015.
- [139] T. Matsuura, K. Hosoda, Y. Kazuta, N. Ichihashi, H. Suzuki, and T. Yomo, “Effects of Compartment Size on the Kinetics of Intracompartamental Multimeric Protein Synthesis,” *ACS Synthetic Biology*, vol. 1, pp. 431–437, Sept. 2012.
- [140] R. Sakamoto, V. Noireaux, and Y. T. Maeda, “Anomalous Scaling of Gene Expression in Confined Cell-Free Reactions,” *Scientific Reports*, vol. 8, p. 7364, May 2018.
- [141] A. Kato, M. Yanagisawa, Y. T. Sato, K. Fujiwara, and K. Yoshikawa, “Cell-Sized confinement in microspheres accelerates the reaction of gene expression,” *Scientific Reports*, vol. 2, pp. 1172–5, Feb. 2012.
- [142] M. Schwarz-Schilling, A. Dupin, F. Chizzolini, S. Krishnan, S. S. Mansy, and F. C. Simmel, “Optimized Assembly of a Multifunctional RNA-Protein Nanostructure in a Cell-Free Gene Expression System,” *Nano Letters*, vol. 18, pp. 2650–2657, Mar. 2018.
- [143] Y. Hori, C. Kantak, R. M. Murray, and A. R. Abate, “Cell-free extract based optimization of biomolecular circuits with droplet microfluidics,” *Lab on a Chip*, vol. 17, pp. 3037–3042, Sept. 2017.
- [144] S. Alberti, A. Gladfelter, and T. Mittag, “Considerations and Challenges in Studying Liquid-Liquid Phase Separation and Biomolecular Condensates,” *Cell*, vol. 176, pp. 419–434, Jan. 2019.
- [145] N.-N. Deng, M. A. Vibhute, L. Zheng, H. Zhao, M. Yelleswarapu, and W. T. S. Huck, “Macromolecularly Crowded Protocells from Reversibly Shrinking Monodisperse Liposomes,” *Journal of the American Chemical Society*, vol. 140, pp. 7399–7402, June 2018.

- [146] E. Sokolova, E. Spruijt, M. M. K. Hansen, E. Dubuc, J. Groen, V. Chokkalingam, A. Piruska, H. A. Heus, and W. T. S. Huck, “Enhanced transcription rates in membrane-free protocells formed by coacervation of cell lysate,” *Proceedings of the National Academy of Sciences of the United States of America*, vol. 110, no. 29, pp. 11692–11697, 2013.
- [147] X. Ge, D. Luo, and J. Xu, “Cell-free protein expression under macromolecular crowding conditions,” *PLoS ONE*, vol. 6, no. 12, p. e28707, 2011.
- [148] T. Y. D. Tang, D. van Swaay, A. deMello, J. L. R. Anderson, and S. Mann, “In vitro gene expression within membrane-free coacervate protocells,” *Chemical Communications*, vol. 51, pp. 11429–11432, June 2015.
- [149] D. van Swaay, T. Y. D. Tang, S. Mann, and A. de Mello, “Microfluidic Formation of Membrane-Free Aqueous Coacervate Droplets in Water,” *Angewandte Chemie*, vol. 127, pp. 8518–8521, May 2015.
- [150] R. C. H. Ruiz, P. Kiatwuthinon, J. S. Kahn, Y. H. Roh, and D. Luo, “Cell-Free Protein Expression from DNA-Based Hydrogel (P-Gel) Droplets for Scale-Up Production,” *Industrial Biotechnology*, vol. 8, pp. 372–377, Dec. 2012.
- [151] J. S. Kahn, R. C. H. Ruiz, S. Sureka, S. Peng, T. L. Derrien, D. An, and D. Luo, “DNA Microgels as a Platform for Cell-Free Protein Expression and Display,” *Biomacromolecules*, vol. 17, pp. 2019–2026, June 2016.
- [152] Y. Jiao, Y. Liu, D. Luo, W. T. S. Huck, and D. Yang, “Microfluidic-Assisted Fabrication of Clay Microgels for Cell-Free Protein Synthesis,” *ACS Applied Materials & Interfaces*, vol. 10, pp. 29308–29313, Aug. 2018.
- [153] S. N. Lai, X. Zhou, X. Ouyang, H. Zhou, Y. Liang, J. Xia, and B. Zheng, “Artificial Cells Capable of Long-Lived Protein Synthesis by Using Aptamer Grafted Polymer Hydrogel,” *ACS Synthetic Biology*, pp. acssynbio.9b00338–20, Dec. 2019.
- [154] P. Stano, “Gene Expression Inside Liposomes: From Early Studies to Current Protocols,” *Chemistry - A European Journal*, vol. 25, pp. 7798–7814, Apr. 2019.
- [155] T. Oberholzer, K. H. Nierhaus, and P. L. Luisi, “Protein expression in liposomes,” *Biochemical and Biophysical Research Communications*, vol. 261, no. 2, pp. 238–241, 1999.

- [156] W. Yu, K. Sato, M. Wakabayashi, T. Nakaishi, E. P. Ko-Mitamura, Y. Shima, I. Urabe, and T. Yomo, "Synthesis of functional protein in liposome.," *Journal of Bioscience and Bioengineering*, vol. 92, no. 6, pp. 590–593, 2001.
- [157] T. Oberholzer and P. L. Luisi, "The use of liposomes for constructing cell models," *Journal of Biological Physics*, vol. 28, no. 4, pp. 733–744, 2002.
- [158] S.-i. M. Nomura, K. Tsumoto, T. Hamada, K. Akiyoshi, Y. Nakatani, and K. Yoshikawa, "Gene Expression within Cell-Sized Lipid Vesicles," *ChemBioChem*, vol. 4, pp. 1172–1175, Nov. 2003.
- [159] K. Ishikawa, K. Sato, Y. Shima, I. Urabe, and T. Yomo, "Expression of a cascading genetic network within liposomes," *FEBS Letters*, vol. 576, pp. 387–390, Oct. 2004.
- [160] Z. Nourian, W. Roelofsen, and C. Danelon, "Triggered Gene Expression in Fed-Vesicle Microreactors with a Multifunctional Membrane," *Angewandte Chemie International Edition*, vol. 51, pp. 3114–3118, Jan. 2012.
- [161] L. R. Arriaga, S. S. Datta, S.-H. Kim, E. Amstad, T. E. Kodger, F. Monroy, and D. A. Weitz, "Ultrathin Shell Double Emulsion Templated Giant Unilamellar Lipid Vesicles with Controlled Microdomain Formation," *Small*, vol. 10, pp. 950–956, Oct. 2013.
- [162] N.-N. Deng, M. Yelleswarapu, and W. T. S. Huck, "Monodisperse Uni- and Multicompartment Liposomes," *Journal of the American Chemical Society*, vol. 138, pp. 7584–7591, June 2016.
- [163] N.-N. Deng, M. Yelleswarapu, L. Zheng, and W. T. S. Huck, "Microfluidic Assembly of Monodisperse Vesosomes as Artificial Cell Models," *Journal of the American Chemical Society*, vol. 139, pp. 587–590, Jan. 2017.
- [164] F. Cuomo, A. Ceglie, A. De Leonadis, and F. Lopez, "Polymer Capsules for Enzymatic Catalysis in Confined Environments," *Catalysts*, vol. 9, pp. 1–18, Jan. 2019.
- [165] A. Schreiber, M. C. Huber, and S. M. Schiller, "Prebiotic Protocell Model Based on Dynamic Protein Membranes Accommodating Anabolic Reactions," *Langmuir*, vol. 35, pp. 9593–9610, June 2019.

- [166] Y.-C. Kwon, G.-H. Hahn, K. M. Huh, and D.-M. Kim, “Synthesis of functional proteins using *Escherichia coli* extract entrapped in calcium alginate microbeads,” *Analytical Biochemistry*, vol. 373, pp. 192–196, Feb. 2008.
- [167] S. Y. Lim, K.-O. Kim, D.-M. Kim, and C. B. Park, “Silica-coated alginate beads for in vitro protein synthesis via transcription/translation machinery encapsulation,” *Journal of Biotechnology*, vol. 143, pp. 183–189, Sept. 2009.
- [168] D. Saeki, S. Sugiura, T. Kanamori, S. Sato, and S. Ichikawa, “Microcompartmentalized cell-free protein synthesis in semipermeable microcapsules composed of polyethylenimine-coated alginate,” *Journal of Bioscience and Bioengineering*, vol. 118, pp. 199–204, Aug. 2014.
- [169] T. Okano, T. Matsuura, Y. Kazuta, H. Suzuki, and T. Yomo, “Cell-free protein synthesis from a single copy of DNA in a glass microchamber,” *Lab Chip*, vol. 12, no. 15, pp. 2704–8, 2012.
- [170] T. Okano, T. Matsuura, H. Suzuki, and T. Yomo, “Cell-free Protein Synthesis in a Microchamber Revealed the Presence of an Optimum Compartment Volume for High-order Reactions,” *ACS Synthetic Biology*, vol. 3, pp. 347–352, June 2014.
- [171] K. Nishimura, T. Matsuura, K. Nishimura, T. Sunami, H. Suzuki, and T. Yomo, “Cell-Free Protein Synthesis inside Giant Unilamellar Vesicles Analyzed by Flow Cytometry,” *Langmuir*, vol. 28, pp. 8426–8432, May 2012.
- [172] T. Sunami, K. Hosoda, H. Suzuki, T. Matsuura, and T. Yomo, “Cellular Compartment Model for Exploring the Effect of the Lipidic Membrane on the Kinetics of Encapsulated Biochemical Reactions,” *Langmuir*, vol. 26, pp. 8544–8551, June 2010.
- [173] P. Stano, E. D’Aguanno, J. Bolz, A. Fahr, and P. L. Luisi, “A Remarkable Self-Organization Process as the Origin of Primitive Functional Cells,” *Angewandte Chemie International Edition*, vol. 52, pp. 13397–13400, Oct. 2013.
- [174] D. Blanken, P. van Nies, and C. Danelon, “Quantitative imaging of gene-expressing liposomes reveals rare favorable phenotypes,” *Physical Biology*, vol. 16, pp. 045002–15, July 2019.

- [175] E. Altamura, P. Carrara, F. D’Angelo, F. Mavelli, and P. Stano, “Extrinsic stochastic factors (solute partition) in gene expression inside lipid vesicles and lipid-stabilized water-in-oil droplets: a review,” *Synthetic Biology*, vol. 3, pp. 167–16, July 2018.
- [176] A. M. Tayar, E. Karzbrun, V. Noireaux, and R. H. Bar-Ziv, “Propagating gene expression fronts in a one-dimensional coupled system of artificial cells,” *Nature Physics*, vol. 11, pp. 1037–1041, Sept. 2015.
- [177] M. Schwarz-Schilling, L. Aufinger, A. Mückl, and F. C. Simmel, “Chemical communication between bacteria and cell-free gene expression systems within linear chains of emulsion droplets,” *Integrative Biology*, vol. 8, no. 4, pp. 564–570, 2016.
- [178] A. Dupin and F. C. Simmel, “Signalling and differentiation in emulsion-based multi-compartmentalized in vitro gene circuits,” *Nature Chemistry*, vol. 11, pp. 1–8, Dec. 2018.
- [179] M. Dwidar, Y. Seike, S. Kobori, C. Whitaker, T. Matsuura, and Y. Yokobayashi, “Programmable Artificial Cells Using Histamine-Responsive Synthetic Riboswitch,” *Journal of the American Chemical Society*, vol. 141, pp. 11103–11114, June 2019.
- [180] S. Majumder, J. Garamella, Y.-L. Wang, M. DeNies, V. Noireaux, and A. P. Liu, “Cell-sized mechanosensitive and biosensing compartment programmed with DNA,” *Chem. Commun.*, vol. 53, no. 53, pp. 7349–7352, 2017.
- [181] J. Garamella, S. Majumder, A. P. L. ORCID: 0000-0002-0309-7018, and V. N. ORCID: 0000-0002-5213-273X, “An Adaptive Synthetic Cell Based on Mechanosensing, Biosensing, and Inducible Gene Circuits,” *ACS Synthetic Biology*, vol. 8, pp. 1–8, July 2019.
- [182] R. Lentini, N. Y. Martín, M. Forlin, L. Belmonte, J. Fontana, M. Cornella, L. Martini, S. Tamburini, W. E. Bentley, O. Jousson, and S. S. Mansy, “Two-Way Chemical Communication between Artificial and Natural Cells,” *ACS Central Science*, vol. 3, pp. 117–123, Jan. 2017.
- [183] A. M. Tayar, E. Karzbrun, V. Noireaux, and R. H. Bar-Ziv, “Synchrony and pattern formation of coupled genetic oscillators on a chip of artificial cells,” *Proceedings of the National Academy of Sciences*, vol. 114, pp. 11609–11614, Oct. 2017.

- [184] R. Lentini, S. P. Santero, F. Chizzolini, D. Cecchi, J. Fontana, M. Marchioretto, C. Del Bianco, J. L. Terrell, A. C. Spencer, L. Martini, M. Forlin, M. Assfalg, M. Dalla Serra, W. E. Bentley, and S. S. Mansy, “Integrating artificial with natural cells to translate chemical messages that direct E. coli behaviour,” *Nature Communications*, vol. 5, p. 4012, May 2014.
- [185] G. Rampioni, F. D’Angelo, M. Messina, A. Zennaro, Y. Kuruma, D. Tofani, L. Leoni, and P. Stano, “Synthetic cells produce a quorum sensing chemical signal perceived by *Pseudomonas aeruginosa*,” *Chemical Communications*, vol. 54, no. 17, pp. 2090–2093, 2018.
- [186] Y. Ding, L. E. Contreras-Llano, E. Morris, M. Mao, and C. Tan, “Minimizing Context Dependency of Gene Networks Using Artificial Cells,” *ACS Applied Materials & Interfaces*, vol. 10, pp. 30137–30146, Aug. 2018.
- [187] K. P. Adamala, D. A. Martin-Alarcon, K. R. Guthrie-Honea, and E. S. Boyden, “Engineering genetic circuit interactions within and between synthetic minimal cells,” *Nature Chemistry*, vol. 9, pp. 431–439, Nov. 2016.
- [188] N. Krinsky, M. Kaduri, A. Zinger, J. Shainsky-Roitman, M. Goldfeder, I. Benhar, D. HersHKovitz, and A. Schroeder, “Synthetic Cells Synthesize Therapeutic Proteins inside Tumors,” *Advanced Healthcare Materials*, vol. 7, pp. 1701163–10, Dec. 2017.
- [189] H. Shum and A. C. Balazs, “Synthetic quorum sensing in model microcapsule colonies,” *Proceedings of the National Academy of Sciences*, vol. 114, pp. 8475–8480, Aug. 2017.
- [190] G. Menon and J. Krishnan, “Design Principles for Compartmentalization and Spatial Organization of Synthetic Genetic Circuits,” *ACS Synthetic Biology*, vol. 8, pp. 1601–1619, June 2019.
- [191] G. Villar, A. D. Graham, and H. Bayley, “A Tissue-Like Printed Material,” *Science (New York, N.Y.)*, vol. 340, no. 6128, pp. 48–52, 2013.
- [192] A. Joesaar, S. Yang, B. Bögels, A. van der Linden, P. Pieters, B. V. V. S. P. Kumar, N. Dalchau, A. Phillips, S. Mann, and T. F. A. de Greef, “DNA-based communication in populations of synthetic protocells,” *Nature Nanotechnology*, vol. 14, pp. 369–378, Apr. 2019.

- [193] A. J. Genot, A. Baccouche, R. Sieskind, N. Aubert-Kato, N. Bredeche, J. F. Bartolo, V. Taly, T. Fujii, and Y. Rondelez, “High-resolution mapping of bifurcations in nonlinear biochemical circuits,” *Nature Chemistry*, vol. 8, pp. 760–767, June 2016.
- [194] M. Weitz, J. Kim, K. Kapsner, E. Winfree, E. Franco, and F. C. Simmel, “Diversity in the dynamical behaviour of a compartmentalized programmable biochemical oscillator,” *Nature Chemistry*, vol. 6, pp. 295–302, Feb. 2014.
- [195] J. Selberg, M. Gomez, and M. Rolandi, “The Potential for Convergence between Synthetic Biology and Bioelectronics,” *Cell Systems*, vol. 7, pp. 231–244, Sept. 2018.
- [196] G. Etienne, M. Kessler, and E. Amstad, “Influence of Fluorinated Surfactant Composition on the Stability of Emulsion Drops,” *Macromolecular Chemistry and Physics*, vol. 218, pp. 1600365–10, Oct. 2016.
- [197] C.-H. Choi, D. A. Weitz, and C.-S. Lee, “One Step Formation of Controllable Complex Emulsions: From Functional Particles to Simultaneous Encapsulation of Hydrophilic and Hydrophobic Agents into Desired Position,” *Advanced Materials*, vol. 25, pp. 2536–2541, Mar. 2013.
- [198] X.-h. Ge, Y.-h. Geng, Q.-c. Zhang, M. Shao, J. Chen, G.-s. Luo, and J.-h. Xu, “Four reversible and reconfigurable structures for three-phase emulsions: extended morphologies and applications,” *Scientific Reports*, vol. 7, pp. 1–9, Feb. 2017.
- [199] C.-X. Zhao, D. Chen, Y. Hui, D. A. Weitz, and A. P. J. Middelberg, “Controlled Generation of Ultrathin-Shell Double Emulsions and Studies on Their Stability,” *ChemPhysChem*, vol. 18, pp. 1393–1399, Mar. 2017.
- [200] A. Vian, V. Favrod, and E. Amstad, “Reducing the shell thickness of double emulsions using microfluidics,” *Microfluidics and Nanofluidics*, vol. 20, pp. 1–9, Nov. 2016.
- [201] A. Vian, B. Reuse, and E. Amstad, “Scalable production of double emulsion drops with thin shells,” *Lab Chip*, vol. 18, no. 13, pp. 1936–1942, 2018.
- [202] R. Rošic, J. Pelipenko, J. Kristl, P. Kocbek, M. Bešter-Rogač, and S. Baumgartner, “Physical characteristics of poly (vinyl alcohol) solutions in relation to electrospun nanofiber formation,” *European Polymer Journal*, vol. 49, pp. 290–298, Feb. 2013.

- [203] A. Urrios, C. Parra-Cabrera, N. Bhattacharjee, A. M. Gonzalez-Suarez, L. G. Rigat-Brugarolas, U. Nallapatti, J. Samitier, C. A. DeForest, F. Posas, J. L. Garcia-Cordero, and A. Folch, “3D-printing of transparent bio-microfluidic devices in PEG-DA,” *Lab on a Chip*, vol. 16, pp. 2287–2294, June 2016.
- [204] Y. Kim, K. Castro, N. Bhattacharjee, and A. Folch, “Digital Manufacturing of Selective Porous Barriers in Microchannels Using Multi-Material Stereolithography,” *Micromachines*, vol. 9, pp. 125–10, Mar. 2018.
- [205] M. B. Browning and E. Cosgriff-Hernandez, “Development of a Biostable Replacement for PEGDA Hydrogels,” *Biomacromolecules*, vol. 13, pp. 779–786, Feb. 2012.
- [206] R. H. Cole, T. M. Tran, and A. R. Abate, “Double Emulsion Generation Using a Polydimethylsiloxane (PDMS) Co-axial Flow Focus Device,” *Journal of Visualized Experiments*, no. 106, pp. 1–7, 2015.
- [207] E. Loiseau, F. Niedermair, G. Albrecht, M. Frey, A. Hauser, P. A. Rhs, and A. R. Studart, “Strong Microcapsules with Permeable Porous Shells Made through Phase Separation in Double Emulsions,” *Langmuir*, vol. 33, pp. 2402–2410, Feb. 2017.
- [208] X. Huang, M. Li, D. C. Green, D. S. Williams, A. J. Patil, and S. Mann, “Interfacial assembly of protein-polymer nano-conjugates into stimulus-responsive biomimetic protocells,” *Nature Communications*, vol. 4, no. 1, p. 2239, 2013.
- [209] A. Rotem, A. R. Abate, A. S. Utada, V. Van Steijn, and D. A. Weitz, “Drop formation in non-planar microfluidic devices,” *Lab on a Chip*, vol. 12, no. 21, pp. 4263–6, 2012.
- [210] M. Ugrinic, A. Zambrano, S. Berger, S. Mann, T. Y. D. Tang, and A. deMello, “Microfluidic formation of proteinosomes,” *Chemical Communications*, vol. 54, pp. 287–290, Dec. 2017.
- [211] D. T. Gonzales, C. Zechner, and T. Y. D. Tang, “Building synthetic multicellular systems using bottom-up approaches,” *Current Opinion in Systems Biology*, vol. 24, pp. 56–63, Dec. 2020.
- [212] D. Stadlbauer, J. Tan, K. Jiang, M. M. Hernandez, S. Fabre, F. Amanat, C. Teo, G. A. Arunkumar, M. McMahon, C. Capuano, K. Twyman, J. Jhang, M. D. Nowak, V. Simon,



- E. M. Sordillo, H. Bakel, and F. Krammer, “Repeated cross-sectional sero-monitoring of SARS-CoV-2 in New York City,” *Nature*, vol. 369, pp. 1–15, Dec. 2020.
- [213] E. C. Hughes, J. A. R. Amat, J. Haney, Y. A. Parr, N. Logan, N. Palmateer, S. Nickbakhsh, A. Ho, P. Cherepanov, A. Rosa, A. McAuley, A. Broos, I. Herbert, U. Arthur, A. M. Szemiel, C. Roustan, E. Dickson, R. N. Gunson, M. Viana, B. J. Willett, and P. R. Murcia, “SARS-CoV-2 serosurveillance in a patient population reveals differences in virus exposure and antibody-mediated immunity according to host demography and healthcare setting,” *The Journal of infectious diseases*, Dec. 2020.
- [214] H.-H. Chang, S. I. J. Peck, and K. Ran, “Serologic Evaluation of Healthcare Workers Caring for COVID-19 Patients in the Republic of Korea,” *fmicb-11-587613.tex*, vol. 11, pp. 1–6, Nov. 2020.
- [215] P. C. H. PhD, F. P. H. PhD, B. L. H. MD, M. n. F. S. MD, P. C. J. S. MD, L. s. P. V. MS, N. A. N. PhD, P. L. C. P. MD, P. O. A. D. PhD, M. N. B. MD, G. D. V. PhD, P. A. M. B. M. MD, P. F. C. B. MD, P. A. s. J. D. B. PhD, and P. C. G. V. MD, “SARS-CoV-2 antibody prevalence in Brazil: results from two successive nationwide serological household surveys,” *The Lancet Global Health*, vol. 8, pp. e1390–e1398, Sept. 2020.
- [216] S. S. PhD, A. W. MS, G. P. PhD, A. S. A. PhD, S. A. L. PhD, H. l. n. B. PhD, D. De Ridder MSc, D. P. PhD, S. S. PhD, K. M. MSc, S. Y. MSc, I. A. V. MSc, P. O. K. PhD, P. S. H. MD, P. K. M. P.-B. MD, P. D. T. MD, P. D. P. MD, L. G. t. MD, P. F. o. C. MD, P. I. E. MD, P. N. V. MD, B. M. PhD, P. A. F. MD, P. L. K. MD, and P. I. G. PhD, “Sero-prevalence of anti-SARS-CoV-2 IgG antibodies in Geneva, Switzerland (SEROCoV-POP): a population-based study,” *The Lancet*, vol. 396, pp. 313–319, Aug. 2020.
- [217] E. A. West, D. Anker, R. Amati, A. Richard, A. Wisniak, A. Butty, E. Albanese, M. Bochud, A. Chiolerio, L. Crivelli, S. Cullati, V. d’Acremont, A. M. Epure, J. Fehr, A. Flahault, L. Fornerod, I. Frank, A. Frei, G. Michel, S. Gonseth, I. Guessous, M. Imboden, C. R. Kahlert, L. Kaufmann, P. Kohler, N. Mösl, D. Paris, N. Probst-Hensch, N. Rodondi, S. Stringhini, T. Vermes, F. Vollrath, M. A. Puhan, E. Albanese, R. Amati, A. Amendola, D. Anker, A. M. Annoni, A. Azman, F. Bally, B. Balmer, H. Baysson, D. Berthod, J. Blankenberger, M. Bochud, P. Bodenmann, M. Bopp, A. Butty, A. L. Camerini, C. Cap-

- peli, C. Carmelli, A. Chiolero, P. Collombet, L. Corna, J. Crawford, L. Crivelli, S. Cullati, A. Cusini, V. D'Acremont, C. De Pietro, A. Deschamps, S. Droz, A. Dumoulin, O. Duperrex, J. Dupraz, M. Egger, N. Engler, A. M. Epure, S. Estoppey, M. Fadda, V. Faivre, J. Fehr, A. Felappi, M. Fiordelli, A. Flahault, L. Fornerod, C. F. Corti, M. Frangville, I. Frank, G. Franscella, A. Frei, D. Gille, G. Michel, S. G. Nusslé, A. Gouzowski, J. Guggisberg, H. Günthard, F. Gutzwiller, L. Incici, E. Jendly, R. Jung, C. Kahlert, L. Kaiser, L. Kaufmann, M. Kaufmann, S. Kessler, P. Kohler, S. Kriemler, L. Lenoir, S. Levati, B. Maeschli, J.-L. Magnin, E. Masserey, R. Morese, N. Möslé, N. Noël, M. Orhant, J. Pasquier, F. Pennacchio, D. Petrovic, S. Pfister, A. Picazio, C. Prandi, G. Piumatti, J. Portier, N. Probst-Hensch, C. Pugin, M. Puhon, T. Radtke, A. Richard, C.-F. Robert, P.-Y. Rodondi, N. Rodondi, E. Salberg, J. S. Zozaya, V. Schlüter, V. Schneider, A. Steiner-Dubuis, J. Sumer, I. Tall, J. Thabard, M. Tonolla, N. Troillet, A. Ulyte, S. Vassaux, T. Vermes, F. Vollrath, V. von Wyl, E. West, A. Wisniak, M.-E. Zaballa, and C. Zuppinger, "Corona Immunitas: study protocol of a nationwide program of SARS- CoV-2 seroprevalence and seroepidemiologic studies in Switzerland," *International Journal of Public Health*, vol. 65, pp. 1529–1548, Oct. 2020.
- [218] C. Fenwick, A. Croxatto, A. T. Coste, F. Pojer, C. André, C. Pellaton, A. Farina, J. Campos, D. Hacker, K. Lau, B.-J. Bosch, S. Gonseth Nussle, M. Bochud, V. d'Acremont, D. Trono, G. Greub, and G. Pantaleo, "Changes in SARS-CoV-2 Spike versus Nucleoprotein Antibody Responses Impact the Estimates of Infections in Population-Based Seroprevalence Studies.," *Journal of Virology*, pp. 1–33, Nov. 2020.
- [219] J. L. Garcia-Cordero, C. Nembrini, A. Stano, J. A. Hubbell, and S. J. Maerkl, "A high-throughput nanoimmunoassay chip applied to large-scale vaccine adjuvant screening," *Integrative Biology*, vol. 5, pp. 650–658, Feb. 2013.
- [220] J. L. Garcia-Cordero and S. J. Maerkl, "A 1024-sample serum analyzer chip for cancer diagnostics.," *Lab on a Chip*, vol. 14, pp. 2642–2650, Aug. 2014.
- [221] C. S. Kosack, A.-L. Page, and P. R. Klatser, "A guide to aid the selection of diagnostic tests.," *Bulletin of the World Health Organization*, vol. 95, pp. 639–645, Sept. 2017.

- [222] R. W. Peeling, K. K. Holmes, D. Mabey, and A. Ronald, “Rapid tests for sexually transmitted infections (STIs): the way forward,” *Sexually Transmitted Infections*, vol. 82, no. suppl 5, pp. v1–v6, 2006.
- [223] B. G. Andryukov, 1 Somov Research Institute of Epidemiology and Microbiology, Vladivostok, Russian Federation, and 2 Far Eastern Federal University (FEFU), Vladivostok, Russian Federation, “Six decades of lateral flow immunoassay: from determining metabolic markers to diagnosing COVID-19,” *AIMS Microbiology*, vol. 6, no. 3, pp. 280–304, 2020.
- [224] A. T. Coste, K. Jatton, M. Papadimitriou-Olivgeris, G. Greub, and A. Croxatto, “Comparison of SARS-CoV-2 serological tests with different antigen targets,” *Journal of Clinical Virology*, vol. 134, pp. 104690–7, Jan. 2021.
- [225] S. E. Conklin, K. Martin, Y. C. Manabe, H. A. Schmidt, J. Miller, M. Keruly, E. Klock, C. S. Kirby, O. R. Baker, R. E. Fernandez, Y. J. Eby, J. Hardick, K. Shaw-Saliba, R. E. Rothman, P. P. Caturegli, A. D. Redd, A. A. R. Tobian, E. M. Bloch, H. B. Larman, T. C. Quinn, W. Clarke, and O. Laeyendecker, “Evaluation of Serological SARS-CoV-2 Lateral Flow Assays for Rapid Point of Care Testing,” *Journal of Clinical Microbiology*, pp. 1–27, Nov. 2020.
- [226] A. M. Hashem, R. Y. Alhabbab, A. Algaissi, M. A. Alfaleh, S. Hala, T. S. Abujamel, M.-Z. ElAssouli, A. A. AL-Somali, F. S. Alofi, A. A. Khogeer, A. A. Alkayyal, A. B. Mahmoud, N. A. M. Almontashiri, and A. Pain, “Performance of Commercially Available Rapid Serological Assays for the Detection of SARS-CoV-2 Antibodies,” *Pathogens*, vol. 9, pp. 1067–10, Dec. 2020.
- [227] R. Mulchandani, H. E. Jones, S. Taylor-Phillips, J. Shute, K. Perry, S. Jamarani, T. Brooks, A. Charlett, M. Hickman, I. Oliver, S. Kaptoge, J. Danesh, E. Di Angelantonio, A. E. Ades, D. H. Wyllie, and EDSAB-HOME and COMPARE Investigators, “Accuracy of UK Rapid Test Consortium (UK-RTC) ”AbC-19 Rapid Test” for detection of previous SARS-CoV-2 infection in key workers: test accuracy study,” *BMJ*, vol. 371, p. m4262, Nov. 2020.
- [228] B. Meyer, G. Torriani, S. Yerly, L. Mazza, A. Calame, I. Arm-Vernez, G. Zimmer, T. Agoritsas, J. Stirnemann, H. Spechbach, I. Guessous, S. Stringhini, J. Pugin, P. Roux-Lombard, L. Fontao, C. A. Siegrist, I. Eckerle, N. Vuilleumier, L. Kaiser, and Geneva Center for

- Emerging Viral Diseases, “Validation of a commercially available SARS-CoV-2 serological immunoassay,” *Clinical microbiology and infection : the official publication of the European Society of Clinical Microbiology and Infectious Diseases*, vol. 26, pp. 1386–1394, Oct. 2020.
- [229] N. N. Nguyen, M. B. Mutnal, R. R. Gomez, H. N. Pham, L. T. Nguyen, W. Koss, A. Rao, A. C. Arroliga, L. Wang, D. Wang, Y. Hua, P. R. Powell, L. Chen, C. C. McCormack, W. J. Linz, and A. A. Mohammad, “Correlation of ELISA method with three other automated serological tests for the detection of anti-SARS-CoV-2 antibodies,” *PLoS ONE*, vol. 15, pp. e0240076–9, Oct. 2020.
- [230] T. W. McDade, E. M. McNally, A. S. Zelikovich, R. D’Aquila, B. Mustanski, A. Miller, L. A. Vaught, N. L. Reiser, E. Bogdanovic, K. S. Fallon, and A. R. Demonbreun, “High seroprevalence for SARS-CoV-2 among household members of essential workers detected using a dried blood spot assay,” *PLoS ONE*, vol. 15, pp. e0237833–8, Aug. 2020.
- [231] G. L. Morley, S. Taylor, S. Jossi, M. Perez-Toledo, S. E. Faustini, E. Marcial-Juarez, A. M. Shields, M. Goodall, J. D. Allen, Y. Watanabe, M. L. Newby, M. Crispin, M. T. Drayson, A. F. Cunningham, A. G. Richter, and M. K. O’Shea, “Sensitive Detection of SARS-CoV-2-Specific Antibodies in Dried Blood Spot Samples,” *Emerging Infectious Diseases*, vol. 26, pp. 2970–2973, Dec. 2020.
- [232] S. J. Moat, W. M. Zelek, E. Carne, M. J. Ponsford, K. Bramhall, S. Jones, T. El-Shanawany, M. P. Wise, A. Thomas, C. George, C. Fegan, R. Steven, R. Webb, I. Weeks, B. P. Morgan, and S. Jolles, “Development of a high-throughput SARS-CoV-2 antibody testing pathway using dried blood spot specimens,” *Annals of Clinical Biochemistry: International Journal of Laboratory Medicine*, pp. 000456322098110–9, Dec. 2020.
- [233] B. U. W. Lei and T. W. Prow, “A review of microsampling techniques and their social impact,” *Biomedical Microdevices*, vol. 21, pp. 1–30, July 2019.
- [234] L. A. Leuthold, O. Heudi, J. Déglon, M. Raccuglia, M. Augsburger, F. Picard, O. Kretz, and A. Thomas, “New Microfluidic-Based Sampling Procedure for Overcoming the Hematocrit Problem Associated with Dried Blood Spot Analysis,” *Analytical Chemistry*, vol. 87, pp. 2068–2071, Feb. 2015.

- [235] M. G. M. Kok and M. Fillet, “Volumetric absorptive microsampling: Current advances and applications,” *Journal of Pharmaceutical and Biomedical Analysis*, vol. 147, pp. 288–296, Jan. 2018.
- [236] W. F. Garcia-Beltran, T. E. Miller, G. Kirkpatrick, A. Nixon, M. G. Astudillo, D. Yang, L. M. Mahanta, M. Murali, A. S. Dighe, J. Lennerz, J. Thierauf, V. Naranbhai, and A. J. Iafrate, “Remote fingerstick blood collection for SARS-CoV-2 antibody testing,” *Archives of Pathology & Laboratory Medicine*, pp. 1–15, Dec. 2020.
- [237] C. Klumpp-Thomas, H. Kalish, M. Drew, S. Hunsberger, K. Snead, M. P. Fay, J. Mehalko, A. Shunmugavel, V. Wall, P. Frank, J.-P. Denson, M. Hong, G. Gulten, S. Messing, J. Hicks, S. Michael, W. Gillette, M. D. Hall, M. Memoli, D. Esposito, and K. Sadtler, “Standardization of enzyme-linked immunosorbent assays for serosurveys of the SARS-CoV-2 pandemic using clinical and at-home blood sampling,” *medRxiv*, May 2020.
- [238] D. R. Mayo and W. H. Beckwith, “Inactivation of West Nile virus during serologic testing and transport,” *Journal of Clinical Microbiology*, vol. 40, pp. 3044–3046, Aug. 2002.
- [239] S. Tripathi, Y. V. B. Kumar, A. Agrawal, A. Prabhakar, and S. S. Joshi, “Microdevice for plasma separation from whole human blood using bio- physical and geometrical effects,” *Scientific Reports*, vol. 6, pp. 1–15, June 2016.
- [240] A. Homsy, P. D. van der Wal, W. Doll, R. Schaller, S. Korsatko, M. Ratzer, M. Ellmerer, T. R. Pieber, A. Nicol, and N. F. de Rooij, “Development and validation of a low cost blood filtration element separating plasma from undiluted whole blood,” *Biomicrofluidics*, vol. 6, pp. 012804–9, Mar. 2012.
- [241] T. A. Crowley and V. Pizziconi, “Isolation of plasma from whole blood using planar micro-filters for lab-on-a-chip applications,” *Lab Chip*, vol. 5, no. 9, pp. 922–8, 2005.
- [242] D. Forchelet, S. Béguin, T. Sajic, N. Bararpour, Z. Pataky, M. Frias, S. Grabherr, M. Augsb-urger, Y. Liu, M. Charnley, J. Déglon, R. Aebersold, A. Thomas, and P. Renaud, “Separa-tion of blood microsamples by exploiting sedimentation at the microscale,” *Scientific Reports*, vol. 8, pp. 14101–9, Sept. 2018.

- [243] M. A. MacMullan, A. Ibrayeva, K. Trettner, L. Deming, S. Das, F. Tran, J. R. Moreno, J. G. Casian, P. Chellamuthu, J. Kraft, K. Kozak, F. E. Turner, V. I. Slepnev, and L. M. Le Page, “ELISA detection of SARS-CoV-2 antibodies in saliva,” *Scientific Reports*, vol. 10, pp. 1–8, Nov. 2020.
- [244] P. Zhou, X.-L. Yang, X.-G. Wang, B. Hu, L. Zhang, W. Zhang, H.-R. Si, Y. Zhu, B. Li, C.-L. Huang, H.-D. Chen, J. Chen, Y. Luo, H. Guo, R.-D. Jiang, M.-Q. Liu, Y. Chen, X.-R. Shen, X. Wang, X.-S. Zheng, K. Zhao, Q.-J. Chen, F. Deng, L.-L. Liu, B. Yan, F.-X. Zhan, Y.-Y. Wang, G.-F. Xiao, and Z.-L. Shi, “A pneumonia outbreak associated with a new coronavirus of probable bat origin,” *Nature*, vol. 579, no. 7798, pp. 270–273, 2020.
- [245] E. Dong, H. Du, and L. Gardner, “An interactive web-based dashboard to track COVID-19 in real time,” *The Lancet Infectious Diseases*, vol. 20, no. 5, pp. 533–534, 2020.
- [246] J. Perez-Saez, S. A. Lauer, L. Kaiser, S. Regard, E. Delaporte, I. Guessous, S. Stringhini, A. S. Azman, S.-P. S. Group, D. Alioucha, I. Arm-Vernez, S. Bahta, J. Barbolini, H. Baysson, R. Butzberger, S. Cattani, F. Chappuis, A. Chiovini, P. Collombet, D. Courvoisier, D. D. Ridder, E. D. Weck, P. D’ippolito, A. Daeniker, O. Desvachez, Y. Dibner, C. Dubas, J. Duc, I. Eckerle, C. Eelbode, N. E. Merjani, B. Emery, B. Favre, A. Flahault, N. Francioli, L. Gétaz, A. Gilson, A. Gonul, J. Guérin, L. Hassar, A. Hepner, F. Hovagemyan, S. Hurst, O. Keiser, M. Kir, G. Lamour, P. Lescuyer, F. Lombard, A. Mach, Y. Malim, E. Marchetti, K. Marcus, S. Maret, C. Martinez, K. Massiha, V. Mathey-Doret, L. Mattera, P. Matute, J.-M. Maugey, B. Meyer, T. Membrez, N. Michel, A. Mitrovic, E. M. Mohbat, M. Nehme, N. Noël, H.-K. Oulevey, F. Pardo, F. Pennacchio, D. Petrovic, A. Picazio, G. Piumatti, D. Pittet, J. Portier, G. Poulain, K. Posfay-Barbe, J.-F. Pradeau, C. Pugin, R. B. Rakotomiamanana, A. Richard, C. R. Fine, I. Sakvarelidze, L. Salzmänn-Bellard, M. Schellongova, S. Schrempft, M. S. Miranda, M. Stimec, M. Tacchino, S. Theurillat, M. Tomasini, K.-G. Toruslu, N. Tounsi, D. Trono, N. Vincent, G. Violot, N. Vuilleumier, Z. Waldmann, S. Welker, M. Will, A. Wisniak, S. Yerly, M.-E. Zaballa, and A. Z. Valle, “Serology-informed estimates of SARS-CoV-2 infection fatality risk in Geneva, Switzerland,” *The Lancet Infectious Diseases*, 2020.
- [247] F. Krammer and V. Simon, “Serology assays to manage COVID-19,” *Science*, vol. 368, no. 6495, pp. 1060–1061, 2020.

- [248] F. Amanat, D. Stadlbauer, S. Strohmeier, T. H. O. Nguyen, V. Chromikova, M. McMahon, K. Jiang, G. A. Arunkumar, D. Jurczynszak, J. Polanco, M. Bermudez-Gonzalez, G. Kleiner, T. Aydillo, L. Miorin, D. S. Fierer, L. A. Lugo, E. M. Kojic, J. Stoeve, S. T. H. Liu, C. Cunningham-Rundles, P. L. Felgner, T. Moran, A. García-Sastre, D. Caplivski, A. C. Cheng, K. Kedzierska, O. Vapalahti, J. M. Hepojoki, V. Simon, and F. Krammer, “A serological assay to detect SARS-CoV-2 seroconversion in humans,” *Nature Medicine*, vol. 26, no. 7, pp. 1033–1036, 2020.
- [249] S. Stringhini, A. Wisniak, G. Piumatti, A. S. Azman, S. A. Lauer, H. Baysson, D. D. Ridder, D. Petrovic, S. Schrempft, K. Marcus, S. Yerly, I. A. Vernez, O. Keiser, S. Hurst, K. M. Posfay-Barbe, D. Trono, D. Pittet, L. Gétaz, F. Chappuis, I. Eckerle, N. Vuilleumier, B. Meyer, A. Flahault, L. Kaiser, and I. Guessous, “Seroprevalence of anti-SARS-CoV-2 IgG antibodies in Geneva, Switzerland (SEROCoV-POP): a population-based study,” *The Lancet*, vol. 396, no. 10247, pp. 313–319, 2020.
- [250] X. Xu, J. Sun, S. Nie, H. Li, Y. Kong, M. Liang, J. Hou, X. Huang, D. Li, T. Ma, J. Peng, S. Gao, Y. Shao, H. Zhu, J. Y.-N. Lau, G. Wang, C. Xie, L. Jiang, A. Huang, Z. Yang, K. Zhang, and F. F. Hou, “Seroprevalence of immunoglobulin M and G antibodies against SARS-CoV-2 in China,” *Nature Medicine*, vol. 26, no. 8, pp. 1193–1195, 2020.
- [251] D. F. Gudbjartsson, G. L. Norddahl, P. Melsted, K. Gunnarsdottir, H. Holm, E. Eythorsson, A. O. Arnthorsson, D. Helgason, K. Bjarnadottir, R. F. Ingvarsson, B. Thorsteinsdottir, S. Kristjansdottir, K. Birgisdottir, A. M. Kristinsdottir, M. I. Sigurdsson, G. A. Arnadottir, E. V. Ivarsdottir, M. Andresdottir, F. Jonsson, A. B. Agustsdottir, J. Berglund, B. Eirisdottir, R. Fridriksdottir, E. E. Gardarsdottir, M. Gottfredsson, O. S. Gretarsdottir, S. Gudmundsdottir, K. R. Gudmundsson, T. R. Gunnarsdottir, A. Gylfason, A. Helgason, B. O. Jensson, A. Jonasdottir, H. Jonsson, T. Kristjansson, K. G. Kristinsson, D. N. Magnusdottir, O. T. Magnusson, L. B. Olafsdottir, S. Rognvaldsson, L. l. Roux, G. Sigmundsdottir, A. Sigurdsson, G. Sveinbjornsson, K. E. Sveinsdottir, M. Sveinsdottir, E. A. Thorarensen, B. Thorbjornsson, M. Thordardottir, J. Saemundsdottir, S. H. Kristjansson, K. S. Josefsson, G. Masson, G. Georgsson, M. Kristjansson, A. Moller, R. Palsson, T. Gudnason, U. Thorsteinsdottir, I. Jonsdottir, P. Sulem, and K. Stefansson, “Humoral Immune Response to SARS-CoV-2 in Iceland,” *New England Journal of Medicine*, 2020.

- [252] M. Pollán, B. Pérez-Gómez, R. Pastor-Barriuso, J. Oteo, M. A. Hernán, M. Pérez-Olmeda, J. L. Sanmartín, A. Fernández-García, I. Cruz, N. F. d. Larrea, M. Molina, F. Rodríguez-Cabrera, M. Martín, P. Merino-Amador, J. L. Paniagua, J. F. Muñoz-Montalvo, F. Blanco, R. Yotti, E.-C. S. Group, F. Blanco, R. G. Fernández, M. Martín, S. M. Navarro, M. Molina, J. F. Muñoz-Montalvo, M. S. Hernández, J. L. Sanmartín, M. Cuenca-Estrella, R. Yotti, J. L. Paniagua, N. F. d. Larrea, P. Fernández-Navarro, R. Pastor-Barriuso, B. Pérez-Gómez, M. Pollán, A. Avellón, G. Fedele, A. Fernández-García, J. O. Iglesias, M. T. P. Olmeda, I. Cruz, M. E. F. Martinez, F. D. Rodríguez-Cabrera, M. A. Hernán, S. P. Fernández, J. M. R. Aguirre, J. M. N. Marí, B. P. Borrás, A. B. P. Jiménez, M. Rodríguez-Iglesias, A. M. C. Gascón, M. L. L. Alcaine, I. D. Suárez, O. S. Álvarez, M. R. Pérez, M. C. Sanchís, C. J. V. Gomila, L. C. Saladrigas, A. H. Fernández, A. Oliver, E. C. Feliciano, M. N. G. Quintana, J. M. B. Fernández, M. A. H. Betancor, M. H. Febles, L. M. Martín, L.-M. L. López, T. U. Miota, I. D. B. Población, M. S. C. Pérez, M. N. V. Fernández, T. M. Enríquez, M. V. Arranz, M. D.-G. González, I. Fernández-Natal, G. M. Lobón, J. L. M. Bellido, P. Ciruela, A. M. i. Casals, M. D. Botías, M. A. M. Maeso, D. P. d. Campo, A. F. d. Castro, R. L. Ramírez, M. F. E. Retamosa, M. R. González, M. S. B. Lobeiras, A. F. Losada, A. Aguilera, G. Bou, Y. Caro, N. Marauri, L. M. S. Blanco, I. d. C. González, M. H. Pascual, R. A. Fernández, P. Merino-Amador, N. C. Castro, A. T. Lizcano, C. R. Almagro, M. S. Hernández, N. A. Elizaga, M. E. Sanz, C. E. Baquedano, A. B. Bascaran, S. I. Tamayo, L. E. Otazua, R. B. Benarroch, J. L. Flores, and A. V. d. l. Villa, “Prevalence of SARS-CoV-2 in Spain (ENE-COVID): a nationwide, population-based seroepidemiological study,” *The Lancet*, vol. 396, no. 10250, pp. 535–544, 2020.
- [253] M. Emmenegger, E. D. Cecco, D. Lamparter, R. P. B. Jacquat, D. Ebner, M. M. Schneider, I. C. Morales, D. Schneider, B. Dogancay, J. Guo, A. Wiedmer, J. Domange, M. Imeri, R. Moos, C. Zografou, C. Trevisan, A. Gonzalez-Guerra, A. Carrella, I. L. Dubach, C. L. Althaus, C. K. Xu, G. Meisl, V. Kosmoliaptsis, T. Malinauskas, N. Burgess-Brown, R. Owens, J. Mongkolsapaya, S. Hatch, G. R. Screaton, K. Schubert, J. D. Huck, F. Liu, F. Pojer, K. Lau, D. Hacker, E. Probst-Mueller, C. Cervia, J. Nilsson, O. Boyman, L. Saleh, K. Spanaus, A. v. Eckardstein, D. J. Schaer, N. Ban, C.-J. Tsai, J. Marino, G. F. X. Schertler, N. Ebert, V. Thiel, J. Gottschalk, B. M. Frey, R. Reimann, S. Hornemann, A. M. Ring, T. P. J. Knowles, I. Xenarios, D. I. Stuart, and A. Aguzzi, “Early peak and rapid decline of SARS-



- CoV-2 seroprevalence in a Swiss metropolitan region,” *medRxiv*, 2020.
- [254] M. Norman, T. Gilboa, A. F. Ogata, A. M. Maley, L. Cohen, E. L. Busch, R. Lazarovits, C.-P. Mao, Y. Cai, J. Zhang, J. E. Feldman, B. M. Hauser, T. M. Caradonna, B. Chen, A. G. Schmidt, G. Alter, R. C. Charles, E. T. Ryan, and D. R. Walt, “Ultrasensitive high-resolution profiling of early seroconversion in patients with COVID-19,” *Nature Biomedical Engineering*, pp. 1–8, 2020.
- [255] J. D. Whitman, J. Hiatt, C. T. Mowery, B. R. Shy, R. Yu, T. N. Yamamoto, U. Rathore, G. M. Goldgof, C. Whitty, J. M. Woo, A. E. Gallman, T. E. Miller, A. G. Levine, D. N. Nguyen, S. P. Bapat, J. Balcerek, S. A. Bylsma, A. M. Lyons, S. Li, A. W.-y. Wong, E. M. Gillis-Buck, Z. B. Steinhart, Y. Lee, R. Apathy, M. J. Lipke, J. A. Smith, T. Zheng, I. C. Boothby, E. Isaza, J. Chan, D. D. Acenas, J. Lee, T. A. Macrae, T. S. Kyaw, D. Wu, D. L. Ng, W. Gu, V. A. York, H. A. Eskandarian, P. C. Callaway, L. Warriar, M. E. Moreno, J. Levan, L. Torres, L. A. Farrington, R. P. Loudermilk, K. Koshal, K. C. Zorn, W. F. Garcia-Beltran, D. Yang, M. G. Astudillo, B. E. Bernstein, J. A. Gelfand, E. T. Ryan, R. C. Charles, A. J. Iafrate, J. K. Lennerz, S. Miller, C. Y. Chiu, S. L. Stramer, M. R. Wilson, A. Manglik, C. J. Ye, N. J. Krogan, M. S. Anderson, J. G. Cyster, J. D. Ernst, A. H. B. Wu, K. L. Lynch, C. Bern, P. D. Hsu, and A. Marson, “Evaluation of SARS-CoV-2 serology assays reveals a range of test performance,” *Nature Biotechnology*, pp. 1–10, 2020.
- [256] D. O. Andrey, P. Cohen, B. Meyer, G. Torriani, S. Yerly, L. Mazza, A. Calame, I. Arm-Vernez, I. Guessous, S. Stringhini, P. Roux-Lombard, L. Fontao, T. Agoritsas, J. Stirnemann, J.-L. Reny, C.-A. Siegrist, I. Eckerle, L. Kaiser, and N. Vuilleumier, “Head-to-Head Accuracy Comparison of Three Commercial COVID-19 IgM/IgG Serology Rapid Tests,” *Journal of Clinical Medicine*, vol. 9, no. 8, p. 2369, 2020.
- [257] F. Rudolf, H.-M. Kaltenbach, J. Linnik, M.-T. Ruf, C. Niederhauser, B. Nickel, D. Gyax, and M. Savic, “Clinical Characterisation of Eleven Lateral Flow Assays for Detection of COVID-19 Antibodies in a Population,” *medRxiv*, p. 2020.08.18.20177204, 2020.
- [258] S. J. Maerkl and S. R. Quake, “A Systems Approach to Measuring the Binding Energy Landscapes of Transcription Factors,” *Science*, vol. 315, no. 5809, pp. 233–237, 2007.

- [259] J. L. Garcia-Cordero and S. J. Maerkl, “Mechanically Induced Trapping of Molecular Interactions and Its Applications,” *Journal of Laboratory Automation*, vol. 21, pp. 356–367, May 2016.
- [260] J. L. Garcia-Cordero, C. Nembrini, A. Stano, J. A. Hubbell, and S. J. Maerkl, “A high-throughput nanoimmunoassay chip applied to large-scale vaccine adjuvant screening,” *Integrative Biology*, vol. 5, no. 4, pp. 650–658, 2013.
- [261] J. L. Garcia-Cordero and S. J. Maerkl, “A 1024-sample serum analyzer chip for cancer diagnostics,” *Lab on a Chip*, vol. 14, no. 15, pp. 2642–2650, 2013.
- [262] T. Thorsen, S. J. Maerkl, and S. R. Quake, “Microfluidic Large-Scale Integration,” *Science*, vol. 298, no. 5593, pp. 580–584, 2002.
- [263] M. M. Remy, M. Alfter, M.-N. Chiem, M. T. Barbani, O. B. Engler, and F. Suter-Riniker, “Effective chemical virus inactivation of patient serum compatible with accurate serodiagnosis of infections,” *Clinical Microbiology and Infection*, vol. 25, no. 7, pp. 907.e7–907.e12, 2018.
- [264] P. M. Fordyce, D. Gerber, D. Tran, J. Zheng, H. Li, J. L. DeRisi, and S. R. Quake, “De novo identification and biophysical characterization of transcription-factor binding sites with microfluidic affinity analysis,” *Nature Biotechnology*, vol. 28, no. 9, pp. 970–975, 2010.
- [265] M. Thevis, A. Knoop, M. S. Schaefer, B. Dufaux, Y. Schrader, A. Thomas, and H. Geyer, “Can dried blood spots (DBS) contribute to conducting comprehensive SARS-CoV-2 antibody tests?,” *Drug Testing and Analysis*, vol. 12, no. 7, pp. 994–997, 2020.
- [266] C. Klumpp-Thomas, H. Kalish, M. Drew, S. Hunsberger, K. Snead, M. P. Fay, J. Mehalko, A. Shunmugavel, V. Wall, P. Frank, J.-P. Denson, M. Hong, G. Gulten, S. Messing, J. Hicks, S. Michael, W. Gilette, M. D. Hall, M. Memoli, D. Esposito, and K. Sadtler, “Standardization of enzyme-linked immunosorbent assays for serosurveys of the SARS-CoV-2 pandemic using clinical and at-home blood sampling,” *medRxiv*, 2020.
- [267] J. L. Garcia-Cordero and S. J. Maerkl, “Multiplexed surface micropatterning of proteins with a pressure-modulated microfluidic button-membrane,” *Chemical Communications*, vol. 49, no. 13, pp. 1264–1266, 2012.

- [268] M. Geertz, D. Shore, and S. J. Maerkl, “Massively parallel measurements of molecular interaction kinetics on a microfluidic platform,” *Proceedings of the National Academy of Sciences*, vol. 109, no. 41, pp. 16540–16545, 2012.
- [269] F. Piraino, F. Volpetti, C. Watson, and S. J. Maerkl, “A Digital–Analog Microfluidic Platform for Patient-Centric Multiplexed Biomarker Diagnostics of Ultralow Volume Samples,” *ACS Nano*, vol. 10, no. 1, pp. 1699–1710, 2016.
- [270] B. Meyer, G. Torriani, S. Yerly, L. Mazza, A. Calame, I. Arm-Vernez, G. Zimmer, T. Agoritsas, J. Stirnemann, H. Spechbach, I. Guessous, S. Stringhini, J. Pugin, P. Roux-Lombard, L. Fontao, C.-A. Siegrist, I. Eckerle, N. Vuilleumier, L. Kaiser, and f. t. G. C. f. E. V. Diseases, “Validation of a commercially available SARS-CoV-2 serological immunoassay,” *Clinical Microbiology and Infection*, vol. 26, no. 10, pp. 1386–1394, 2020.
- [271] R. G. F. Alvim, T. M. Lima, D. A. S. Rodrigues, F. F. Marsili, V. B. T. Bozza, L. M. Higa, F. L. Monteiro, D. P. B. Abreu, I. C. Leitao, R. S. Carvalho, R. M. Galliez, T. M. P. P. Castineiras, A. Nobrega, L. H. Travassos, A. Tanuri, O. C. Ferreira, A. M. Vale, and L. R. Castilho, “An affordable anti-SARS-COV-2 spike protein ELISA test for early detection of IgG seroconversion suited for large-scale surveillance studies in low-income countries,” *medRxiv*, 2020.
- [272] M. G. Chibwana, K. C. Jere, R. kamng’ona, J. Mandolo, V. Katunga-Phiri, D. Tembo, N. Mitole, S. Musasa, S. Sichone, A. Lakudzala, L. Sibale, P. Matambo, I. Kadwala, R. L. Byrne, A. Mbewe, M. Y. R. Henrion, B. Morton, C. Phiri, J. Mallewa, H. C. Mwandumba, E. R. Adams, S. B. Gordon, and K. C. Jambo, “High SARS-CoV-2 seroprevalence in Health Care Workers but relatively low numbers of deaths in urban Malawi,” *medRxiv*, 2020.
- [273] D. Wrapp, N. Wang, K. S. Corbett, J. A. Goldsmith, C.-L. Hsieh, O. Abiona, B. S. Graham, and J. S. McLellan, “Cryo-EM structure of the 2019-nCoV spike in the prefusion conformation,” *Science (New York, N.Y.)*, vol. 367, pp. 1260–1263, Mar. 2020.
- [274] R. Verplaetse and J. Henion, “Hematocrit-Independent Quantitation of Stimulants in Dried Blood Spots: Pipet versus Microfluidic-Based Volumetric Sampling Coupled with Automated Flow-Through Desorption and Online Solid Phase Extraction-LC-MS/MS Bioanalysis,” *Analytical Chemistry*, vol. 88, pp. 6789–6796, June 2016.

- [275] I. McWilliam, M. C. Kwan, and D. Hall, “Inkjet Printing for the Production of Protein Microarrays,” in *Protein Microarrays: Methods and Protocols* (U. Korf, ed.), pp. 345–361, Totowa, NJ: Humana Press, 2011.
- [276] J. C. Stark, T. Jaroentomeechai, T. D. Moeller, J. M. Hershewe, K. F. Warfel, B. S. Moricz, A. M. Martini, R. S. Dubner, K. J. Hsu, T. C. Stevenson, B. D. Jones, M. P. DeLisa, and M. C. Jewett, “On-demand biomanufacturing of protective conjugate vaccines,” *Science Advances*, vol. 7, p. eabe9444, Feb. 2021.
- [277] K. S. Boles, K. Kannan, J. Gill, M. Felderman, H. Gouvis, B. Hubby, K. I. Kamrud, J. C. Venter, and D. G. Gibson, “Digital-to-biological converter for on-demand production of biologics,” *Nature Publishing Group*, vol. 35, pp. 672–675, July 2017.
- [278] M. Emmenegger, E. De Cecco, D. Lamparter, R. P. B. Jacquat, D. Ebner, M. M. Schneider, I. C. Morales, D. Schneider, B. Doğancı, J. Guo, A. Wiedmer, J. Domange, M. Imeri, R. Moos, C. Zografou, C. Trevisan, A. Gonzalez-Guerra, A. Carrella, I. L. Dubach, C. L. Althaus, C. K. Xu, G. Meisl, V. Kosmoliaptsis, T. Malinauskas, N. Burgess-Brown, R. Owens, S. Hatch, J. Mongkolsapaya, G. R. Screaton, K. Schubert, J. D. Huck, F. Liu, F. Pojer, K. Lau, D. Hacker, E. Probst-Müller, C. Cervia, J. Nilsson, O. Boyman, L. Saleh, K. Spanaus, A. von Eckardstein, D. J. Schaer, N. Ban, C.-J. Tsai, J. Marino, G. F. X. Schertler, N. Ebert, V. Thiel, J. Gottschalk, B. M. Frey, R. Reimann, S. Hornemann, A. M. Ring, T. P. J. Knowles, I. Xenarios, D. I. Stuart, and A. Aguzzi, “Early peak and rapid decline of SARS-CoV-2 seroprevalence in a Swiss metropolitan region,” *medRxiv*, 2020.
- [279] L. R. Arriaga, E. Amstad, and D. A. Weitz, “Scalable single-step microfluidic production of single-core double emulsions with ultra-thin shells,” *Lab on a Chip*, vol. 15, pp. 3335–3340, July 2015.
- [280] D. Wrapp, N. Wang, K. S. Corbett, J. A. Goldsmith, C.-L. Hsieh, O. Abiona, B. S. Graham, and J. S. McLellan, “Cryo-EM structure of the 2019-nCoV spike in the prefusion conformation,” *Science*, vol. 367, no. 6483, pp. 1260–1263, 2020.



## Grégoire Michielin

April 15, 1986

Av. Sainte-Luce 14 | 1003 Lausanne | Switzerland

+41 (0)76 585 53 44

gregoire.michielin@epfl.ch

linkedin.com/in/gregoiremichielin

### MEDICAL EXPERIENCE

#### Clinical Internships

- Pediatrics, Hôpital Inter cantonal de la Broye, Payerne, May 2015
- Pediatric Neurology, British Columbia Children's Hospital, Vancouver, August 2015
- Internal Medicine, PMU, Lausanne, November-December 2015
- General surgery, Hôpital Riviera-Chablais, Montreux, January 2016
- Neurology, CHUV, Lausanne, February 2016

#### Core Clinical Rotations, Centre Hospitalier Universitaire Vaudois, Lausanne

- Internal Medicine, Surgery, Pediatrics, Psychiatry, Family Medicine, Emergency, Palliative Care, Ophthalmology, Otorhinolaryngology, Dermatology (Spring semester 2014)

#### Summer Observership, Neuropediatrics

- Centre Hospitalier Universitaire Vaudois, Lausanne, August 2013

### RESEARCH EXPERIENCE

#### Doctoral Student, Prof. Sebastian Maerkl's group (LBNC)

École polytechnique fédérale de Lausanne, November 2016 – present

- Cell-free expression systems for therapeutic enzyme biomanufacturing
- Microfluidic production of biocompatible semi-permeable capsules for active biomolecules encapsulation
- Microfluidic nano-immunoassays for anti-SARS-CoV-2 antibodies detection in dried blood spots obtained from decentralized blood microsampling

#### Research Internships

- Neurobiology, Service de Biomedecine, CHUV, Lausanne, June 2015
- Neurobiology, Boston Children's Hospital, Boston, October 2015

#### Master Student, Prof. Dubikovskaya's group (LCBIM)

École Polytechnique Fédérale de Lausanne (EPFL), September 2013 – February 2016

- Development of blood brain barrier permeable probes for in vivo bioluminescent imaging in the brain.

#### Master Student and Research Assistant, Molecular Modelling group

Swiss Institute of Bioinformatics, Lausanne, August 2009 – March 2011

- Homology modelling of  $\alpha_5\beta_1$  integrin. Docking of several ligands on  $\alpha_5\beta_1$  and  $\alpha_v\beta_3$  integrins. Structure-activity relationship study.

### PUBLICATIONS

- Michielin G., Amstad E. and Maerkl S.J. Direct encapsulation of active biomolecules in semi-permeable microcapsules templated from double-emulsions, *In preparation*
- Swank Z, Michielin G, Yip HM, Cohen P, Andrey DO, Vuilleumier N, et al. A high-throughput microfluidic nano-immunoassay for detecting anti-SARS-CoV-2 antibodies in serum or ultra-low volume dried blood samples. medRxiv. Cold Spring Harbor Laboratory Press; 2020 Oct 29;26:1033–5. DOI: 10.1101/2020.10.07.20208280
- Laohakunakorn, N., Grasemann, L., Lavickova, B., Michielin, G., Shahein, A., Swank, Z. and Maerkl, S.J. (2019). Bottom-up construction of complex biological systems with cell-free synthetic biology. Front Bioeng Biotechnol. 2020 Mar 24;8:431–26. DOI: 10.3389/fbioe.2020.00213

## TEACHING EXPERIENCE

### Hacking medicine mini-hackathon organizer

- Organized and animated a mini-hackathon in a doctoral-level course “The making of an innovative medicine” by Prof. Roger Clerc at EPFL – Autumn semester 2019

### Summer school main organizer

- Shaping the future of (bio)-medicine 2019 (sfm2019.epfl.ch) – May 2019

### Teaching Assistant

- iGEM 2018: “Capoeira” cell-free production of personalized cancer vaccine and companion monitoring (nominated for best therapeutics and best software)
- iGEM 2017: “Aptasense” cell-free protein detection with sandwich aptamer assay and toehold switches (nominated for best diagnostics and best software) / educational cell-free minikit (award for best education and public engagement)

### Tutor and Private Teacher

- Collège Champittet, Pully, August 2010 – August 2015  
Academic tutoring of boarding school pupils.  
Private teacher in chemistry, physics, biology and mathematics.  
Supervise extracurricular activities during the evening and the weekends.

### Chemistry Teacher

- École Roche et École Cap, Lausanne, August 2009 – August 2010  
Teacher for standard and high level chemistry for high school students.

### Teaching Assistant

- École Polytechnique Fédérale de Lausanne, March 2006 – February 2010  
Supervision of practical work in analytical chemistry and general chemistry.  
Support for groups of 6 to 16 students. Correction and evaluation of reports.  
Presentation of safety rules, theoretical and practical concepts.

---

## EDUCATION

### École de Médecine, Faculté de Biologie et de Médecine, Université de Lausanne

- September 2013 – October 2016  
Master of Medicine, Swiss Federal Diploma
- September 2011 – July 2013  
Bachelor of Medicine

### USMLE, Step 1

- December 2014, Score: 207

### Chemistry Section, School of Basic Sciences, École Polytechnique Fédérale de Lausanne

- September 2008 – March 2010  
Master of Science in Molecular and Biological Chemistry, 5.38/6
- September 2004 – July 2008  
Bachelor of Science in Chemistry

---

## LANGUAGES

**French** native language

**English** professional working proficiency, TOEFL iBT: 114/120 (August 2014)

**German** limited working proficiency

**Italian** limited working proficiency

---

## HONORS & AWARDS

**2016** SNSF MD-PhD Fellowship

**2015** M-Day Award: Master Project Short Talk (3' presentation)

**2004** SVSN Award (Société vaudoise des Sciences naturelles)  
High School Diploma Thesis entitled “La solidité des noeuds”.  
<http://wp.unil.ch/svsn/soutien-a-la-releve/prix-svsn/>